

**Analysis of heat-induced localization of  
ESCRTIII core and associated proteins to mRNP granules  
in *A. thaliana***

Inaugural-Dissertation  
zur  
Erlangung des Doktorgrades  
der Mathematisch-Naturwissenschaftlichen Fakultät  
der Universität zu Köln

vorgelegt von  
Heike Wolff  
aus Köln

Köln, 2019

Berichterstatter: Prof. Dr. Martin Hülskamp<sup>1</sup>  
(Gutachter) Prof. Dr. Jane Parker<sup>2</sup>

Prüfungsvorsitzender: Prof. Dr. Niels Gehring<sup>3</sup>

Tag der mündlichen Prüfung: 03.09.2018

<sup>1</sup> Botanisches Institut, Universität zu Köln, Zülpicher Str. 47b 50674, Köln

<sup>2</sup> Max-Planck-Institut für Pflanzenzüchtungsforschung, Carl-von-Linné-Weg 10, 50829, Köln

<sup>3</sup> Institut für Genetik, Universität zu Köln, Zülpicher Str. 47a 50674, Köln

## Table of Contents

Table of Contents .....	3
List of Figures .....	6
List of Tables.....	7
List of Abbreviations.....	8
Abstract .....	12
Zusammenfassung.....	13
1 Introduction .....	15
1.1 Membrane trafficking in <i>A. thaliana</i> .....	15
1.2 Vacuolar protein sorting by the ESCRT system .....	18
1.3 The ESCRTIII core and associated protein complex .....	21
1.4 Composition and function of P-bodies and SGs .....	26
1.5 Aim of work .....	33
2 Material and Methods.....	34
2.1 Plasmids .....	34
2.2 Primers .....	35
2.3 Organisms .....	37
2.4 Plant techniques.....	39
2.4.1 Plant growth conditions.....	39
2.4.2 Seed sterilization .....	39
2.4.3 Crossing.....	39
2.4.4 Heat stress treatment .....	39
2.4.5 Transient transformation by particle bombardment .....	39
2.4.6 Confocal microscopy.....	40
2.4.7 FM4-64 staining and BFA treatment.....	41
2.5 Molecular biology techniques .....	41
2.5.1 RNA extraction and cDNA synthesis.....	41
2.5.2 Polymerase Chain Reaction (PCR) .....	41
2.5.3 Gateway cloning.....	42
2.5.4 Plasmid purification, restriction digestion and sequencing.....	43
2.5.5 Generation of chemical competent <i>E. coli</i> cells .....	43
2.5.6 Transformation of <i>E. coli</i> cells .....	44
2.6 Biochemical techniques.....	44
2.6.1 Co-immunoprecipitation .....	44
2.6.2 In solution/on-bead digest .....	45

## Table of Contents

---

2.6.3	StageTip purification .....	46
2.6.4	LC-MS/MS analysis .....	46
2.6.5	SDS-PAGE .....	47
2.6.6	Coomassie staining .....	47
2.6.7	Immunoblotting (Western blotting).....	47
2.7	Protein-protein interaction assays.....	48
2.7.1	Protein-protein interaction analysis by Y2H .....	48
2.7.2	Protein-protein interaction analysis by LUMIER.....	50
2.8	Computational analysis.....	51
2.8.1	Colocalization quantification.....	51
2.8.2	Intrinsically Disordered Region (IDR) analysis of protein sequences .....	51
2.8.3	Filtering and classification of interactome candidates.....	52
2.8.4	Statistical analysis.....	53
3	Results .....	54
3.1	Y2H of ESCRTIII core and associated proteins with mRNP granule components.....	54
3.2	Heat-dependent subcellular protein localization of SKD1 .....	57
3.3	Colocalization of SKD1 with P-body, SG, and endosomal marker proteins.....	61
3.3.1	Colocalization of SKD1 with mRNP proteins in transient double transformations .....	61
3.3.2	Colocalization quantification of SKD1 with mRNP granule markers.....	66
3.3.3	Colocalization quantification in transgenic marker lines .....	69
3.4	Subcellular localization of ESCRTIII core and associated proteins.....	76
3.4.1	<i>In-silico</i> analysis of IDRs in ESCRTIII core and associated proteins.....	77
3.4.2	Heat stress-dependent localization of ESCRTIII core and associated proteins.....	84
3.4.3	Colocalization study of ESCRTIII core and associated proteins with SKD1-AQ.....	88
3.4.4	Colocalization study of ESCRTIII core and associated proteins with UBP1b.....	91
3.4.5	Colocalization quantification of ESCRTIII core and associated proteins with UBP1b .....	94
3.5	Heat-dependent interactome of SKD1.....	97
3.5.1	Experimental approach and statistics of the heat-dependent SKD1 interactome .....	97
3.5.2	Characterization of the SKD1 interactome by GO and functional classification .....	100
3.5.3	Selection and cloning of SKD1 interactome candidates.....	104
3.5.4	Heat stress-dependent subcellular localization of the SKD1 interactome candidates .....	108
3.5.5	Colocalization analysis of SKD1 interactome candidates with UBP1b .....	111
3.5.6	Colocalization analysis of interactome candidates with SKD1 .....	115
3.5.7	Validation of candidate interactions with SKD1 by Y2H and LUMIER assays .....	118
3.6	Impact of heat stress on PIN2 protein trafficking.....	122
4	Discussion.....	126

---

4.1	SKD1 associates with mRNP granules after heat stress independent of endosomes .....	127
4.2	Some ESCRTIII associated, but no core proteins localize to mRNP granules .....	129
4.3	Membrane trafficking and new mRNP granule proteins are in the SKD1 interactome .....	131
4.4	What is the functional relevance of SKD1 relocalization under heat stress?.....	135
5	Appendix .....	138
6	References .....	169
7	Danksagung.....	184
8	Erklärung zur Dissertation .....	185

## List of Figures

Figure 1.1. Membrane trafficking in the endomembrane system of <i>A. thaliana</i> . .....	16
Figure 1.2. The ESCRT system in <i>A. thaliana</i> . .....	19
Figure 1.3. Removal of the ESCRTIII core complex by the ESCRTIII associated complex. ....	23
Figure 1.4. Sequestration of mRNAs and proteins into mRNP granules during cellular stress. ....	28
Figure 3.1. Subcellular localization of SKD1-YFP. ....	57
Figure 3.2. Subcellular localization of GFP-SKD1 in transgenic <i>A. thaliana</i> plants. ....	59
Figure 3.3. FM4-64 staining of <i>35S::GFP-SKD1</i> roots. ....	60
Figure 3.4. Colocalization of SKD1 with P-body marker proteins. ....	62
Figure 3.5. Colocalization of SKD1 with SG marker proteins. ....	64
Figure 3.6. Transient transformation of <i>35S::GFP-SKD1</i> leaves with mCHERRY-UBP1b. ....	65
Figure 3.7. Colocalization quantification of SKD1 with mRNP granule markers after heat stress. ....	67
Figure 3.8. Confocal imaging of <i>35S::GFP-SKD1x35S::PAB2-mRFP</i> . ....	70
Figure 3.9. Confocal imaging of the <i>35S::GFP-SKD1x35S::mCHERRY-ARA7</i> line. ....	71
Figure 3.10. Confocal imaging of crossed mRNP granule and endosomal marker lines. ....	73
Figure 3.11. Colocalization quantification of stable lines after heat stress treatment. ....	74
Figure 3.12. Comparison of predictor categories .....	81
Figure 3.13. Percentages of IDRs and long IDRs in ESCRTIII core and associated proteins. ....	83
Figure 3.14. Heat-dependent subcellular localization of ESCRTIII core and associated proteins. ....	86
Figure 3.15. Colocalization of ESCRTIII core and associated proteins with SKD1-AQ. ....	90
Figure 3.16. Colocalization of ESCRTIII core and associated proteins with UB1b after heat stress. ....	92
Figure 3.17. Colocalization quantification of ESCRTIII core and associated proteins with UB1b. ....	94
Figure 3.18. Strategy, test blot, and candidate filtering of the SKD1 interactome approach. ....	98
Figure 3.19. Individual functional classifications of the SKD1 interactome candidates. ....	102
Figure 3.20. Heat stress-dependent subcellular localization of membrane trafficking candidates. ....	109
Figure 3.21. Heat stress-dependent subcellular localization of the RNA metabolism candidates. ....	110
Figure 3.22. Colocalization analysis of membrane trafficking candidates with mCHERRY-UBP1b. ....	112
Figure 3.23. Colocalization analysis of RNA metabolism candidates with mCHERRY-UBP1b. ....	114
Figure 3.24. Colocalization analysis of membrane trafficking candidates with SKD1-mCHERRY. ....	116
Figure 3.25. Colocalization analysis of RNA metabolism candidates with SKD1-mCHERRY. ....	117
Figure 3.26. Subcellular localization of PIN2-GFP after heat stress or BFA treatment. ....	123
Figure 3.27. FM4-64 staining of heat or BFA treated <i>ProPIN2::PIN2-GFP</i> roots. ....	124
Figure A.1. Subcellular localization of free YFP and mCHERRY-UBP1b before and after heat. ....	145
Figure A.2. Representative pictures of the positive controls for the colocalization quantification. ....	146
Figure A.3. Colocalization of ESCRTIII core and associated proteins with SKD1. ....	153
Figure A.4. Colocalization of membrane trafficking candidates with mCHERRY-SKD1-AQ. ....	163
Figure A.5. Colocalization of RNA metabolism candidates with mCHERRY-SKD1-AQ. ....	164
Figure A.6. Test of SKD1 expression and purification from HEK293TN cells. ....	167

## List of Tables

Table 2.1. General plasmids used in this study .....	34
Table 2.2. Sequences of primers used in this study.....	35
Table 2.3. List of used organisms .....	37
Table 2.4. List of used and generated <i>A. thaliana</i> transgenic lines.....	38
Table 2.5. PCR reaction and program .....	42
Table 2.6. Composition of BP- and LR-reactions.....	43
Table 2.7. Summary of detected and identified peptides in the LC-MS/MS analysis .....	52
Table 3.1. Previously identified protein interactions of ESCRTIII and P-body components. ....	54
Table 3.2. Summary of tested ESCRTIII protein interactions with mRNP granule proteins.....	55
Table 3.3. Statistical analysis of colocalization between transient double transformations.....	68
Table 3.4. Statistical significance analysis of colocalization between the stable lines. ....	75
Table 3.5. Percentages of predicted IDR content within ESCRTIII, P-body and SG proteins. ....	79
Table 3.6. Statistical analysis of colocalization between ESCRTIII core and associated proteins .....	95
Table 3.7. PANTHER GO enrichment analysis of SKD1 shared interactors. ....	101
Table 3.8 List of SKD1 interactome candidates selected for further analysis. ....	105
Table 3.9. Summary of localizations and interactions of the SKD1 interactome candidates.....	121
Table A.1. List of specific plasmids used or generated in this study. ....	138
Table A.2. Y2H of ESCRTIII core and associated proteins with mRNP granule proteins.....	141
Table A.3. PCCs of transiently double transformed epidermal leaf cells. ....	147
Table A.4. Statistical analysis of colocalization between transient double transformations.....	148
Table A.5. PCCs of stable lines.....	149
Table A.6. Statistical analysis of colocalization between the stable lines.....	150
Table A.7. Predicted IDR content .....	151
Table A.8. PCCs of ESCRTIII core or associated proteins and UBP1b. ....	154
Table A.9. Statistical analysis of colocalization of ESCRTIII core and associated proteins .....	155
Table A.10. List of filtered SKD1 interactome candidates. ....	156
Table A.11. Results of SKD1 interactome Y2H assays. ....	165
Table A.12. Results of SKD1 interactome LUMIER assay. ....	166
Table A.13. Quantification of PIN2-GFP aggregates. ....	168

## List of Abbreviations

Abbreviation	Name
'	Minutes
''	Seconds
3'	3' prime end of DNA or RNA molecule
3-AT	3-Amino-1,2,4-triazole
35S <i>CaMV</i>	35S promoter of the Cauliflower mosaic virus
5'	5' prime end of DNA or RNA molecule
AAA	ATPases Associated with diverse cellular Activities
AALP	ALEURAIN-LIKE PROTEASE
ADP	Adenosine diphosphate
AN	ANGUSTIFOLIA
ATP	Adenosine triphosphate
ARF-GEF	ADP-RIBOSYLATION FACTOR GUANINE-EXCHANGE FACTOR
BAR	BFA-ADP RIBOSYLATED SUBSTRATE
BEACH	Beige And Chediak Higashi
BFA	Brefeldin A
bp	base pairs
Caf1	Ccrf Associated Factor
Ccr4	Carbon201 Catabolite Repressor 4
CCT	Complex Chaperonin-Containing T complex
Cdc48	Cell Division Cycle 48
CDS	Coding Sequence
CHMP	CHARGED MULTIVESICULAR BODY PROTEIN
CFP	cyan fluorescent protein
CML38	CALMODULINLIKE 38
COP	COAT PROTEIN COMPLEX
CORVET	class C core vacuole/endosome tethering
CPY	CARBOXYPEPTIDASE Y
CtBP	C-terminal Binding Protein
d	Day
DCP	Decapping Protein
Did4	DOA4-independent degradation protein 4
Dhh1	DEXD/H-box helicase 1
dNTPs	deoxyribonucleotides
DNA	deoxyribonucleic acid
Doa4	Degradation of alpha 4
DTT	Dithiothreitol
EAP	ELL ASSOCIATED PROTEIN
Edc3	Enhancer of Decapping 3
EE	Early endosomes

## List of Abbreviations

---

Abbreviation	Name
eIF2 $\alpha$	Eukaryotic translation Initiation Factor 2 $\alpha$
ER	Endoplasmic reticulum
ESCRT	Endosomal Sorting Complex Required For Transport
FDR	False discovery rate
FLOT1	FLOTTILIN-LIKE PROTEIN 1
FLS2	FLAGELLIN SENSING 2
FREE1	FYVE DOMAIN PROTEIN REQUIRED FOR ENDOSOMAL SORTING
FYVE	Fab-1, YGL023, Vps27, and EEA1
<i>g</i>	<i>g</i> -force
G3BP	Ras-GAP SH3 domain Binding Protein
GAL4-AD	GAL4 Activation Domain
GAL4-BD	GAL4 Binding Domain
GFP	green fluorescent protein
GL2	GLABRA 2
GRF2/9	GENERAL REGULATORY FACTOR 2/9
GRP2/7	GLYCINE RICH PROTEIN 2/7
GO	Gene Ontology
GTP	guanosine triphosphate
H	Histidine
h	hours
HOPS	homotypic fusion and vacuole protein sorting
HRS	HEPATOCTE GROWTH FACTOR-REGULATED TYROSINE KINASE SUBSTRATE
Hse1	Hbp STAM EAST1
Hsp	Heat Shock Protein
Hz	Hertz
IDR	Intrinsically Disordered Region
ILV	intraluminal vesicle
ISTL1	INCREASED SODIUM TOLERANCE1-LIKE 1
JACoP	Just Another Colocalization Plugin
kb	kilo base
L	Leucine
LC	Low Complexity
LC-MS/MS	Liquid chromatography- tandem mass spectrometry
LE	Late endosomes
LIP5	LYST INTERACTING PROTEIN 5
LFQ	Label-free quantification
LOS4	LOW EXPRESSION OF OSMOTICALLY RESPONSIVE GENES 4
Lsm	Sm-like
LUMIER	Luminescence-based mammalian interactome mapping
m7GpppN	7-methylguanosine 5'-triphosphate
MCM	MINI-CHROMOSOME MAINTENANCE
MIM	MIT Interacting Motif
MIT	Microtubule Interacting and Transport
mRFP	monomeric RFP

## List of Abbreviations

---

Abbreviation	Name
mRNA	messenger ribonucleic acid
mRNP	mRNA-ribonucleoprotein
mTQ	mTURQUOISE
MVBs	Multivesicular bodies
Mvb12p	Multivesicular Body 12
MS	Murashige and Skoog
NAD(H)	Nicotinamide adenine dinucleotide (H) <sup>+</sup>
NCBI	National Center for Biotechnology Information
Not	Negative on Tata
NTF2	NUCLEAR TRANSPORT FACTOR 2
o/n	over night
PABs	Poly(A) Binding Proteins
PANTHER	Protein analysis through evolutionary relationships
Pat1	Protein Associated With Topoisomerase1
P-bodies	Processing bodies
PBST	Phosphate buffer saline with 0.1% Tween20
PCC	Pearson's correlation coefficient
PCR	Polymerase Chain Reaction
PIN	PIN-FORMED
PIP1-1	PLASMA MEMBRANE INTRINSIC PROTEIN 1-1
PM	Plasma membrane
PROS	POSITIVE REGULATOR OF SKD1
ProtA	protein A from <i>Staphylococcus aureus</i>
PI(3)P	Phosphatidylinositol 3-phosphate
Rab	Ras-related in brain
RBP	RNA-BINDING PROTEIN
RE	Recycling endosome
RFP	red fluorescent protein
RLI	Relative Luminescence Intensity
ROI	Region of Interest
RRM	RNA Recognition Motif
RT	Room temperature
RUXF	SMALL NUCLEAR RIBONUCLEOPROTEIN F
Rvb	RuvB-like
SD	Selection Dropout
SDS-PAGE	Sodiumdodecylsulfate polyacrylamide gel electrophoresis
SEC13A	SECRETORY13 A
SG	Stress granule
SKD1	SUPPRESSOR OF K(+) TRANSPORT GROWTH DEFECT 1
SKD1-AQ	ATPase-defective version, contains K178A and E234Q mutation
SNARE	Soluble NSF attachment protein receptor
Snf7	Sucrose Non Fermenting 7
SPI	SPIRRIG
STAM1/2	SIGNAL TRANSDUCING ADAPTOR MOLECULE 1 AND 2

## List of Abbreviations

---

Abbreviation	Name
SUBA	Subcellular localization database for Arabidopsis proteins
TAIR	The Arabidopsis Information Resource
T	Tryptophan
TCP-1	T-complex protein 1
TEAB	Triethylammonium bicarbonate buffer
TGN	trans-Golgi network
TIA1	T-CELL RESTRICTED INTRACELLULAR ANTIGEN 1
TIA1-R	TIA1-RELATED
TOL	TARGET OF MYB1-LIKE
TORC1	TARGET OF RAPAMYCIN COMPLEX 1
TSG101	TUMOR SUSCEPTIBILITY GENE 101
TTG1	TRANSPARENT TESTA GLABRA 1
UAP56A	HOMOLOG OF HUMAN U2AF65-ASSOCIATED PROTEIN
UBP1	OLIGOURIDYLATE BINDING PROTEIN 1
UBP12	UBIQUITIN-SPECIFIC PROTEASE 12
<i>UBQ10</i>	<i>UBIQUITIN 10</i> gene promoter
V-ATPases	vacuolar H <sup>+</sup> ATP-ases
VCS	VARICOSE
VPS	Vacuolar protein sorting
VSR	VACUOLAR SORTING RECEPTOR
Vta1	Vacuolar protein sorting-associated protein 1
w/o	without
XRN	EXORIBONUCLEASE
Y2H	Yeast two Hybrid
YFP	yellow fluorescent protein

## Abstract

Endosomes are key sorting compartments in the endomembrane system, including the sorting of transmembrane proteins for degradation. This is achieved by a endocytic event in which the cargo-enriched endosomal membrane buds away from the cytosol and releases an intraluminal vesicle (ILV) into the endosomal lumen. Endosomes that contain ILVs are called multivesicular bodies (MVBs) and ILVs together with their cargo are finally degraded by the fusion of MVBs with the vacuole.

ILV formation is executed by evolutionary conserved multi-protein complexes that are called the Endosomal Sorting Complex Required for Transport (ESCRT) system. The late steps of ILV formation are regulated by the ESCRTIII core and associated complex, in which the AAA-ATPase SUPPRESSOR OF K(+) TRANSPORT GROWTH DEFECT 1 (SKD1) is the key enzyme. Recent studies in *Arabidopsis thaliana* showed that SPIRRIG, a stimulator of SKD1 function in MVB formation, has also a function in the stress-dependent formation of Processing bodies (P-bodies). P-bodies, together with stress granules, are two classes of mRNA-ribonucleoprotein (mRNP) granules that sequester mRNAs during stress-induced polysome disassembly.

To see, if other late acting ESCRTIII proteins are associated with mRNP granules, an exhaustive colocalization study was performed. This study showed that SKD1 changes its subcellular localization after heat stress to mRNP granules, independent of MVBs. Other ESCRTIII associated proteins, but none of the tested ESCRTIII core proteins, colocalized to mRNP granule markers. The sequestration of SKD1 and some of its cofactors in mRNP granules led to the hypothesis, that ESCRT trafficking might be temporarily blocked during heat stress. First evidence supporting this hypothesis was gained by the study of the subcellular localization of PIN-FORMED 2, which is transported by ESCRT, after heat stress. In a broader approach, the interactome of SKD1 was analyzed. Several proteins known to associate with mRNP granules were identified, such as members of the chaperonin-containing T-complex or the P-body protein VARICOSE. In addition, new potential interactions with other membrane trafficking proteins, such as members of the homotypic fusion and vacuole protein sorting (HOPS)/class C core vacuole/endosome tethering (CORVET) complex, were identified. A subcellular localization analysis confirmed the association of some candidates with mRNP granules after heat stress and indicated that proteins of other membrane trafficking routes might also be recruited to mRNP granules by heat stress.

## Zusammenfassung

Eine zentrale Funktion von Endosomen ist das Sortieren von Proteinen für den Transport innerhalb des Endomembransystems. Dies beinhaltet das Sortieren von Transmembranproteinen für den Abbau in der Vakuole. Ein kompletter Abbau wird ermöglicht, indem durch eine vom Zytosol abgewandte Abschnürung der endosomalen Membran, in der die Transmembranproteine angereichert sind, ein intraluminäres Vesikel (ILV) geformt wird. Endosomen, die ILVs enthalten, werden als „multivesicular bodies“ (MVBs) bezeichnet. ILVs und die sich darin befindenden Transmembranproteine werden schließlich komplett abgebaut durch die Fusion des MVBs mit der Vakuole.

Die Bildung von ILVs wird durch mehrere evolutiv konservierte Multiprotein-Komplexe reguliert, welche zusammen als das „Endosomal Sorting Complex Required for Transport“ (ESCRT) System bezeichnet werden. Die letzten Schritte der ILV Bildung werden durch den ESCRTIII Kern und assoziierten Komplex reguliert. In diesem Prozess ist die AAA-ATPase „SUPPRESSOR OF K(+) TRANSPORT GROWTH DEFECT 1“ (SKD1) das zentrale Enzym. Neue Studien in *Arabidopsis thaliana* zeigten, dass SPIRRIG, ein Regulator von SKD1, auch eine Funktion in der stressabhängigen Formation von sogenannten „processing bodies“ (P-bodies) hat. P-bodies sowie „stress granules“ repräsentieren zwei Klassen von mRNA-Ribonukleoproteinaggregaten, die als „mRNP granules“ bezeichnet werden und Transkripte nach dem stressinduzierten Zerfall von Polysomen in sich konzentrieren.

Um zu untersuchen, ob auch andere spät agierende ESCRTIII Proteine in Assoziation mit mRNP granules sind, wurde eine umfassende Kollokalisationsstudie durchgeführt. In dieser Studie wurde gezeigt, dass SKD1 seine subzelluläre Lokalisation nach Hitzestress ändert und mit mRNP granules kollokalisiert. Diese Umlagerung der Lokalisation ist unabhängig von MVBs. Die beobachtete Konzentrierung von SKD1 und einiger seiner Kofaktoren in mRNP granules führte zu der Hypothese, dass ESCRT-abhängige Transportprozesse möglicherweise während akutem Hitzestress blockiert werden. Durch die Analyse der subzellulären Lokalisation des durch ESCRT transportierten Proteins „PIN-FORMED 2“ nach Hitzestress wurden erste Ergebnisse gesammelt, die in diese Richtung deuten. In einem weiteren, allgemeineren Experiment wurde das Interaktom von SKD1 untersucht. Hierbei wurden einige Proteine identifiziert, von denen bekannt ist, dass sie eine Funktion in mRNP granules haben, wie zum Beispiel Proteine des „chaperon-containing T-complex“ oder das P-body Protein „VARICOSE“. Zusätzlich wurden neue potentielle Proteininteraktionen zwischen SKD1 und

anderen Membrantransportproteinen identifiziert, wie beispielsweise mit Komponenten des „homotypic fusion and vacuole protein sorting (HOPS)/class C core vacuole/endosome tethering (CORVET)“ Komplexes. Die subzelluläre Lokalisationsanalyse einiger Interaktomkandidaten bestätigte deren Assoziation mit mRNP granules nach Hitzestress und deutete darauf hin, dass auch Proteine aus anderen Membrantransportprozessen durch Hitzestress in mRNP granules gelangen.

# 1 Introduction

## 1.1 Membrane trafficking in *A. thaliana*

A hallmark of all eukaryotic cells is the presence of a sophisticated membrane system that tightly regulates cellular uptake and transport of macromolecules and proteins, biosynthetic and degradation processes, as well as signaling cascades. This system is called the endomembrane system and consists of several membrane-enclosed organelles which constantly exchange content either via vesicle trafficking, direct interactions or maturation processes. The endomembrane system includes the nuclear envelope, the endoplasmic reticulum (ER), the Golgi apparatus, the trans-Golgi network (TGN), the plasma membrane (PM), endosomes and lysosomes or vacuoles in fungi and plants. The exchange of lipids, proteins or macromolecules between the compartments is called protein or membrane trafficking.

Membrane trafficking routes between the different compartments can be classified according to the directionality of cargo transport. For example, transport from the PM over endosomes to the TGN, from the Golgi to the ER, or from late endosomes to the TGN is classified as retrograde or endocytic transport. Trafficking from the ER to the Golgi network and subsequently to the PM is called anterograde or secretory transport. Another mode of anterograde protein trafficking is transport of enzymes to the lytic compartment, which is often called vacuolar protein sorting in plants. Cargo vesicles are generated by membrane deformation which is mediated by different coat proteins. With the help of adaptor complexes, vesicle coat subunits polymerize at the donor membrane and thereby introduce necessary membrane curvature for vesicle budding (Lee and Hwang et al., 2014).

Nearly all trafficking routes lead over endosomes. This circumstance makes endosomes the primary sorting compartment of eukaryotes. Endosomes, which fuse with endocytic vesicles, are called early endosomes (EEs) in yeast and animals and exhibit a tubular shape. From there, internalized cargo, such as activated receptors or ion channels, can either be directed to the TGN, to lysosomes/vacuoles for degradation via late endosomes (LEs, also called multivesicular bodies/MVBs) or back to the PM via recycling endosomes (REs). The different classes of endosomes are categorized based on different attributes such as lipid composition, accessory proteins, luminal acidification and morphology. Cargo transport between the different endosomal classes mainly occurs via maturation of the endosomal structure (Huotari and Helenius, 2011). This is initiated by the subsequent exchange of associated Rab (Ras-

related in brain) GTPases. For example, the outer membrane of EEs is enriched with the Rab GTPase Rab5, which regulates vesicle to EE fusion (Gorvel et al., 1991). Subsequently, Rab5 is exchanged for Rab7 which initiates the recruitment of additional MVB-specific accessory proteins (Méresse et al., 1995, Rink et al., 2005). Another Rab-regulated step of endosome maturation is the recruitment of specific fusion machineries which allow homo- and heterotypic membrane fusions between endosomes (Nickerson et al., 2009).

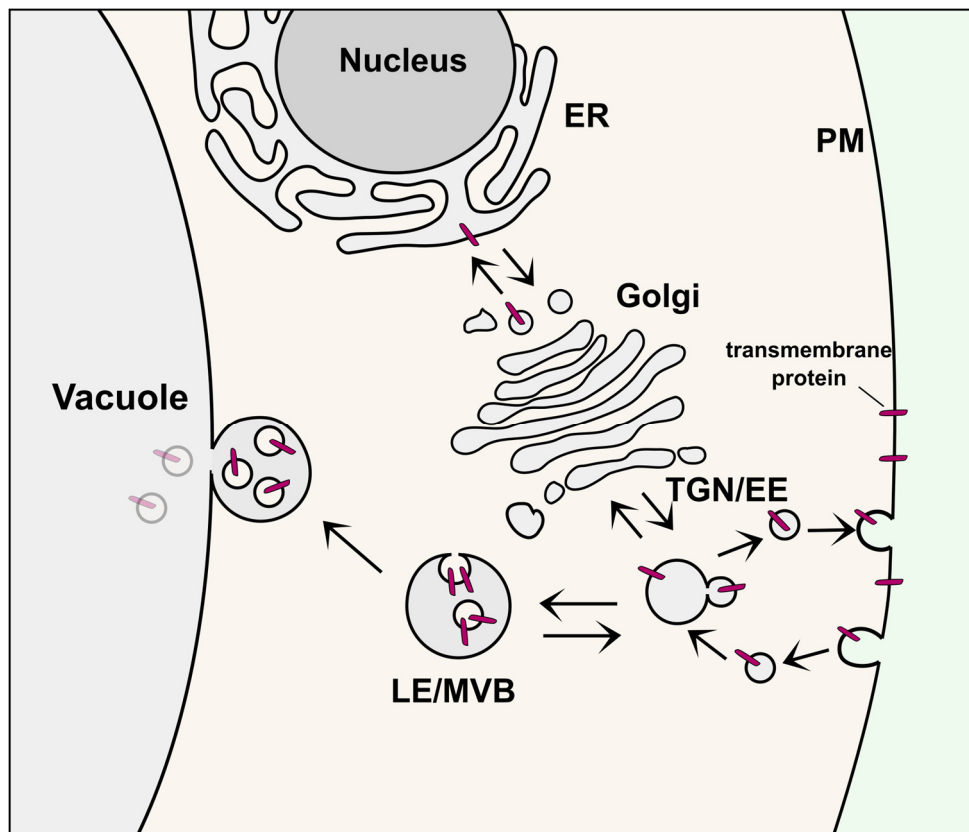


**Figure 1.1. Membrane trafficking in the endomembrane system of *A. thaliana*.** This scheme represents the main trafficking routes of transmembrane proteins in the endomembrane system. After synthesis and membrane integration in the ER, transmembrane proteins are transported via vesicles to the Golgi. From there, they enter the TGN either via cisternal maturation or vesicle transport. The TGN also functions as EE and RE in plants. At the TGN/EE, vesicles are formed that carry the transmembrane proteins and release them into the PM by fusion. The protein trafficking from the ER to the PM is called anterograde or secretory transport. Transmembrane proteins can also be removed from the cell surface via endocytosis and vesicle fusion with the TGN/EE. This direction of transport is called retrograde transport. If transmembrane proteins are determined to be degraded (e.g. via ubiquitination), they remain in the membrane of a TGN/EE, which matures into an LE/MVB. In a second invagination event, which is executed by the ESCRT system, the transmembrane proteins are internalized into an ILV. The final fusion of the LE/MVB releases ILVs into the lumen of the vacuole, where they are completely degraded.

The morphology of endosomes correlates with the function they exert. A morphological hallmark of MVBs is the presence of intraluminal vesicles (ILVs). ILVs are an architectural necessity for the complete degradation of transmembrane proteins by fusion with lysosomes/vacuoles. They are formed by invagination and fission of the MVBs' outer membrane, away from the cytosol (Huotari and Helenius, 2011). This process is regulated by highly ordered multi-protein complexes which functions together as the Endosomal Complex Required for Transport (ESCRT) system, which will be explained in detail in Chapter 1.2 and 1.3.

The general membrane transport processes and the regulating proteins are conserved between yeast, animal and plant cells. However, plant endosomes exhibit some differences compared to their mammalian or yeast counterparts (Contento and Bassham, 2012). Plants do not contain endosomal structures reminiscent of the tubular EEs and REs. Instead, the TGN provides the first contact site for endocytosed content and also sorts cargo back to the PM. Therefore, the plant TGN is often called TGN/EE (Bolte et al., 2004; Viotti et al., 2011, Figure 1.1).

The importance of membrane trafficking in plant development is demonstrated by the protein sorting of the PIN (PIN-FORMED) auxin efflux channels. PIN proteins regulate the directed efflux of auxin out of cells, thereby building up spatial auxin minima and maxima which are crucial for embryogenesis, cell polarity and gravitropism (Grunewald and Friml, 2010). Mutants of the PIN1 protein reveal severe developmental defects (e.g. lack of stem organs) while *pin2* roots show no gravitropism (Gälweiler et al., 1998; Chen et al., 1998; Luschnig et al., 1998; Müller et al., 1998). The directionality of auxin efflux mediated by PIN proteins depends on their polar distribution at the PM. For example, PIN1 localizes to the basal PM (towards the shoot) in root vascular tissue while PIN2 accumulates at the apical site of root epidermal cells (Gälweiler et al., 1998; Müller et al., 1998). PIN1 and 2 undergo constant endocytic recycling from the PM to the TGN and are partially degraded in the vacuole via MVB trafficking. This was shown by experiments with Brefeldin A (BFA), a fungal toxin and inhibitor of ARF-GEFs (ADP-RIBOSYLATION FACTOR GUANINE-EXCHANGE FACTORS, general regulators of vesicle coat formation), and by staining with the styryl dye FM4-64, which is internalized via endocytosis and subsequently stains all membranous compartments (Geldner et al., 2001; Bolte et al., 2004; Paciorek et al., 2005; Kleine-Vehn et al., 2006; Dhonukshe et al., 2007; Spitzer et al., 2009).

### 1.2 Vacuolar protein sorting by the ESCRT system

Plant vacuoles are multifunctional organelles. Not only do they provide a storage or degradation compartment for the cell, but also generate, together with the cell wall, the necessary turgor for cell growth and cell rigidity. In vegetative tissues, such as leaves, mature cells contain a central lytic vacuole which takes up nearly all of the cells volume. Therefore, the maintenance of the vacuole's volume and metabolic activity is of utmost importance for plants. This is achieved by constant vacuolar trafficking of proteins and membranes via endosomal structures (Xiang et al., 2013). Vacuolar enzymes, such as proteases and hydrolases, are transported from the TGN to the plant vacuole by binding to VSRs (VACUOLAR SORTING RECEPTORS), which are integrated in the outer membrane of MVBs. The fusion of the MVB outer membrane with the tonoplast releases the enzymes in the vacuolar lumen. V-ATPases (Vacuolar ATPases), which acidify the lytic vacuole, are transported in a similar way (Contento and Bassham, 2012). The fusion of MVBs with the tonoplast also releases ILVs in the vacuolar lumen, where they are completely degraded. The majority of PM transmembrane proteins, such as PINs, are degraded via ILVs. The cargo sorting, membrane invagination and the final release into the MVB lumen is regulated by the ESCRT system.

The ESCRT system was first characterized in the context of vacuolar protein sorting (VPS) in yeast and ongoing research showed that the majority of ESCRT proteins are conserved among eukaryotic species. In addition, more and more cellular processes, which involve membrane invagination and abscission events away from the cytosol, are found to depend on the ESCRT machinery (e.g. enveloped virus budding, exosomes, cytokinetic abscission, nuclear envelope reassembly, and autophagosomes, Gao et al., 2017). The identification of the ESCRT system in yeast was achieved by classical mutant screens, which focused on aberrant endosomal morphologies. A subset of the mutants (17 genes) exhibited a distinctive phenotype of enlarged and malformed MVBs which were termed class E compartments (Rieder et al., 1996; Conibear and Stevens, 1998). The careful and systematic analysis of vacuolar cargo transport (e.g. soluble Cpy/Carboxypeptidase Y) in these mutants revealed the different steps of MVB cargo sorting and led to the description of the ESCRT system.

The ESCRT system can be divided in 5 multi-protein complexes based on their function: ESCRT0, ESCRTI, ESCRTII, ESCRTIII core, and ESCRTIII associated. The early functioning ESCRT complexes are involved in cargo recognition via ubiquitin and sequestration (ESCRT0 to II) while the late acting ESCRT complexes regulate membrane invagination and fission (ESCRTIII and associated). The proteins of the complexes are present in the cytosol and are

subsequently recruited to the endosomal membrane in a hierarchal manner (Gao et al., 2017, Figure 1.2).

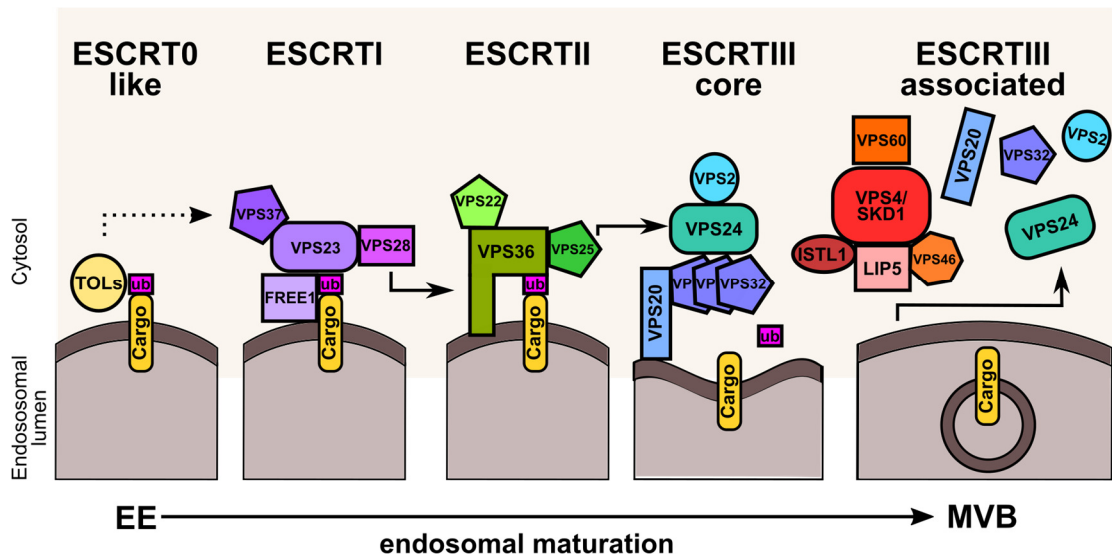


**Figure 1.2. The ESCRT system in *A. thaliana*.** The complete degradation of ubiquitinated transmembrane proteins is achieved by their internalization into ILVs. ILV formation is a part of the maturation of EEs to MVBs and is executed by the ESCRT system. The ESCRT system is divided into 5 multi-protein complexes, which regulate the different steps of cargo recognition and enrichment (ESCRT0 to ESCRTII), as well as invagination and fission (ESCRTIII core and associated) in a hierarchal manner. No plant homologs of the ESCRT0 proteins have been identified. TOL proteins are thought to recognize ubiquitinated cargo (e.g. transmembrane proteins) and to subsequently recruit the pre-assembled ESCRTI complex to the endosomal membrane. ESCRTI consist of VPS23, VPS37, VPS28 and the plant-specific FREE1, which directly binds to membranes via its FYVE domain. VPS28 recruits the preassembled ESCRTII (VPS36, VPS22, and VPS25) complex via interaction with VPS36, which also directly binds to ubiquitinated cargo. The ESCRTIII core complex (VPS20, VPS32, VPS24, and VPS2) is not pre-assembled in the cytosol and subunits are subsequently recruited. During invagination, the in the membrane enriched cargo is deubiquitinated by additional factors. ILV formation is finalized by recruitment of the ESCRTIII associated complex (VPS4/SKD1, LIP5, VPS60, VPS46, and ISTL1), which removes the oligomerized ESCRTIII core subunits from the membrane. For *A. thaliana* VPS60, no direct function in ESCRT trafficking has been shown yet, but is expected based on homology. Model and graphical representation based on Gao et al., 2017.

In yeast and animals, the ESCRT0 complex consists of 2 subunits, the Vps27/HRS (HEPATOCYTE GROWTH FACTOR-REGULATED TYROSINE KINASE SUBSTRATE) protein and the Hse1/STAM1/2 (Hbp STAM EAST1, SIGNAL TRANSDUCING ADAPTOR MOLECULE 1 AND 2) protein (Bilodeau et al., 2002). Both proteins bind directly to membranes and also contain an ubiquitin-binding motif that allows the recognition of K63 polyubiquitinated cargo (Ren and Hurley, 2010; Lange et al., 2012). Homologs of the ESCRT0 complex have not been identified in plants and in the majority of other eukaryotic lineages. The

*A. thaliana* genome encodes several TOL (TARGET OF MYB1-LIKE) proteins which contain a similar membrane-binding domain as ESCRT0, bind ubiquitin and have been shown to regulate the vacuolar trafficking of PIN2 (Blanc et al., 2009; Korbei et al., 2013).

After cargo recognition and sequestration, ESCRT0 recruits the pre-assembled ESCRTI complex from the cytosol (Bache et al., 2003; Katzmann et al., 2003; Lu et al., 2003). Yeast and animal ESCRTI consists of 4 proteins: Vps23/TSG101 (TUMOR SUSCEPTIBILITY GENE 101), Vps28, Vps37 and Mvb12p (Multivesicular Body 12, Katzmann et al., 2001; Garrus et al., 2001; Kostelansky et al., 2007). Ubiquitin and ESCRT0 recognition is mediated via Vps23/TSG101 (Bilodeau et al., 2003; Katzmann et al., 2003). The recruitment of the ESCRTII complex is mediated by a C-terminal helical bundle structure (Pineda-Molina et al., 2006).

No Mvb12-like protein has been identified in *A. thaliana* but two protein versions of Vps23 (ELCH/VPS23.1 and VPS23.2), Vps28 (VPS28.1 and VPS28.2) and Vps37 (VPS37.1 and VPS37.2) are present (Leung et al., 2008). Mutants of the *A. thaliana* ELCH protein show defects in cytokinesis and trichome development (Spitzer et al., 2006). Single mutants of *vps37-1* and *vps28-2* show no growth phenotype under normal conditions but are compromised in the endosomal uptake and degradation of the FLS2 (FLAGELLIN SENSING 2) receptor which mediates plant immune responses (Spallek et al., 2013). Several studies showed that the *A. thaliana* ESCRTI complex contains an additional, plant specific component which is called FREE1 (Fab-1, YGL023, Vps27, and EEA1/FYVE, FYVE DOMAIN PROTEIN REQUIRED FOR ENDOSOMAL SORTING). FREE1 binds PI(3)P (Phosphatidylinositol 3-phosphate) via its conserved FYVE domain and ubiquitin with a C-terminal domain. Loss of FREE1 function leads to seedling death, which coincides with the presence of aberrant endosomal structures (Gao et al., 2014, Kolb et al., 2015).

The ESCRTII complex provides the link between the early acting and the late acting ESCRT complexes. It consists of Vps22/EAP30 (ELL ASSOCIATED PROTEIN 30), Vps36/EAP45 and two Vps25/EAP20 proteins which together form a Y-shaped structure (Schmidt et al., 1999; Kamura et al., 2001; Babst et al., 2002a; Teo et al., 2004; Wernimont and Weissenhorn, 2004). Vps36 mediates PI(3)P and ubiquitin binding and is the contact site for the ESCRTI protein Vps28. (Slagsvold et al., 2005; Teo et al., 2006; Gill et al., 2007). Recruitment of the ESCRTIII complex is mediated by association of the two Vps25 proteins with Vps20 (Teo et al., 2004). In contrast to the other ESCRT proteins, only one homolog of each ESCRTII protein exists in *A. thaliana*. VPS25 and VPS22 have not been functionally characterized yet, but a recent study

from Wang and colleagues showed that they form, together with VPS36, a putative ESCRTII complex in plants (Wang et al., 2017). Furthermore, this study showed that the ubiquitin binding activity of VPS36 is conserved in plants and that it regulates MVB biogenesis and protein trafficking to the vacuole.

### **1.3 The ESCRTIII core and associated protein complex**

The ESCRTIII complex and its associated proteins only assemble into functional complexes when they associate with the endosomal membrane. This dynamic polymerization distinguishes the ESCRTIII subunits from the ones of ESCRTI and II, which are already assembled in stable heteropolymers in the cytosol. The ESCRTIII complex consists of four core subunits and three related subunits in yeast. It finalizes, together with the ATPase Vps4/SKD1 (SUPPRESSOR OF K(+) TRANSPORT GROWTH DEFECT 1) and its regulator Vta1/LIP5 (Vacuolar protein sorting-associated protein 1, LYST INTERACTING PROTEIN 5), the invagination and fission of ILVs (Hurley and Hanson, 2010). Since the ESCRTIII related proteins regulate Vps4/SKD1 activity and are not essential for the first steps of membrane invagination and fission, they are referred to as the ESCRTIII associated complex in this study.

Babst and colleagues were the first to study the recruitment of the four ESCRTIII core proteins in yeast: Vps20, Snf7 (Sucrose Non Fermenting 7)/Vps32, Vps24 and Vps2/ Did4 (DOA4-independent degradation protein 4, Babst et al. 1998 and 2002b). They showed by co-immunoprecipitations that the ESCRTIII components preferably interact with each other at membranes. Vps20 and Snf7 are required for membrane association of the ESCRTIII complex while Vps24 and Vps2 are necessary for Vps4 recruitment. Vps20 nucleates the oligomerization of Snf7 in a filamentous spiral structure, which forms a curved dome and is the driving force of membrane invagination (Lin et al., 2005; Hanson et al., 2008; Shen et al., 2014; McCullough et al, 2015). The oligomerization of Snf7 is terminated by Vps24-dependent recruitment of Vps2, which in turn initiates the disassembly of the ESCRTIII complex via Vps4 recruitment (Teis et al., 2008). The human ESCRTIII core homologues are called CHMP (CHARGED MULTIVESICULAR BODY PROTEIN) and their structural characterization, together with the yeast proteins, revealed the physical attributes that allow ESCRTIII to assemble and polymerize specifically on membranes (Howard et al., 2001; von Schwedler et al., 2003).

The ESCRTIII proteins are similar in size and share a specific architecture. The N-terminus is enriched in basic amino acids while the C-terminus is acidic (Muzioł et al., 2006). They do not contain known membrane binding domains (e.g. PH or FYVE) and only Vps20 is myristoylated and binds directly to the ESCRTII complex (Babst et al., 2002b; Bowers et al., 2004).

Membrane binding is mediated by the basic N-terminal part of the ESCRTIII proteins and is based on electrostatic interactions (Lin et al., 2005). In addition, a small N-terminal membrane insertion motif was identified, which contributes to membrane association (Buchkovic et al., 2013). The membrane-interacting, basic N-terminus forms a flexible helical hairpin structure, which is built up by four  $\alpha$ -helices (Muziol et al., 2006; Shen et al., 2014). The acidic C-terminal region also contains an  $\alpha$ -helix and one or two MIM (Microtubule Interacting and Transport, MIT Interacting Motif) domains which mediate the interaction with the MIT domain of Vps4/SKD1 and Vta1/LIP5 (Scott et al., 2005; Obita et al., 2007; Stuchell-Brereton et al., 2007; Skalicky et al., 2012). The C-terminal region has an autoinhibitory effect on ESCRTIII membrane binding and oligomerization since its competing for interaction with the N-terminal hairpin (Muziol et al., 2006; Zamborlini et al., 2006; Shim et al., 2007). All ESCRTIII proteins, with the exception of Vps20, are present in the cytosol in a “closed”, monomeric state in which the C-terminus is folded against the N-terminal hairpin. Membrane association and interaction with the other ESCRTIII core subunits releases the C-terminal helix and allows oligomerization. This conformational shift is initiated by Vps20, which was shown to maintain an open conformation in the cytosol (Henne et al., 2012; Schuh et al., 2015).

The three ESCRTIII associated proteins Did2/Vps46/CHMP1, Vps60/CHMP1 and Ist1 share the coiled-coil structure of the ESCRTIII core components. They are not primarily involved in membrane invagination but recruit and regulate the activity of the Vps4/SKD1 ATPase (Amerik et al., 2000; Kranz et al., 2001; Babst et al., 2002b; Nickerson et al., 2006; Dimaano et al., 2007). Yeast studies revealed that the weak class E phenotype of  $\Delta$ *ist1*,  $\Delta$ *did2* and  $\Delta$ *vps60* mutants is only partially synergistic (Rue et al., 2008). This indicated that the three ESCRTIII associated proteins modulate Vps4/SKD1-activity differently.

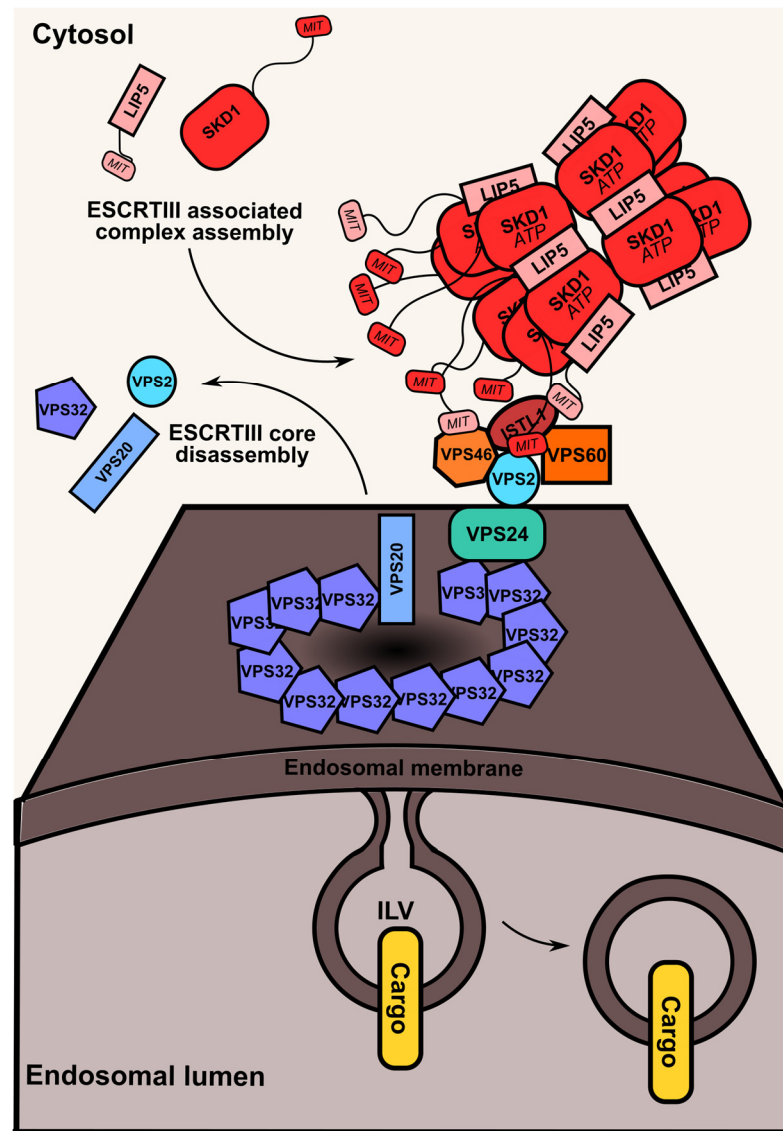


**Figure 1.3. Removal of the ESCRTIII core complex by the ESCRTIII associated complex.** The ESCRTIII core complex introduces membrane curvature for ILV formation by oligomerization. ESCRTIII core and associated proteins are not pre-assembled in the cytosol, but form oligomers when in contact with the endosomal membrane and with each other. VPS20 nucleates the oligomerization of VPS32, which form filamentous and restricting spirals. Oligomerization is finalized by VPS24-dependent VPS2 recruitment, which finally recruits the ESCRTIII associated complex. The AAA-ATPase SKD1 forms an active barrel structure together with its cofactor LIP5 when bound to ATP and when in physical contact with other ESCRTIII proteins. The MIT domains of SKD1 and LIP5 interact with the MIM domains of the ESCRTIII core proteins. Hydrolysis-driven conformational changes of SKD1 remove the core proteins from the endosomal membrane. The ESCRTIII core subunits are released in the cytosol in a closed conformation that inhibits oligomerization. The other ESCRTIII associated proteins ISTL1, VPS46, and VPS60 are thought to stimulate SKD1 oligomerization and thereby its' ATPase function. The removal of ESCRTIII core proteins from the endosomal membrane is a prerequisite for the final scission of the ILV and its release into the endosomal lumen. Model and graphical representation based on Schmidt and Teis, 2012.

Vps4/SKD1 and its cofactor Vta1/Lip5 do not share the classical ESCRTIII protein structure. Vps4/SKD1 is an ATPase of the AAA (ATPases Associated with diverse cellular Activities) class I. It contains one central ATPase cassette which is built up by one large, highly conserved AAA-ATPase domain and a smaller, less conserved AAA-ATPase domain (Scott et al., 2005b; Azmi et al., 2006; Vajjhala et al., 2006; Xiao et al., 2007). Endosomal recruitment and the majority of protein interactions occur via an N-terminal MIT-domain, which is connected to the ATPase cassette by a long, flexible linker (Babst et al., 1998; Lottridge et al., 2006; Stuchell-Brereton et al., 2007; Obita et al., 2007). When inactive (ADP bound or absence of nucleotides), Vps4/SKD1 is present in the cytosol as a monomer or homodimer. Recruitment to the endosomal membrane by ESCRTIII core and associated proteins as well as ATP binding initiate the oligomerization of Vps4 in a barrel shaped, double ring structure consisting of 12 or 14 subunits (Hartmann et al., 2008; Landsberg et al., 2009). The activated Vps4/SKD1-oligomer disassembles the ESCRTIII complex by sequential interactions via its MIT-domain. Conformational changes, which are driven by ATP hydrolysis, detach the proteins from each other and from the membrane, and release them in their “closed”, monomeric conformation into the cytosol (Scott et al., 2005a, Figure 1.3). The disassembly of the ESCRTIII complex by Vps4/SKD1 is essential for the final step of membrane fission in the process of ILV formation. When Vps4/SKD1 function is diminished, abnormally large MVBs with incomplete ILVs are formed, vacuolar or lysosomal transport is blocked and the upstream ESCRT proteins accumulate at MVBs (Finken-Eigen et al., 1997; Babst et al., 1998; Fujita et al., 2003). If Vps4/SKD1 actively participates in membrane fission or simply guarantees, that enough ESCRTIII subunits are present in the cytosol for multiple rounds of ILV formation, is part of the current discussion (Alonso Y Adell and Teis, 2011).

The cofactor Vta1/LIP5 co-assembles in the Vps4/SKD1 barrel structure and enhances its hydrolytic activity (Scott et al., 2005a; Azmi et al., 2006; Lottridge et al., 2006; Xiao et al., 2008; Azmi et al., 2008). Vta1/LIP5 contains two N-terminal MIT domains for ESCRTIII interaction and a C-terminal Vps4/SKD1-binding domain which are connected via a long, flexible linker. The co-assembly of Vta1/LIP5 subunits into the Vps4/SKD1 barrel increases the number of free MIT-domains that interact with the ESCRTIII proteins and thereby enhances substrate engagement. In parallel to the last steps of ESCRTIII-driven membrane invagination fission, the sequestered cargoes of the MVB pathway are deubiquitinated (Alonso Y Adell and Teis, 2011).

All 4 ESCRTIII core proteins are present in *A. thaliana* with two or three homologues (in this study referred to as VPS20.1/VPS20.2, VPS32.1/VPS32.2, VPS24.1/VPS24.2, and VPS2.1/VPS2.2/VPS2.3, Winter and Hauser, 2006). So far, only mutants of the VPS2.1 and VPS2.2 protein were isolated, which are embryonic lethal or have a root growth phenotype, respectively (Katsiarimpa et al., 2011; Ibl et al., 2012). Studies of yeast and human proteins showed that C-terminal modification of ESCRTIII components can have a dominant-negative effect on ESCRT disassembly and thereby on MVB maturation and cargo transport (Martin-Serrano et al., 2003; Strack et al., 2003; Zamborlini et al., 2006; Teis et al. 2008). This was confirmed for *A. thaliana* in transient expression assay with C-terminal deletion/ modification versions of the ESCRTIII proteins (Richardson et al., 2011; Katsiarimpa et al., 2011; Cai et al., 2014).

Similar to the ESCRTIII core proteins, all isoforms of the associated proteins are present with at least one homolog in *A. thaliana* (in this study referred to as VPS46.1/VPS46.2, VPS60.1/VPS60.2, and ISTL/ISTL1-like, Winter and Hauser, 2006; Leung et al., 2008; Buono et al., 2016). Interestingly, gene duplication and diversification led to the presence of 12 ISTL proteins from which only ISTL1 has been shown to synergistically function to LIP5 in ESCRT trafficking. Mutant *lip5* plants exhibit overall normal growth under non-stress conditions but are impaired in basal pathogen defenses responses, heat and salt stress responses as well as root gravitropism (Wang et al., 2014 and 2015, Buono et al., 2016). The double mutants of *istl1* and *lip5* are impaired in growth, fertility and show early senescence. Furthermore, MVBs of the double mutant contain fewer, but larger ILVs than the wild type or single mutants (Buono et al., 2016). Double mutants of the two Did2 homologs VPS46.1 and VPS46.2 also show a reduced number of ILVs which coincides with PIN mislocalization. The disruption of polar auxin transport causes severe embryo deformation and early seedling death (Spitzer et al., 2009). Although no mutants of the *A. thaliana* AAA-ATPase SKD1 were isolated so far, studies using dominant-negative versions confirmed its involvement in MVB formation. *In-vitro* assays confirmed its ATPase activity, which is also stimulated by the addition of LIP5 (Haas et al., 2007; Shahriari et al., 2010a). The transient or inducible expression of ATPase-dead versions of SKD1 causes the formation of aberrantly large MVBs with reduced ILV numbers and inhibits the transport of vacuolar cargo. Furthermore, the expression of mutated SKD1 under the control of the epidermal cell-specific promoter of *GL2* (*GLABRA 2*) revealed that the loss of SKD1 causes cell expansion phenotypes, vacuolar fragmentation and inhibits seed coat mucilage production (Shariaria et al., 2010a and b). Those severe phenotypes led to the assumption that SKD1 loss is lethal for *A. thaliana*.

A plant specific and late acting ESCRTIII associated protein was identified in a yeast two hybrid screen. PROS (POSITIVE REGULATOR OF SKD1, Reyes et al., 2014) contains an internal MIM domain, stimulates the ATPase activity of SKD1 *in vitro* and causes a cell expansion phenotype when silenced. With the *A. thaliana* SPI (SPIRRIG) proteins, another positive regulator of SKD1 function was recently identified in our group (Steffens et al., 2017). SPI is a member of the BEACH (Beige and Chediak Higashi) domain protein family, which is associated with and involved in membrane trafficking events (Cullinane et al., 2013). *A. thaliana spi* mutants have cell expansion phenotypes which includes twisted trichomes, short root hairs and reduced complexity of epidermal pavement cells (Saedler et al., 2009). In addition, the central vacuoles of root hairs are fragment, which points to a function of SPI in vacuolar trafficking. Protein interaction studies confirmed a direct interaction of SPI with SKD1 and LIP5. Furthermore, *spi* and *lip5* double mutants exhibit defects in cargo trafficking of the vacuolar proteases CPY and AALP (ALEURAIN-LIKE PROTEASE) as well as a seed coat mucilage phenotype reminiscent of the one in plants expressing ATPase-deficient SKD1 under the *GL2* promoter (Shahriari et al 2010b; Steffens et al., 2017).

Interestingly, a new cellular function of SPI was identified, which is thought to be unrelated to ESCRT-dependent trafficking. It was shown that the SPI protein is involved in the posttranscriptional regulation of salt-stress responsive mRNAs via the recruitment to and the formation of so-called Processing bodies (P-bodies, Steffens et al., 2015). P-bodies are a class of microscopically visible, membrane-less mRNA-ribonucleoprotein (mRNP) granules, which are involved in the selective degradation of transcripts, especially after the onset of cellular stress. Their function and composition, as well as the function of the related stress Granules (SGs) are explained in detail in the next chapter.

### **1.4 Composition and function of P-bodies and SGs**

After transcription and maturation, eukaryotic mRNAs in conjunction with mRNPs are shuttled out of the nucleus. At the nuclear pore, transcripts have to pass quality-control which determines whether they enter the cytosol for translation or if they are subjected to degradation. Once in the cytosol, the eukaryotic translation initiation complex binds the 5' cap structure (7-methylguanosine 5'-triphosphate, m7Gppp) of transcripts and initiates ribosome assembly. PABs (Poly(A) Binding Proteins) which bind the 3' poly(A) tail of transcripts, have been shown to interact with proteins of the translation initiation complex. This protein interaction across the length of the transcript leads to mRNA circulation which reduces ribosome disassociation and enhances protein synthesis (Gallie, 2014; Chantarachot and Bailey-Serres, 2018). The

complexes formed by translation initiation proteins, functional ribosomes and additional accessory proteins such as PABs are called polysomes and are the active sites of protein translation.

Cellular stresses such as starvation, hypoxia or heat stress trigger the phosphorylation of eIF2 $\alpha$  (eukaryotic translation Initiation Factor 2  $\alpha$ ), which causes polysome disassembly. From there, mRNAs are either transported in association with a stalled pre-initiation complex to SGs or are transported to another, closely related class of mRNP granules, the so-called P-bodies (also known as GW182-containing bodies, Anderson and Kedersha, 2008). Both classes of mRNP granules share some associated proteins and have been shown to exchange protein and mRNA content via docking and fusion events in mammals and yeast (Kedersha et al., 2005; Buchan et al., 2009, Figure 1.4). The formation of mRNP granules depends on the presence of polysome-released transcripts in the cytosol. This is demonstrated by the observation that treatment of cells with cycloheximide, a translation elongation inhibitor which “traps” transcripts in polysomes, prevents mRNP granule formation. Treatment with the early translation termination-inducing drug puromycin increases the number of mRNP granules (Anderson and Kedersha, 2008).

Though they are considered to be somewhat similar, P-bodies are distinguishable from SGs by the presence of DCPs (Decapping Proteins), which initiate 5' to 3' mRNA decay. Therefore, P-bodies are thought to primarily function in transcript degradation while SGs provide a transient cytosolic storage compartment for mRNAs (Buchan and Parker, 2009). However, transport into P-bodies does not always lead to mRNA degradation since transcripts can re-enter translation after stress removal (Bregues et al., 2005; Bhattacharyya et al., 2006; Aizer et al., 2014).

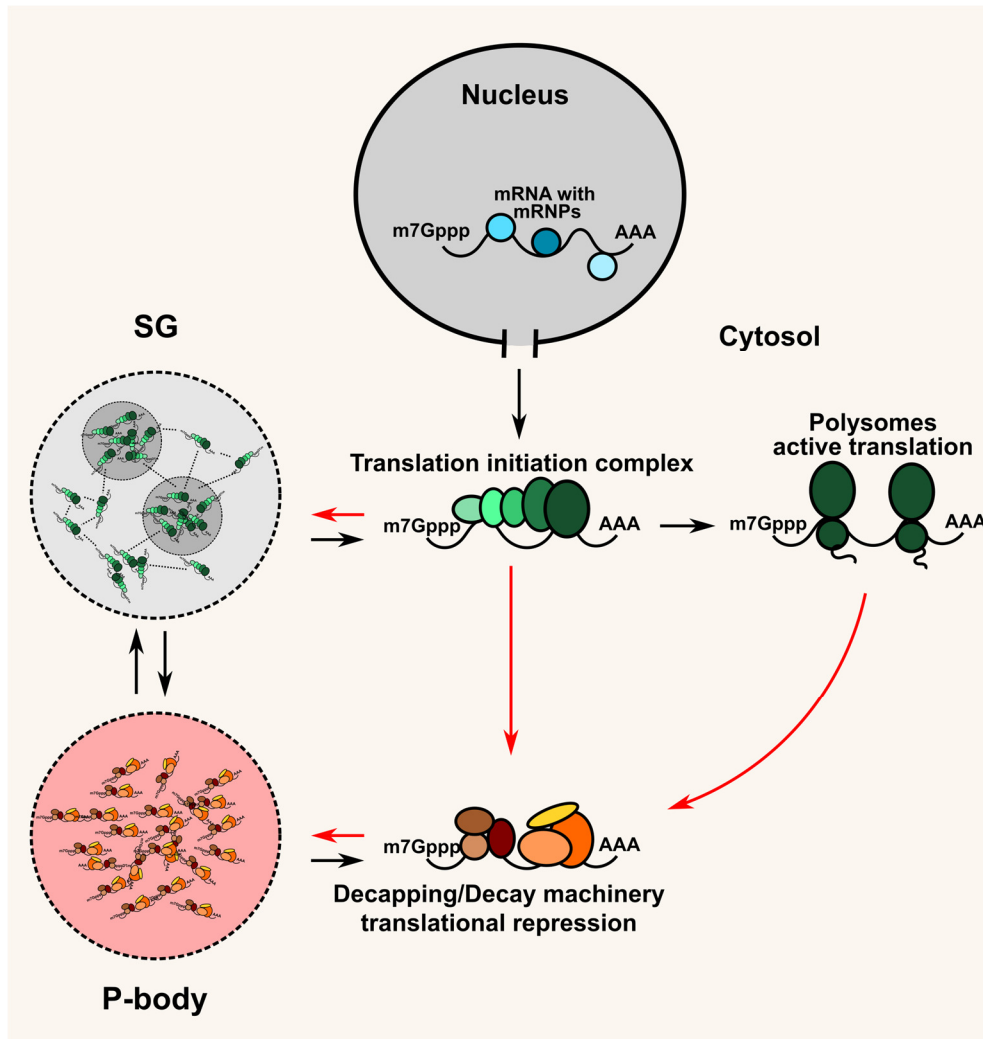


**Figure 1.4. Sequestration of mRNAs and proteins into mRNP granules during cellular stress.** Mature mRNAs (m7Gppp cap and poly(A) tail) are shuttled out of the nucleus in conjunction with different mRNPs (e.g. export factors, quality control components). In the cytosol, the translation initiation complex (eIF4E, eIF4G, eIF2, eIF3, and 40S ribosomal subunit, green proteins) assembles onto mRNAs. The additional recruitment of the 60S ribosomal subunits and enhancing factors such as PABs initiate protein translation in polysomes. Cellular stress (e.g. starvation, infection, heat stress, red arrow) induces the disassembly of polysomes and promotes the sequestration of mRNAs into P-bodies or SGs, which are two classes of mRNP granules. P-bodies, that contain proteins of the Decapping complex (e.g. Dcp1, Dcp2, Dhh1, red/brown proteins)/ Decay machinery (e.g. Xrn1, Pat1, Lsm1-7, orange/yellow proteins), are also present in the absence of stress, and are a place of mRNA degradation. SGs, that contain several proteins of the translation initiation complex and PABs, are specifically formed after stress, and are thought to function in transcript stabilization. SGs and P-bodies have been shown to exchange proteins and mRNAs, and are also found in physical contact with each other. The dynamic in- and efflux of proteins into mRNP granules has been described as a mode of liquid-liquid phase separation. This is thought to depend on weak IDR-driven interactions in SG shells (light grey), while more stable, globular domain driven interactions with proteins and mRNAs are predominant in SG cores (dark grey). After stress removal, mRNAs from both granules can re-enter translation and the granules disassemble. Alternatively, they are removed from the cell via autophagy. Model and graphical representation based on Protter and Parker, 2016.

As mentioned, the hallmark of P-bodies is the presence of DCPs. In mammals and yeast, the Dcp1/Dcp2 holoenzyme, with Dcp2 being the catalytic subunit, cleaves the 5'-cap of mRNAs (Beelman et al., 1996; Dunckley et al., 1999 and 2001; Lykke-Andersen, 2002; Steiger et al., 2003). Several decapping activators and mRNA decay components have been shown to be enriched in P-bodies such as the RNA helicase Dhh1(DEXD/H-box helicase 1), the deadenylated mRNA binding Lsm1-7 (Sm-like) -Pat1 (Protein Associated With Topoisomerase1)-complex, Edc3 (Enhancer of Decapping 3) as well as the 5' to 3' exoribonuclease Xrn1 which executes the final transcript decay (Hatfield et al., 1996; Bouveret et al., 2000; Tharun et al., 2000; Bonnerot et al., 2001; Sheth and Parker, 2003; Cougot et al., 2004; Fenger-Grøn et al., 2005). Decapping is preceded by the deadenylation of the 3' poly(A) tail via the Ccr4-Caf1-Not complex (Carbon201 Catabolite Repressor 4, Ccrf Associated Factor, Negative on Tata, Chen et al., 2002; Tucker et al., 2001; Parker and Song, 2004).

The transcript degradation machinery and its localization to P-bodies is conserved in plants (Chantarachot and Bailey-Serres, 2018). In *A. thaliana*, the DCP1 protein, together with VCS (VARICOSE)/EDC4, stimulate the enzymatic activity of DCP2 and forms the core decapping complex. Mutants of the three decapping complex proteins share similar phenotypes consisting of reduced cell expansion (dwarfism), disorganization of vascular tissues and epidermal cell growth defects, which are finally lethal after cotyledon emergence (Xu et al., 2006). With DCP5, an additional co-factor of mRNA decapping activity was identified. Although DCP5 does not directly stimulate DCP2 activity, it promotes mRNA degradation via interaction with DCP1 and VCS, accumulates in P-bodies and is necessary for targeted translational repression during seed germination (Xu and Chua, 2009). The final step of 5' to 3' mRNA decay is mediated by XRN4 in plants (Kastenmayer and Green, 2000). Although *xrn4* mutants do not share the drastic phenotypes of the other decapping components, the loss of XRN4 function effects the regulation of seed dormancy, heat stress responses as well as viral infection (Jaag and Nagy, 2009; Peng et al., 2011; Merret et al., 2013; Nguyen et al., 2015; Basbous-Serhal et al., 2017).

Yeast and mammalian SGs have been distinguished from P-bodies by the presence of the 40S small ribosomal subunit, proteins of the stalled translation initiation complex (tenary complex-deficient) such as eIF3, the eIF4F complex (eIF4E, eIF4A and eIF4G) and eIF4B as well as PABs such as PAB1 (Kedersha et al., 2005; Anderson and Kedersha, 2008). In contrast to the other translation initiation complex components, the 5'-cap binding eIF4E protein has also been found in yeast and mammalian P-bodies (Ferraiuolo et al., 2005; Kedersha et al., 2005). The

mammalian TIA1 (T-CELL RESTRICTED INTRACELLULAR ANTIGEN 1) and TIA1-R (TIA1-RELATED) proteins contain three N-terminal RRM (RNA Recognition Motifs), bind to poly(A)-tail of mRNAs and have been shown to function downstream of eIF2 $\alpha$  phosphorylation by mediating the enrichment of stalled translation initiation complexes in SGs (Tian et al., 1991; Kedersha et al., 1999). Under normal conditions, TIA1 and TIA1-R constantly shuttle between the cytosol and nucleus. Upon the onset of stress, they accumulate in the cytosol. Here, a prion-like domain enables self-aggregation that promotes SG assembly (Gilks et al., 2004). Although not always essential for SG formation, TIA1 and TIA1-R as well as their yeast counterparts have been shown to be of high importance for granule formation since overexpression of TIA1 alone can induce the formation of SGs in the absence of stress (Gilks et al., 2004; Protter and Parker, 2016). Another core SG protein, which initiates granule nucleation, is the endonuclease G3BP (Ras-GAP SH3 domain Binding Protein). G3BP contains a C-terminal RRM and an N-terminal NTF2-like (NUCLEAR TRANSPORT FACTOR 2) domain which mediates recruitment to SGs (Tourrière et al., 2003; Jain et al., 2016).

The analysis of *A. thaliana* SGs is still an emerging field in plant science, yet several studies investigated their composition and function (Chantarachot and Bailey-Serres, 2018). For example, the translation initiation factors eIF4E and eIF3B have been shown to localize in distinct cytosolic foci upon heat stress treatment (Weber et al., 2008; Suzuki et al., 2015). The UBP1 (OLIGOURIDYLATE BINDING PROTEIN 1) and the RBP45/47 (RNA-BINDING PROTEIN 45/47) family proteins are related to human TIA1 and share the overall domain structure of 3 RRMs and a prion-like domain (Lorkovic et al., 2000; Weber et al., 2008; Sorenson and Bailey-Serres, 2014). Similar to the TIA1 proteins, RBP47b has been shown to change its localization from a nuclear and cytoplasmic to a granular localization during heat, salt and hypoxia stress (Weber et al., 2008; Lokdarshi et al., 2016). Furthermore, it was shown that the prion-like domain of RBP47b is necessary for SG association, similar to the one of TIA1 (Gilks et al., 2004; Weber et al., 2008). Three *A. thaliana* UBP1 proteins have been characterized in the context of mRNP granules. The UBP1c protein was shown to reversibly localize in distinct cytosolic granules during hypoxia which contained poly(A)-mRNAs as well as the PAB2 protein and UBP1a. Seedling survival during hypoxia was reduced in *ubp1c* mutant plants and this loss in viability correlated with the selected sequestration of mRNAs (Sorenson and Bailey-Serres, 2014). The UBP1b protein was shown to aggregate into SGs upon heat stress treatment and mutant plants are salt-stress sensitive (Weber et al., 2008; McCue et al., 2012; Nguyen et al., 2016). Furthermore, overexpression lines of UBP1b are hypersensitive to heat stress while they exhibit an enhanced sensitivity to abscisic acid signaling. Both

phenotypes were linked to an enhanced stabilization of stress-relevant transcripts (Nguyen et al. 2016 and 2017). *A. thaliana* PAB proteins are also classified as closely related to the human TIA1 protein. PAB2 as well as PAB8 have been shown to localize in SGs during hypoxia or after heat stress treatment (Weber et al., 2008; Sorenson and Bailey-Serres, 2014; Bhasin and Hülskamp, 2017). A putative plant homolog of the NTF2-like RRM containing protein G3BP was also identified in *A. thaliana* (Krapp et al., 2017). The authors showed in transient expression assays that *A. thaliana* G3BP localizes to SGs in a heat stress-dependent manner.

In addition to classical RNA binding proteins, an increasing number of studies show that a variety of proteins with no known DNA or RNA binding activity are sequestered in SGs during cellular stress (Jain et al., 2016). One example in *A. thaliana* is the calcium sensor protein CML38 (CALMODULINLIKE 38) which localizes in SGs during hypoxia in a calcium-dependent manner. This change in localization correlates with a reduced tolerance of hypoxia in *cml38* mutant plants as well as the co-precipitation of known mRNP granule components in an interactome study (Lokdarshi et al., 2016). Another example is the AN (ANGUSTIFOLIA) protein (Bhasin and Hülskamp, 2017). It contains a CtBP (C-terminal Binding Protein) domain found in translational co-repressors that sense the redox state of the cell and a BAR (BFA-ADP RIBOSYLATED SUBSTRATE) domain known to function in membrane trafficking events (Colanzi et al., 2013). AN localizes in distinct cytoplasmic foci during salt and heat stress. Moreover, the association and interaction with SG proteins depends on the NAD(H) binding site within the CtBP domain. SG size was reduced and number was increased in *an* mutants and they were hyposensitive to changing salt and osmotic growth conditions. This led to the hypothesis that AN is a cellular redox sensor that modulates SG formation (Bhasin and Hülskamp, 2017). Previous studies showed that the AN protein also partially co-localizes to the TGN (Minamisawa et al., 2011). Thus, in addition to the previously mentioned SPI protein, AN provides another example for a protein that is involved in or associated with membrane trafficking events as well as mRNP granule formation.

A prominent example of a protein with no known RNA binding or modification activity that is integrated into SGs during cellular stress is TORC1 (TARGET OF RAPAMYCIN COMPLEX 1, Kedersha et al., 2013). TORC1 and TORC2 are two multiprotein complexes that together form the conserved TOR kinase, which regulates the metabolic state of eukaryotic cells. TORC1 is located at the lysosomal/vacuolar membrane under normal growth conditions where it is active and promotes biosynthetic processes. Amino acid deprivation, hypoxia as well as heat stress inhibit TOR signaling, leading to the halt of biosynthesis and the promotion of

catabolic processes (Efeyan et al., 2013). Studies in yeast and human cells revealed that the inhibition of TOR signaling during heat stress or arsenite induced hypoxia correlates with the sequestration of TOC1 in SGs (Takahara and Maeda, 2012; Wippich et al., 2013). The disassembly of SGs after stress removal correlated with the relocalization of TORC1 to lysosomal/vacuolar membranes and re-activation of TOR signaling.

Prion-like domains have been shown to be a driving force in the formation of mRNP granules (e.g. TIA1). They represent a subclass of Intrinsically Disordered Regions (IDRs), also known as Low Complexity (LC) regions. IDRs are amino acid stretches within a protein sequence that are not organized in secondary structures and are considered to be flexible linker regions between globular domains (Protter and Parker, 2016). IDRs are overrepresented in proteins known to be in mRNP granules. *In-vitro* studies using protein fragments of IDRs from mRNP granule components showed that they form dynamic aggregates with molecular diffusion rates reminiscent of liquid-liquid-phase separation, thus leading to the hypothesis that weak, but broad multivalent interactions of IDRs are the driving force of mRNP granule formation (Lin et al., 2015; Molliex et al., 2015). Proteomic analysis of mammalian and yeast SGs further showed that mRNP granules consist of a core and a shell structure whereby interactions between core components are thought to be mainly globular domain driven (e.g. RRM interaction with mRNAs) and specific while associated proteins of the shell structure rely on dynamic, but weak IDR interactions (Jain et al., 2016).

The same study showed that stability of SGs is ATP dependent and that specific ATP-dependent remodeling complexes such as the CCT complex (chaperonin-containing T complex) or the RNA helicase complex Rvb (RuvB-like) actively modulate assembly and disassembly of SGs. Furthermore, different chaperone proteins, such as Hsp70 (Heat shock protein 70) and Hsp40, have been found in mRNP granules and were shown to regulate the disassembly of SGs (Protter and Parker, 2016). The AAA-ATPase Cdc48 (Cell Division Cycle 48) was shown to remove ubiquitinated proteins from SGs, thereby contributing to their disassembly. This subsequent removal of proteins is discussed to prime SGs for clearance via autophagy, which provides an additional mode of mRNP granule clearance from the cytosol. (Buchan et al., 2013)

## 1.5 Aim of work

Previous studies in our group revealed a connection between ESCRT-dependent protein trafficking and mRNP granule formation in *A. thaliana*. It was shown that the SPI protein is involved in vacuolar transport by stimulating the activity of SKD1 in the process of MVB formation. An additional function of SPI was found in the regulation of salt stress responses by selective sequestration of mRNAs into P-bodies, thereby modulating transcript levels. An initial yeast two hybrid experiment indicated several potential protein interactions between P-body and ESCRTIII core and associated proteins, providing evidence for a general link between ESCRT-dependent trafficking and mRNP granules. To further investigate this potential, and so far unknown, link between the two cellular pathways, the repetition and extension of the yeast two hybrid study was carried out. The study was complemented by an exhaustive cellular localization and co-localization study of ESCRTIII core and ESCRTIII associated components with P-body and SG components after heat stress treatment, which is known to promote the formation of mRNP granules. The cellular localization of SKD1 was hereby of particular interest, since it executes the rate-limiting and essential step of ESCRTIII removal from MVBs. Another objective was the study of the effect of heat stress on ESCRT-dependent PIN2 trafficking and how it would correlate to potential protein relocalizations. Finally, with the help of an interactome approach, the general influence of heat stress on SKD1 protein interactions was tested.

## 2 Material and Methods

### 2.1 Plasmids

Table 2.1. General plasmids used in this study

Name	Attributes and use	Resistance in <i>E. coli</i>	Reference/Origin
<b>pDONR201</b>	Gateway cloning; Donor vector	Kanamycin	Invitrogen
<b>pDONR207</b>	Gateway cloning; Donor vector	Gentamycin	Invitrogen
<b>pENTRA-w/o-ccdB</b>	Gateway cloning; Generation of empty backbones as control; Donor vector	Kanamycin	Campeu et al., 2009
<b>pAS</b>	N-terminal fusion of GAL4-BD; Tryptophan biosynthesis gene; expression in yeast; Y2H	Ampicillin/Carbenicillin	Clontech
<b>pACT</b>	N-terminal fusion of GAL4-AD; Leucine biosynthesis gene; expression in yeast; Y2H	Ampicillin/Carbenicillin	Clontech
<b>pENSG-YFP</b>	N-terminal fusion of YFP; <i>35S CaMV</i> plant expression; Subcellular localization analysis	Ampicillin/Carbenicillin	Feys et al., 2005
<b>pEXSG-YFP</b>	C-terminal fusion of YFP; <i>35S CaMV</i> plant expression; Subcellular localization analysis	Ampicillin/Carbenicillin	Feys et al., 2005
<b>pEXSG-CFP</b>	C-terminal fusion of CFP; <i>35S CaMV</i> plant expression; Subcellular localization analysis	Ampicillin/Carbenicillin	Feys et al., 2005
<b>pPACIFIC</b>	C-terminal fusion of mTURQUOISE; <i>35S CaMV</i> plant expression; Subcellular localization analysis	Ampicillin/Carbenicillin	M. Jakoby
<b>pAMARENA</b>	N-terminal fusion of mCHERRY; <i>35S CaMV</i> plant expression; Subcellular localization analysis	Ampicillin/Carbenicillin	M. Jakoby GenBank ID: FR695428
<b>pAMARENA-UBQ10</b>	N-terminal fusion of mCHERRY; <i>UBQ10</i> plant expression; Subcellular localization analysis	Ampicillin/Carbenicillin	M. Jakoby
<b>pAUBERGINE</b>	C-terminal fusion of mCHERRY; <i>35S CaMV</i> plant expression; Subcellular localization analysis	Ampicillin/Carbenicillin	M. Jakoby, GenBank ID: FR695428
<b>pTREX-dest30-ProtA</b>	N-terminal fusion with protein-A; expression in HEK cells; LUMIER assay	Ampicillin/Carbenicillin	Blasche et al., 2013
<b>pTREX-dest-30-YFP</b>	N-terminal fusion with YFP; expression in HEK cells; LUMIER assay	Ampicillin/Carbenicillin	A. Steffens
<b>pcDNA3-RLuc</b>	N-terminal fusion with Renilla luciferase; expression in HEK cells; LUMIER assay	Ampicillin/Carbenicillin	Blasche et al., 2013

All vectors used in this study contain a Gateway cassette that allows the introduction of genes of interest via recombination. Table 2.1 summarizes the attributes of the general donor and destination vectors used in this study. The plasmid expressing SKD1 under its endogenous promoter (not listed, *ProSKD1::SKD1-YFP*) was generated by removal of the *35S Cauliflower mosaic virus (CaMV)* promoter (restriction digestion with *AscI/XhoI*) from the pEXSG-YFP plasmid and the ligation of a fragment which contained the upstream sequence of the *SKD1* gene (1.2 kb) upstream of the ATG, generated with J1439 *AscI-proVPS4* 5'-ggggcgcgcCTTGGTTAATTATCACCTAAAATAG-3' and J1440 *XhoI-proVPS4* 5'-ccctcgAGGGTTTTACAAGAGAAATTGAAATTC-3' primers, M. Jakoby, unpublished). The specific vectors, which were generated and used in this study, are listed in Table A.1.

## 2.2 Primers

Table 2.2 summarizes the primer sequences, which were used for the coding sequence (CDS) amplification of the interactome candidates and the addition of gateway sites (bolt sequences). Furthermore, the used sequencing primers are listed. All primers were purchased from Sigma-Aldrich/Merck.

**Table 2.2. Sequences of primers used in this study.**

Gene/Primer	ATG (isoform)	5' to 3' sequence
VPS18 fwd	AT1G12470.1	GGGGACAAGTTTGTACAAAAAAGCAGGCTTAATGGATCAAGGAA GGCAAGT
VPS18 rew	AT1G12470.1	GGGGACCACTTTGTACAAGAAAGCTGGGTATCMAACAGGCAAA GAAATGGTCCTCTG
VPS41 fwd	AT1G08190.1	GGGGACAAGTTTGTACAAAAAAGCAGGCTTAATGGCTGCGGTTCT CGCCTGAAAACGG
VPS41 rew	AT1G08190.1	GGGGACCACTTTGTACAAGAAAGCTGGGTATCMCCGAGCGGAC GCAGCGGCGGC
GRF2 fwd	AT1G78300.1	GGGGACAAGTTTGTACAAAAAAGCAGGCTTAATGGCGTCTGGGC GTGAAGAGTTCGT
GRF2 rew	AT1G78300.1	GGGGACCACTTTGTACAAGAAAGCTGGGTATCMCTGCTGTTCTCT CGGTCGGTTTTGG
SEC13A fwd	AT3G01340.1	GGGGACAAGTTTGTACAAAAAAGCAGGCTTAATGCCTCCTCAGA AGATTGAAACTGG
SEC13A rew	AT3G01340.1	GGGGACCACTTTGTACAAGAAAGCTGGGTATCMTGGCTCAACA ACAGTCACTTGTTCT
ISTL1 fwd	AT1G34220.1	GGGGACAAGTTTGTACAAAAAAGCAGGCTTAATGTCGATGCTCG ATTCCTTCTCAA
ISTL1 rew	AT1G34220.1	GGGGACCACTTTGTACAAGAAAGCTGGGTATCMCGAATCATGG GCGGGTCTTGATT
GRF9 fwd	AT2G42590.3	GGGGACAAGTTTGTACAAAAAAGCAGGCTTAATGGGTTCTGGAA AAGAGCGTGACAC
GRF9 rew	AT2G42590.3	GGGGACCACTTTGTACAAGAAAGCTGGGTATCMATTTGATTTAC CCCAGTAAAGGA
PIP1-1 fwd	AT3G61430.1	GGGGACAAGTTTGTACAAAAAAGCAGGCTTAATGGAAGGCAAG GAAGAAGACGTTAG
PIP1-1 rew	AT3G61430.1	GGGGACCACTTTGTACAAGAAAGCTGGGTATCMGCTTCTGGACT TGAAGGGGATGGC
VCL1/VPS16 fwd	AT2G38020.1	GGGGACAAGTTTGTACAAAAAAGCAGGCTTAATGGCAAACGTGT CTGTTGCTGCGGA

<b>Gene/Primer</b>	<b>ATG (isoform)</b>	<b>5' to 3' sequence</b>
<b>VCL1/VPS16 rew</b>	AT2G38020.1	<b>GGGGACCACTTTGTACAAGAAAGCTGGGTATCMGGAGGCTCCTT</b> GGAAAGGCATTAA
<b>FLOT1 fwd</b>	AT5G25250.1	<b>GGGGACAAGTTTGTACAAAAAAGCAGGCTTAATGTTCAAAGTTG</b> CAAGAGCGTCACA
<b>FLOT1 rew</b>	AT5G25250.1	<b>GGGGACCACTTTGTACAAGAAAGCTGGGTATCMGCTGCGAGTC</b> ACTTGCTTCGGTTC
<b>eIF4B1 fwd</b>	AT3G26400.1	<b>GGGGACAAGTTTGTACAAAAAAGCAGGCTTAATGTGCGAAAAGCTT</b> GGGGTGGAAATTGG
<b>eIF4B1 rew</b>	AT3G26400.1	<b>GGGGACCACTTTGTACAAGAAAGCTGGGTATCMCCATCCTTCCC</b> TAGAGGAAGACCT
<b>RUXF fwd</b>	AT4G30220.2	<b>GGGGACAAGTTTGTACAAAAAAGCAGGCTTAATGGCGTTTGTAT</b> GTATGTGTGTTTT
<b>RUXF rew</b>	AT4G30220.2	<b>GGGGACCACTTTGTACAAGAAAGCTGGGTATCMGTCTTGATCAG</b> CGTCTTCAAGCTC
<b>UAP56A fwd</b>	AT5G11170.1	<b>GGGGACAAGTTTGTACAAAAAAGCAGGCTTAATGGGAGACGCTA</b> GAGACAACGAAGC
<b>UAP56A rew</b>	AT5G11170.1	<b>GGGGACCACTTTGTACAAGAAAGCTGGGTATCMAGAAGGCATG</b> TAGGTTGAAGTATC
<b>UBP12 fwd</b>	AT5G06600.1	<b>GGGGACAAGTTTGTACAAAAAAGCAGGCTTAATGACTATGATGA</b> CTCCGCCTCCCGT
<b>UBP12 rew</b>	AT5G06600.1	<b>GGGGACCACTTTGTACAAGAAAGCTGGGTATCMATTGTATATTT</b> TTACCGGCTTCTC
<b>NTF2 fwd</b>	AT5G60980.2	<b>GGGGACAAGTTTGTACAAAAAAGCAGGCTTAATGGCACAGCAGG</b> AAGCTAGTCCTTC
<b>NTF2 rew</b>	AT5G60980.2	<b>GGGGACCACTTTGTACAAGAAAGCTGGGTATCMAGATGAACCA</b> CCACCTCGAGCTCC
<b>LOS4 fwd</b>	AT3G53110.1	<b>GGGGACAAGTTTGTACAAAAAAGCAGGCTTAATGGCGGATACGG</b> TAGAGAAAGTTCC
<b>LOS4 rew</b>	AT3G53110.1	<b>GGGGACCACTTTGTACAAGAAAGCTGGGTATCMCTCGTCCAGCA</b> GGCCAGCTTCCTT
<b>RRM fwd</b>	AT3G23900.1	<b>GGGGACAAGTTTGTACAAAAAAGCAGGCTTAATGGCTTCAGATC</b> GTGGTTCTGCAGC
<b>RRM rew</b>	AT3G23900.1	<b>GGGGACCACTTTGTACAAGAAAGCTGGGTATCMTGACTTAAGA</b> ATAATCCTTTTCTC
<b>CML10 fwd</b>	AT2G41090.1	<b>GGGGACAAGTTTGTACAAAAAAGCAGGCTTAATGGCGAATAAGT</b> TCACTAGACAACA
<b>CML10 rew</b>	AT2G41090.1	<b>GGGGACCACTTTGTACAAGAAAGCTGGGTATCMAGAAAACAAC</b> GCTTCGAACAAATF
<b>eIF4B seq</b>	AT3G26400.1	ATTATCAACATCATCAGCTC
<b>VPS18 seq1</b>	AT1G12470.1	AGTGATGGAAGTGAAGCAGT
<b>VPS18 seq2</b>	AT1G12470.1	GACATAGGCGCAATGCATAT
<b>UBP12 seq1</b>	AT5G06600.1	ATAAGTGTGCTGCTTCGACA
<b>UBP12 seq2</b>	AT5G06600.1	AGTATGTTGAAGTTGAACGT
<b>RRM seq</b>	AT3G23900.1	CTTTGTTTTCTCATCATCT
<b>eIF4B1 seq2</b>	AT3G26400.1	GTGCTTGCCTTTTCCCTGCA
<b>Sequencing primer 1</b>		TCGCGTTAACGCTAGCATGGATCTC
<b>Sequencing primer 2</b>		GTAACATCAGAGATTTTGAGACACGGGCCAGAGCTGCAGCTG

## 2.3 Organisms

Table 2.3 summarizes all organisms used in this study. The different transgenic *A. thaliana* lines, which were used or generated in this study, are listed separately in Table 2.4.

**Table 2.3. List of used organisms**

Species	Name/Strain/Line	Attributes	Reference/Origin
<i>A. thaliana</i>	Columbia (Col-0)	wild type	WT-02, TAIR
<i>E. coli</i>	DH5- $\alpha$	F <sup>-</sup> , $\phi$ 80 <i>lacZ</i> $\Delta$ M1, $\Delta$ ( <i>lacZYA-argF</i> ), U169, <i>deoR</i> , <i>recA1</i> , <i>endA1</i> , <i>hsdR17</i> , ( <i>r</i> <sup>k</sup> -, <i>m</i> <sup>k</sup> +), <i>phoA</i> , <i>supE44</i> , <i>thi-1</i> , <i>gyrA96</i> , <i>relA1</i> , - $\lambda$	(Hanahan, 1983).
<i>E. coli</i>	DH10B	F <sup>-</sup> , <i>gyrA462endA1</i> , <i>glnV44</i> , $\Delta$ ( <i>sr1-recA</i> ), <i>mcrBmrr</i> , <i>hsdS20</i> ( <i>r</i> <sub>B</sub> <sup>-</sup> , <i>m</i> <sub>B</sub> <sup>-</sup> ), <i>ara14</i> , <i>galK2</i> , <i>lacY1</i> , <i>proA2</i> , <i>rpsL20</i> ( <i>Smr</i> ), <i>xyl5</i> $\Delta$ <i>leumt11</i>	(Miki et al. 1992).
<i>S. cerevisiae</i>	AH109	<i>MATatrp1-901</i> , <i>leu2-3,112</i> <i>ura3-52</i> , <i>his3-200</i> , <i>gal4</i> $\Delta$ , <i>gal80</i> $\Delta$ , <i>LYS2::GAL1UAS-GAL1TATA-HIS3</i> , <i>MEL1 GAL2UAS-GAL2TATA-ADE2</i> , <i>URA3::MEL1UAS-MEL1TATA-lacZ</i>	(CLONTECH, James et al. 1996)
<i>H. sapiens</i>	HEK293TN	Pseudoviral Lenti Particle Producer Cell Line	BioCat/SBI LV900A-1)

Table 2.4. List of used and generated *A. thaliana* transgenic lines

Name of line	Recombinant Protein (ATG)	Plasmid (selection in plants)	Reference/Origin
<b>35S::GFP-SKD1 (Col-0)</b>	GFP-SKD1 (AT2G27600)	pCambia 1300 (Hygromycin B or Kanamycin)	Haas et al., 2007
<b>35S::PAB2-mRFP (Col-0)</b>	PAB2-mRFP (AT4G34110)	pGWB 554 (Hygromycin B)	Sorenson and Bailey-Serres, 2014.
<b>35S::mCHERRY-ARA7 (Co-0)</b>	mCHERRY-ARA7 (AT4G19640)	pAMARENA (Glufosinate)	A. Steffens, unpublished
<b>35S::DCP5-TURQUOISE (Col-0)</b>	DCP5-TURQUOISE (AT1G26110)	pPACIFIC (Glufosinate)	M. Jakoby, unpublished
<b>35S::YFP-RHA1 (Col-0)</b>	YFP-RHA1 (AT5G45130)	pNIGEL07 (Glufosinate)	Geldner et al., 2009
<b>35S::YFP-w/o (Col-0)</b>	YFP CFP (not visible)	pENSG-YFP-w/o (Glyphosate) pENSG-CFP-w/o (Glufosinate)	I. Schultheiß Araújo, unpublished
<b>ProPIN2::PIN2-GFP (eir1-1)</b>	PIN2-GFP (AT5G57090)	pBRL	Abas et al., 2006
<b>35S::GFP-SKD1x 35S::PAB2-mRFP (Col-0)</b>	GFP-SKD1 PAB2-mRFP	pCambia 1300 pGWB 554	This study
<b>35S::GFP-SKD1x 35S::mCHERRY-ARA7 (Col-0)</b>	GFP-SKD1 mCHERRY-ARA7	pCambia 1300 pAMARENA	This study
<b>35S::DCP5-TURQUOISEx 35S::mCHERRY-ARA7 (Co-0)</b>	DCP5-TURQUOISE mCHERRY-ARA7	pPACIFIC pAMARENA	This study
<b>35S::YFP-RHA1x 35S::PAB2-mRFP (Col-0)</b>	YFP-RHA1 PAB2-mRFP	pNIGEL07 pGWB 554	This study
<b>35S::DCP5-TURQUOISEx 35S::PAB2-mRFP (Col-0)</b>	DCP5-TURQUOISE PAB2-RFP	pPACIFIC pGWB 554	This study
<b>ProPIN2::PIN2-GFPx 35S::mCHERRY-ARA7</b>	PIN2-GFP mCHERRY-ARA7	pBRL pAMARENA	This study

## 2.4 Plant techniques

### 2.4.1 Plant growth conditions

*A. thaliana* seeds were put on soil or on ½ MS agar plates (Murashige and Skoog, 1962, 2.2 g MS powder [Duchefa], pH 5.6-5.8 with 1 M NaOH, 8 g/l agar, with H<sub>2</sub>O to 1 l, autoclave) and stratified for at least 2 d) at 4°C in the dark. Afterwards, the plants were grown under long day conditions (16 h light, 8 h darkness) at 21°C and with an average light intensity of 100 ± 20 µmol/m<sup>2</sup>s.

### 2.4.2 Seed sterilization

*A. thaliana* seeds were surface sterilized before they were placed on ½ MS agar plates. For this, seeds were submerged in 70% ethanol for 5', followed by 2% NaOCl for 3'. Finally, the seeds were washed twice with sterile H<sub>2</sub>O.

### 2.4.3 Crossing

Transgenic lines were crossed by removing the anthers of the receiving flower with forceps. Then, the stigma of the receiving flower is pollinated with the anthers of the crossing partner. All steps were executed under a binocular microscope. The female, receiving line is noted first, the pollen donor second.

### 2.4.4 Heat stress treatment

The subjection of *A. thaliana* plants to a heat stress of 40°C has been shown to trigger the formation of SGs. Heat stress treatment at 40°C for 50' was used to induce mRNP granules. For confocal imaging, transiently transformed rosette leaves were placed on ½ MS plates, sealed with surgical tape and put in an incubator for 50' at 40°C. Imaging occurred immediately after treatment. The same procedure was used for rosette leaves of transgenic lines.

For the imaging of root epidermal cells, 5-10 d old seedlings grown on vertical ½ MS plates were transferred in tubes with liquid ½ MS and placed into a heating block. Here, the control plants were also submerged in liquid ½ MS, but kept at RT.

### 2.4.5 Transient transformation by particle bombardment

For subcellular localization and colocalization analysis, epidermal cells of non-flowering *A. thaliana* (Col-0) rosette leaves were transiently transformed using a particle gun (Biolistic Particle Delivery system PDS-1000 / He<sup>TM</sup>, BIO RAD). This method uses DNA-coated micro particles, here gold particles, which are accelerated by a burst of high-pressure helium gas to

penetrate plant cells. If the nucleus is hit, plasmid DNA gets expressed but is not stably integrated into the genome.

For single and double transformations, 5  $\mu$ l gold particles (30 mg/ $\mu$ l, diameter 1  $\mu$ m, Biolistic®1.0 Micron gold, BioRad) were coated with plasmid DNA (0.6  $\mu$ g for each construct) using 2.5 M CaCl<sub>2</sub> (10  $\mu$ l) and spermidine (4  $\mu$ l). The reaction was filled up with H<sub>2</sub>O to a final volume of 20  $\mu$ l and shaken vigorously for 10'. Coated gold particles were sedimented (9300 g for 10'') and subsequently washed with 70% ethanol (50  $\mu$ l), ethanol absolute (20  $\mu$ l) and finally resuspended in 12  $\mu$ l ethanol absolute. The coated gold particles were loaded onto macro carriers (plastic discs) and placed in the particle gun. A helium burst of 900 psi accelerated the gold particles and allowed cell wall penetration. Rosette leaves were placed on ½ MS agar plates, sealed with tape and incubated in the dark at RT for 14-17 h until confocal microscopy analysis

### **2.4.6 Confocal microscopy**

Subcellular protein localization and colocalization was analyzed by confocal microscopy using a Leica TCS SP8 (Leica Microsystems). Images were collected with an HC PL APO 20x/0.75 IMM CORR CS2 combinatorial objective (H<sub>2</sub>O for immersion in this study) or an HCX PL Fluotar 10x/0.30 dry objective. CFP and mTURQUOISE (mTQ) were excited at 405 nm (Diode 405) and emission was detected between 460 and 500 nm. GFP and YFP were excited at 488 nm (Argon laser) and detected between 500 nm and 530 nm, and 510 and 540 nm, respectively. Monomeric RFP (mRFP) and mCHERRY were excited at 561 nm (DPSS561) and detected between 590 and 640 nm. FM4-64 dye was excited at 514 nm (Argon laser) and emission was detected between 600 and 680 nm. Emitted signals were detected with hybrid detectors (Leica HyD) or photomultiplier (PMT) detectors.

In double transformations, the signals of fluorescent proteins were captured with separate detectors and by sequential scanning (between lines) to prevent crosstalk. Samples were scanned bidirectional, with a speed of 700 Hz or 1000 Hz and with a line average of 1-3 (stacks) or 3-16 (single planes). Stacks of leaf epidermal cells were scanned every 1.04  $\mu$ m and total stack size depended on cell thickness (approximately 15-60  $\mu$ m). Stacks were depicted and analyzed as signal maximum projections. If not described otherwise, laser intensities were kept constant for imaging before and after heat stress. The pictures were not modified, except for brightness and contrast. If not described otherwise, CFP and mTQ signals are depicted in cyan, GFP and YFP signals in yellow, and mRFP, mCHERRY, and FM4-64 in magenta. The ImageJ 1.51 freeware was used for image composition and preparation (Schneider et al., 2012).

### **2.4.7 FM4-64 staining and BFA treatment**

Roots of *A. thaliana* seedlings grown on ½ MS plates (5-7 d) were stained with FM4-64 dye (Synaptored™ C2, Merck) for the identification of membranous structures by confocal microscopy. For this, FM4-64 was added to liquid ½ MS medium to a final concentration of 50 µM (Ueda et al., 2002). For Figure 3.3, Chapter 3.2, roots were incubated in medium containing the dye for 5', incubated in dye-free medium for 2 h at RT and were finally subjected to heat treatment before imaging. For Figure 3.27, the roots were incubated 10' in liquid medium with the dye and then subjected to heat treatment in the same medium. The BFA-treated roots were incubated with FM4-64 and BFA in parallel for 50'. Roots were treated with a final concentration of 50 µM BFA (stock 35 mM in EtOH, Roth) either for 90' (Figure 3.26) or 50' (Figure 3.27) before imaging (Kleine-Vehen et al., 2008). The corresponding amount of ethanol (1 µl to 711 µl liquid ½ MS) was given to the control roots.

## **2.5 Molecular biology techniques**

### **2.5.1 RNA extraction and cDNA synthesis**

Total RNA was extracted from *A. thaliana* Col-0 seedlings or flowers with the RNeasy kit (Qiagen) following the manufacturer's protocol. For the transcription of mRNA into cDNA, the First Strand cDNA Synthesis Kit (ThermoScientific) was used according to the instructions of the manufacturer. Hereby, the synthesis was done with oligo(dT) primer for total poly(A) mRNA amplification.

### **2.5.2 Polymerase Chain Reaction (PCR)**

The CDS of the interactome candidates was generated from flower or seedling cDNA by PCR. Hereby, primers were used which added recombinant *attB* Gateway sites to the ends of the CDS. Furthermore, the primer contained a degenerate site allowing the introduction of a stop codon or a glycine for C-terminal fusions. Table 2.5 lists the different interactome candidate versions, which were generated. CDS were amplified using the Phusion High-Fidelity DNA Polymerase (Thermo Scientific).

**Table 2.5. PCR reaction and program**

Reaction		Amplification program		
Component	Amount/Concentration	Step	Temperature	Duration
<b>Phusion Buffer</b>	4 $\mu$ l	<b>1.</b>	98°C	30''
<b>dNTP</b>	0.8 $\mu$ l (10 mM)	<b>2.</b>	98°C	10''
<b>Forward Primer</b>	0.8 $\mu$ l (10 mM)	<b>3.</b>	primer annealing temperature	30''
<b>Reverse Primer</b>	0.8 $\mu$ l (10 mM)	<b>4.</b>	72°C	CDS length (1000 bp in 30'')
<b>cDNA</b>	0.8 $\mu$ l	<b>5.</b>	72°C	10'
<b>Phusion</b>	0.2 $\mu$ l	Repeat step 2 to 4 35 times		
<b>H<sub>2</sub>O</b>	13 $\mu$ l			

### 2.5.3 Gateway cloning

The Gateways cloning system (Invitrogen) is a quick alternative for classical cloning. It is based on site specific recombination of the bacteriophage lambda, which exchanges its DNA via a specific sequence (*attP*) into the chromosome of its bacterial host (*attB*). The recombination is carried out by phage integrase and a bacterial host integration factor. After recombination and the integration of phage DNA, the integration specific sequences are changed (*attL* for left, *attR* for right). Gateway-compatible donor vectors (e.g. pDONR201) contain *attP* sites and PCR products, which are flanked by *attB* sites, can be integrated by a BP-reaction. The resulting entry vectors contain a DNA fragment of interest flanked by *attL* sites, which can be introduced into a Gateway-compatible destination vector (e.g. pENSG-YFP, contains *attR* sites) by an LR-reaction. Donor and Destination vectors contain a toxic *ccdB* gene between the recombination sites, which enhances the selection of positive clones. Empty donor and destination vectors are amplified in the *E.coli* strain DB3.1, which is resistant against the *ccdB* gene. PCR products were integrated into entry vectors by a BP-reaction. The genes of interest in the donor vectors were integrated in different destination vectors by LR-reactions. After 1-16 h at RT, the reactions were transformed in competent *E. coli* DH5 $\alpha$  cells.

**Table 2.6. Composition of BP- and LR-reactions.**

<b>BP-reaction</b>		<b>LR-reaction</b>	
<b>Component</b>	<b>Amount/Concentration</b>	<b>Component</b>	<b>Amount/Concentration</b>
<b>PCR product</b>	1.75 $\mu$ l (100 ng/ $\mu$ l)	<b>Donor vector</b>	0.5 $\mu$ l (150 ng/ $\mu$ l)
<b>Donor vector</b>	0.25 $\mu$ l (150 ng/ $\mu$ l)	<b>Destination vector</b>	0.25 $\mu$ l (150 ng/ $\mu$ l)
<b>BP Clonase (ThermoScientific)</b>	0.5 $\mu$ l	<b>LR Enzyme Mix (ThermoScientific)</b>	0.5 $\mu$ l
		<b>H<sub>2</sub>O</b>	1.25 $\mu$ l

#### 2.5.4 Plasmid purification, restriction digestion and sequencing

After transformation and amplification in *E. coli* DH5 $\alpha$  cells, plasmids were extracted from the cells using the GeneJET Plasmid MiniPrep Kit (ThermoScientific) according to the manufacturer's protocol. Approximately 200-400 ng/ $\mu$ l plasmid DNA was extracted from DH5 $\alpha$  cells and subjected to restriction digestion (3  $\mu$ l plasmid DNA, 0.3  $\mu$ l BsrGI, 2  $\mu$ l Tango Buffer, ThermoScientific) and gel electrophoresis. Plasmids, which showed correct band patterns after restriction digestion, were sent for sequencing to GATC (Light Run, Eurofins Genomics) using plasmid DNA and sequencing primer.

#### 2.5.5 Generation of chemical competent *E. coli* cells

DH5 $\alpha$  and DB3.1 cells were made competent for heat shock-induced transformation by the RbCl<sub>2</sub> method. For that, an o/n culture (10 ml  $\psi$ broth medium) was inoculated and incubated at 37°C under agitation. The main culture (200 ml  $\psi$ broth medium, 20 g BactoPeptone, 5 g Bacto yeast extract, 4 g MgSO<sub>4</sub> x 7H<sub>2</sub>O, 0.746 g KCl, with H<sub>2</sub>O to 1 l) was inoculated with 3 ml of the o/n culture and cells were grown at 37°C under agitation until an OD<sub>600</sub> of 0.5 was reached (approximately 2-3 h). The cells were put on ice (15'), collected by centrifugation (10', 4°C at 650 g) and resuspended in 1 ml Tfb1 medium (1.21 g RbCl<sub>2</sub>, 0.99 g MnCl<sub>2</sub> x 4H<sub>2</sub>O, 0.15 g CaCl<sub>2</sub>x 2H<sub>2</sub>O, 15 ml glycerol 100%, with H<sub>2</sub>O to 1 l). After resuspension of the cell pellet, Tfb1 medium was added to a final volume of 15 ml and kept on ice for 2 h. The cells were collected (10', 4°C at 650 g), resuspended in 2 ml Tfb2 (0.024 g RbCl<sub>2</sub>, 0.221 g CaCl<sub>2</sub>x 2H<sub>2</sub>O, 0.042 g 3-(*N*-morpholino)-propanesulfonic acid, 3 ml glycerol 100%, with H<sub>2</sub>O to 20 ml) medium and aliquots of 50  $\mu$ l were generated. The aliquots were frozen in liquid nitrogen and kept at -80°C.

### 2.5.6 Transformation of *E. coli* cells

*E. coli* DH5 $\alpha$  (amplification of plasmids generated by BP or LR reactions) and DB3.1 (amplification of empty Gateway cassette-containing plasmids) cells were transformed with plasmid DNA using the following protocol: 50  $\mu$ l of chemically competent cells were added to the LR or BP reaction mix and incubated on ice for 20'. For retransformations, 0.5  $\mu$ l of plasmid DNA was used. After the incubation on ice, cells were subjected to a heat shock at 42°C for 1' and subsequently placed on ice for 5'. The cells were mixed with 800  $\mu$ l LB medium (10 g BactoPepton, 5 g Bacto yeast extract, 10 g NaCl, with H<sub>2</sub>O to 1 l, Bertani, 1951) w/o antibiotics and incubated at 37°C for 1 h. Afterwards, cells were collected (6000 g for 5'), resuspended in 50  $\mu$ l LB medium and plated on LB agar plates (16 g agar to 1 l LB medium) containing corresponding antibiotics for selection. The plates were kept at 37°C o/n and colonies were picked on the next day. For a standard MiniPrep, 4 ml of LB medium (with corresponding antibiotics) were inoculated and grown at 37°C o/n under agitation.

## 2.6 Biochemical techniques

### 2.6.1 Co-immunoprecipitation

The co-immunoprecipitation experiment was performed to study the interactome of SKD1. For that, the GFP Isolation kit (Miltenyi Biotec) was used. The immunoprecipitation was performed with the provided solutions and following the manufacturer's protocol with modifications. Until protein elution, all centrifugation, incubation, and flow-through steps were performed at 4 °C. Rosette leaves of 2.5 week old soil grown plants (not flowering) of the *35S::GFP-SKD1* and the *35S::YFP-w/o* line were either subjected to heat treatment or kept at RT (control) before harvest (3 replicates each, 12 samples in total). During the heat treatment (40°C 50'), the pots were covered with a petridish to prevent evaporation. For each sample, leaves of 5 plants were combined and quickly frozen in liquid nitrogen.

The leaf material was grinded in a mortar with liquid nitrogen, weighed and mixed with modified GFP Isolation kit lysis buffer (940  $\mu$ l lysis buffer, 10  $\mu$ l 1 M Dithiothreitol/DTT, 50  $\mu$ l of a Roche cOmplete™ Protease Inhibitor Cocktail Pill dissolved in 2 ml lysis buffer). The grinded leaf material (120-160 mg) was mixed with the corresponding volume of lysis buffer (500  $\mu$ l lysis buffer to 100 mg material) and incubated for 30' whereby the samples were inverted every 5' to prevent sedimentation of the material. Cell debris was removed by centrifugation (1000 g, 5') and the supernatant was collected. An additional centrifugation step (12000 g, 5') removed all remaining residues and input controls were taken for the test of immunoprecipitation (3.5.1, Figure 3.18) Same amounts of lysates (450  $\mu$ l) were mixed with  $\alpha$ -

GFP magnetic beads (90  $\mu$ l) and incubated for 60' under slow agitation. The  $\mu$ MACS columns were placed in a magnetic separator and equilibrated with 550  $\mu$ l unmodified lysis buffer. The columns were loaded with the samples, the flow through was collected and reloaded onto the columns for a second time. The columns were washed four times with washing buffer 1 (200  $\mu$ l) and one time with washing buffer 2 (100  $\mu$ l). Afterwards, the magnetic separator with the columns was transferred to RT.

For the immunoprecipitation test, 20  $\mu$ l preheated elution buffer (90°C) were added to the columns and incubated for 5'. The repeated addition of 50  $\mu$ l hot elution buffer released the bound proteins from the beads and final samples were collected and subjected to SDS-PAGE (sodium dodecyl sulfate polyacrylamide gel electrophoresis).

For the analysis of the SKD1 interactome, 20  $\mu$ L urea buffer (8 M urea in 50 mM triethylammonium bicarbonate/TEAB) were added to the columns, removed from the magnetic separator and incubated for 10'. The proteins, together with the beads, were eluted from the columns by the addition of 50  $\mu$ l urea buffer (final volume of samples: 50  $\mu$ l).

### **2.6.2 In solution/on-bead digest**

To analyze all co-precipitated proteins by liquid chromatography and tandem mass spectrometry analysis (LC-MS/MS analysis), an in-solution/on-bead digest of the proteins was performed. The protocol and the used solutions were provided by the Proteomics Core Facility Cologne.

To each sample, DTT was added to a final concentration of 5 mM (0.25  $\mu$ l 1 M DTT), mixed and incubated at 37°C for 1 h. Next, chloroacetamide (2.54  $\mu$ l 750 mM) was added to the samples to a final concentration of 40 mM, mixed and incubated in the dark at RT for 30'. The first digestion was performed by Lys-C protease (0.5  $\mu$ g/ $\mu$ l). For that, 0.5  $\mu$ l Lys-C protease were added and the samples were incubated at 25°C for 4 h. The samples were diluted with 150  $\mu$ l TEAB (pH 8.5, 50 mM) to a final urea concentration below 2 M. The second digestion was started with the addition of 2.5  $\mu$ l Trypsin (1  $\mu$ g/ $\mu$ l) and was finished after o/n incubation at 25°C. On the next day, the digestion was stopped by acidification with formic acid to a final concentration of 1% (4  $\mu$ l of 50% formic acid). The beads were removed from the samples by centrifugation at 15.000 g for 5'. The centrifugation was repeated until no beads were present in the supernatant (yellow-brownish color).

### 2.6.3 StageTip purification

The next step was the loading of the samples onto StageTips for removal of salts and other contaminants before MS/MS analysis. Protocol, chemicals and styrene-divinylbenzene–reversed phase sulfonate discs-containing C18 StageTips were provided by the Proteomic Core Facility Cologne.

The StageTips were equilibrated by subsequent addition and removal of methanol (20  $\mu$ l, 600 g 1'), 0.1% formic acid in 80% acetonitrile (20  $\mu$ l, 600 g 1'), 0.1% formic acid in H<sub>2</sub>O (20  $\mu$ l, 600 g 1.5') and 0.1% formic acid in H<sub>2</sub>O (20  $\mu$ l, 600 g 2'). The acidified and bead-free samples were centrifuged (15700 g, 5') and samples were loaded onto the StageTips and centrifuged at 600 g for 5'. The StageTips were subsequently washed with 30  $\mu$ l 0.1% formic acid in H<sub>2</sub>O (600 g 3') and two times with 30  $\mu$ l formic acid in 80% acetonitrile (600 g 3'). The StageTips were dried with a syringe and stored at 4°C until LC-MS/MS analysis.

### 2.6.4 LC-MS/MS analysis

The LC-MS/MS analysis and the bioinformatical analysis were performed by the Proteomics Core Facility Cologne. The following paragraphs summarize the technical information provided by the facility.

The samples were subjected to LC using an EASY nLC 1200 UPLC (Thermo Scientific) which was connected to a Q-Exactive Plus (Thermo Scientific) mass spectrometer. Chromatographic separation occurred on an analytical column which was prepared by the Proteomic Facility. The column was 50 cm high and 75  $\mu$ m in diameter and packed with 2.7  $\mu$ m Poroshell EC 120 C18 (Agilent). The peptides were loaded with 0.1% formic acid in H<sub>2</sub>O and separated at a constant flow rate (250 nl/min) using a gradient (8-40% of 0.1% formic acid in H<sub>2</sub>O within 40', 95% of 0.1% formic acid in H<sub>2</sub>O within 10'). This was followed by washing and the equilibration of the column. The Q-Exactive Plus mass spectrometer was set to the data-dependent acquisition mode and scans were started with following settings: 300-1750 m/z (resolution 70000), isolation of the 10 most abundant peptides within a 1.8 Tz window, higher-energy collisional dissociation fragmentation of isolated peptides at 27% of the normalized collision energy. The maximum injection time was 108 ms as the automatic gain control target was 5e<sup>5</sup> charges. Orbitrap detection of product ions had a resolution of 35000 and precursors were excluded dynamically for 20''.

The raw data of the MS<sup>2</sup> spectra was analyzed by S. Müller, Proteomics Core Facility Cologne, using Maxquant software (version 1.5.2.8.) set to default parameters. As a reference, the

Uniprot ARATH.fasta database (download 16.06.2017) was used, which included common contaminants. The protein and peptide spectrum matches (PSM) false discovery rates (FDRs) were estimated using the target-decoy approach (1% Protein FDR and 1% PSM FDR). Only peptides that had a length of at least 7 amino acids were counted and the carbamidomethylation of cysteins was included as a fixed modification. Variable modifications (Oxidation and Acetyl) were included in the analysis. The match between runs option was enabled and used to boost the number of identifications and label-free quantification (LFQ) was performed using default settings.

### **2.6.5 SDS-PAGE**

Proteins extracted from leaf tissue or HEK293TN cells were mixed 1:1 (volume/volume) with SDS sample buffer (50 mM Tris/HCl pH 6.8; 10% Glycerol, 2% SDS, 0.1% Bromophenol Blue; 100 mM DTT) and cooked for 10' at 99°C. The PAGE was performed with 10% SDS separation gels (5 ml gel: 1.9 ml H<sub>2</sub>O, 1.7 ml acrylamide mix [Rotiphorese Gel 30, Roth], 1.3 ml 1.5 M Tris pH 8.8, 50 µl 10% SDS, 50 µl 10% ammoniumpersulfate, 2 µl tetramethylethylenediamine). The stacking gels (1 ml) were composed as following: 0.68 ml H<sub>2</sub>O, 0.17 acrylamide mix, 0.13 ml 1.5 M Tris/HCl pH 6.8, 10 µl 10% SDS, 10 µl 10% ammoniumpersulfate, 1 µl tetramethylethylenediamine). As a marker, the PageRuler Prestained was used (10 to 180 kDa, ThermoScientific). For the test of the immunoprecipitation, 15 µl of input control and eluate were applied to the gel. For the test of SKD1 expression in HEK cells, 15 µl of the diluted supernatants and 2 µl of the pellets were applied. The PAGE ran in SDS-electrophoresis buffer (3.03 g Tris, 18.1 g glycine, 10 ml 10% SDS, up to 1 l with H<sub>2</sub>O) at 20 mA/gel for 1.5 h.

### **2.6.6 Coomassie staining**

To detect the total protein amount in samples, SDS gels were stained with colloidal Coomassie solution (0.02% Coomassie Brilliant Blue G250 [Serva], 5% aluminiumsulfate-18-hydrate, 10% ethanol absolute, 2% orthophosphoric acid). Gels were submerged in the staining solution and incubated at RT over night under agitation. On the next day, excessive staining was removed by washing with H<sub>2</sub>O until clear protein bands were visible.

### **2.6.7 Immunoblotting (Western blotting)**

For semi-dry immunoblotting, gels were rinsed in cathode buffer (100 ml Roti<sup>®</sup>Blot 2K [Roth], 50 ml methanol, 850 ml H<sub>2</sub>O) and placed onto a polyvinylidenfluoride-membrane (Roth), which was activated with methanol. The gel and membrane were placed between two Whatman papers, which were rinsed in cathode or anode (100 ml Roti<sup>®</sup>Blot 2A [Roth], 50 ml methanol,

850 ml H<sub>2</sub>O) buffer, and proteins were transferred from the gel to the membrane by semi-dry blotting at 40 mA over 17 h at 8°C. Membranes were blocked in 5% milk in phosphate buffer saline and 0.1% Tween20 (PBST, 8 g NaCl, 0.2 g KCl, 1.44 g Na<sub>2</sub>HPO<sub>4</sub>, 0.24 g KH<sub>2</sub>PO<sub>4</sub>, with H<sub>2</sub>O to 1 l, 1 ml Tween20) for 30'. YFP and SKD1-YFP were detected using mouse  $\alpha$ -GFP antibody (1:2000, Roche) diluted in 5% milk (PBST) for 1 h under agitation. After washing (3 times with 15 ml PBST for 10'), the membrane was incubated with the second goat  $\alpha$ -mouse antibody (1:10000, Sigma–Aldrich/Merck), which was coupled to horseradish peroxidase for chemiluminescence detection (West Femto Maximum Sensitivity Substrate Kits, Thermo Scientific) with a LAS4000 (Amersham).

## 2.7 Protein-protein interaction assays

### 2.7.1 Protein-protein interaction analysis by Y2H

The yeast-two-hybrid (Y2H) method is an *in-vivo* assay to test protein-protein interactions. First described by Fields and Song (1989), it utilizes the eukaryotic transcription factor GAL4 to drive the protein-protein interaction-dependent expression of a histidine (H) biosynthesis. The yeast strain *AH109* is incompetent of leucine (L), tryptophan (W) and H biosynthesis. Yeast cells are transformed with the pAS vector, which encodes for a recombinant version of the bait protein in fusion with the DNA Binding Domain of GAL4 (GAL4-BD). The prey protein is encoded on the pACT vector as a recombinant fusion version with the GAL4 Activation Domain (GAL4-AD). The vectors encode for W (pAS) and L (pACT) biosynthesis genes which are used for selection of transformed cells. The GAL4-BD and GAL4-AD are only in a functional distance when the bait and prey protein interact with each other. If this is the case, the functional GAL4 transcription factor binds to the *GAL4* promoter, which drives the expression of an H biosynthesis gene (stably transformed in the AH109 yeast strain). The identification of protein interactions was determined by colony growth on selection dropout (SD) agar plates without L, W and H, also termed interaction medium (5 g ammonium sulfate, 1.7 g yeast nitrogen base, 0.6 g drop-out supplement w/o leucine, histidine, tryptophan [Difco], 100 mg adenine, and 18 g agar, with H<sub>2</sub>O to 1 l, pH 5.8, autoclave, addition of glucose to a final concentration of 2%). 3-Amino-1,2,4-triazole (3-AT), which is a competitive inhibitor of the upstream activating sequence of the *GAL4* promoter, can be added to the SD-LWH plates to adjust for autoactivation (0 mM, 5 mM, 15 mM, 30 mM). Autoactivation of the bait protein was detected by colony growth of the negative control (GFP-AD).

The yeast cells were transformed with the two vectors using the LiAc method (modified from Gietz et al., 1995). For that, cells were grown in 10 ml liquid YPAD medium (10 g yeast extract,

20 g Difco peptone, 100 mg adenine, pH 5.8, with H<sub>2</sub>O to 950 ml, autoclave, addition of glucose to final a concentration of 2%) o/n. To inoculate the main YPAD culture (50 ml), 0.5-1 ml of the suspension were used. After incubation at 30°C for approximately 3-4 h under agitation, the culture reached an OD<sub>600</sub>=0.7-1, which is sufficient for 10-15 transformations. The cells were collected from the medium by centrifugation (2600 g for 5') and washed with 0.1 M LiAc (pH 7.5). After an additional centrifugation step (2600 g for 5'), the transformation agents were added to the cells: 240 µl polyethylene glycol 3350, 36 µl 1 M LiAC, 50 µl ssDNA [2 mg/ml, cooked at 100°C for 10'], and 25 µl H<sub>2</sub>O per transformation. The suspension was mixed and 350 µl were added to approximately 0.6 µg of plasmid DNA for each construct. Transformation occurred at 42°C for 40' under agitation. Afterwards, the cells were collected by centrifugation (3300 g, 30'') and resuspended in 100 µl H<sub>2</sub>O and plated on SD-LW medium (addition of 20 mg/l H) to identify positive transformants.

After 5-7 d, colonies were picked from the SD-LW plates, resuspended in water and transferred onto SD-LWH plates by stamping. In addition to the stamping onto the interaction medium, the resuspended cells were also transferred to an SD-LW plate to confirm the viability of the cells. Technical replicates were defined as two pools of 3-7 colonies from one transformation, which are separately transferred to the interaction medium. A biological replicate was defined as an independent transformation of yeast cells. An interaction of a bait and prey protein was defined as positive, if the corresponding negative control showed no colony growth at the same 3-AT concentration at the day of evaluation (7-11 days after transfer). For the interaction test of the ESCRTIII core and associated proteins with mRNP granule components, each interaction was tested with at least 2 biological and 2 technical replicates (Chapter 3.1 and Appendix, Table A.2). Here, a tested combination was considered positive if half of the transferred colonies showed growth. For the analysis of the interactions of SKD1 with the interactome candidates, each interaction was tested in 3 biological with 3 technical replicates. Here, a combination was considered positive if it showed the same degree of colony growth as the weakest, established positive control (LIP5 with SKD1, 2 out of 9 colonies, Chapter 3.5.7 and Appendix, Table A.11).

Used positive controls for ESCRTIII core and associated protein with mRNP granule proteins: LIP5 *versus* SKD1 and DCP5 *versus* DCP1.

Used positive controls for SKD1 and interactome candidates: SKD1 *versus* LIP5/VPS32.1/VPS32.2/ VPS60.1/ VPS60.2.

### 2.7.2 Protein-protein interaction analysis by LUMIER

The LUMIER (Luminescence-based mammalian interactome mapping) assay was initially described by Barrios-Rodiles and colleagues and modified by Pesch and colleagues (Barrios-Rodiles et al., 2005; Pesch et al., 2013). LUMIER is a pulldown-based assay in which a bait protein fused to protein A (ProtA) from *Staphylococcus aureus* (pTREX) and a prey protein fused to the luciferase of *Renilla reniformis* are coexpressed in HEK293TN cells. Protein interaction is detected by luminescence after precipitation.

Constructs of modified bait (ProtA-SKD1, pTREX) and prey proteins (Renilla-interactome candidates, pcDNA3) were cotransfected into HEK293TN cells ( $1 \times 10^6$ , 6-well plates) using 0.6  $\mu$ g plasmid DNA of each construct and 20  $\mu$ l TurboFect transfection reagent (ThermoScientific). DNA and transfection reagent were mixed with 1.5 ml serum-free medium (Dulbecco's Modified Eagle Medium, Merck), incubated for 15' at RT and added to the cells. Another 2 ml medium were added and the cells were incubated for 48 h at 37°C. Medium was removed and the cells were collected and washed twice with 1 ml ice cold PBS. In between, cells were gently pelleted at 600 g for 5'. All centrifugation steps were done at 4°C. Cell lysis was induced by the addition of 450  $\mu$ l ice cold lysis buffer (79.1 ml H<sub>2</sub>O, 11 ml 10% Triton-X, 5.5 ml 5 M NaCl, 2.2 ml Na<sub>2</sub>EDTA pH 8.0, sterile filtrate, add 200  $\mu$ l of a Roche cOmplete™ Protease Inhibitor Cocktail Pill dissolved in 10 ml H<sub>2</sub>O to 10 ml lysis buffer). The cells were shaken and incubated for 1 h on ice. Cell debris was removed from lysates by centrifugation (21,380 g 15'). Input samples were taken (test of general expression levels of interactome candidates) and 100  $\mu$ l of the lysates were mixed with 5  $\mu$ l sheep anti-rabbit IgG-coated magnetic beads (Dynabeads M280 [Invitrogen], prewashed with PBS, 2 or 3 technical replicates). Lysates and beads were incubated for 2 h on ice. Afterwards, the beads were collected using a magnetic stand and washed 5 times with 50  $\mu$ l ice cold PBS). The beads were resuspended in 50  $\mu$ l PBS and luminescence was measured by a microtiter plate reader (FLUOstar OPTIMA, BMG Labtech) after the addition of 70  $\mu$ l Renilla buffer (27.44 ml H<sub>2</sub>O, 11 ml 5 M NaCl, 11 ml K<sub>2</sub>PO<sub>4</sub> pH 5.1, Na<sub>2</sub>EDTA pH 8.0, 0.225 ml 10 % bovine serum albumin [weight/volume], substrate: Coelenterazine synthesized, 1  $\mu$ l/ml [P.J.K]). Protein interactions were determined to be present, if the Relative Luminescence Intensity (RLI) was 1.5 fold higher than the background control (ProtA-SKD1 with Renilla-w/o). As positive controls, the interaction of SKD1 with VPS32.1, VPS60.1, and LIP5 were tested. As control for the assay, the in LUMIER established interaction of TTG1 (TRANSPARENT TESTA GLABRA 1) and GL3 was used (B. Zhang unpublished).

## 2.8 Computational analysis

### 2.8.1 Colocalization quantification

The quantitative colocalization studies of Chapter 3.3.2 and Chapter 3.4.5 were performed with transiently double transformed epidermal leaf cells, the study in Chapter 3.3.3 was performed with epidermal leaf cells of stable transgenic lines. Maximum projections of stacks were generated by confocal microscopy. Laser intensities were kept constant within datasets and kept in a range that minimized overexposure but allowed the detection of as many granules as possible. For each combination, 10 cells (transient transformation) or 10 equally sized leaf areas (stable lines) were analyzed. Unlabeled extracellular background signals and labeled cellular structures, which are not of interest in the respective study, can artificially inflate quantified overlaps (Dunn *et al.*, 2010). Therefore, three regions of interest (ROIs) per cell/leaf area were defined, which excluded the majority of membrane and nuclear signals and contained at least five granular structures (if granules were formed) in each channel. Examples of ROIs are given in the respective figures. For the quantification of the signal overlap, the Pearson's correlation coefficient (PCC) was used which is defined as following:

$$PCC = \frac{\sum_i (A_i - \bar{A}) \times (B_i - \bar{B})}{\sqrt{\sum_i (A_i - \bar{A})^2 \times \sum_i (B_i - \bar{B})^2}}$$

where  $A_i$  and  $B_i$  are signal intensities of pixel  $i$  in the two compared channels.  $\bar{A}$  and  $\bar{B}$  refer to mean signal intensities of the whole image for each channel (Manders *et al.*, 1992; Dunn *et al.*, 2011). A PCC of 1 indicates perfect co-occurrence of two signals, a PCC of 0 a random distribution, and a PCC of -1 indicates perfect negative correlation. PCCs for the different ROIs were calculated with the ImageJ Plugin JACoP (Just Another Colocalization Plugin, Bolte and Cordelieres, 2006). As positive control, the same protein (UBP1b) was expressed in cells with two different fluorescent tags (YFP and mCHERRY). As a negative control, one channel of the positive control was tilted by 180° and again analyzed for colocalization.

### 2.8.2 Intrinsically Disordered Region (IDR) analysis of protein sequences

A subset of *A. thaliana* P-body, SG, ESCRTIII core, and ESCRTIII associated proteins were analyzed for the presence of IDRs. For this, protein sequences of the representative gene models taken from TAIR (The Arabidopsis Information Resource) were subjected to the DisEMBL 1.5 and GlobPlot 2.3 online tools (standard settings, Linding *et al.*, 2003; Linding, 2003). DisEMBL predicts the presence of loops and H-loops, a class of secondary structures that fall not in the category of structured  $\alpha$ -helices,  $3_{10}$ -helices or  $\beta$ -strands. GlobPlot defines disordered regions

based on the likelihood of a residue to be in a second structure or in a random coil. Percentages of disorder were calculated based on the total protein length. The exact sequence stretches, which were predicted to be disordered by DisEMBL and GlobPlot, are given in Appendix, Table A.7 for the different analyzed proteins.

### 2.8.3 Filtering and classification of interactome candidates

To identify interactors of SKD1 under control condition and after heat treatment, proteins from GFP-SKD1-expressing and YFP-expressing plants were isolated by co-immunoprecipitation and analyzed by LC-MS/MS (Chapter 3.5). LFQs, a normalized relative measurement for protein abundance, were calculated if at least 2 peptides were identified for one protein. This was also the criterion for the presence of a protein within a sample. Table 2.7 summarizes the number of detected and identified peptides for each sample and the number of proteins, which were identified.

**Table 2.7. Summary of detected and identified peptides in the LC-MS/MS analysis**

Sample	MS/MS	MS/MS identified [%]	Peptide sequences identified	Proteins identified
<b>YFP control 1</b>	15834	32,60	4534	530
<b>YFP control 2</b>	14886	26,27	3455	511
<b>YFP control 3</b>	12180	23,99	2765	527
<b>YFP heat 1</b>	15863	32,16	4408	636
<b>YFP heat 2</b>	11262	18,43	2028	414
<b>YFP heat 3</b>	14663	25,73	3426	599
<b>GFP-SKD1 control 1</b>	14295	32,55	4408	1169
<b>GFP-SKD1 control 2</b>	16384	43,91	6272	1592
<b>GFP-SKD1 control 3</b>	15800	41,96	5705	1432
<b>GFP-SKD1 heat 1</b>	13116	24,79	3105	913
<b>GFP-SKD1 heat 2</b>	15769	38,77	5599	1322
<b>GFP-SKD1 heat 3</b>	16076	41,87	6102	1420

In all samples combined, 2409 different proteins were identified. The highest iBAQ value (normalized measurement of protein abundance between samples, Schwanhäusser et al., 2011) was calculated for SKD1 (in all GFP-SKD1 samples). All proteins, which were present in at least one replicate of the YFP control or heat samples, were removed from the candidate list. From the remaining 1425 proteins, only the ones, which were present in three GFP-SKD1 replicates of one condition, were included (control: 146, heat: 132). The majority of proteins were present in both lists. (159, in at least two replicates) while 15 were control specific and 18 were heat specific (in none or one replicate of the other condition). Differences in relative

protein abundances between control and heat treated samples were analyzed, if at least two values were measured for each condition (Students-T analysis, present in two replicates). No significant differences were identified between the samples and q-values (p-values corrected for multiple testing) were all above the cutoff value (5% false discovery rate, q-value  $\leq 0.05$ ).

Gene ontology (GO) analysis was performed using the PANTHER classification System (Thomas et al., 2003; Mi et al., 2010). The classification was performed using default settings and candidate lists were compared to the whole *A. thaliana* genome. Overrepresented classes (q-value  $\leq 0.05$ ) within the PANTHER GO-Slim Biological Process and Cellular Component categories were listed with the number of identified proteins and the fold enrichment relative to the number of all *A. thaliana* protein in this class.

In addition to the GO analysis, the interactome candidates were individually classified. For this, annotations and literature were analyzed for each candidate using TAIR (Appendix, Table A.10). Based on the identified annotations and the aim of analysis (identification of membrane trafficking and mRNP granule proteins), proteins were grouped in following categories: protein folding, protein processing, membrane trafficking, RNA metabolism, mitochondria and chloroplast, and others. Proteins in the others category are not necessarily lacking description or are not annotated, but were not able to be grouped in one of the before mentioned classes. The subcellular localization of the candidates was either described in the literature or predicted by SUBA4 consensus prediction (Subcellular Localization Database For *Arabidopsis* Proteins, Hooper *et al.*, 2017).

### **2.8.4 Statistical analysis**

Statistical analysis was done with RStudio (RStudio: Integrated Development for R. RStudio, Inc., Boston, MA). Datasets were tested for normality using Shapiro-Wilk-test. The Welch's two sample t-test was used for significance analysis between normally distributed datasets. The Wilcoxon-Mann-Whitney-test was used to compare normally distributed set to not normally distributed sets.

### 3 Results

#### 3.1 Y2H of ESCRTIII core and associated proteins with mRNP granule components.

A recent study in our group showed that the SPI protein is a positive regulator of protein transport from MVBs to the lytic vacuole in *A. thaliana*. This positive effect is executed by direct interaction with LIP5 and their synergistic activation of SKD1 enzyme activity (Steffens et al., 2017). Furthermore, the SPI protein was found to directly interact with the P-body core protein DCP1 and to regulate P-body assembly during salt stress (Steffens et al., 2015). This link of MVB protein trafficking and P-body formation raised the question whether other proteins involved in MVB biogenesis and P-body formation interact with each other. This question was addressed by an Y2H assay which pointed to a potential protein-protein interaction network between members of the ESCRT system and proteins found in P-bodies (A. Steffens, unpublished).

**Table 3.1. Previously identified protein interactions of ESCRTIII and P-body components.**

		P-bodies					
		DCP1	DCP2	DCP5	VCS	eIF4E1	XRN4
<b>ESCRTIII</b> associated	<b>LIP5</b>	-	-	-	-	-	-
	<b>SKD1</b>	<b>interaction</b>	<b>interaction</b>	<b>interaction</b>	-	<b>interaction</b>	-
	<b>VPS46.1</b>	<b>interaction</b>	-	<b>interaction</b>	-	-	-
	<b>VPS46.2</b>		-	<b>interaction</b>	-	-	-
<b>ESCRTIII</b> core	<b>VPS20.1</b>	-	-	<b>interaction</b>	-	-	-
	<b>VPS24.1</b>	-	-	<b>interaction</b>	-	-	<b>interaction</b>
	<b>VPS32.1</b>	<b>interaction</b>	-	-	-	-	<b>interaction</b>
	<b>VPS32.2</b>	-	-	-	-	<b>interaction</b>	<b>interaction</b>

Table 3.1 summarizes the preliminary results testing interactions of ESCRTIII core and associated proteins with P-body proteins. The proteins SKD1, VPS46.1, VPS46.2, VPS20.1, VPS24.1, VPS32.1, and VPS32.2 showed interactions with at least one P-body protein. SKD1

showed the highest number of interactions (DCP1, DCP5, DCP2, and eIF4E) while LIP5 showed no interactions.

To confirm and further investigate a potentially broad interaction between ESCRTIII and P-body proteins, an exhaustive Y2H assay was performed. ESCRTIII core (VPS20.1, VPS24.1, VPS32.1, VPS32.2, VPS2.1, VPS2.2, and VPS.2.3) and ESCRTIII associated proteins (SKD1, LIP5, VPS46.1, VPS46.2, VPS60.1, and VPS60.2) were tested for potential protein interactions with known P-body proteins (DCP1, DCP2, DCP5, XRN4, and eIF4E). The analysis was extended to proteins found in SGs (UBP1b, PAB2, RBP47bb, GRP7, RBP45bb, and GRP2). The mammalian homolog of eIF4E has been found in both, P-bodies and SGs (Ferraiuolo et al., 2005; Kedersha et al., 2005). In the context of this study, it is classified as a P-body protein. The ESCRTIII proteins were fused to the GAL4-BD while the mRNP granule components were fused to the GAL4-AD.

**Table 3.2. Summary of tested ESCRTIII protein interactions with mRNP granule proteins.**

GAL4-AD \ GAL4-BD		P-bodies						SGs					
		DCP1	DCP2	DCP5	VCS	eIF4E1	XRN4	UBP1b	PAB2	RBP47 <sub>b</sub>	GRP7	RBP45 <sub>b</sub>	GRP2
ESCRTIII associated	LIP5	5mM	-	5mM	-	-	-	-	5mM	5mM	15mM	5mM	-
	SKD1	-	-	-	-	-	-	-	-	-	-	-	-
	VPS46.1	-	-	-	-	-	-	-	-	-	-	-	-
	VPS46.2	-	-	-	-	-	-	-	-	-	-	0mM	-
	VPS60.1	30mM	-	-	30mM	-	-	-	30mM	-	-	30mM	-
	VPS60.2	30mM	-	-	30mM	-	-	30mM	30mM	-	-	30mM	-
ESCRTIII core	VPS20.1	-	-	-	-	-	-	-	-	-	-	-	-
	VPS24.1	-	-	-	-	-	-	-	-	-	-	-	-
	VPS32.1	-	-	-	-	-	-	-	-	-	-	-	-
	VPS32.2	-	-	-	-	-	-	-	-	-	-	-	-
	VPS2.1	-	-	-	-	-	-	-	-	-	-	-	-
	VPS2.2	-	-	-	-	-	-	-	-	-	-	-	-
	VPS2.3	-	-	-	-	-	-	-	-	-	-	-	-

Table 3.2 summarizes the obtained results of this study. Each interaction was tested with at least two biological and two technical replicates. A combination was determined as a positive protein interaction if in at least half of the tests colony growth was present on the interaction medium. Further, colony growth needed to occur at a higher 3-AT concentration than in the corresponding negative control (GFP fused to the GAL4-AD). The highest 3-AT concentration, which still allowed colony growth, is indicated in the Table.

In contrast to the previously assessed data, only few potential interactions were identified. While none of the tested ESCRTIII core proteins showed interactions with the different mRNP granule components, some interactions were observed for the ESCRTIII associated proteins: LIP5 interacts with DCP1, DCP5, PAB2, RBP47b, GRP7, and RBP45b. The VPS46.1 protein interacts with RBP45b, VPS60.1 with DCP1, VCS, PAB2, and RBP45b. VPS60.2 interacts with DCP1, VCS, UBP1B, PAB2, and RBP45b. The positive interactions of VPS60.1 and VPS60.2 have to be taken with caution since both proteins showed autoactivation in the negative controls, reaching even a 3-AT concentration of 30 mM in one experiment (Appendix, Table A.2). SKD1, which showed the highest number of potential interactions in previous studies, showed none in this analysis. However, several potential protein interactions with P-body and SG proteins were identified for its direct interactor and regulator LIP5.

Similar to their yeast and mammalian homologues, the *A. thaliana* LIP5, VPS46 and VPS60 proteins have been categorized as ESCRTIII associated proteins based on their function in SKD1 activity regulation (Hurley and Hanson et al., 2010, Richardson et al., 2011). The loss of LIP5, VPS46.1, or VPS46.2 (single mutants) has no consequences for plant growth under normal conditions (Haas et al., 2007; Spitzer et al., 2009). In contrast to that, SKD1 loss seems to be lethal in *A. thaliana* since no homozygous mutant has been isolated so far. Further, studies in plant cells using a dominant-negative variant of SKD1 showed that the loss of SKD1 function inhibits protein trafficking to the vacuole and causes the formation of aberrantly large MVBs called class E compartments (Haas et al, 2007; Shahriari et al., 2010). These attributes make SKD1 a key component of ESCRT-mediated trafficking in *A. thaliana*.

Though this study did not confirm direct potential interactions of SKD1 with mRNP granule components, the essential role of SKD1 in MVB trafficking, combined with the fact that regulators of SKD1 interact with mRNP components, make it an interesting candidate to further study the relation between ESCRTIII proteins and mRNP granules.

### 3.2 Heat-dependent subcellular protein localization of SKD1

The investigation of a potential link between ESCRTIII proteins and mRNP granules was continued by studying the subcellular localization of SKD1 after a treatment which is known to induce and/or increase mRNP formation.

SKD1 in its native form and in fusion with fluorescent proteins has been described to be evenly distributed in the cytosol and to occasionally localize in dot-like structures representing MVBs (Haas et al., 2007). The majority of the signal is found in the cytosol, illustrating the transient association of SKD1 with MVBs (Shahriari et al., 2010). Further, a nuclear localization of SKD1 has been described. This has been interpreted as partial degradation artifact of SKD1 in fusion with GFP (Haas et al., 2007). However, new studies reveal that the mammalian homolog of SKD1 and other ESCRTIII proteins function in nuclear envelope maintenance, providing an alternative explanation for SKD1 signal in *A. thaliana* nuclei (Olmos et al., 2015; Vietri et al., 2015).

For the localization study by confocal microscopy, SKD1 was fused with YFP at the C-terminus (SKD1-YFP). A putative SKD1 promoter fragment (1.2 kb upstream of the *A. thaliana* SKD1 start codon) was used for gene expression. *A. thaliana* epidermal leaf cells were transiently transformed by particle bombardment.

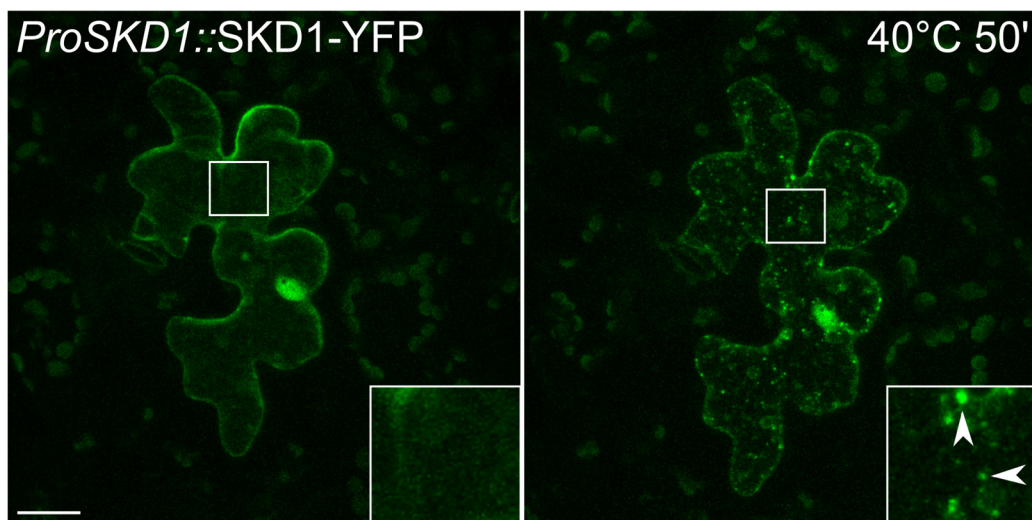


**Figure 3.1. Subcellular localization of SKD1-YFP.** Epidermal cells of *A. thaliana* Col-0 rosette leaves were transiently transformed by particle bombardment with a construct expressing SKD1-YFP under the control of the putative *A. thaliana* SKD1 promoter. Cells were imaged by confocal microscopy with the same laser intensities before (left column) and after heat treatment at 40°C for 50' (right column). Depicted are maximum projections of stacks. Arrow heads indicate SKD1-YFP labeled granules after heat treatment. Bar = 20  $\mu$ m.

As shown in Figure 3.1, SKD1-YFP was mainly present in the cytosol and nearly no dot-like structures were visible, which is in accordance with previous localization studies. In addition, a nuclear signal was visible.

The localization analysis was extended to stress conditions known to initiate mRNP granule formation. An easily applicable and robust way to induce mRNP granule formation is heat treatment. For this, a temperature of approximately 40°C is usually used in *A. thaliana* localization studies. Treatment duration is more variable (40' to 90', Bhasin and Hülskamp, 2017, Motomura et al., 2015). A heat stress treatment at 40°C for 50' was chosen for this study.

Upon heat stress, the overall signal intensity of SKD1-YFP was comparable to the one of non-stressed cells, indicating no drastic increase of protein levels. However, the localization changed. In addition to the cytosolic and nuclear signal, structures, which can be described as dot-like or granular, were observed. Their size averaged at  $0.547 \pm 0.333 \mu\text{m}^2$  (50 structures/cell, data from two cells). Plane-by-plane analyses of the stacks point to a distribution of the dots at the cell periphery rather than within the central vacuole. Therefore it is likely that the granular structures are located within the cytosol.

In order to exclude the possibility that the heat-dependent shift of localization is caused by the method of transformation (particle bombardment), an *A. thaliana* line stably expressing SKD1 was analyzed. The established Col-0 line overexpressing GFP-SKD1 under the *35S CaMV* promoter was used (Haas et al., 2007).

Figure 3.2 shows the localization of GFP-SKD1 in epidermal leaf (upper row) and root cells (lower row). Again, under non-stress conditions, the GFP-SKD1 protein localizes to the nucleus and cytoplasm and is found in granular structures after heat treatment. This result reinforces the observation that the SKD1 protein changes its subcellular localization upon heat treatment independent of transformation method, tissue, expression strength, or the orientation of modification (C-terminal or N-terminal modification).

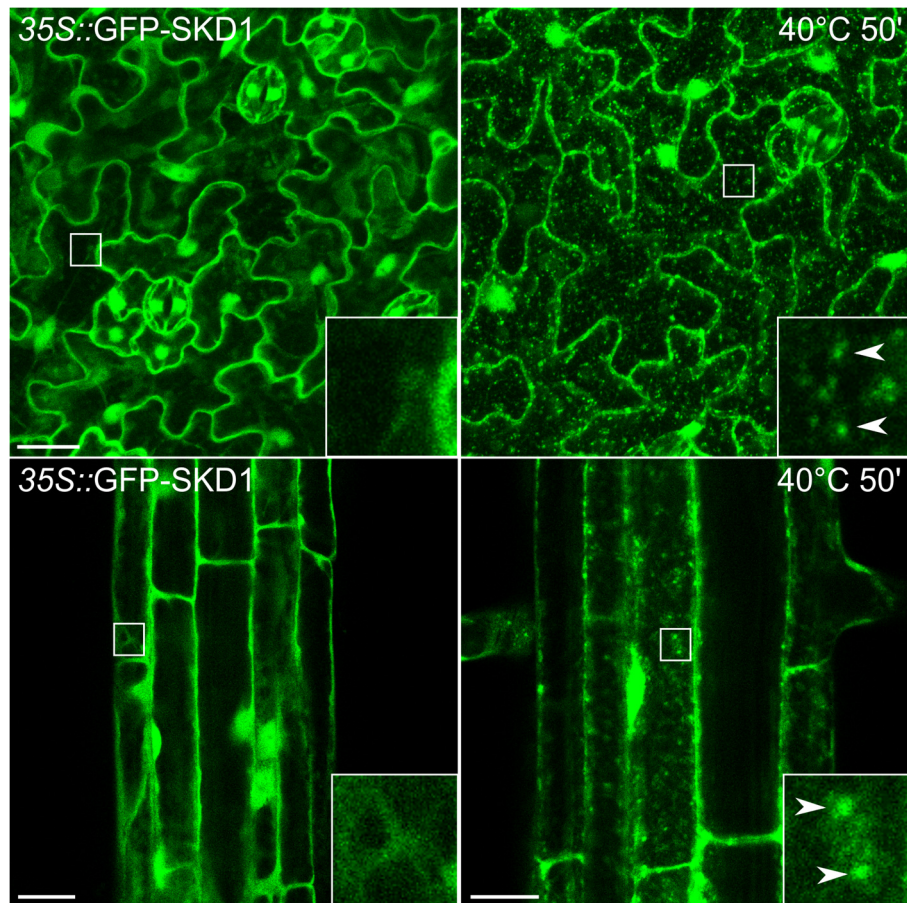


**Figure 3.2. Subcellular localization of GFP-SKD1 in transgenic *A. thaliana* plants.** Col-0 plants stably overexpressing GFP-SKD1 (*35S::GFP-SKD1*) were used for analysis (Haas et al., 2007). The localization of the GFP-SKD1 protein was evaluated by confocal microscopy in epidermal cells of rosette leaves (upper row) and roots (lower row) of 7 d old seedlings grown on vertical  $\frac{1}{2}$  MS plates before (left columns) or after (right column) heat treatment (40°C for 50'). Same leaves/roots, but not the exact same areas were analyzed before and after heat treatment and laser intensities were adjusted. Depicted are maximum projections of stacks for epidermal leaf cells and single planes for epidermal root cells. Arrow heads indicate GFP-SKD1 granules after heat treatment. Bar = 20  $\mu$ m

The next step was to further investigate the identity of the granular structures in which SKD1 localizes in. SKD1 is known to mediate the final step of intraluminal vesicle formation at late endosomes, thereby creating MVBs (Gao et al., 2017). Further, SKD1 has been described to be occasionally visible at MVBs in fluorescent studies (Haas et al., 2007, Shahriari et al., 2010). Therefore, it is conceivable that the heat-induced granular structures might represent MVBs. To test this hypothesis, roots of the stable *35S::GFP-SKD1* line were stained with the styryl dye FM4-64. FM4-64 is a well-known and widely used membrane staining dye to study endocytic processes and endomembrane system dynamics. Upon exposure to FM4-64, the plasma membrane is immediately stained and the dye is distributed via endocytic processes throughout the vesicular network (including the tonoplast). When integrated into the outer layer

of phospholipid bilayer membranes, FM4-64 becomes fluorescent (Bolte et al., 2004). If the heat-induced SKD1 granules are membranous (like MVBs), a local increase of FM4-64 signal is expected.

A representative staining result (five roots analyzed) is depicted in Figure 3.3. Again, GFP-SKD1 is visible in heat-induced granules in the cytosol. The FM4-64 signal is in distinct dot-like structures. In addition, signal is detectable at the periphery of the cells, outlining the cell shape (staining of tonoplast and/or PM). Interestingly, no local FM4-64 signal increase at the site of GFP-SKD1 granules is observable. This suggests that the distinct structures stained by FM4-64 and the GFP-SKD1 labeled granules represent two different populations. These findings suggest that heat stress-induced SKD1 granules are membrane-free structures.

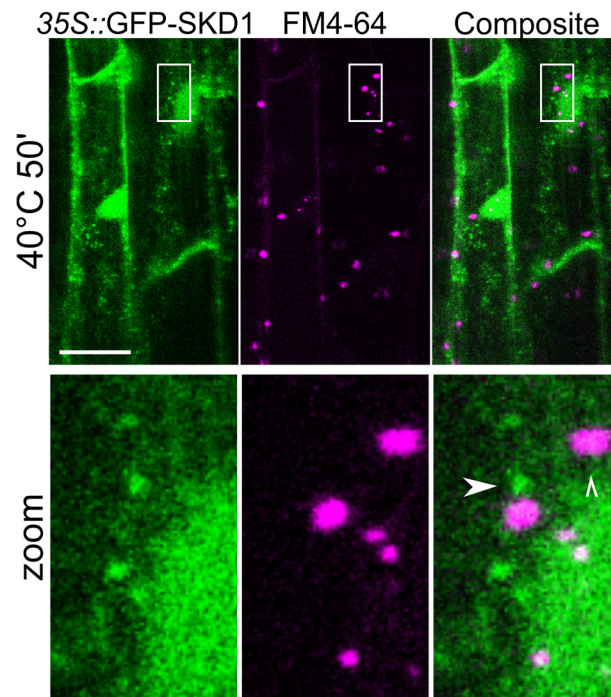


**Figure 3.3. FM4-64 staining of 35S::GFP-SKD1 roots.** Roots of 35S::GFP-SKD1 plants grown for 5 or 7 d on vertical ½ MS were stained with 50 µM FM4-64 in ½ MS liquid medium for 5 minutes. Roots were incubated at room temperature for 2 h and then subjected to heat treatment (40°C for 50'). Root epidermal cells of the proximal transformation zone/early elongation zone were analyzed by confocal microscopy. Depicted are single planes. Arrow heads indicate GFP-SKD1 labeled granules and empty arrow heads indicate structures stained by FM4-64. Bar = 20 µm.

### **3.3 Colocalization of SKD1 with P-body, SG, and endosomal marker proteins**

The above described results suggest that heat stress triggers SKD1 to localize in membrane-free granular aggregates in the cytosol. A hallmark of mRNP granules is the absence of a structure-limiting membrane and since SPI, the direct interactor of SKD1, localizes to P-bodies upon cellular stress, it is conceivable to presume that SKD1 also localizes to mRNP granules. This part of the study tested a potential association of SKD1 with mRNP granules by colocalization analyses with different marker proteins of P-bodies and SGs. In addition, the localization of well-established endosomal marker proteins in the context of mRNP granules was examined.

#### **3.3.1 Colocalization of SKD1 with mRNP proteins in transient double transformations**

In a first step to further assess the identity of the heat stress-induced SKD1 granules, a colocalization study was performed. For this, epidermal cells of Col-0 rosette leaves were double transformed by particle bombardment with a construct overexpressing SKD1 in C-terminal fusion with YFP or mCHERRY and a construct overexpressing either the P-body protein DCP1 in C-terminal fusion with CFP, DCP5 in C-terminal fusion with YFP or eIF(iso)4E in N-terminal fusion with YFP. DCP1 and DCP5 are both positive regulators of the decapping enzyme DCP2 and crucial components of the decapping complex in *A. thaliana* (Xu et al., 2006, Xu and Chua, 2009). As mentioned before, the mammalian elongation initiation factor eIF4E has been found in SGs and P-bodies and was used as a P-body protein in the context of this study (Ferraiuolo et al., 2005; Kedersha et al., 2005). Here, the plant-specific family member eIF(iso)4E was used for colocalization analysis.

Figure 3.4 depicts representative results for DCP1, DCP5 and eIF(iso)4E localization. DCP1-CFP localized in large and distinct granular aggregates in the cytosol which represent P-bodies (Xu et al., 2006). As seen before, SKD1-YFP showed a cytosolic distribution and a nuclear signal. In contrast to single transformations, few large aggregates of SKD1-YFP protein were visible under non-stress conditions and these aggregates colocalized with DCP1-CFP. Previous observations of DCP1 overexpression in plant cells showed that DCP1 can recruit even weakly interacting proteins into P-bodies (D. Gagliardi, personal communication). This phenomenon might also be seen here for SKD1-YFP. After heat stress treatment, more granular SKD1-YFP structures were visible which strongly colocalized with DCP1-CFP.

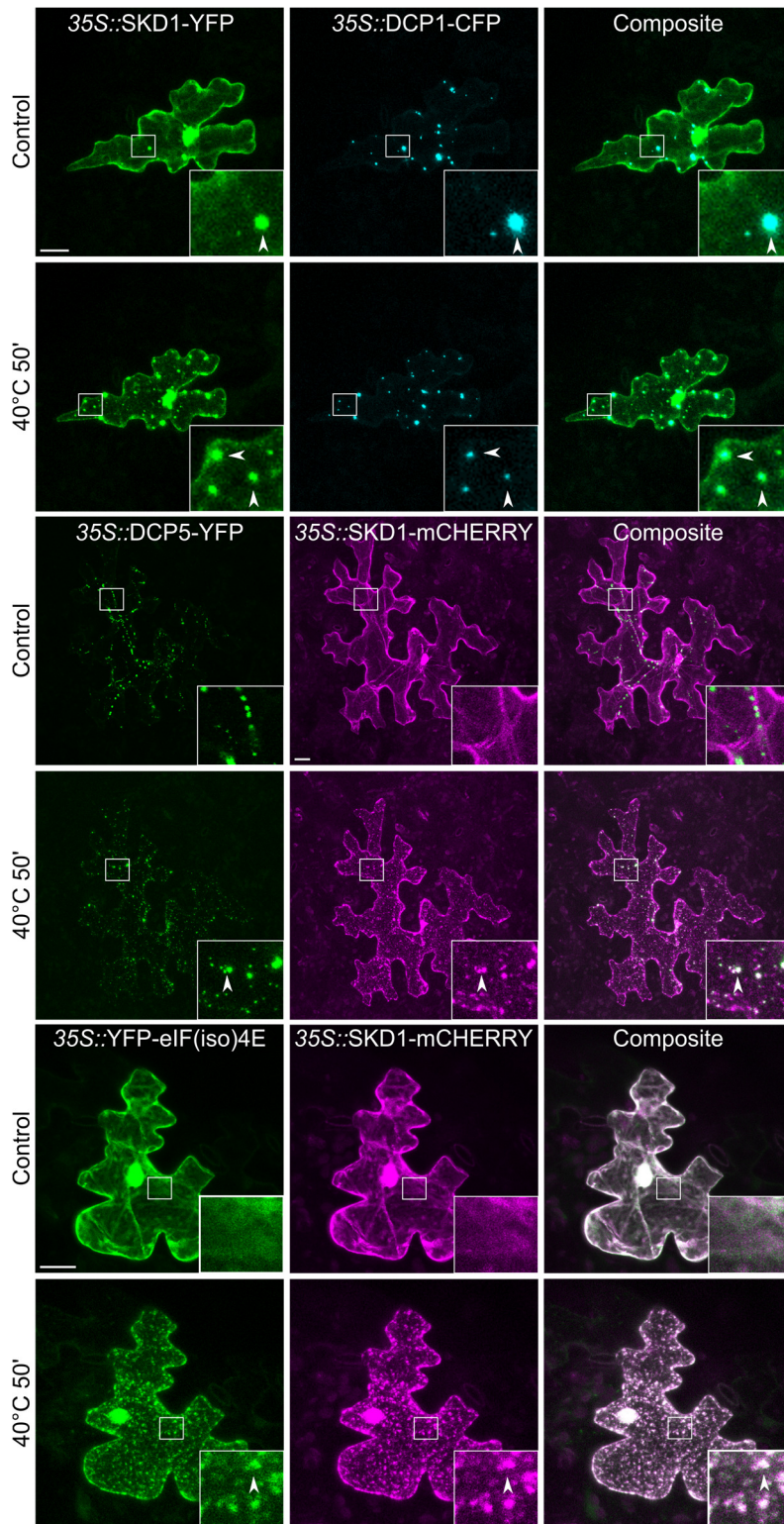


**Figure 3.4. Colocalization of SKD1 with P-body marker proteins.** Epidermal cells of *A. thaliana* Col-0 rosette leaves were transiently transformed by particle bombardment with a construct overexpressing either SKD1-YFP (row 1-2) or SKD1-mCHERRY (row 3-6). In addition, cells were either cotransformed with a construct overexpressing DCP1-CFP (row1-2), DCP1-YFP (row3-4), or YFP-eIF(iso)4E (row 5-6). The same cells were imaged by confocal microscopy with the same laser intensities before and after heat treatment at 40°C for 50'. Depicted are representative maximum projections of stacks. Arrow heads indicate colocalizing structures. Bar = 20  $\mu$ m.

Similar to DCP1, DCP5-YFP localized to granular structures in the cytosol. In comparison to DCP1, they appeared to be smaller in size and to increase in number upon heat stress. In contrast to DCP1, the coexpression of DCP5-YFP did not induce any aggregation of SKD1-mCHERRY in the absence of stress. Heat stress induced the colocalization of SKD1-mCHERRY and DCP5-YFP in granules.

The YFP-eIF(iso)4E proteins exhibited a different localization than DCP1 and DCP5. It was evenly distributed in the cytosol and nucleus and shifted to a granular localization, which coincided with SKD1, upon heat stress treatment. This pattern of localization is reminiscent of SG marker proteins (aggregation under stress) rather than P-body proteins (aggregation also in the absence of stress, Stoecklin and Kedersha, 2013). Thus, the *A. thaliana* eIF(iso)4E protein might not be primarily found in P-bodies but in SGs.

In addition to the P-body marker proteins, SKD1 was tested for colocalization with the stress granule proteins UBP1b, RBP47b, and PAB2. UBP1b is a component of pre-mRNA splicing and shares sequence homology with the mammalian TIA1. It localizes in the nucleus and is transported into the cytoplasm where it aggregates in stress granules upon heat stress. RBP47b is also a TIA1 homolog and has been shown to localize to SGs upon heat stress (Lambermon et al., 2000; Weber et al., 2008). PAB proteins are universal core components of SGs in eukaryotes and the *A. thaliana* PAB2 protein localizes in the cytosol under non-stress conditions and is found in SGs upon hypoxia as well as heat stress (Anderson and Kedersha, 2008; Sorenson and Bailey-Serres, 2014; Bhasin and Hülkamp, 2017).

As described in the literature, mCHERRY-UBP1b is visible in the nucleus under non-stress conditions and undergoes a localization shift to granular structures in the cytosol (SGs) under heat stress (Figure 3.5). Cotransformed SKD1-YFP is also present in granular structures after heat stress which strongly colocalize with the mCHERRY-UBP1b protein. This shift in SKD1 localization can be accounted to the protein characteristics of SKD1 rather than the fused YFP, since localization studies of overexpressed free YFP with mCHERRY-UBP1B do not show aggregation of YFP upon heat stress treatment (see Appendix, Figure A.1).

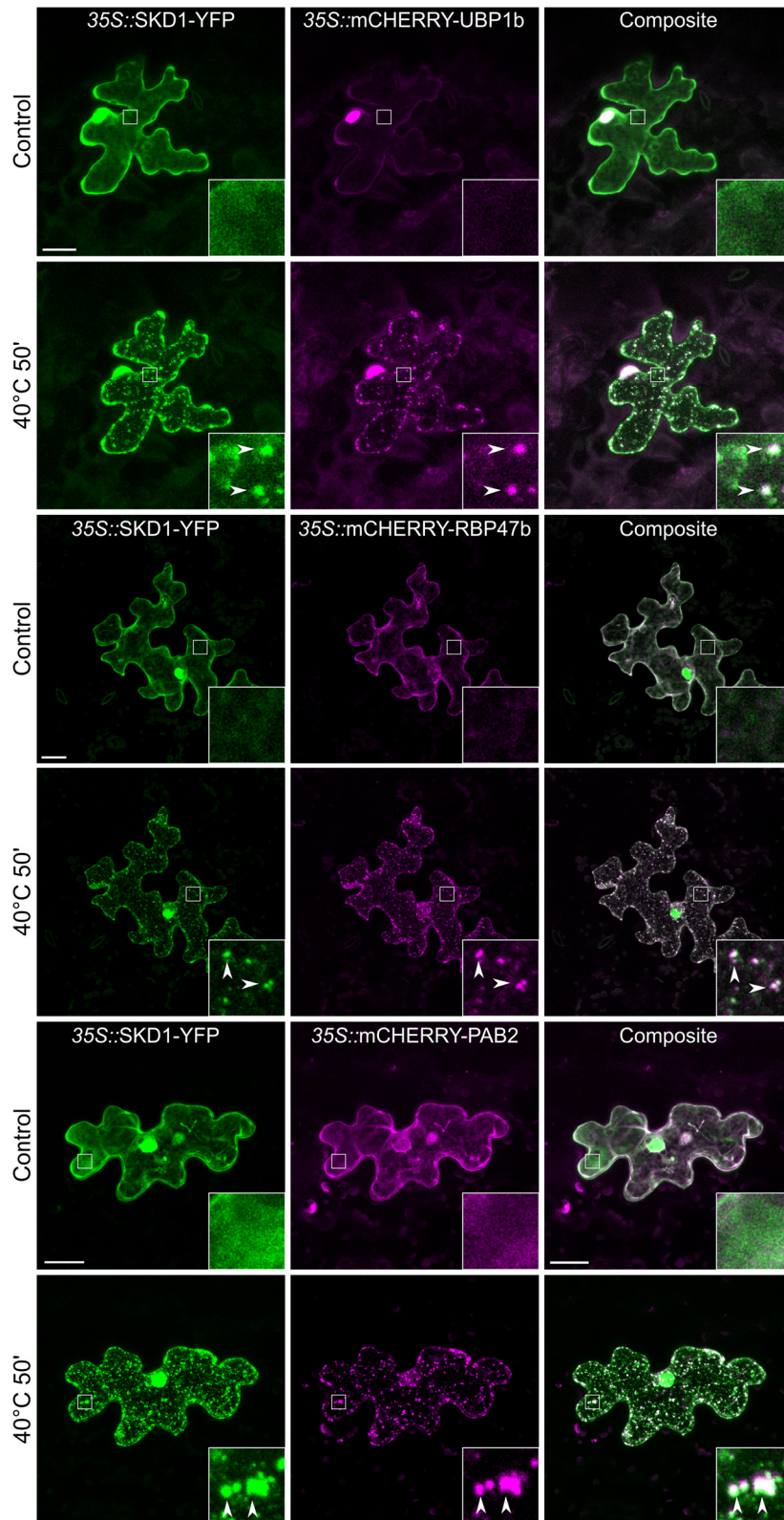


**Figure 3.5. Colocalization of SKD1 with SG marker proteins.** *A. thaliana* Col-0 rosette leaves were transiently transformed with a construct overexpressing SKD1-YFP. In addition, cells were either cotransformed with a construct overexpressing mCHERRY-UBP1b (row1-2), mCHERRY-RBP47b (row3-4), or mCHERRY-PAB2 (row 5-6). The same cells were imaged by confocal microscopy with the same laser intensities before and after heat treatment at 40°C for 50'. Depicted are representative maximum projections of stacks. Arrow heads indicate colocalizing structures. Bar = 20  $\mu$ m.

*A. thaliana* RBP47b was shown to localize in the nucleus and to SGs upon heat stress (Weber et al., 2008). In this study, mCHERRY-RBP47b was not present in the nucleus but dispersed in the cytosol. Nonetheless, heat stress induced the formation of mCHERRY-RBP47b-labeled granules which colocalized with SKD1-YFP. The mCHERRY-PAB2 protein localized to the cytosol and in granules after heat stress treatment which also coincided with SKD1-YFP granules.

In addition to the double transient transformations, the stable *35S::GFP-SKD1* line was transiently transformed with the construct overexpressing mCHERRY-UBP1b. The fact that the particle bombardment method transforms only single cells allowed a side-by-side comparison of cells only expressing GFP-SKD1 and a cell additionally expressing mCHERRY-UBP1b.

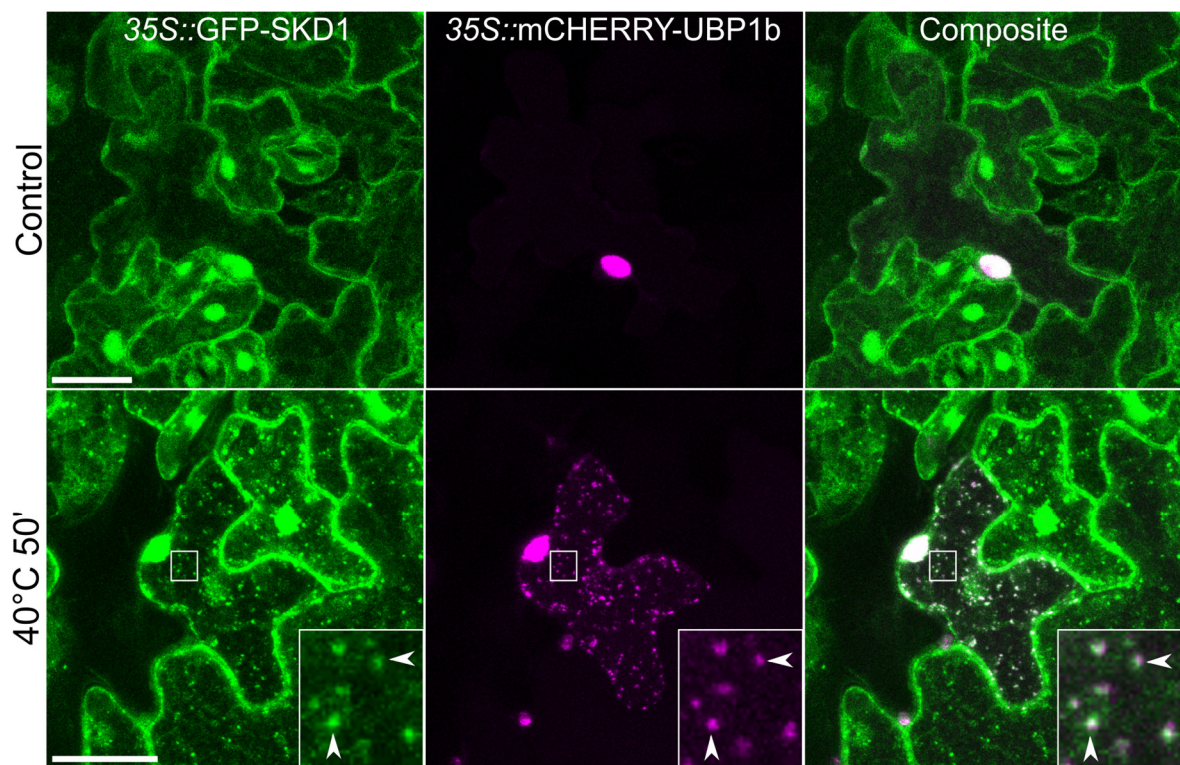


**Figure 3.6. Transient transformation of *35S::GFP-SKD1* leaves with mCHERRY-UBP1b.** Epidermal leaf cells of the stable *35S::GFP-SKD1* line were transiently transformed by particle bombardment with a construct overexpressing mCHERRY-UBP1b. Different cells were imaged by confocal microscopy before and after heat treatment at 40°C for 50'. Depicted are representative maximum projections of stacks. Arrow heads indicate colocalizing structures. Bar = 20  $\mu$ m.

The single transient transformation of mCHERRY-UBP1b exhibited the same localization as the double transient transformation: The mCHERRY-UBP1b protein is in the nucleus before and in granules after heat stress. Again, GFP-SKD1 strongly colocalizes with mCHERRY-UBP1B in the granules (Figure 3.6). The GFP-SKD1 labeled granules in the neighboring cells resemble the ones in the transiently transformed cell in size and number, providing evidence that the coexpression of UB1B does not influence the localization of GFP-SKD1.

In summary, the observed colocalization of SKD1 with P-body and SG granule marker indicates that the SKD1 protein does associate with mRNP granules during heat stress.

### **3.3.2 Colocalization quantification of SKD1 with mRNP granule markers**

To further evaluate the association of SKD1 with different mRNP granule marker proteins, their colocalization after heat treatment was quantified. By this, potential differences in colocalization were investigated. Stacks of transiently double transformed leaf epidermal cells were generated and ROIs containing granules were defined as described in Chapter 2.8.1. The Pearson's correlation coefficient (PCC) was used for granule colocalization quantification (Manders et al., 1992).

Positive and negative controls are recommended in quantitative colocalization studies to permit a meaningful interpretation of the obtained results. Here, constructs overexpressing YFP-UBP1b and mCHERRY-UBP1b were double transformed and evaluated for colocalization. The images of mCHERRY-UBP1b were rotated by 180° and again analyzed for colocalization, mimicking random colocalization. In addition to the double transformation of YFP-UBP1b and mCHERRY-UBP1b, cells were double transformed with YFP-UBP1b and mCHERRY-PAB2. Thereby it was possible to estimate the colocalization coefficient that can be expected for two proteins known to localize to SGs.

A PCC of 1 indicates absolute co-occurrence of signals in two channels, a value of -1 represents exclusive signal occurrence (negative correlation), and a value of 0 indicates a random distribution of signals. In this study, the highest level of colocalization was detected for the positive control (YFP-UBP1b/mCHERRY-UBP1b) with a mean correlation coefficient of 0.75 ( $\pm 0.1$  standard deviation). This value represents maximal measurable colocalization within the experimental setup. The measurement of the negative control (UBP1b/UBP1b tilt) gave a coefficient of 0.02 ( $\pm 0.08$ ) and all measured coefficients were significantly higher than the negative control (Table 3.3).

## Results

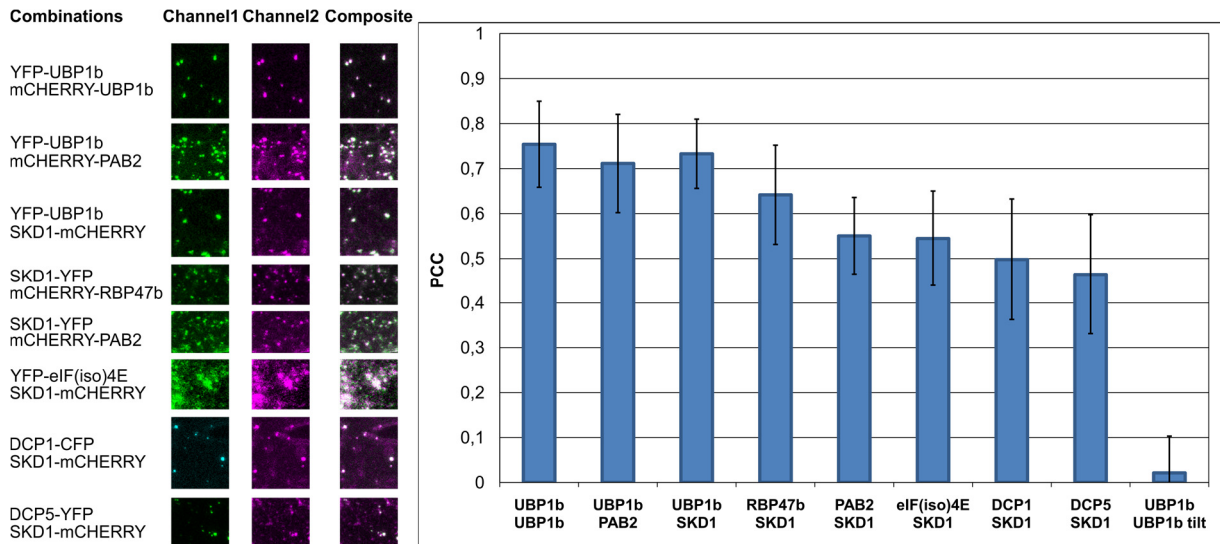


**Figure 3.7. Colocalization quantification of SKD1 with mRNP granule markers after heat stress.** Epidermal leaf cells of Col-0 plants were transiently double transformed by particle bombardment for colocalization quantification. All used constructs overexpressed the respective protein under the control of the *35S CaMV* promoter. The SKD1 protein was expressed in C-terminal fusion with YFP or mCHERRY and an mRNP granule marker fused to another fluorescent protein was cotransformed (YFP-UBP1b, mCHERRY-RBP47b, mCHERRY-PAB2, YFP-eIF(iso)4E, DCP1-CFP, or DCP5-YFP). The transformed cells were subjected to heat stress treatment at 40°C for 50' and maximum projections of stacks were generated. For each combination, 10 cells were imaged and three ROIs were analyzed for fluorescent signal overlap using the PCC (ImageJ, JACoP). Representative ROIs of the different combinations are depicted on the left. The mean overlaps of the different combinations are shown in the histogram on the right. Error bars indicate standard deviation. As positive controls, cells were cotransformed with YFP-UBP1b and mCHERRY-UBP1b or mCHERRY-PAB2. As a negative control, one channel of the YFP/mCHERRY-UBP1b pictures was rotated by 180° before analysis.

The UBP1b and PAB2 overlap was similar to the one of the positive control ( $0.71 \pm 0.11$ ). Interestingly, the colocalization coefficient of SKD1 and UBP1b was also not significantly lower ( $0.73 \pm 0.08$ ). The colocalization of SKD1 with the other two SG markers, RBP47b ( $0.64 \pm 0.11$ ) and PAB2 ( $0.55 \pm 0.09$ ), was significantly lower than with UBP1b. The colocalization coefficient of SKD1 and eIF(iso)4E overlap ( $0.55 \pm 0.11$ ) was similar to the one with PAB2.

The P-body proteins DCP1 ( $0.5 \pm 0.14$ ) and DCP5 ( $0.46 \pm 0.13$ ) were comparable to each other in their overlap with SKD1 and showed no significant differences. Intermediate PCCs are often ambiguous and hard to interpret in terms of positive correlation. Since the maximal coefficient in this study was 0.754, all of the obtained values are relatively high and can be considered to represent positive correlation.

## Results

**Table 3.3. Statistical analysis of colocalization between transient double transformations.** All datasets were normally distributed with the exception of UBP1b-UBP1b (Shapiro-Wilk-test). Normally distributed datasets were evaluated for significant colocalization differences using the Welch's two sample t-test. For comparisons with the UBP1b/UBP1b dataset, the Wilcoxon-Mann-Whitney-test was used. Significance level are indicated as following: n.s. = not significant,  $p < 0.05 = *$ ,  $p < 0.01 = **$ ,  $p < 0.001 = ***$ ). Detailed p-values are listed in Appendix, Table A.4.

	UBP1b UBP1b	UBP1b PAB2	UBP1b SKD1	RBP47b SKD1	PAB2 SKD1	eIF(iso)4E SKD1	DCP1 SKD1	DCP5 SKD1	UBP1b UBP1b tilt
UBP1b UBP1b		n.s.	n.s.	***	***	***	***	***	***
UBP1b PAB2	n.s.		n.s.	*	***	***	***	***	***
UBP1b SKD1	n.s.	n.s.		***	***	***	***	***	***
RBP47b SKD1	***	*	***		***	***	***	***	***
PAB2 SKD1	***	***	***	***		n.s.	n.s.	**	***
eIF(iso)4E SKD1	***	***	***	***	n.s.		n.s.	*	***
DCP1 SKD1	***	***	***	***	n.s.	n.s.		n.s.	***
DCP5 SKD1	***	***	***	***	**	*	n.s.		***
UBP1b UBP1b tilt	***	***	***	***	***	***	***	***	

Overall, the quantification of SKD1 colocalization with mRNP granule markers showed a non-random localization of the observed overlaps. Furthermore, the localization of SKD1 correlates strongly with the localization of UBP1b and RBP47b after heat stress and, to a lesser extent, with PAB2, eIF(iso)4E, DCP1 and DCP5. The reduced colocalization of SKD1 with proteins known to be mainly present in P-bodies might indicate that the SKD1 localizes primarily to SGs after heat treatment and partially to P-bodies.

### 3.3.3 Colocalization quantification in transgenic marker lines

The results of the transient colocalization study showed that the SKD1 protein colocalizes to mRNP granules upon heat stress. To further validate these results, the localization of SKD1 in respect to an SG marker protein in stable transgenic lines was investigated. For this, the stable *35S::GFP-SKD1* line was crossed to a line overexpressing the PAB2 protein C-terminally fused to mRFP (*35S::PAB2-mRFP*, Sorenson and Bailey-Serres, 2014). The generated *35S::GFP-SKD1x35S::PAB2-mRFP* line was analyzed for colocalization in the F2 generation.

Representative images of leaf and root epidermal cells of the *35S::GFP-SKD1x35S::PAB2-mRFP* line before and after heat stress treatment are presented in Figure 3.8. GFP-SKD1 and PAB2-mRFP localize to the cytosol under non-stress conditions in both cell types. Similar to the transient results, PAB2-mRFP does not localize to the nucleus. Under heat stress, PAB2-mRFP changes its localization and is found in granular structures with GFP-SKD1. The majority of granules are labeled by both proteins. This result confirmed once more the heat-dependent colocalization of the SKD1 protein with SGs.

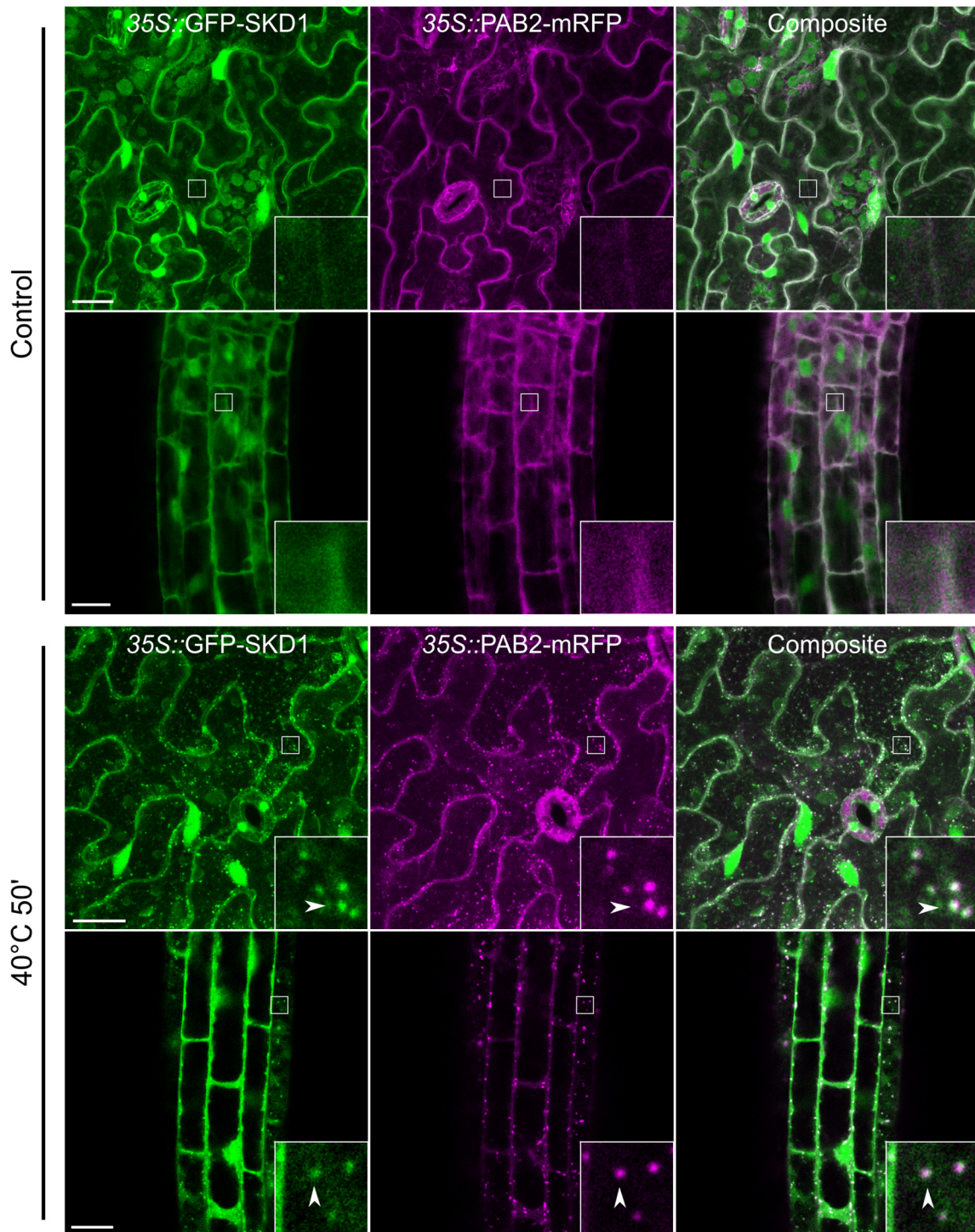


**Figure 3.8. Confocal imaging of *35S::GFP-SKD1* x *35S::PAB2-mRFP*.** The previously analyzed *35S::GFP-SKD1* line was crossed to a line expressing PAB2-mRFP under the *35S CaMV* overexpression promoter (*35S::PAB2-mRFP*, Sorenson and Bailey-Serres, 2014) and plants of the F2 generation were analyzed for subcellular protein localization. Epidermal cells of rosette leaves and root epidermal cells of 7 d old seedlings grown on vertical ½ MS plates were imaged by confocal microscopy before and after heat treatment (40°C for 50'). The same leaves/roots but not the exact same areas were analyzed before and after heat treatment. Depicted are maximum projections of stacks for leaf epidermal cells and single planes for epidermal root cells. Arrow heads indicate colocalizing structures. Bar = 20 µm.

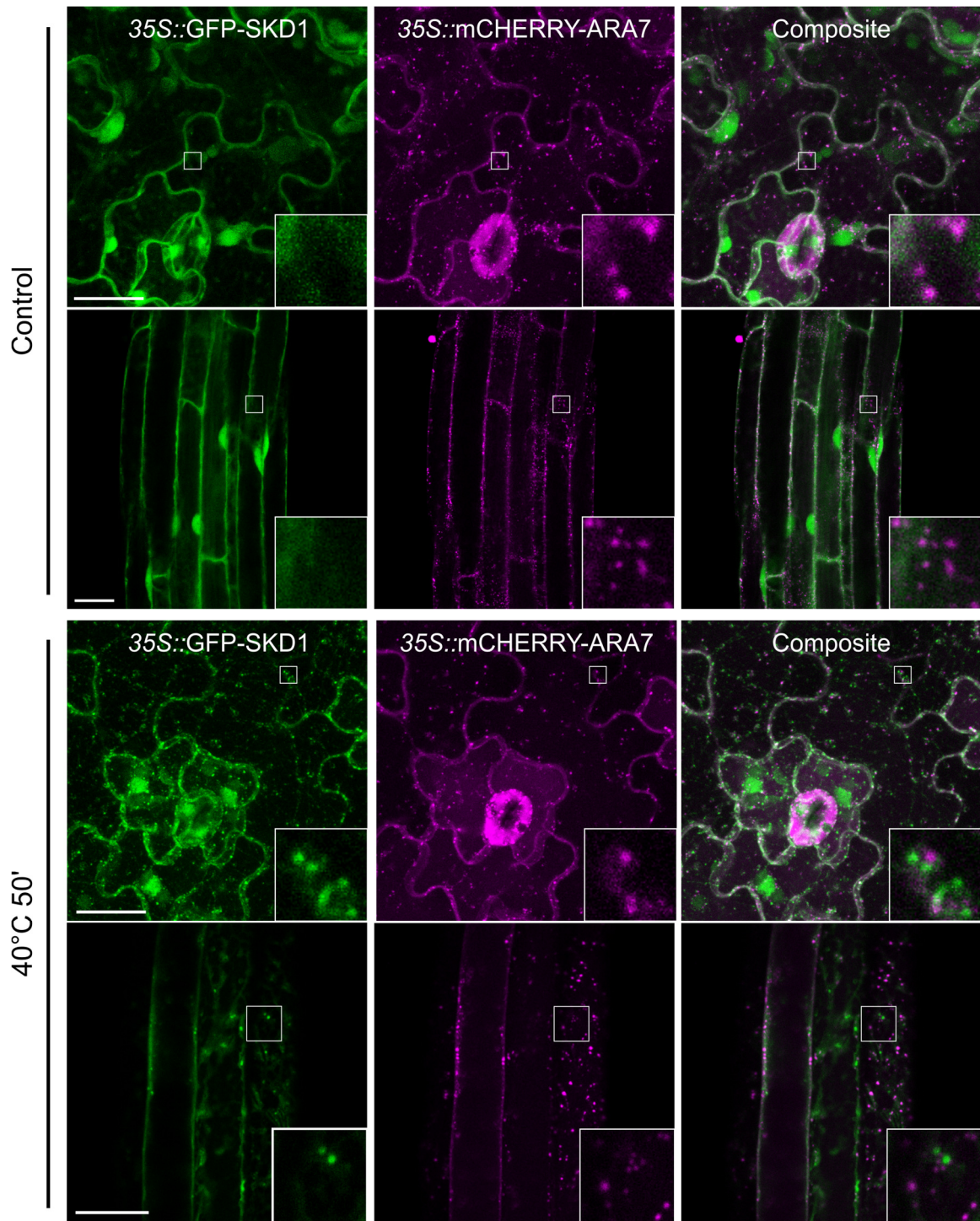


**Figure 3.9. Confocal imaging of the *35S::GFP-SKD1x35S::mCHERRY-ARA7* line.** The previously analyzed *35S::GFP-SKD1* line was crossed to a line overexpressing mCHERRY-ARA7 (*35S::mCHERRY-ARA7*, A. Steffens, unpublished) and plants of the F2 generation were analyzed for subcellular protein localization. The same leaves/roots but not the exact same areas were analyzed before and after heat treatment (40°C, 50'). Depicted are maximum projections of stacks for epidermal leaf cells and single planes for epidermal root cells. Bar = 20  $\mu$ m.

Another, so far not discussed, potential explanation for the granular localization of SKD1 after heat stress might be inhibited dissociation of SKD1 from MVB membranes. Under these circumstances, the colocalization of SKD1 with mRNP granules would rather represent a general colocalization of MVBs with mRNP granules. The observation that GFP-SKD1 granules are not stained by the membrane dye FM4-64 in *A. thaliana* roots (Chapter 3.2, Figure 3.3) weakens this hypothesis. Nonetheless, this possible explanation was further tested by analyzing the localization of heat-induced SKD1 granules in relation to the late endosomal marker protein ARA7/RabF2b, a plant Rab5-related GTPase (Ueda et al., 2001; Lee et al., 2004). The transgenic *35S::GFP-SKD1* line was crossed to a stable line expressing mCHERRY-ARA7 under the *35S* overexpression promoter (*35S::mCHERRY-ARA7*, A. Steffens unpublished). Epidermal leaf and root cells of the F2 generation were analyzed by confocal microscopy for heat-dependent protein localization.

As depicted in Figure 3.9, the simultaneous overexpression of mCHERRY-ARA7 does not influence the localization of GFP-SKD1, which is still present in the nucleus and evenly distributed in the cytosol under non-stress conditions. The ARA7 protein localizes to punctate structures in the cytosol, which have been characterized as MVBs in previous studies (Lee *et al.*, 2004). Upon heat stress, GFP-SKD1 is localized in granules which do not colocalize with the mCHERRY-ARA7-labeled structures. This result indicates that the SKD1 protein alone, rather than in association with MVBs, colocalizes to mRNP granules upon heat stress conditions.

The study was extended to a direct analysis of colocalization of well established mRNP granule markers and late endosomal markers. To this end, transgenic lines either expressing a fluorescently marked endosomal protein or a marked mRNP granule protein were crossed and F2 plants were analyzed by confocal microscopy. The SG marker line *35S::PAB2-mRFP* was crossed to a line overexpressing YFP-RHA1 (*35S::YFP-RHA1*, Gelder et al., 2009). RHA1 shares high amino acid similarity with ARA7 and is also involved in vacuolar trafficking and localizes to MVBs (Sohn et al., 2003, Lee et al., 2004). Further, the P-body marker line *35S::DCP5-TURQUOISE* (DCP5-mTQ, M. Jakoby unpublished) was crossed to the *35S::mCHERRY-ARA7* line. In addition, a *35S::DCP5-mTQx35S::PAB2-mRFP* line was generated. P-bodies and SGs are highly dynamical structures known to interchange proteins and mRNAs (Buchan and Parker, 2009). Thus, the DCP5 and PAB2 protein overlap was of interest.

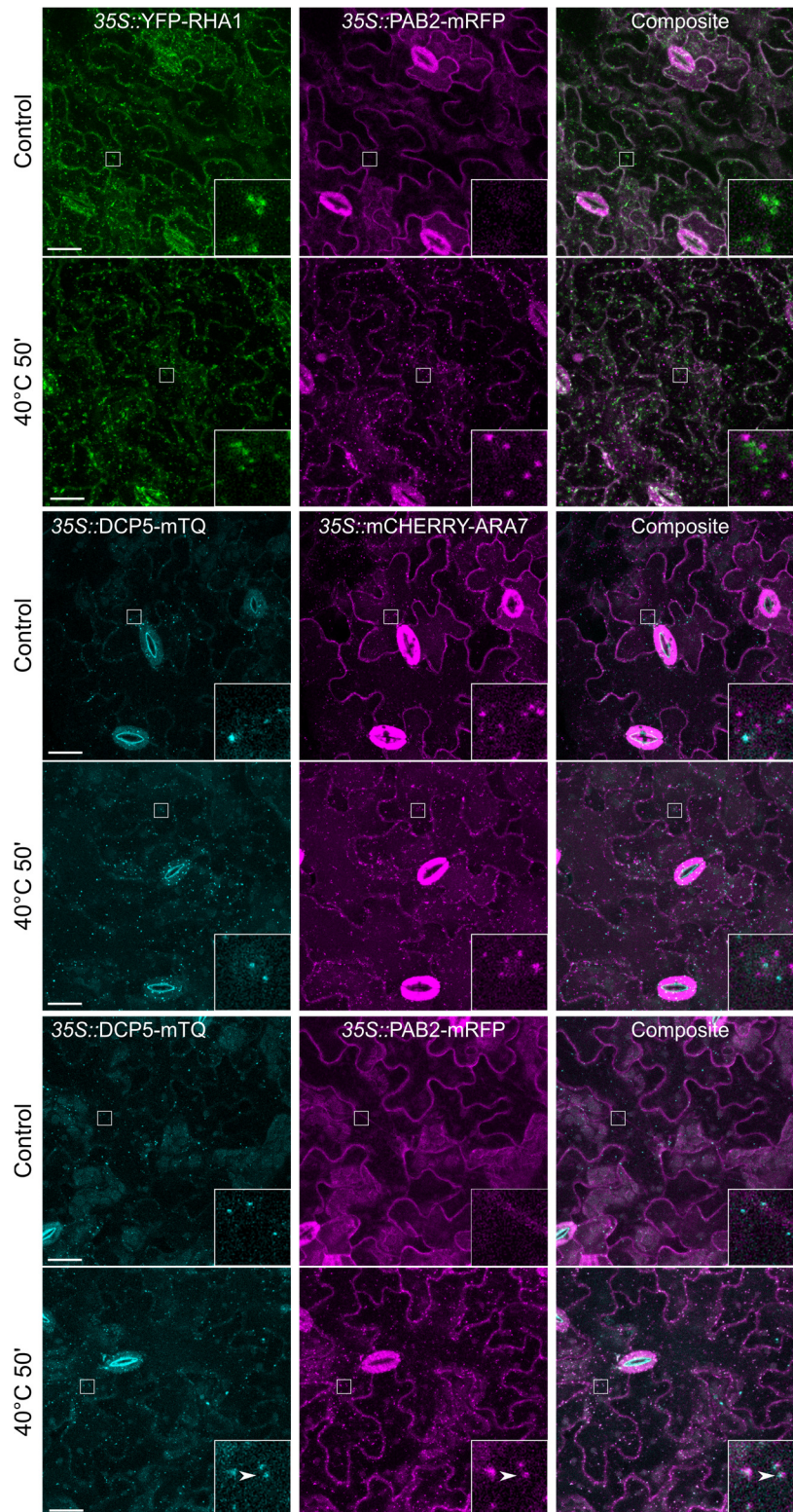


**Figure 3.10. Confocal imaging of crossed mRNP granule and endosomal marker lines.** Following stable lines expressing an endosomal marker (YFP-RHA1, mCHERRY-ARA7) and/or and mRNP granule marker (PAB2-mRFP, DCP5-mTQ) were generated by crossing: *35S::YFP-RHA1x35S::PAB2-mRFP* (row 1-2), *35S::DCP5-mTQx35S::mCHERRY-ARA7* (row 3-4), and *35S::DCP5-mTQx35S::PAB2-mRFP* (row 5-6). Plants of the F2 generation were analyzed for subcellular protein localization before and after heat treatment (40°C for 50'). The same leaves but not the exact same areas were analyzed before and after heat treatment. Depicted are maximum projections of stacks. Arrow heads indicate colocalizing structures. Bar = 20  $\mu$ m.

## Results

Representative pictures of the generated lines are shown in Figure 3.10. In the *35S::YFP-RHA1x35S::PABP-mRFP* transgenic line, the YFP-RHA1 protein localizes to distinct punctate structures in the cytosol, similar to ARA7. After heat stress treatment, PAB2-mRFP is also found in cytosolic granules, yet the YFP-RHA1 and PAB2-mRFP structures do not appear to co-occur within the cell. In the *35S::DCP5-mTQx35S::mCHERRY-ARA7*, both proteins localize in granular structures independent of heat stress, but neither under non-stress conditions nor after heat stress treatment, the structures appear to colocalize. In contrast, the DCP5-mTQ and PAB2-mRFP proteins showed a considerable degree of co-occurrence after heat treatment.

Similar to the transient colocalization study, the signal overlap of the different marker proteins after heat treatment was quantified using the PCC. The leaf epidermal cells of the transgenic lines were imaged by confocal microscopy. As a negative control, images of the mRFP channel of the *35S::GFP-SKD1x35S::PAB2-mRFP* line were tilted by 180° and analyzed for signal overlap.

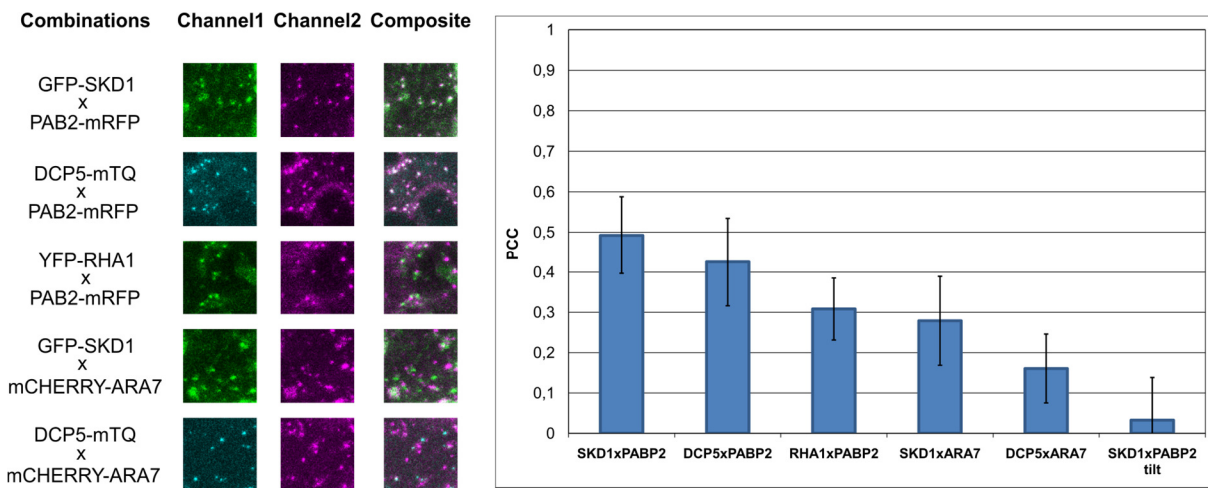


**Figure 3.11. Colocalization quantification of stable lines after heat stress treatment.** Epidermal leaf cells of the crossed stable lines *35S::GFP-SKD1x35S::PAB2-mRFP*, *35S::GFP-SKD1x35S::mCHERRY-ARA7*, *35S::DCP5-mTQx35S::PAB2-mRFP*, *35S::YFP-RHA1x35S::PABP-mRFP*, *35S::GFP-SKD1x 35S::mCHERRY-ARA7*, and *35S::DCP5-mTQx35S::mCHERRY-ARA7* were imaged for colocalization quantification. Leaves were subjected to heat stress treatment at 40°C for 50' and maximum projections of stacks were generated. For each combination, 10 leaf areas were imaged and three ROIs were analyzed for fluorescent signal overlap using the PCC. Representative ROIs of the different combinations are depicted on the left. The mean overlaps for the different combinations are shown in the histogram on the right. Error bars indicate standard deviation. As a negative control, pictures of one channel of the *35S::GFP-SKD1x 35S::PAB2-mRFP* line were rotated by 180° before analysis.

**Table 3.4. Statistical significance analysis of colocalization between the stable lines.** All datasets were normally distributed (Shapiro-Wilk-test). Significant colocalization differences were tested by the Welch's two sample t-test (n.s. = not significant,  $p < 0.05 = *$ ,  $p < 0.01 = **$ ,  $p < 0.001 = ***$ ). Detailed p-values are listed in Appendix, Table A.6.

	SKD1x PAB2	DCP5x PAB2	RHA1x PAB2	SKD1x ARA7	DCP5x ARA7	SKD1/ PAB2 tilt
SKD1x PAB2		**	***	***	***	***
DCP5x PAB2	**		***	***	***	***
RHA1x PAB2	***	***		n.s.	***	***
SKD1x ARA7	***	***	n.s.		***	***
DCP5x ARA7	***	***	***	***		***
SKD1/ PAB2 tilt	***	***	***	***	***	

The strongest positive correlation of localization was identified for GFP-SKD1 and PAB2-mRFP with a mean value of  $0.49 (\pm 0.10)$ , Figure 11). This overlap is significantly lower than the overlap identified for the transient double transformation ( $0.55 \pm 0.09$ , p-value 0.018). A previous quantitative colocalization study of PAB2 and the AN protein showed that the overlap in transient cells was higher than in transgenic cells (Bhasin and Hülkamp, 2017). This observation was not exhaustively explained, but different protein proportionality and altered signal intensity were discussed as an explanation. Nevertheless, a PCC of 0.49 indicates a considerable degree of co-occurrence in the context of this study (highest obtained coefficient is 0.75 for YFP-UBP1B/mCHERRY-UBP1B in transient colocalization study). The overlap of DCP5-mTQ and PAB2-mRFP ( $0.43 \pm 0.05$ ) is significantly lower than the overlap of GFP-SKD1 and PAB2-mRFP, but is still considerably high. This indicates a partial overlap of the P-body marker protein DCP5 with PAB2, which so far has only been described to localize to SGs.

The quantification of YFP-RHA1 and PAB2-mRFP co-occurrence results in a PCC of  $0.31 \pm 0.10$ , which is significantly lower than the coefficient of GFP-SKD1/ PAB2-mRFP and DCP5-TURQUOISE/ PAB2-mRFP, but comparable to the result of GFP-SKD1/mCHERRY-ARA7 ( $0.28 \pm 0.07$ ). This fits the hypothesis that the heat induced GFP-SKD1 structures

represent mRNP granules (similar to PAB2-mRFP) while mCHERRY-ARA7 and YFP-RHA1 label late endosomal structures. The lowest overlap was shared between DCP5-TURQUOISE and mCHERRY-ARA7 ( $0.16 \pm 0.06$ ).

Altogether, the analysis of the transgenic marker lines confirmed the observation that SKD1 localizes to mRNPs upon heat stress. In addition, it was demonstrated that known marker proteins of late endosomal structures do not colocalize with heat-induced SKD1 granules or mRNP granule proteins. These results provide further evidence that the association of SKD1 with mRNP granules upon heat stress is independent of endosomal structures.

### **3.4 Subcellular localization of ESCRTIII core and associated proteins**

So far, the results of this study showed that the SKD1 protein localizes to mRNP granules upon heat stress. This shift in localization appears to be independent of membrane association, since formed SKD1 granules are neither enriched in FM4-64 staining (Chapter 3.2, Figure 3.3) nor colocalize to the late endosomal marker protein ARA7 (Chapter 3.3.3, Figure 3.9). The previously obtained Y2H data and the Y2H data generated in this study (Chapter 3.1, Table 3.1 and Table 3.2) indicate potential interactions between several ESCRTIII core and associated proteins and mRNP granule components.

All ESCRTIII core proteins as well as the associated proteins VPS46.1/VPS46.2, VPS60.1/VPS60.2, and ISTL1 share similar architectural features: an N-terminal  $\alpha$ -helical hairpin which is supported by additional shorter helical structures and a flexible C-terminal  $\alpha$ -helix which can fold back and mask the hairpin structure (closed conformation, auto-inhibition). The hairpin is overall negatively charged and provides the membrane-binding interface of ESCRTIII proteins. Further, it contains residues which are essential for protein interactions amongst the ESCRTIII subunits. Only upon release of the C-terminal  $\alpha$ -helix from the hairpin structure (open conformation), endosomal membrane association and polymer formation can occur (Muzioł et al., 2006; Bajorek et al., 2009;). In general, the ESCRTIII proteins are in the monomeric closed state when present in the cytosol and in the open oligomerized state when bound to membranes. The cycling of the ESCRTIII subunits from the membrane-bound to the monomeric state in the cytosol is executed by SKD1 and its associated regulators (Babst et al., 1998, Shim et al., 2007). The *A. thaliana* LIP5 protein does not share the typical domain structure of the ESCRTIII core and most of the ESCRTIII associated proteins. It has been shown that the yeast LIP5 homolog Vta1 interacts with SKD1 via a conserved C-terminal region. Interactions with other ESCRTIII components are mediated over two N-terminal MIT-domains (Azmi et al., 2008; Xiao et al., 2008).

This part of the study addressed the question whether other ESCRTIII proteins exhibit a heat-dependent localization shift similar to the one of SKD1. Another part of the study was to see whether the different ESCRTIII core and associated components localize differently after heat stress treatment, despite their overall high similarity in domain structure.

### **3.4.1 *In-silico* analysis of IDRs in ESCRTIII core and associated proteins**

A part of the current discussion about the dynamic nature of mRNP granules involves the question whether their assembly represents liquid-liquid phase separation and what role IDRs (Intrinsically Disordered Regions) play in this process. IDRs, also known as LC (Low Complexity) regions, are linear peptide stretches outside of globular domains without regular secondary structure elements. Most of the time, IDRs have a low amino acid complexity and do not contain stretches of hydrophobic amino acids, which could initiate protein folding. Functions of IDRs include being flexible linker between globular domains, sites of posttranslational modification and serving as “interaction hubs” since they allow specific, but weak and variable protein-protein interactions (Dunker et al. 2002, Protter and Parker, 2016). IDR-enriched proteins have been shown to be relevant in diverse cellular processes such as cell cycle-control, chaperone activity or transcription regulation (Iakoucheva et al., 2002; Tompa et al., 2006; Xie et al., 2007). Further, IDRs are enriched in mRNP granule components and are relevant for aggregation and granule formation (Gilks et al., 2004; Decker et al., 2007; Reijns et al., 2008; Kato et al., 2012; Jain et al., 2016).

The implication that the presence of IDRs increases the likelihood of a protein to locate to mRNP granules raised the question, whether there is a considerable degree of disorder in *A. thaliana* ESCRTIII proteins and if this disorder correlates with aggregation upon heat stress. To investigate this aspect, protein sequences of ESCRTIII core and associated proteins were analyzed with two different online tools: DisEMBL and GlobPlot (Linding et al., 2003; Linding, 2003). The machine-learning based DisEMBL tool predicts the presence of loops (or coils) and hot loops (H-loops) within an amino acid sequence. Loops are defined as secondary structures which do not fall in the category of  $\alpha$ -helices,  $3_{10}$ -helices or  $\beta$ -strands (Kabsch and Sander, 1983). H-loops are a subset of the loops defined by DisEMBL and are predicted to have a higher degree of mobility and thus are more likely to be disordered. The GlobPlot predictor calculates the sum of propensities (probability of a residue to be in a secondary structure or in a random coil) of amino acids and defines regions of globularity and disorder within protein sequences.

The IDR analysis was performed on amino acid sequences of ESCRTIII core and associated proteins which have been previously analyzed in the Y2H experiment (Chapter 3.1). To

compare the degrees of disorder to a group of proteins known to aggregate in mRNP granules, the *A. thaliana* mRNP granule components, which were also analyzed in the Y2H experiment, were included in the analysis. The protein sequences (representative gene models) were extracted from The Arabidopsis Information Resource (TAIR) and subjected to analysis with the DisEMBL and GlobPlot tool.

Table 3.5 summarizes the results of the IDR analysis. The exact protein regions, which were predicted to be disordered, are given in Appendix, Table A.7. To compare the degree of disorder, the percentage of residues in IDRs is used. Another criterion to evaluate protein disorder is the presence of long continuous IDRs ( $\geq 30$  residues) since they are more likely to have functional relevance (Ward et al., 2004).

**Table 3.5. Percentages of predicted IDR content within ESCRTIII, P-body and SG proteins.** The Percentages of IDRs in respect to total protein length predicted by DisEMBL and GlobPlot are indicated. Percentages of amino acids (aa) in long IDRs are indicated in bold and italic. The total number of aa in IDRs or long IDRs are shown in brackets.

			DisEMBL		GlobPlot
		Protein length [aa]	% of aa in loops	% of aa in H-loops	% of aa in disordered region
ESCRTIII core	VPS20.1	243	29% (70) <b>24% (58)</b>	30% (72) <b>18% (43)</b>	5% (11) <b>none</b>
	VPS24.1	229	16% (37) <b>none</b>	34% (77) <b>none</b>	<b>none</b> <b>none</b>
	VPS32.1	194	26%(51) <b>15%(30)</b>	21% (41) <b>none</b>	7% (13) <b>none</b>
	VPS32.2	219	26% (57) <b>none</b>	28% (63) <b>16% (35)</b>	9% (20) <b>none</b>
	VPS2.1	225	24% (53) <b>none</b>	27% (60) <b>none</b>	6% (13) <b>none</b>
	VPS2.2	243	32% (77) <b>14% (35)</b>	44% (108) <b>31% (76)</b>	3% (7) <b>none</b>
	VPS2.3	210	24% (51) <b>none</b>	36% (75) <b>19% (39)</b>	8% (16) <b>none</b>
ESCRTIII associated	LIP5	421	73% (308) <b>55% (230)</b>	31% (54) <b>none</b>	58% (253) <b>54%(227)</b>
	SKD1	435	54% (233) <b>32% (141)</b>	14% (62) <b>9% (41)</b>	23% (101) <b>9% (41)</b>
	VPS46.1	203	20% (41) <b>none</b>	30% (60) <b>20% (41)</b>	10% (20) <b>none</b>
	VPS46.2	203	19% (39) <b>none</b>	35% (72) <b>26% (53)</b>	9% (19) <b>none</b>
	VPS60.1	235	53% (124) <b>26% (62)</b>	29% (67) <b>15% (35)</b>	32% (75) <b>17% (40)</b>
	VPS60.2	272	52% (141) <b>23% (63)</b>	20% (54) <b>12% (33)</b>	29% (80) <b>15% (42)</b>
P-body	DCP1	367	54% (198) <b>43% (157)</b>	21% (76) <b>none</b>	46% (168) <b>46%(168)</b>
	DCP2	386	60% (230) <b>23% (89)</b>	39% (151) <b>15% (56)</b>	15% (56) <b>none</b>

		DisEMBL		GlobPlot	
		Protein length [aa]	% of aa in loops	% of aa in H-loops	% of aa in disordered region
	<b>DCP5</b>	611	96% (584) <b>92% (561)</b>	33% (204) <b>21% (131)</b>	72% (438) <b>59% (362)</b>
	<b>VCS</b>	1344	60% (793) <b>47% (629)</b>	19% (258) <b>4% (56)</b>	25% (336) <b>10% (130)</b>
	<b>eIF4E1</b>	235	63% (148) <b>60% (140)</b>	15% (35) <b>none</b>	25% (58) <b>none</b>
	<b>XRN4</b>	947	66% (626) <b>45% (426)</b>	18% (173) <b>9% (88)</b>	34% (318) <b>15% (145)</b>
<b>SG</b>	<b>UBP1b</b>	419	64% (270) <b>45% (187)</b>	9% (36) <b>none</b>	23% (95) <b>8% (33)</b>
	<b>PAB2</b>	629	64% (405) <b>37% (234)</b>	25% (159) <b>5% (33)</b>	25% (179) <b>13% (81)</b>
	<b>RBP47b</b>	435	76% (332) <b>64% (280)</b>	22% (97) <b>16% (69)</b>	32% (141) <b>11% (46)</b>
	<b>GRP7</b>	176	77% (135) <b>62% (109)</b>	41% (73) <b>none</b>	56% (99) <b>52% (92)</b>
	<b>RBP45b</b>	405	71% (286) <b>58% (235)</b>	25% (103) <b>13% (52)</b>	43% (176) <b>17% (70)</b>
	<b>GRP2</b>	158	40% (64) <b>21% (33)</b>	23% (37) <b>none</b>	53% (83) <b>33% (52)</b>

In a first step, the overall degree of disorder between the different functional protein groups (ESCRTIII core, ESCRTIII associated, P-body and SG) as well as the different prediction categories (DisEMBL: loop and H-loop, GlobPlot: disordered region) were compared. For this, mean values of each functional protein group, for ESCRTIII total and mRNPs total was generated. The obtained mean percentages of amino acids in IDRs and in long IDRs are plotted in Figure 3.12.

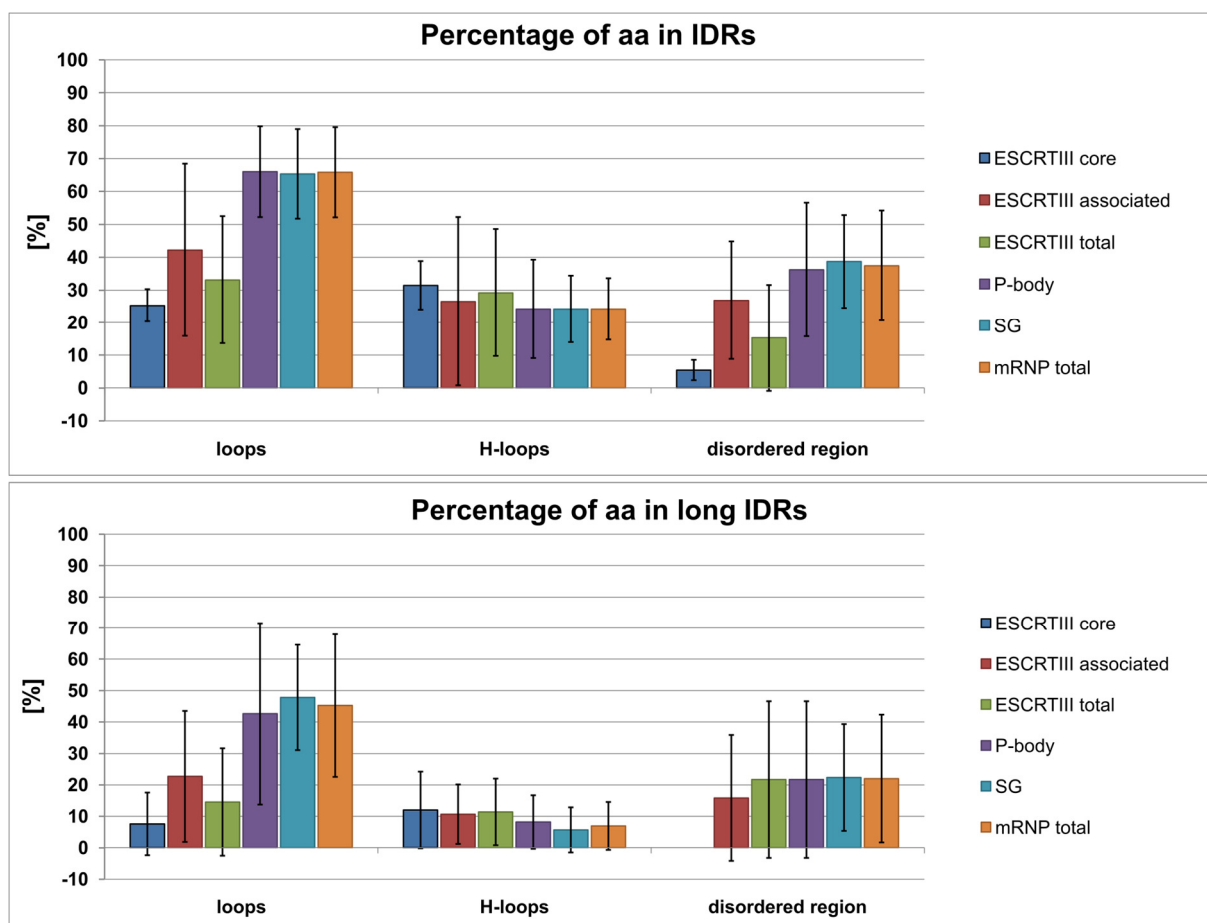


**Figure 3.12. Comparison of predictor categories based on mean IDR content in analyzed functional protein groups.** Histograms of the mean percentages of aa in IDRs and long IDRs within the functional group of ESCRTIII core, ESCRTIII associated, P-body, and SG proteins. ESCRTIII total indicates the mean IDR/long IDR content of all tested ESCRTIII proteins, mRNP total indicates the content for all tested P-body and SG proteins. IDRs were predicted by the DisEMBL (loop, H-loop) and GlobPlot (disordered region) tool (Linding et al., 2003; Linding, 2003). Long IDRs are defined as all stretches of disorder that include 30 or more residues. Error bars represent standard deviation.

The highest degree of disorder for nearly all functional protein groups was predicted by the DisEMBL loop category, followed by the disordered region category of GlobPlot and the H-loop category (DisEMBL). Only for the ESCRTIII core proteins more residues were predicted

to be disordered by the H-loop ( $31 \pm 7\%$ ) than the loop ( $25 \pm 5\%$ ) category. This is surprising since the H-loop category is described as a subset of the loop category.

The loop category of the DisEMBL tool seems to be less conservative than the other two prediction groups. Nonetheless, the same trends in disorder are observable when comparing the predictions of the loop category and the disordered region category: P-body and SG proteins share a similar degree of disorder (mRNP total, loop:  $66 \pm 13\%$ , disordered region:  $37 \pm 18\%$ ) while ESCRTIII core and associated proteins are less disordered (ESCRTIII total, loop:  $33 \pm 19\%$ , disordered region:  $15 \pm 16\%$ ). These strong differences are no longer present in the H-loop category (H-loop ESCRTIII total:  $29 \pm 19\%$ , mRNP total:  $24 \pm 9\%$ ).

As mentioned before, an additional aspect of protein disorder evaluation is the presence and percentage of residues in long IDRs. The mean percentages of amino acids in long IDRs are depicted in the lower histogram in Figure 3.12. Logically, the overall percentage of residues in IDRs is decreased if only stretches of 30 amino acids or more are considered. Strikingly, the same trends in disorder percentage between the different functional proteins groups are still present in the loop category (ESCRTIII total:  $15 \pm 17\%$ , mRNP total:  $45 \pm 23\%$ ). This is not the case for the H-loop and disordered region category. Thus, the correlation between degree of disorder and presence of long IDRs is only reflected by the loop category. This might be explained by more conservative parameters of the H-loop and disordered region algorithms.

After the comparison of the different prediction tools and categories with each other, the degree of disorder within each ESCRTIII core and associated protein was analyzed. For this, the absolute percentages of amino acids in the different classes of IDRs or long IDRs were plotted (Figure 3.13).

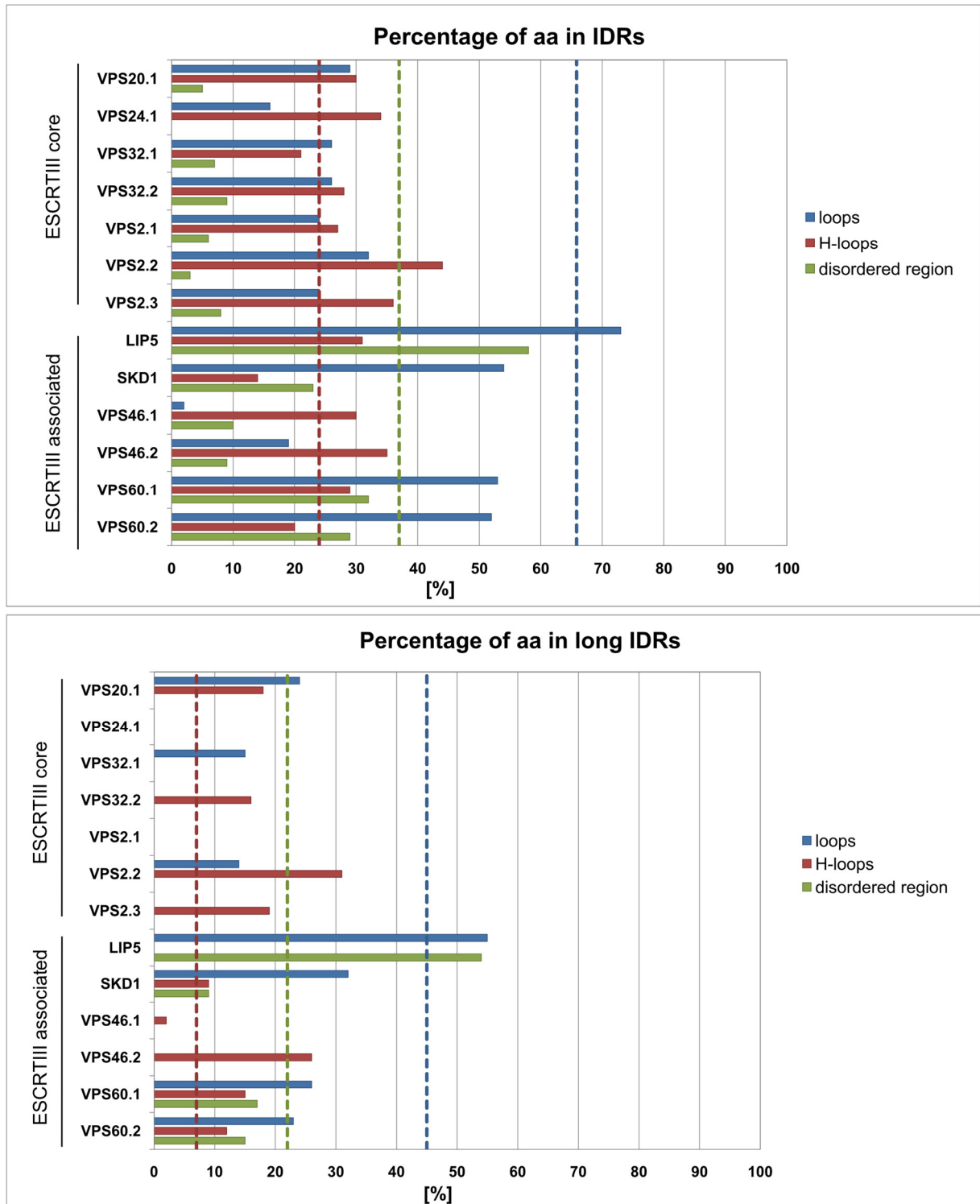


**Figure 3.13. Percentages of IDRs and long IDRs in ESCRTIII core and associated proteins.** The percentages of aa in IDRs or long IDRs predicted by DisEMBL (loop, H-loop) and GlobPlot (disordered region) for the analyzed *A. thaliana* ESCRTIII core and associated proteins are presented in the histograms. As a reference, the mean percentage of disorder of all tested mRNP granule components is indicated as vertical dashed lines for each predictor category.

The vertical lines in the histograms indicate the mean percentage of disorder of the analyzed mRNP granule proteins. By plotting the individual ESCRTIII proteins, it becomes evident that the majority of them shares a comparable degree of disorder over all analyzed categories (loops, H-loops and disordered region). The exceptions are LIP5, SKD1 and, to a lesser extent, VPS60.1 and VPS60.2. LIP5 and SKD1 do not share the same domain structure as the other analyzed ESCRTIII proteins (N-terminal  $\alpha$ -hairpin and C-terminal  $\alpha$ -helix connected by a flexible linker) and therefore, it is not surprising that they display a different degree of disorder. A particularly low percentage of VPS24.1, VPS46.1, and VPS46.2 residues are predicted to be in IDRs.

The percentage of amino acids that are predicted to be in long IDRs (Figure 3.13, bottom) is once more elevated in LIP5, SKD1, VPS60.1 and VPS60.2 in comparison to the other ESCRTIII proteins. For VPS24.1 and VPS2.2, no long IDR was identified and for VPS32.1, VPS2.3, VPS46.1 and VPS46.2 only one predictor category found long IDRs.

A large-scale study from 2013 by Pietrosemoli and colleagues examined the prevalence of IDRs in the *A. thaliana* proteome (Pietrosemoli et al., 2013). They showed that approximately 60% of the *A. thaliana* proteins contain one long IDR and a degree of disorder between 0- 30%. A protein was considered highly disordered, if over 50% of the amino acids were predicted to be in an IDR and roughly 30% of the *A. thaliana* proteins fall in this category. All but one (GRP2) of the analyzed P-body and SG proteins fulfill this requirement for the loop category. As mentioned, the mRNP granule components were included in the analysis as a reference and this result strengthens the confidence in the predictions for the ESCRTIII core and associated proteins. The LIP5, SKD1, VPS60.1, and VPS60.2 protein can be considered highly disordered while the other analyzed ESCRTIII proteins display an average degree of disorder. SKD1, similar to the mRNP granule components, has been shown to form granules upon heat stress and to colocalize to mRNP granules. It is now of interest to see whether the high degree of disorder of LIP5, VPS60.1 or VPS60.2 correlates with a tendency to form granules.

### **3.4.2 Heat stress-dependent localization of ESCRTIII core and associated proteins.**

This part of the study addressed the question whether other ESCRTIII proteins show a similar shift in localization upon heat stress treatment like SKD1. For this, the localization of the ESCRTIII core components VPS2.2, VPS24.1, and VPS32.1 as well as the associated proteins LIP5, VPS60.2, VPS46.1, and its homolog VPS46.2 were analyzed. An additional objective was to investigate if the ATPase function of SKD1 is relevant for a heat-dependent localization shift. The exchange of Lys178 to Ala (K178A) and Glu234 to Gln (E234Q, combined referred

to as SKD1-AQ) diminishes ATP binding and hydrolysis activity of SKD1 which leads to the block of MVB biogenesis and endosomal swelling (Babst et al. 1998; Haas et al. 2007; Shahriari et al. 2010).

Epidermal leaf cells of Col-0 plants were transiently transformed with constructs overexpressing ESCRTIII core and associated proteins in fusion with fluorescent proteins. Representative subcellular localizations of the recombinant proteins before and after heat stress are shown in Figure 3.14. For clarity, all fluorescent signals (YFP and mCHERRY) are depicted in green.

It has been reported that C-terminal fusions of mammalian VPS32 (CHMP4) and VPS46 (CHMP1) with GFP cause endosomal swelling reminiscent of the dominant-negative effect of SKD1-AQ. This has been explained with the loss of the autoinhibitory effect of the C-terminal  $\alpha$ -helix, which results in increased membrane association. Further, this increased filament formation at the MVB membrane reduces the accessibility of VPS32 and thus it cannot be removed by SKD1 (Howard et al., 2001; Zamborlini et al., 2006; Hanson et al., 2008). This effect was also observed in this study by transiently transforming epidermal leaf cells of the transgenic *35S::GFP-SKD1* line with a construct overexpressing VPS32.1-mCHERRY (Appendix, Figure A.3). Larger aggregates of VPS32.1-mCHERRY were visible which seemed to “trap” the GFP-SKD1 protein. By using an N-terminal fluorescent fusion of VPS32.1, this effect was no longer observed (Appendix, Figure A.3).

As shown in Figure 3.14, heat-stress had no apparent effect on the localization of mCHERRY-VPS32.1. The majority of signal was evenly distributed throughout the cytosol and some larger punctuate structures, presumably MVBs, were visible.

Contrary to the subcellular localization of C-terminal modified VPS32.1, no large aggregates were observed when VPS24.1-YFP was coexpressed with SKD1-mCHERRY (Appendix, Figure A.3). This implies that the *A.thaliana* VPS24.1 protein is not sensitive to C-terminal recombination. As depicted in Figure 3.14, VPS24.1-YFP was visible in the cytosol and changed upon heat-stress to a granular localization, similar to SKD1.

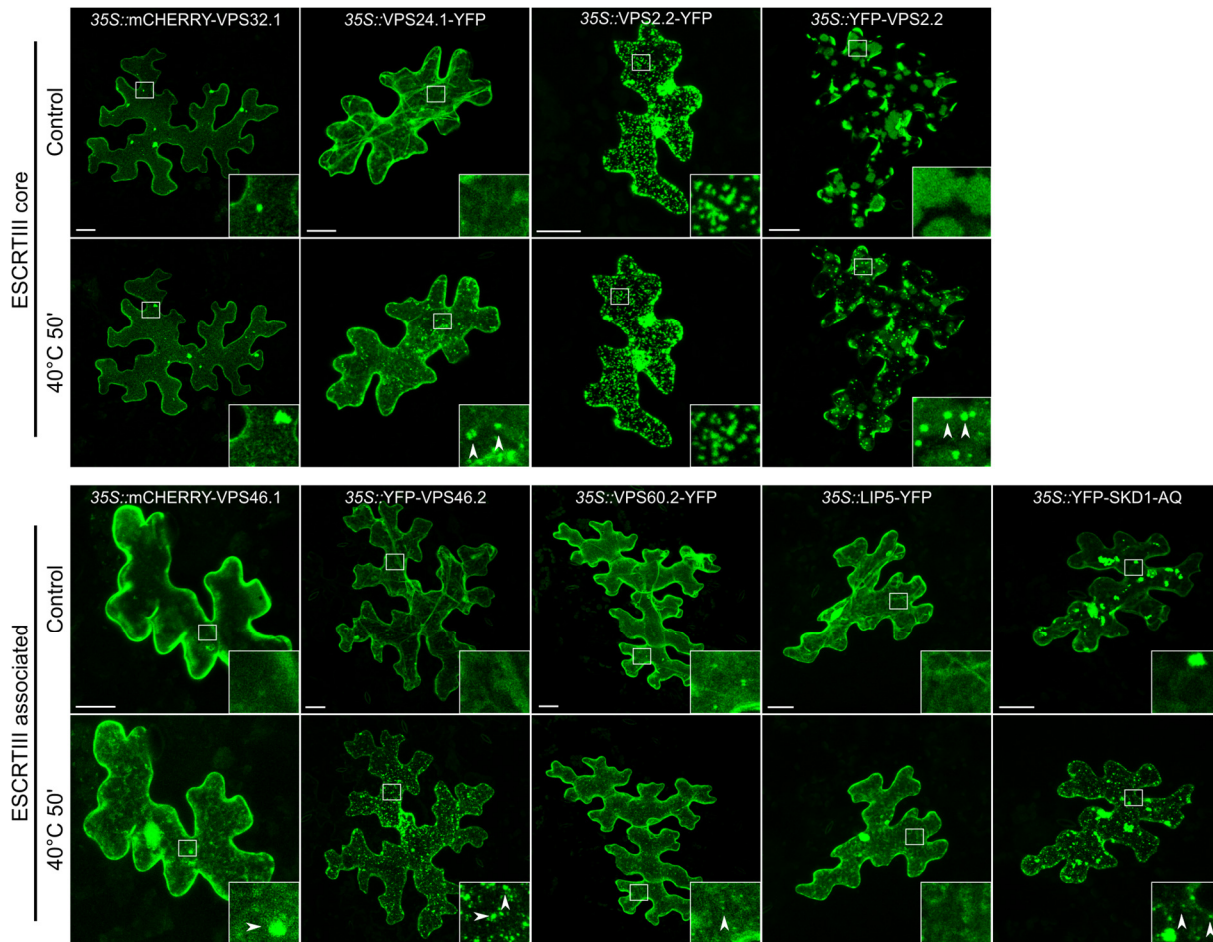


**Figure 3.14. Heat-dependent subcellular localization of ESCRTIII core and associated proteins.** *A. thaliana* epidermal leaf cells were transiently transformed by particle bombardment with a construct overexpressing ESCRTIII core or associated protein fused to YFP or mCHERRY. For clarity, all imaged cells are depicted in green, independent of the fused fluorescent protein. The following recombinant versions of the ESCRTIII proteins were analyzed: mCHERRY-VPS32.1, VPS24.1-YFP, VPS2.2-YFP, YFP-VPS2.2, mCHERRY-VPS46.1, YFP-VPS46.2, VPS60.2-YFP, and LIP5-YFP. In addition, the localization of the mutated ATPase variant SKD1-AQ was studied (YFP-SKD1-AQ, Shahriari et al. 2010). The same cells were imaged by confocal microscopy with the same laser intensities before and after heat treatment at 40°C for 50'. Depicted are representative maximum projections of stacks. Arrow heads indicate granules which formed after heat treatment. Bar = 20  $\mu$ m.

The *A. thaliana* VPS2.2 protein was previously analyzed in a study by Ibl and colleagues. They showed that C-terminal fusion of VPS2.2 does not diminish its cellular function since the root growth phenotype of *vps2.2*  $-/-$  mutants expressing VPS2.2-GFP was restored. Further, the subcellular localization of VPS2.2-GFP expressed under its endogenous promoter was described as predominantly endosomal with some signal in the nucleus and plasma membrane (Ibl et al., 2011). Here, VPS2.2-YFP showed a strong, granular signal with some larger aggregation in proximity to the nucleus (Figure 3.14). Heat-stress did not alter the granular localization.

The strong aggregation of VPS2.2-YFP was striking and raised the question whether overexpression of the protein might cause a dominant-negative effect similar to the one of VPS32.1-mCHERRY. This hypothesis was tested by coexpression of the SKD1 protein. As shown in Appendix, Figure A.3, overexpression of VPS2.2-YFP causes the formation of SKD1-mCHERRY labeled granules which colocalize to VPS2.2-YFP. Hence it is likely that the C-terminal modification in combination with the overexpression of VPS2.2 causes an inhibition of ESCRTIII protein recycling from the endosomal membrane.

The trapping of the VPS2.2 protein at endosomal membranes might block a potential localization shift upon heat treatment. Therefore it was tested, if the N-terminal modification of VPS2.2 is not limiting the mobility of the protein. A previous study analyzed the localization of *A. thaliana* VPS2 proteins in protoplasts and showed that N-terminally modified versions mainly localize to the cytosol (no inhibitory effect, Katsiarimpa et al., 2011). By overexpressing YFP-VPS2.2 in epidermal leaf cells, a different localization was observed (Figure 3.14, maximum projection). Here, the cells showed bright patches of fluorescent signal. The analysis of the imaged cells slide by slide revealed that the YFP-VPS2.2 signal was concentrated at the rims of the cell. This localization might represent a concentration of YFP-VPS2.2 at distinct plasma membrane regions. In contrast to the C-terminally modified version of VPS2.2, YFP-VPS2.2 was visible in granules after heat treatment. Further, it did not cause SKD1-mCHERRY to localize in aggregates when coexpressed (Appendix, Figure A.3).

VPS46.1 and VPS46.2 were both fused N-terminally with mCHERRY or YFP (Figure 3.14). The two homologs share 95% sequence similarity (blastp, Altschul et al., 1997) but show some differences in their stress dependent localization. Both proteins were evenly distributed in the cytosol. After heat stress, YFP-VPS46.2 formed very pronounced granules while YFP-VS46.1 granules were less apparent and defined. These results indicate that the VPS46.2 protein might be more prone to aggregation than VPS46.1.

The C-terminal fusion of VPS60.2 to fluorescent proteins caused no large cellular aggregation (Appendix, Figure A.3). Before heat stress treatment, VPS60.2-YFP localized in the cytosol and in few punctate structures which presumably represent MVBs (Figure 3.14). The localization of VPS60.2 did not change drastically upon heat stress treatment, but a few very small granular structures were visible in some cells

Previous studies showed, that C-terminal modification of LIP5 does not influence its functionality since *lip5-1* mutants transformed with a construct overexpressing LIP5-GFP

showed restored resistance against *Pseudomonas syringae* (PstDC3000) infection (Wang et al., 2014). Figure 3.14 demonstrates that LIP5-YFP localized evenly in the cytosol and the nucleus. This localization of LIP5 has been previously described and coexpression of either wild type or mutant SKD1 enhances its endosomal localization (Wang et al., 2014). In addition, Wang and colleagues described in 2015 an increase in granular LIP5-GFP localization after heat-stress treatment in 2015 (Wang et al., 2015). Surprisingly, a shift in localization was not observed in this study.

As previously mentioned, the localization of a non-functional ATPase version of SKD1 (SKD1-AQ) was investigated. Figure 3.14 shows that the subcellular localization of YFP-SKD1-AQ differed strongly from the wild type protein (Chapter 3.2, Figure 3.1 and Figure 3.2). In addition to the cytosolic and nuclear signal, large aggregates were visible throughout the plant cell. The expression of SKD1-AQ has a dominant-negative effect and causes the formation of aberrantly large endosomal structures called class E compartments (Babst et al., 1998; Haas et al., 2007; Shariari et al., 2010). These large aggregates were still visible upon heat-stress treatment, yet additional small granules were present, similar to those seen for wild type SKD1. Thus, it seems like the ATPase function is not relevant for SKD1 granule formation.

In summary, the ESCRTIII core protein VPS24.1 and the ESCRTIII associated protein VPS46.2 changed their localization from predominantly cytosolic to granular upon heat stress. VPS46.1 and VPS60.2 showed some granulation upon heat treatment. These results are unexpected in view of the results of the IDR analysis (Chapter 3.4.1). Following the assumption that a high degree of protein disorder correlates to the likelihood to form aggregates, it was expected to see a localization shift of LIP5 and VPS60.2. Only VPS60.2 showed some mild granulation upon heat stress. In addition, the rather highly ordered VPS46.2 showed stronger aggregation than expected. Hence, the degree of disorder seems to be a weak predictor for heat stress-dependent aggregation in the case of ESCRTIII proteins.

### **3.4.3 Colocalization study of ESCRTIII core and associated proteins with SKD1-AQ**

The previous Chapter analyzed the localization of recombinant ESCRTIII core and associated proteins under non-stress condition as well as after heat stress treatment (Figure 3.14). Further, the influence of fluorescently labeled ESCRTIII proteins on SKD1 localization was tested when the modifications were suspected to cause a dominant-negative effect. However, this approach did not test whether an N- or C-terminal modification diminishes the capability of the ESCRTIII core and associated proteins to interact with each other and to localize to MVBs in *A. thaliana*

cells. A potential loss of membrane association might also influence their localization behavior under heat stress.

Babst and colleagues showed that the majority of ESCRTIII core proteins are not found in association with membranes but are dispersed in the cytosol under normal conditions in yeast. This was attributed to the highly efficient ESCRTIII disassembly activity of VPS4 (yeast SKD1 homolog). Indeed, over 90% of ESCRTIII proteins were found to be associated with endosomal membranes in *vps4*  $\Delta$  cells by localization and biochemical studies (Babst et al., 2002). Hence, the easiest way to investigate the capacity of the modified ESCRTIII proteins to associate with membranes would be their localization analysis in *skd1* mutants. Unfortunately, the loss of SKD1 is lethal in plants since no homozygous *skd1* mutants was ever successfully isolated (M. Jakoby, personal communication). An elegant solution to this problem is the coexpression of the dominant-negative SKD1-AQ variant. SKD1-AQ expression has been shown to mimic the effect of Vps4 protein loss in yeast (Babst et al., 1998; Haas et al., 2007; Shariari et al., 2010). A similar approach was used in a study by Katsiarimpa and colleagues in which they coexpressed SKD1-EQ in *A. thaliana* protoplasts and analyzed the colocalization of VPS2.1, VPS2.2, VPS2.3, and VPS24.1 with the SKD1-EQ induced class E compartments (Katsiarimpa et al., 2011).

Epidermal leaf cells of *A. thaliana* plants were once more transiently transformed with a construct overexpressing an ESCRTIII core or associated protein (same fusion orientation as in Chapter 3.4.2) and a construct either expressing YFP-SKD1-AQ or mCHERRY-SKD1-AQ. Representative pictures of the colocalization analysis are shown in Figure 3.15. For clarity, all ESCRTIII core and associated proteins are depicted in green and SKD1-AQ is depicted in magenta, independent of the fused fluorescent protein.

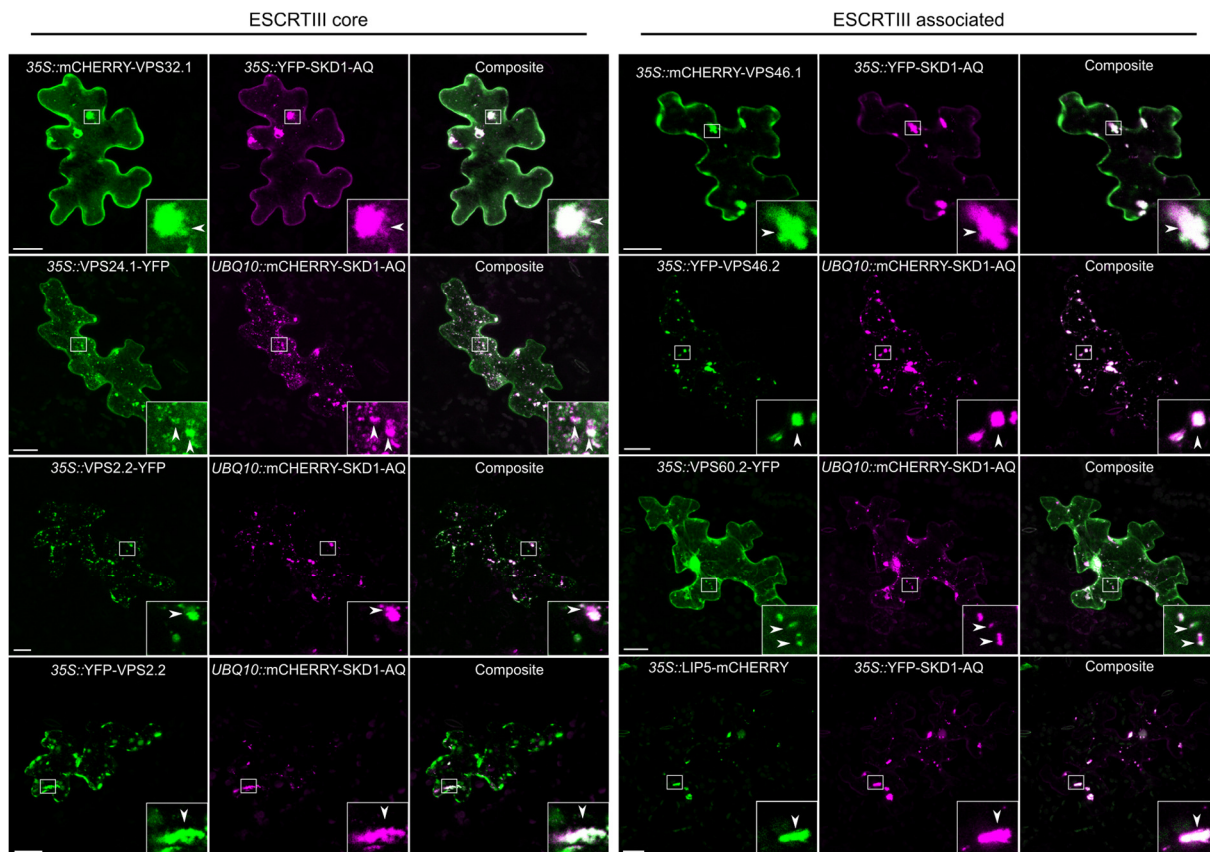


**Figure 3.15. Colocalization of ESCRTIII core and associated proteins with SKD1-AQ.** Epidermal cells of *A. thaliana* Col-0 leaves were transiently transformed with a construct overexpressing SKD1-AQ in N-terminal fusion with a fluorescent protein and a construct overexpressing an ESCRTIII core or associated protein. The following recombinant versions of the ESCRTIII proteins were analyzed: mCHERRY-VPS32.1, VPS24.1-YFP, VPS2.2-YFP, YFP-VPS2.2, mCHERRY-VPS46.1, YFP-VPS46.2, VPS60.2-YFP, and LIP5-mCHERRY. The cells were imaged by confocal microscopy and maximum projections generated from stacks are depicted. Arrow heads indicate colocalization with SKD1-AQ. Bar = 20  $\mu$ m.

As expected, the YFP/mCHERRY-SKD1-AQ protein localized in large aggregates in the transformed plant cells, inducing and labeling class E compartments. The ESCRTIII core proteins mCHERRY-VPS32.1 and VPS24.1-YFP colocalized to the SKD1-AQ labeled structures. Since neither VPS2.2-YFP nor YFP-VPS2.2 showed the expected mainly cytosolic localization under normal conditions, both recombinant variants were tested for colocalization with SKD1-AQ. Figure 3.15 demonstrates that both proteins colocalize with the dominant-negative version of SKD1. As mentioned, the subcellular localization of YFP-VPS2.2 was tested previously in *A. thaliana* protoplasts. There, no association of VPS2.2 with class E compartments was observed (Katsiarimpa et al., 2011). This discrepancy might be explained by the cell model (epidermal cells *versus* protoplasts).

The coexpression of SKD1-AQ also induced the colocalization of ESCRTIII associated proteins mCHERRY-VPS46.1, YFP-VPS46.2, VPS60.2-YFP, and LIP5-mCHERRY with SKD1-AQ in larger cytosolic structures. Thus it is likely that the here used N- and C-terminally modified ESCRTIII proteins are still able to bind to MVB membranes and to each other.

### **3.4.4 Colocalization study of ESCRTIII core and associated proteins with UBP1b**

So far, the localization of the ESCRTIII core and associated proteins was analyzed in respect to heat and during coexpression of a dominant-negative version of SKD1. It was shown that some of the ESCRTIII proteins change their localization upon heat treatment in a similar way as SKD1. To see, whether this shift in localization also indicates a relocation to mRNP granules, a colocalization study was performed. For this, epidermal leaf cells of *A. thaliana* Col-0 plants were transiently double transformed with a construct overexpressing one of the previously tested ESCRTIII core or associated proteins and a construct overexpressing YFP- or mCHERRY-UBP1b. Figure 3.16 shows representative pictures of the analyzed cells. For clarity, all ESCRTIII core and associated proteins are depicted in green and UBP1b in magenta, independent of the fused fluorescent protein.

Chapter 3.4.2 demonstrated that N-terminally modified VPS32.1 did not change its localization upon heat treatment and was visible in larger, punctate structures independent of heat stress. Further, it was shown that these structures are not caused by a dominant-negative effect of N-terminal modification of VPS32.1 (Appendix, Figure A.3). The coexpression of mCHERRY-UBP1b did not change the distinct localization of YFP-VPS32.1 and the two structures did not colocalize after heat stress (Figure 3.16). This result indicates that VPS32.1 does not relocate to SGs upon heat stress and remains at MVBs.

In contrast to VPS32.1, VPS24.1-YFP did change its localization upon heat stress treatment from cytosolic to granular (Figure 3.14). This shift in localization was also visible in coexpression with UBP1b (Figure 3.16). Nevertheless, the formed VPS24.1-YFP and the mCHERRY-UBP1b labeled granules seemed to represent two distinct populations with no apparent overlap. One explanation for this might be that VPS24.1-YFP associates with P-bodies rather than with SGs. However, it is known that several P-body and SG proteins are not exclusively found in their respective compartment (Buchan and Parker, 2009). Further, this study provided evidence that the P-body marker protein DCP5 and SG marker protein PAB2 share a considerable degree of overlap in a transgenic *A. thaliana* line (Chapter 3.3.3, Figure 3.10 and Figure 3.11). Therefore, the hypothesis that VPS24.1-YFP exclusively localizes to P-

bodies after heat stress is unlikely. Another explanation for the granular localization might be an enhanced association with MVB membranes.

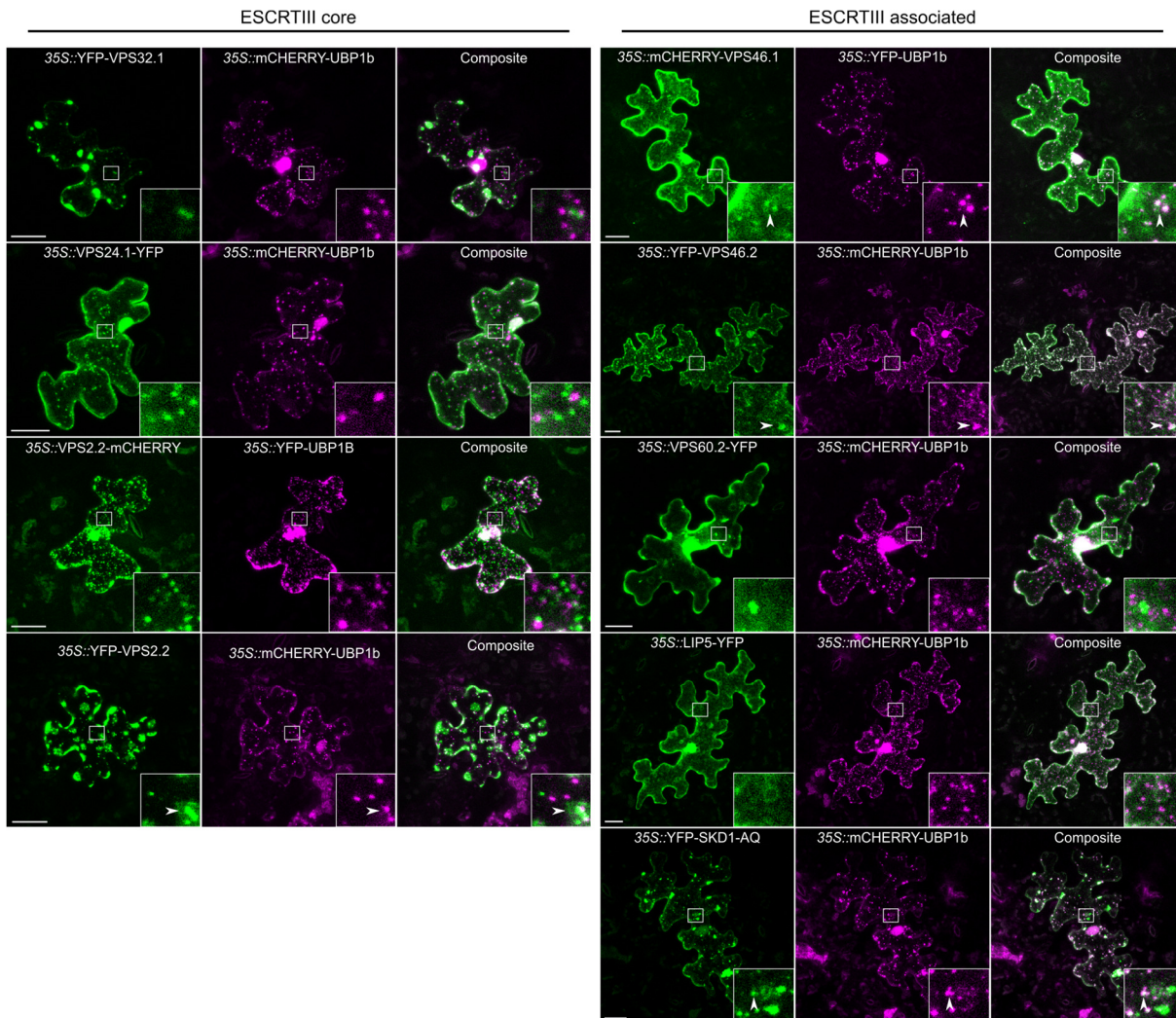


**Figure 3.16. Colocalization of ESCRTIII core and associated proteins with UBQP1b after heat stress.** *A. thaliana* Col-0 leaves were transiently transformed with a construct overexpressing YFP- or mCHERRY-UBQP1 and a construct overexpressing an ESCRTIII core or associated protein fused to YFP or mCHERRY. The following recombinant versions of the ESCRTIII proteins were analyzed: YFP-VPS32.1, VPS24.1-YFP, VPS2.2-YFP, YFP-VPS2.2, mCHERRY-VPS46.1, YFP-VPS46.2, VPS60.2-YFP, LIP5-YFP, and YFP-SKD1-AQ. The transiently transformed leaf cells were subjected to heat stress treatment (40°C 50') and imaged by confocal microscopy. Maximum projections of stacks are depicted. Arrow heads indicate colocalization with UBQP1b. Bar = 20  $\mu$ m.

Both fusion versions of VPS2.2 were tested for colocalization with mCHERRY-UBQP1b. VP2.2.-YFP was shown to localize strongly to granular structures independent of heat treatment (Figure 3.14). These structures are likely to represent enlarged MVBs. Coexpression of mCHERRY-UBQP1b did not change the localization of VPS2.2-YFP and the granular structures labeled by the proteins did not colocalize after heat stress (Figure 3.16). This result further strengthens the hypothesis that MVBs and mRNP granules do not colocalize after heat stress.

The coexpression of N-terminally modified VPS2.2 had no apparent effect on SKD1 localization (Appendix, Figure A.3) and probably no dominant-negative effect on MVB biogenesis. Yet the localization was still unexpected since the protein localized to distinct patches, presumably at the plasma membrane (Figure 3.14). This localization partially changed after heat stress treatment and YFP-VPS2.2 was visible in granular structures. This shift in localization was also visible when mCHERRY-UBP1b was coexpressed and some of the formed YFP-VPS2.2 granules co-occurred with mCHERRY-UBP1b labeled granules. This result suggests that VPS2.2 localizes to SGs upon heat treatment if its membrane-affinity is not altered. However, the localization of both VPS2.2 versions, which were used in this study, is different from what is expected (cytosolic localization or moderate endosomal association). Therefore, a definite statement about the heat-dependent localization of VPS2.2 cannot be made. In future, an additional localization study of VPS2.2 in stable lines, protoplasts, or labeled by a specific antibody might resolve this question.

The ESCRTIII associated proteins mCHERRY-VPS46.1 and YFP-VPS46.2 change their localization upon heat stress from mainly cytosolic to granular (Figure 3.14). The coexpression of YFP- or mCHERRY-UBP1b showed that the mCHERRY-VPS46.1 and YFP-VPS46.2 labeled granules partially colocalized with the SG marker protein. In the previous transient localization study, the C-terminally modified VPS60.2-YFP protein showed some minor granulation after heat stress treatment. The coexpression analysis revealed that mCHERRY-UBP1b granules did not coincide with the few VPS60.2-YFP labeled granules (Figure 3.16). LIP5-YFP did not change its mainly cytosolic localization upon heat treatment in single-transformed leaf epidermal cells, as well as when mCHERRY-UBP1b was coexpressed.

The single transient transformation study showed that SKD1-AQ localized in large aggregates and in small granular structures after heat treatment (Figure 3.14). The coexpression study revealed that YFP-SKD1-AQ colocalized with mCHERRY-UBP1b in smaller granules while some larger YFP-SKD1-AQ structures were not or only partially labeled by the SG marker protein (Figure 3.16). An explanation for this observation could be that only the population of YFP-SKD1-AQ proteins, which is present in the cytosol, changes its localization to mRNPs upon heat stress. The YFP-SKD1-AQ proteins, which are in larger aggregates, are trapped due to the lack of ATPase activity and remain in association with MVB membranes. This result suggests once more that the SKD1 protein and not MVBs as a whole localizes to mRNP granules upon heat stress.

### 3.4.5 Colocalization quantification of ESCRTIII core and associated proteins with UBP1b

To further validate the obtained colocalization results of the ESCRTIII core and associated proteins with UBP1b, a quantification study, similar to the one of Chapter 3.3.1, was performed. Epidermal leaf cells of *A. thaliana* Col-0 plants were transiently double transformed by particle bombardment with a construct overexpressing YFP- or mCHERRY-UBP1b and a construct overexpressing an ESCRTIII core or associated protein fused to a fluorescent protein. The quantification was performed as described in Chapter 2.8.1.

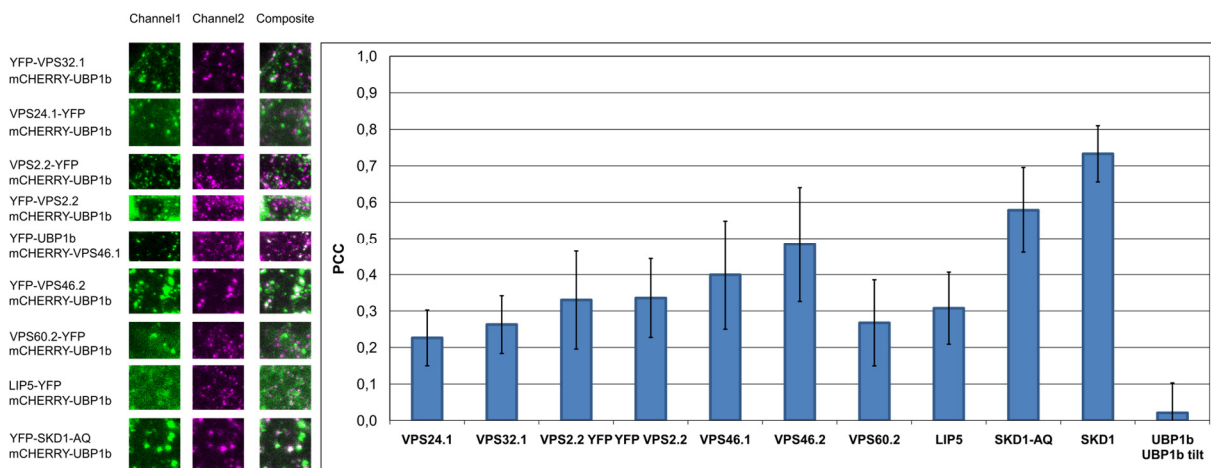


**Figure 3.17. Colocalization quantification of ESCRTIII core and associated proteins with UBP1b.** Epidermal leaf cells of *A. thaliana* Col-0 plants were transiently double transformed by particle bombardment with a construct overexpressing YFP- or mCHERRY-UBP1b and a construct overexpressing an ESCRTIII core or associated protein modified by fusion to YFP or mCHERRY. The same fusion versions of the ESCRTIII core and associated proteins were used as in Chapter 3.4.4. The transformed leaves were subjected to heat stress treatment (40°C 50') and imaged by confocal microscopy. 10 cells were imaged for each combination and maximum projections of stacks were generated. In each cell, three ROIs were defined and analyzed for signal overlap (PCC). On the left, representative ROIs are indicated for each analyzed combination. The histogram on the right represents the mean coefficients for the different combinations (error bars = standard deviation). The overlap of SKD1 with UBP1b (indicated as SKD1) and the negative control UB1b/UBP1b tilt from Chapter 3.3.2 are included in the histogram for comparison.

**Table 3.6. Statistical analysis of colocalization between ESCRTIII core and associated proteins and UBPIb.** All datasets were normally distributed with the exception of VPS46.2 (Shapiro-Wilk-test). Normally distributed datasets were evaluated for significant colocalization differences using the Welch’s two sample t-test. For comparisons with the VPS46.2 dataset, the Wilcoxon-Mann-Whitney-test was used. Significance level are indicated as following: n.s. = not significant,  $p < 0.05 = *$ ,  $p < 0.01 = **$ ,  $p < 0.001 = ***$ ). Detailed p-values are available in Appendix, Table A.9.

	VPS 32.1	VPS 24.1	VPS2.2 YFP	YFP VPS2.2	VPS 46.1	VPS 46.2	VPS 60.2	LIP5	SKD1 AQ	SKD1	UBP1b UBP1b tilt
VPS32.1		n.s.	*	**	***	***	n.s.	n.s.	***	***	***
VPS24.1	n.s.		***	***	***	***	n.s.	***	***	***	***
VPS2.2 YFP	*	***		n.s.	n.s.	***	n.s.	n.s.	***	***	***
YFP VPS2.2	**	***	n.s.		n.s.	***	*	n.s.	***	***	***
VPS46.1	***	***	n.s.	n.s.		n.s.	***	**	***	***	***
VPS46.2	***	***	***	***	n.s.		***	***	**	***	***
VPS60.2	n.s.	n.s.	n.s.	*	***	***		n.s.	***	***	***
LIP5	n.s.	***	n.s.	n.s.	**	***	n.s.		***	***	***
SKD1 AQ	***	***	***	***	***	**	***	***		***	***
SKD1	***	***	***	***	***	***	***	***	***		***
UBP1b UBP1b tilt	***	***	***	***	***	***	***	***	***	***	

Figure 3.17 depicts the analyzed combinations, examples of the analyzed ROIs and the mean PCCs in a histogram. The previously determined coefficient of the SKD1-mCHERRY/ YFP-UBP1b overlap as well as the negative control UBPIb/ UBPIb tilt (Chapter 3.3.2) are plotted for comparison.

The overlap quantification confirmed the impressions gained in the colocalization study of Chapter 3.4.4. The ESCRTIII core components VPS24.1 ( $0.23 \pm 0.08$ ) and VPS32.1 ( $0.26 \pm 0.08$ ) share little signal overlap with UBPIb. A similar weak correlation of localization is observable for the ESCRTIII associated proteins VPS60.2 ( $0.27 \pm 0.12$ ) and LIP5 ( $0.31 \pm 0.10$ ) with UBPIb. Though all measured PCCs are significantly higher than the negative

control, they are less than half of the coefficient determined for SKD1 and UBP1b ( $0.73 \pm 0.08$ ) and probably indicate no or very weak positive correlation.

The PCC of VPS46.1 ( $0.40 \pm 0.15$ ) and VPS46.2 ( $0.48 \pm 0.16$ ) are comparable to each other and are significantly higher than the ones of the other tested ESCRTIII core and associated proteins. The overlap of VPS46.2 with UBP1b is higher than for VPS46.1, although the difference is not significant due to high standard deviation. Nonetheless, this result is in agreement with localization in the experiment described in Chapter 3.4.2 and 3.4.4, in which VPS46.2 showed stronger heat-dependent granulation than VPS46.1.

As previously discussed, the C-terminally modified variant of VPS2.2 seems to be inhibited in endosomal membrane dissociation and does not change its localization upon heat stress treatment. When N-terminally modified, VPS2.2 localizes in distinct patches presumably at the PM but still forms granules which partially coincide with UBP1b granules after heat stress treatment (Figure 3.16). This difference in localization is not reflected by the PCC. The coefficients of VPS2.2-YFP ( $0.33 \pm 0.13$ ) and YFP-VPS2.2 ( $0.34 \pm 0.11$ ) were not significantly different from each other and in general rather low. This can be explained by the large portion of YFP-VPS2.2 which still remained in the unusual patches after heat stress. This result points out once more that the usage of a different transformation system or antibody staining of the endogenous protein might be necessary to determine the heat-dependent subcellular localization of VPS2.2.

Finally, the colocalization coefficient of SKD1-AQ with UBP1b was determined. The signal overlap of this SKD1 variant with UBP1b was still considerably high ( $0.58 \pm 0.12$ ) but significantly lower than the coefficient of the wild type protein. Again, this is in accordance with the observation that some larger SKD1-AQ labeled structures do not or only partially coincide with heat-induced UBP1b granules.

To summarize, the homologous ESCRTIII-associated proteins VPS46.1 and VPS46.2 as well as the dominant-negative SKD1-AQ protein colocalized to a considerable degree with the SG marker protein UBP1b after heat stress treatment. The ESCRTIII core proteins VPS24.1, VPS32.1 and both tested recombinant versions of the VPS2.2 protein showed little signal co-occurrence with UBP1b. The same applies to the ESCRTIII associated components VPS60.2 and LIP5. This is particularly surprising in the case of LIP5 since it contains a considerable degree of disorder (Chapter 3.4.1) and is a strong interactor and stimulator of SKD1 function (Haas et al., 2007; Shahriari et al., 2010). An interesting aspect of this study is that the VPS24.1

protein (and to a lesser extent VPS60.2) shifts its localization from mainly cytosolic to granular after heat stress treatment but does not colocalize significantly with the SG marker UBP1b. All in all, the picture emerges that the heat-triggered association with mRNP granules is not a general feature of ESCRTIII proteins but rather of a subset of proteins.

### **3.5 Heat-dependent interactome of SKD1**

So far this study showed that the SKD1 protein changes its localization from the cytosol to mRNP granules after heat stress. The relocalization seems to be independent of endosomal structures and is reduced when SKD1 association with membranes is enhanced. It was further shown that the ESCRTIII associated proteins VPS46.1 and VPS46.2 undergo a similar shift in localization. However, not all ESCRTIII components exhibit this localization behavior.

The first chapter of this study tested potential protein interactions of the ESCRTIII proteins with known marker proteins of P-bodies and SGs. Some interactions were identified for SKD1 regulating proteins, but none for SKD1 itself. This might indicate that the SKD1 localization shift is dependent on ESCRTIII proteins which interact with mRNP components. An alternative explanation is provided by the nature of mRNP granule formation: A hallmark of mRNP granules is their highly dynamic assembly and ongoing exchange of proteins and mRNAs with other granules or the cytosol. These characteristics are thought to be facilitated by low-affinity protein-protein interactions between IDRs of mRNP granule components (Kedersha et al., 2013). Thus, SKD1 might interact with mRNP granule proteins with low affinity and only under certain cellular conditions. Further, only a subset of proteins was tested for protein interactions and SKD1 might interact with other mRNP granule components. To address this aspect, the heat-dependent *in-vivo* interactome of SKD1 was investigated.

#### **3.5.1 Experimental approach and statistics of the heat-dependent SKD1 interactome**

For the identification of *in-vivo* interactors of SKD1, the established *35S::GFP-SKD1* line was used. The strategy was to co-immunoprecipitate potential interactors of GFP-SKD1 from cell extracts of untreated or heat treated rosette leaves and to analyze the eluted proteins by mass spectrometry. A line overexpressing free YFP without a fused protein (*35S::YFP*) was used as a negative control and subjected to the same treatment regime as the *35S::GFP-SKD1* line. The general outline of the interactome approach is depicted in Figure 3.18.

First, it was tested if the used extraction method and immunoprecipitation allowed the enrichment of free YFP and GFP-SKD1 in respect to total protein content. Further, it was important to see that the GFP-SKD1 protein remained intact and was not degraded to a larger

## Results

extent before or in the process of immunoprecipitation. Hence, the total protein content of rosette leaves of the *35S::GFP-SKD1* and the *35S::YFP* line were extracted following the protocol given in chapter 2.6.1. For the immunoprecipitation, magnetic  $\alpha$ -GFP  $\mu$ MACS (Miltenyi Biotec) were added to the lysates, incubated and applied to the columns. Bound proteins were eluted after several washing steps and subjected to SDS-PAGE followed by immunoblotting with an antibody against GFP or Coomassie staining. Used materials and volumes were kept constant for the protocol test.

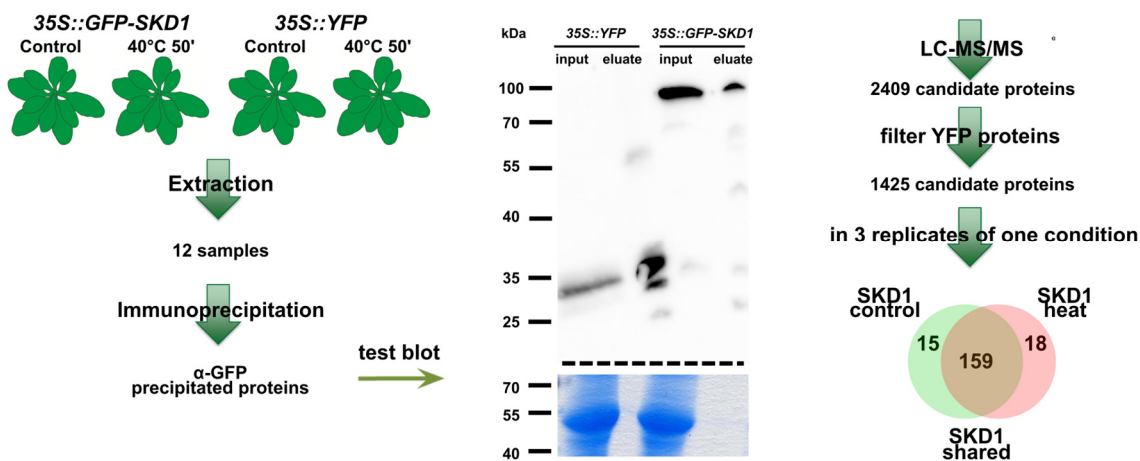


**Figure 3.18. Strategy, test blot, and candidate filtering of the SKD1 interactome approach.** To identify the heat-dependent SKD1 interactome, proteins of rosette leaves of control or heat treated transgenic *35S::GFP-SKD1* plants were extracted and subjected to  $\alpha$ -GFP immunoprecipitation. As a control, leaves from *35S::YFP* plants were used. The enrichment of the target proteins compared to the total protein amount was tested by SDS-PAGE. Same volumes of input and eluate samples were used. YFP (26 kDa) and GFP-SKD1 (77 kDa) were detected with an  $\alpha$ -GFP antibody via immunoblotting (exposure time: 70'') and total protein amount was visualized by Coomassie staining. After confirmation of enrichment, three replicates of each genotype and condition (total: twelve samples) were digested (Lys-C, Trypsin) and subjected to LC-MS/MS analysis. In total, 2409 proteins were identified in all samples. Proteins, which were identified in the YFP replicates, were removed from the candidate list. From the remaining 1425 candidates, only proteins which were identified in three replicates of one condition were considered. This approach resulted in two lists which shared a significant overlap. Proteins, which were present in three replicates of one condition and in two replicates of the other, were combined to the SKD1 shared list (159). Proteins, which were not identified or only in one replicate in the heat treated samples, were listed as SKD1 control candidates (15) and vice versa (SKD1 heat: 18). The scheme of the rosette leaves was modified from H. Wolff, 2016, CEPLAS Planter's Punch.

Figure 3.18 depicts the results of the protocol test for the immunoprecipitation of GFP-SKD1 and free YFP. The molecular weight of GFP-SKD1 amounts to approximately 77 kDa and 26 kDa for free GFP/YFP. In the input control as well as in the eluate of the *35S::GFP-SKD1* plants, a distinct band at approximately 100 kDa is visible. The gel, which was used for blotting, ran slightly uneven and the visible bands of the *35S::GFP-SKD1* samples are more likely to migrate at a height representing a protein size between 70 and 100kDa, which is the range in which GFP-SKD1 is expected. In addition, no strong signals were detected at lower molecular weights, indicating that the majority GFP-SKD1 protein did not undergo degradation during protein extraction or immunoprecipitation. A few very weak additional bands were visible in the eluate of the GFP-SKD1 sample. However, a similar pattern of bands was visible in the eluate of the YFP sample and therefore might be an artifact caused by the used beads. In the *35S::YFP* samples, a distinct band between 25 and 35 kDa was detectable, which fits the expected size of YFP. In the eluate, a second band with slightly lower molecular weight was detected. Though YFP degradation cannot be ruled out, an artifact caused by uneven gel polymerization or movement during protein transfer (e.g. air bubble) could explain this observation since the protein bands show evidence for that (“hole” in the bands).

The comparison of the signal intensities of GFP-SKD1 and YFP to the total protein amount (Coomassie staining) demonstrates that the immunoprecipitation successfully enriched the tagged proteins. The input samples of the *35S::GFP-SKD1* and *35S::YFP* lysates both showed strong staining while nearly no protein was detected in the corresponding eluate (exemplified by the band representing the large Rubisco subunit, approximately 55 kDa).

After the confirmation that the GFP-SKD1 protein was not degraded and successfully enriched compared to total protein content, samples were prepared for mass spectrometry. For each genotype (*35S::GFP-SKD1* versus *35S::YFP*) and condition (control versus heat treatment), proteins from three biological replicates were extracted and subjected to  $\alpha$ -GFP immunoprecipitation (in total twelve samples). Instead of eluting the bound proteins, an in-solution digest was performed on the beads (for details, see Chapter 2.6.2). The generated peptides were subjected to liquid chromatography and tandem mass spectrometry (LC-MS/MS, S. Müller, Proteomics Core Facility Cologne).

In summary, 2409 *A.thaliana* proteins were identified. A prerequisite for a successful interactome analysis is that the target protein is sufficiently enriched in comparison to all identified proteins. The highest intensity-based absolute quantification value (iBAQ value, a

normalized measurement for protein abundance) was measured for peptides of SKD1, making it the most abundant protein in the analyzed *35S::GFP-SKD1* samples.

To increase the stringency of the GFP-SKD1 interactome, all proteins which were identified in one of the six control samples (*35S::YFP* control and heat treatment) were excluded. This eliminated 984 proteins from the potential interactome list. The remaining 1425 proteins were further filtered with the criteria that a protein needed to be identified in all three replicates of one condition of the *35S::GFP-SKD1* samples. This approach resulted in two lists of potential SKD1 interactors: Proteins which were identified in each of the GFP-SKD1 control replicates (146 proteins) and proteins which were identified in each of the GFP-SKD1 heat replicates (132 proteins, for details, see Appendix, Table A.10).

159 proteins were shared between control and heat samples (present in at least 2 replicates). Only 15 proteins of the control samples and 18 proteins of the heat samples were exclusive for the respective condition (found in none or one replicate of the opposite treatment). No heat-dependent significant differences in the list of shared interactors were identified. This indicates that the identified heat-dependent interactome does not differ drastically from the control interactome. This might be explained by transient interactions during heat.

The confidence in an interactome is increased, if known interactors of the bait protein are identified by the used method. Here, two well-established *A. thaliana* ESCRTIII proteins and known SKD1 interactors were identified: ISTL1 and VPS46.2 (Spitzer et al., 2009; Buono et al., 2016). The ISTL1 protein was identified in three control replicates and two heat treated replicates, while the VPS46.2 protein was identified in one control replicate and in three heat replicates.

### **3.5.2 Characterization of the SKD1 interactome by GO and functional classification**

To further elucidate, if potential interactors of SKD1 are involved in a specific biological process or are present in a particular subcellular compartment, a gene ontology (GO) enrichment study was performed. For that, the three interactor sets (SKD1 share, control, and heat) were analyzed with the PANTHER classification System (Thomas et al., 2003; Mi et al., 2010). The frequencies of identified GO categories in the interactome sets were compared to the whole *A.thaliana* genome and overrepresented terms were given with an estimation of significance. Smaller sets of genes decrease the likelihood to identify significant category enrichment. Indeed, for the SKD1 control set, no overrepresented GO terms (biological process and cellular component) were identified and only one for the SKD1 heat set (biological process:

protein folding). For the SKD1 shared interactor set, several overrepresented categories for biological processes and cellular components were identified (Table 3.7).

**Table 3.7. PANTHER GO enrichment analysis of SKD1 shared interactors.** All categories of the PANTHER GO-Slim Biological Process and Cellular Component, which were significantly enriched in the SKD1 shared interactor list ( $q$ -value  $\leq 0.05$ ) compared to the *A. thaliana* genome, are indicated with the respective fold of enrichment.

<b>PANTHER GO-Slim Biological Process</b>	<b>Proteins in category</b>	<b>Fold enrichment</b>
gluconeogenesis	2	20.10
mitochondrion organization	11	17.73
protein folding	13	15.64
tRNA aminoacylation for protein translation	4	11.39
protein targeting	7	7.03
protein complex assembly	7	6.61
protein complex biogenesis	7	6.50
monosaccharide metabolic process	4	6.33
translation	8	4.44
homeostatic process	5	4.38
intracellular protein transport	14	4.21
protein transport	14	3.99
vesicle-mediated transport	11	3.61
protein metabolic process	36	3.51
organelle organization	19	3.46
cellular component organization	22	2.77
cellular component organization or biogenesis	25	2.60
cellular component biogenesis	12	2.59
catabolic process	18	2.38
transport	18	2.13
localization	18	1.95
cellular process	77	1.92
primary metabolic process	57	1.82
metabolic process	72	1.78
<b>PANTHER GO-Slim Cellular Component</b>	<b>Proteins in category</b>	<b>Fold enrichment</b>
mitochondrion	18	7.37
cytosol	30	6.60
vacuole	8	4.15
protein complex	30	3.73
macromolecular complex	34	3.03
cytoplasm	60	2.83
intracellular	68	1.97
cell part	68	1.88
organelle	46	1.72

The top enriched GO categories of the shared SKD1 interactors described unexpected biological functions (e.g. gluconeogenesis, mitochondrial organization, protein folding), yet also several categories were enriched which reflect the known function of SKD1 (intracellular protein transport, vesicle-mediated transport, protein targeting). In terms of enrichment in a specific cellular compartment, the most enriched categories were mitochondrion, cytosol and vacuole.

GO enrichment analyses can give a first impression of the identity and general cellular function of a set of proteins. However, category annotations might not be applicable to a certain experimental question and be fairly superficial. Therefore, the proteins in the different sets were individually analyzed and classified on the basis of database annotations (TAIR) and available literature. Short descriptions of the potential interactors are given in Appendix, Table A.10.

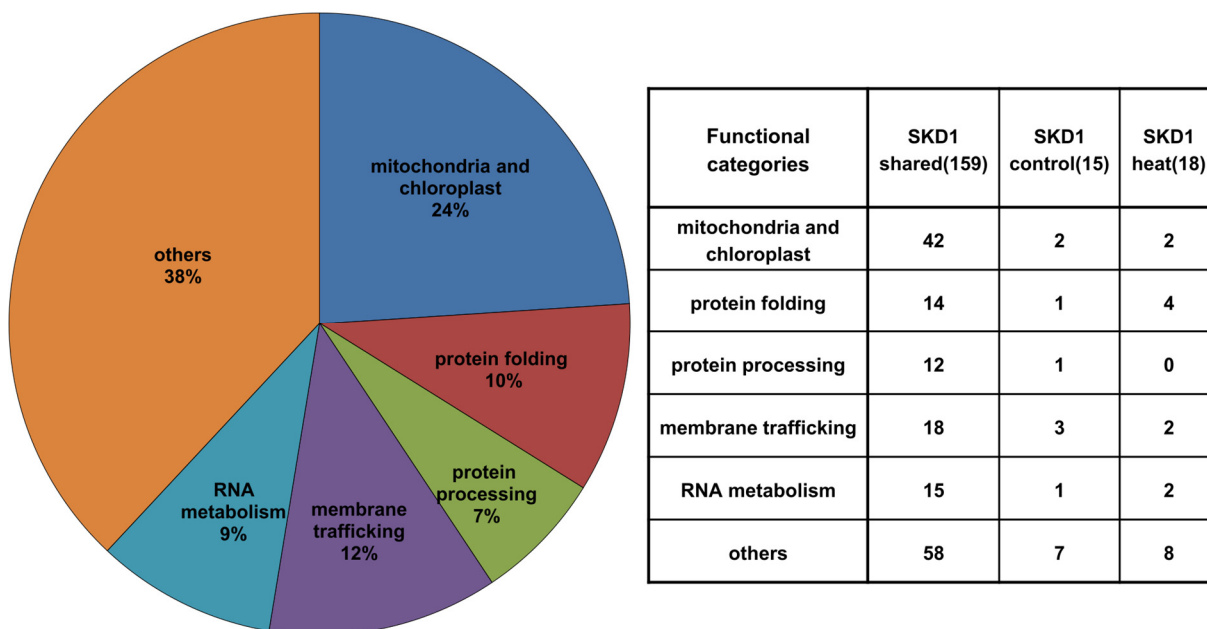


**Figure 3.19. Individual functional classifications of the SKD1 interactome candidates.** Individual descriptions of the SKD1 interactome candidates were made on the basis of database annotations (TAIR) and available literature. On the basis of the descriptions, proteins were sorted in following categories: mitochondria and chloroplast, protein folding, protein processing, membrane trafficking, RNA metabolism, and others. The pie chart depicts the percentage of all proteins which fall in the respective category. The table indicates the number of proteins which fall in these categories.

The SKD1 interactors were grouped based on the individual protein descriptions (Figure 3.19). A high number of proteins was described to be chloroplastic or mitochondrial and might represent false positives since SKD1 is not described to be in these organelles. Thus, they were excluded from further characterization and analysis.

Several interactors were described to be involved in protein folding (chaperones, T-complex protein 1/TCP-1 chaperonins, HSPs) or protein degradation. Proteins of both functional classes have been described to associate with mRNP granules and to prevent abnormal aggregation and promote granule disassembly (Weber et al., 2008; Lokdarshi et al., 2016; Jain et al., 2016; Muthuramalingam et al., 2017; Mateju et al., 2017). A comparison of the identified SKD1 interactors with the interactomes of two characterized SG proteins in *A.thaliana* (RBP45b and CML38) showed some overlap of the interactomes (RBP45b: seven proteins, CML38, 15 proteins, see Appendix, Table A.10). Interestingly, most of the shared interactors were in the protein folding category (Lokdarshi et al., 2016; Muthuramalingam et al., 2017).

SKD1 exerts a well established function in protein trafficking via MVB maturation. Therefore it was interesting to see, which membrane trafficking proteins co-precipitated with SKD1. As previously mentioned, the ESCRTIII associated components ISTL1 and VPS46.2 were indentified. Several vesicle-coating proteins or adaptor proteins were in the list of potential interactors. Further, proteins which are localized over an ESCRT-dependent trafficking route or are involved in this process were identified (PIN polarity establishment proteins, Aquaporin PIP1 family proteins, Spitzer et al., 2009, Keicher et al., 2017; Wang et al., 2017). An interesting finding was that several components of the endosomal tethering complexes CORVET (class C core vacuole/endosome tethering) and HOPS (homotypic fusion and vacuole protein sorting) were identified (Solinger and Spang, 2013). Further, subunits of vacuolar H<sup>+</sup>-ATPases (V-ATPases) which acidify the endosomal lumen in the process of endosomal maturation were among the potential interactors (Nishi and Forgac, 2002).

One aim of the SKD1 interactome analysis was to identify proteins, which associate to mRNP granules, and by that to further elucidate the nature of the relationship of SKD1 with mRNP granules. Therefore, all proteins, which are involved with RNA metabolism, were grouped. This group included several RNA helicases, a CML38 homolog, nucleo-cytoplasmic shuttle proteins, 60S and 30S ribosomal proteins as well as translation initiation factors. Further, the well established P-body protein VCS was identified.

A large number of proteins were not further categorized on the basis of their cellular functions. The majority of those candidates are described to be involved in biosynthetic or metabolic processes. In future, the in-depth classification of these candidates based on their involvement in particular cellular processes might reveal new connections between different pathways and ESCRT-dependent trafficking.

All in all, several interesting potential interactors of SKD1 were identified by this *in-vivo* interactome approach. Though no striking differences between unstressed and heat-induced interactors were identified, there are indications that SKD1 interacts with proteins identified in interactomes of mRNP granule proteins. Further, several proteins which are involved with RNA metabolic processes and potentially localize in mRNP granules were among the interactor candidates.

### **3.5.3 Selection and cloning of SKD1 interactome candidates**

The next step after the identification of new potential SKD1-interacting proteins was the analysis of their subcellular localization in respect to SKD1 and an mRNP granule marker. Furthermore, the confirmation of their interaction with SKD1 via protein-protein interaction assays was planned. For that, the CDS of the representative candidate genes were amplified and cloned in the Gateway-compatible vectors (Chapter 2.5.3 and Appendix, Table A.1).

Several candidates from the group of proteins classified to be involved in RNA metabolism were selected. Further it was of interest to investigate the subcellular localizations and interactions of some of the identified membrane-trafficking proteins. Table 3.8 summarizes the selected candidates from each of the two groups.

**Table 3.8 List of SKD1 interactome candidates selected for further analysis.** For the interactome candidates, the used names, identifier (ATG), CDS sequence length, and short annotations are given. The subcellular localization is either based on literature or on the SUBA consensus prediction (SUBA4, Hooper et al., 2017).

<b>Membrane trafficking</b>					
<b>Full name</b>	<b>Name</b>	<b>ATG</b>	<b>CDS (bp)</b>	<b>Annotations and descriptions</b>	<b>Subcellular localization</b>
VACUOLAR PROTEIN SORTING 18	VPS18	AT1G12470.1	2967	CORVET/HOPS complex, endosome to vacuole fusion	cytosol, endosomal structures, tonoplast
GENERAL REGULATORY FACTOR 2	GRF2	AT1G78300.1	780	14-3-3 protein, PIN polarity establishment	cytosol
GENERAL REGULATORY FACTOR 9	GRF9	AT2G42590.3	831	14-3-3 protein, PIN polarity establishment	cytosol
PLASMA MEMBRANE INTRINSIC PROTEIN 1-1	PIP1-1	AT3G61430.1	861	transmembrane water transporter, transport ESCRT-dependent	PM
SECRETORY13 A (homolog)	SEC13A	AT3G01340.1	909	COPII vesicle budding, protein transport	ER
FLOTTILIN-LIKE PROTEIN 1	FLOT1	AT5G25250.1	1413	membrane invagination, endocytosis	PM, endosomes, cytosol
INCREASED SODIUM TOLERANCE1-LIKE 1	ISTL1	AT1G34220.2	1860	Regulator of SKD1 activity, ESCRTIII associated	nucleus, cytosol, endosomes
<b>RNA metabolism</b>					
<b>Full name</b>	<b>Name</b>	<b>ATG</b>	<b>CDS (bp)</b>	<b>Annotations and descriptions</b>	<b>Subcellular localization</b>
EUKARYOTIC TRANSLATION INITIATION FACTOR 4B1	eIF4B1	AT3G26400.1	1599	translation initiation	cytosol
HOMOLOG OF HUMAN U2AF65-ASSOCIATED PROTEIN	UAP56A	AT5G11170.1	1284	DEAD-box RNA helicase, interacts with nuclear export factors, mRNA splicing	nucleus
LOW EXPRESSION OF OSMOTICALLY RESPONSIVE GENES 4	LOS4	AT3G53110.1	1491	DEAD-box RNA helicase, nuclear envelope and cytosol, mRNA export from nucleus	nuclear envelope, cytosol,
CALMODULIN-LIKE	CML10	AT2G41090.1	576	calmodulin-like calcium-binding protein, calcium-sensor	nucleus, cytosol
UBIQUITIN-SPECIFIC PROTEASE 12	UBP12	AT5G06600.1	3351	deubiquitination, involved in JA signaling and circadian clock regulation	nucleus, cytosol
SMALL NUCLEAR RIBONUCLEOPROTEIN F	RUXF	AT4G30220.2	291	mRNA splicing	nucleus, cytosol
RRM-containing protein	RRM	AT3G23900.1	2964	RRM-containing protein, RNA binding	nucleus
NUCLEAR TRANSPORT FACTOR 2	NTF2	AT5G60980.4	1380	RRM-containing protein, nucleocytoplasmic transport	nucleus, cytosol

From the membrane trafficking components, seven proteins were cloned for further analysis. VPS18 is a component of the conserved HOPS/CORVET multiprotein tethering complex which mediates vacuole-to-vacuole fusions (HOPS) and MVB-vacuole fusions (CORVET) in plants (Takemoto et al., 2018). Several components of this protein complex, or proteins associated with it, were identified in the interactome (VPS18, VPS41, VCL1/VPS16, SYP41 interactor TNO1, Rojo et al., 2001; Vukašinović and Žárský, 2016; Roy and Bassam, 2017). The attempt to amplify VPS41, VCL1, and TNO1 was not successful in this study. Thus, VPS18 was the only HOPS/CORVET component further characterized.

Two 14-3-3 proteins, GRF2 and GRF9, were identified in the interactome. The protein class of 14-3-3 proteins is involved in diverse cellular processes in eukaryotes and regulates the activity and localization of respective target proteins via protein-protein interactions (Mackintosh, 2004). In *A. thaliana* it was shown that 14-3-3 proteins are involved in the establishment of polar cellular localization of PIN proteins via regulating trafficking processes (Keicher et al., 2017). Another cargo protein of ESCRT-dependent trafficking is the PM aquaporin PIP1-1 (Boursiac et al., 2005; Wang et al., 2017).

The *A. thaliana* SEC13A protein is a WD-40 repeat family protein and has not been characterized so far. It is one of two paralogs of the conserved, eukaryotic Sec13 proteins which is a well-known component of the COPII (COAT PROTEIN COMPLEX II) vesicle coat (ER to Golgi protein trafficking, Chung et al., 2016). FLOT1 is a membrane microdomain protein which regulates Clathrin-independent endocytosis and is directed to vacuolar degradation during pathogen attack (Li et al., 2012; Yu et al., 2017). The established ESCRTIII associated component ISTL1 was not analyzed in terms of heat-dependent localization in this study so far (Buono et al. 2016). Therefore, ISTL1 was added to the list of membrane trafficking candidates and cloned for the subcellular localization and protein interaction analysis.

From the list of identified RNA metabolic proteins, eight candidates were chosen and cloned for further analysis. Among them was the translation initiation factor eIF4B1. The eIF4B1 protein is part of the eIF4 group of initiation factors, has RNA binding activity and stimulates the RNA unwinding activity of eIF4A and eIF4F (Bi et al., 2000; Rogers et al., 2001; Mayberry et al., 2009). Mammalian homologs of eIF4B1 and other members of the eIF4 group are regularly found in mRNP granules, making the *A. thaliana* eIF4B1 protein an interesting candidate for further analysis (Buchan and Parker, 2009).

The DEAD-box RNA helicase UAP56A has been described to function in mRNA slicing as well as mRNA export from the nucleus to the cytosol in *A. thaliana* (Kammel et al., 2013, Pfaff et al., 2018). LOS4 is another DEAD-box RNA helicase, which has been shown to regulate mRNA export from the nucleus (Gong et al., 2002 and 2005). Similar to translation initiation factors, RNA helicases are regularly found in granules (Buchan and Parker, 2009; Jain et al., 2016; Bailey-Serres, 2017). UAP56A has even been identified by an interactome approach as potential interactor of CML38, which was shown to localize to mRNP granules during hypoxia in the same study (Lokdarshi et al., 2016). In the SKD1 interactome, another member of the CML protein family was identified. The CML10 protein has been described to regulate the biosynthesis of ascorbic acid in a calcium-dependent manner (Cho et al., 2016).

The deubitinase UBP12 was included in the analysis since the inhibition of the ubiquitin-dependent proteasome system affects mRNP granule formation in human cells (Mazroui et al., 2007). In plants, UBP12 was shown to regulate the protein stability of transcription factors (Jeong et al., 2017; Cui et al., 2013). The RUXF protein is a small nuclear mRNP. It contains an LSM domain and has been shown to regulate alternative splicing in *A.thaliana* (Kanno et al., 2017).

Finally, two RRM-containing proteins were chosen from the candidate list to be further examined. The first one has not been described yet and is simply named RRM in the context of this study. This particular RRM-containing protein was chosen, because it was exclusively identified as an SKD1 interactor after heat stress. The second RRM-containing protein chosen for further analysis was NTF2. In *A. thaliana*, it was shown that NTF2 interacts with a component involved in RNA-mediated gene silencing (Parida et al., 2017). The essential SG component G3BP contains NTF2-like RRMs in mammals and in plants (Tourrière et al., 2003; Krapp et al., 2017). Further, NTF2 was identified in an interactome study of *A. thaliana* SG protein RBP45b as well as in an interactome of the ESCRTIII core component VPS2.2 (Muthuramalingam et al., 2017; Ibl et al., 2012).

The CDS of all listed proteins was successfully amplified from seedling or flower cDNA. For ISTL1 and NTF2, an alternative splice variant (40 aa shorter and 1 aa shorter) was amplified instead of the representative gene model. All sequences were amplified with primers adding Gateway-sites to facilitate the cloning process via BP and LR reactions. Further, the primers contained a degenerate site which allowed the introduction of either a stop codon or a glycine for future C-terminal fusions.

### 3.5.4 Heat stress-dependent subcellular localization of the SKD1 interactome candidates

The analysis of the selected candidates was started with the study of their subcellular localization under normal conditions and after heat stress treatment. For this, the amplified CDS of the candidates were cloned in vectors overexpressing the genes under the control of the 35S *CaMV* promoter and in N- or C-terminal fusion with YFP. Epidermal cells of *A. thaliana* Col-0 rosette leaves were transiently transformed and imaged before and after heat treatment by confocal microscopy. For each candidate, at least five cells were evaluated and representative images are depicted in Figure 3.20 (membrane trafficking candidates) and Figure 3.21 (RNA metabolism candidates).

YFP-VPS18, YFP-GRF2, and YFP-GRF9 exhibited a similar localization: all three proteins were visible in the cytosol and (to some extent) in the nucleus before heat treatment and showed some degree of aggregation after heat treatment (YFP-GR2 rather weak, YFP-GRF9 stronger). These results are in agreement with their predicted or in the literature described localization (Table 3.8).

In contrast to that, the localization of the water channel protein PIP1-1-YFP was not as expected. PIP1-1-YFP was previously shown to localize evenly at the PM of transgenic *A. thaliana* root cells (Wang et al., 2017). In this study, the PIP1-1-YFP protein localized in a net-like structure which presumably represents the ER. This unexpected localization might be caused by defective vesicular transport of PIP1-1 out of the ER. It is not likely that the C-terminal fusion of the fluorescent protein causes PIP1-1 retention in the ER since the same recombinant version was previously used in localization studies (Wang et al., 2017). A possible explanation might be the transient transformation, which sometimes causes proteins to mislocate. The N-terminal fusion version of PIP1-1 showed the same localization as PIP1-1-YFP (data not shown) and was therefore not further analyzed in respect to its subcellular localization.

SEC13A-YFP is predicted to localize to the ER, but showed a cytosolic and nuclear localization in this study. Upon heat stress, the protein was visible in granular structures. FLOT1-YFP was visible in the cytosol and, similar to the other analyzed candidates, showed some weak granular localization after heat stress. The ESCRTIII associated protein ISTL1-YFP was visible in the cytosol and in some dot-like structures which presumably represent MVBs. Heat stress treatment did not change the localization drastically, yet sometimes a few more granular structures were visible.

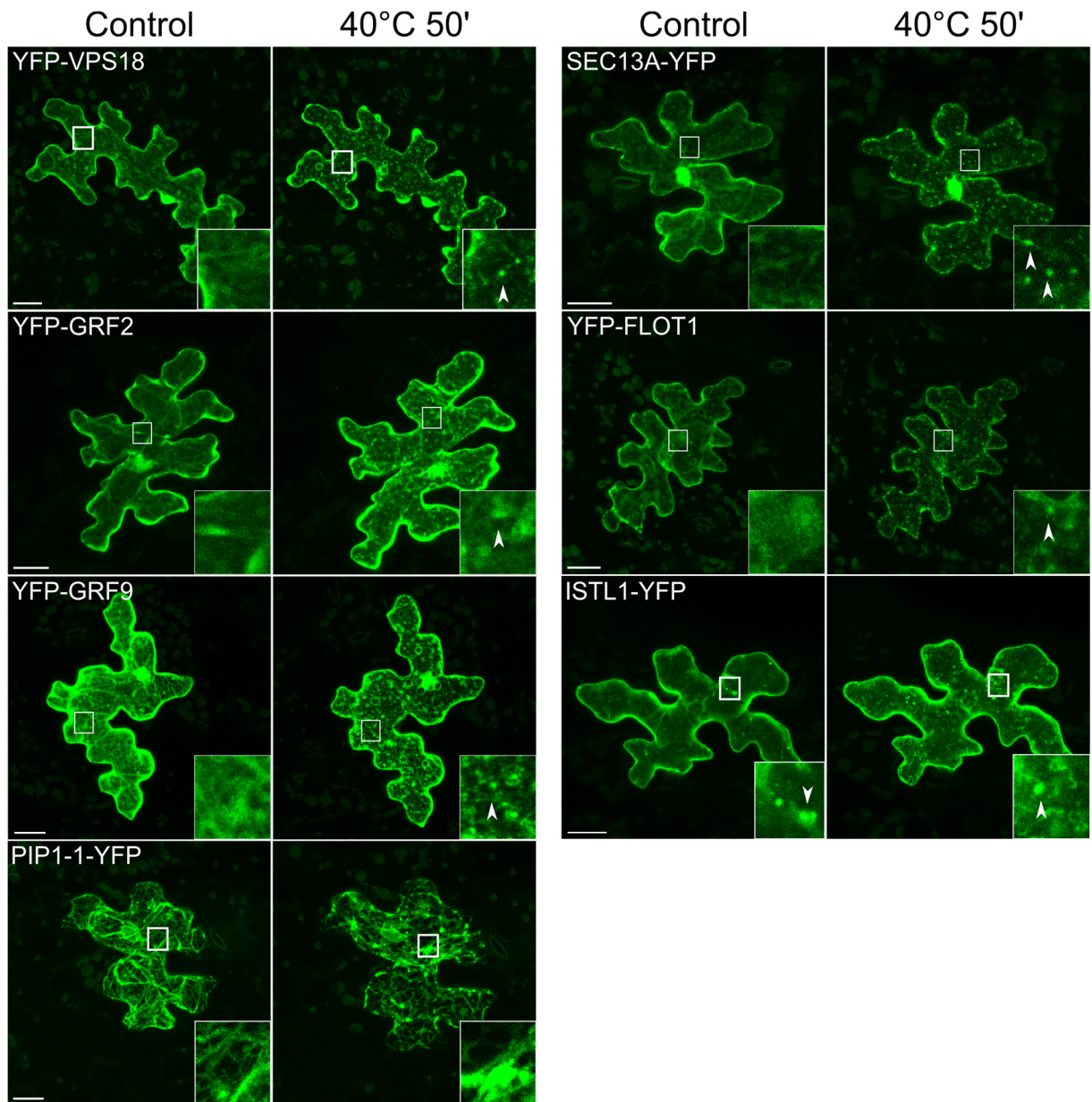


**Figure 3.20. Heat stress-dependent subcellular localization of membrane trafficking candidates.** Epidermal *A. thaliana* Col-0 cells were transiently transformed with a construct overexpressing an SKD1 interactome candidate in N- or C-terminal fusion with YFP. The same cells were imaged by confocal microscopy with the same laser intensities before and after heat stress treatment (40°C 50'). Depicted are representative maximum projections of stacks. Arrow heads indicate cytosolic granules. Bar = 20 μm.

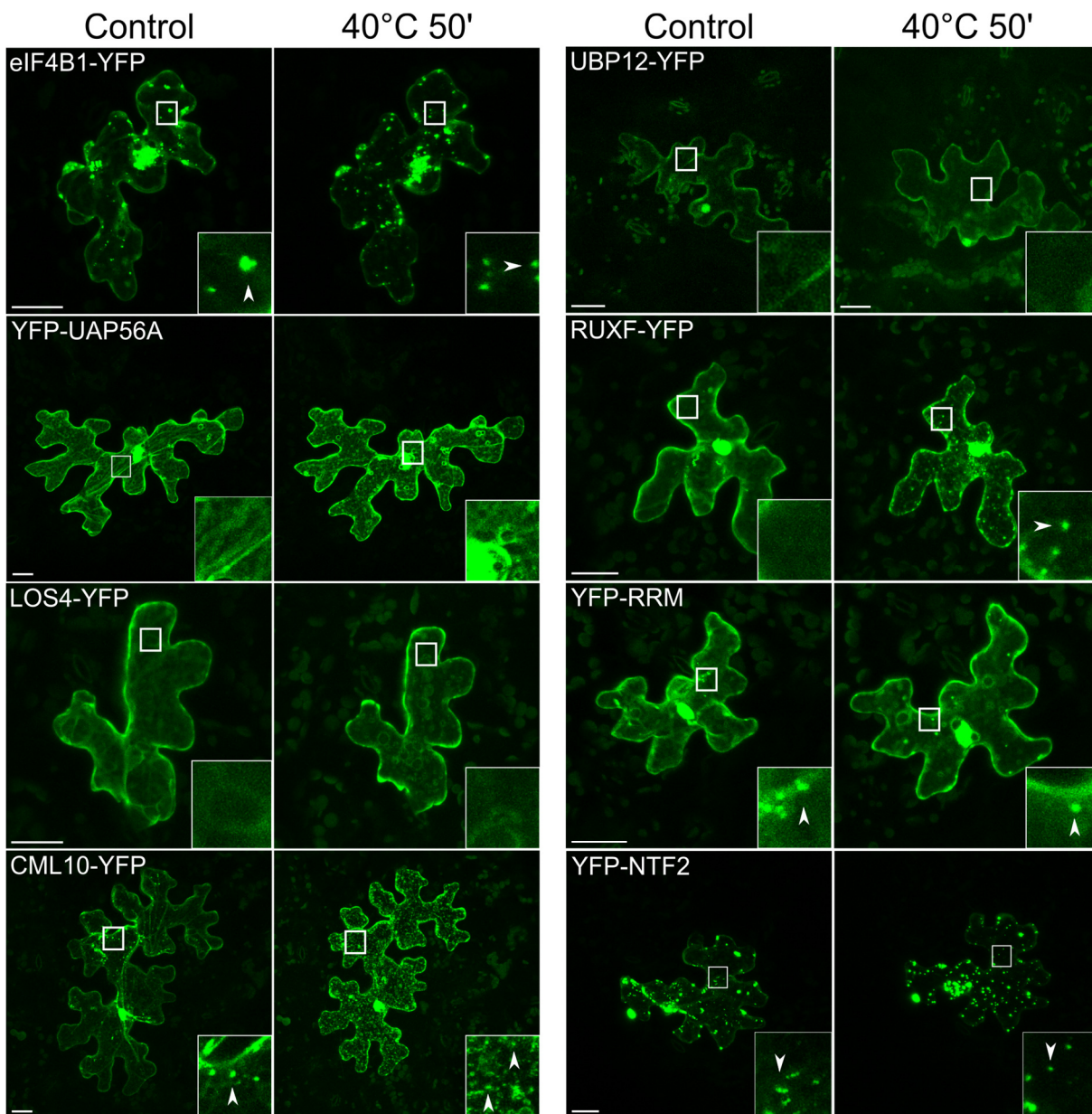


**Figure 3.21. Heat stress-dependent subcellular localization of the RNA metabolism candidates.** Epidermal *A. thaliana* Col-0 cells were transiently transformed, treated, and imaged as described in Figure legend Figure 3.20. For UBP12-YFP, different cells are depicted before and after heat treatment. Arrow heads indicate cytosolic granules. Bar = 20  $\mu$ m.

The translation initiation factor eIF4B1-YFP was visible in very distinct cytosolic granules before and, in slightly stronger ones, after heat treatment. The RNA-helicase YFP-UAP56A was visible in the cytosol and nucleus, though only a nuclear localization has been described so far in *A. thaliana* (Kammel *et al.*, 2013). The second analyzed RNA-helicase, LOS4, was described to localize in the cytosol and to be specifically enriched at the nuclear rim (Gong *et al.*, 2005). A similar localization was observed in this study for LOS4-YFP. Both RNA-helicases did not change their localization upon heat treatment.

The calcium sensor CML10 is predicted to localize to the cytosol and the nucleus. A similar localization was observed in this study for CML10-YFP with additional distinct granules in the cytosol. Heat stress treatment increased the aggregation of CML10-YFP and several smaller granules were visible. The deubiquitination enzyme UBP12 localized to the cytosol and nucleus and did not change its localization after heat stress. Under normal conditions, RUXF-YFP was either visible in larger aggregates (not shown) or evenly distributed in the cytosol. After heat treatment, it localized in distinct small granules.

YFP-RRM was also visible in granules before and after heat treatment, yet its granulation was not very pronounced. In contrast to that, the other analyzed RRM-containing protein, YFP-NTF2, was nearly exclusively in granules before and even stronger after heat treatment.

In summary, all of the analyzed membrane trafficking candidates and six of the eight analyzed RNA metabolism candidates exhibited some degree of granule formation upon heat stress treatment. However, all of the membrane trafficking candidates showed only weak granulation and were evenly distributed in the cytosol under control conditions. The RNA-metabolism candidates localized in more distinct granules, sometimes even in the absence of heat stress.

### **3.5.5 Colocalization analysis of SKD1 interactome candidates with UBP1b**

The next step was to see, whether the observed granular localization of the SKD1 interacting proteins represents an association with mRNP granules. For this, leaf epidermal cells were once more transformed with the constructs overexpressing the candidate genes in fusion to YFP. In addition, mCHERRY-UBP1b was co-transformed as SG marker. The Figure 3.22 and Figure 3.23 show representative pictures of transformed cells before and after heat treatment.

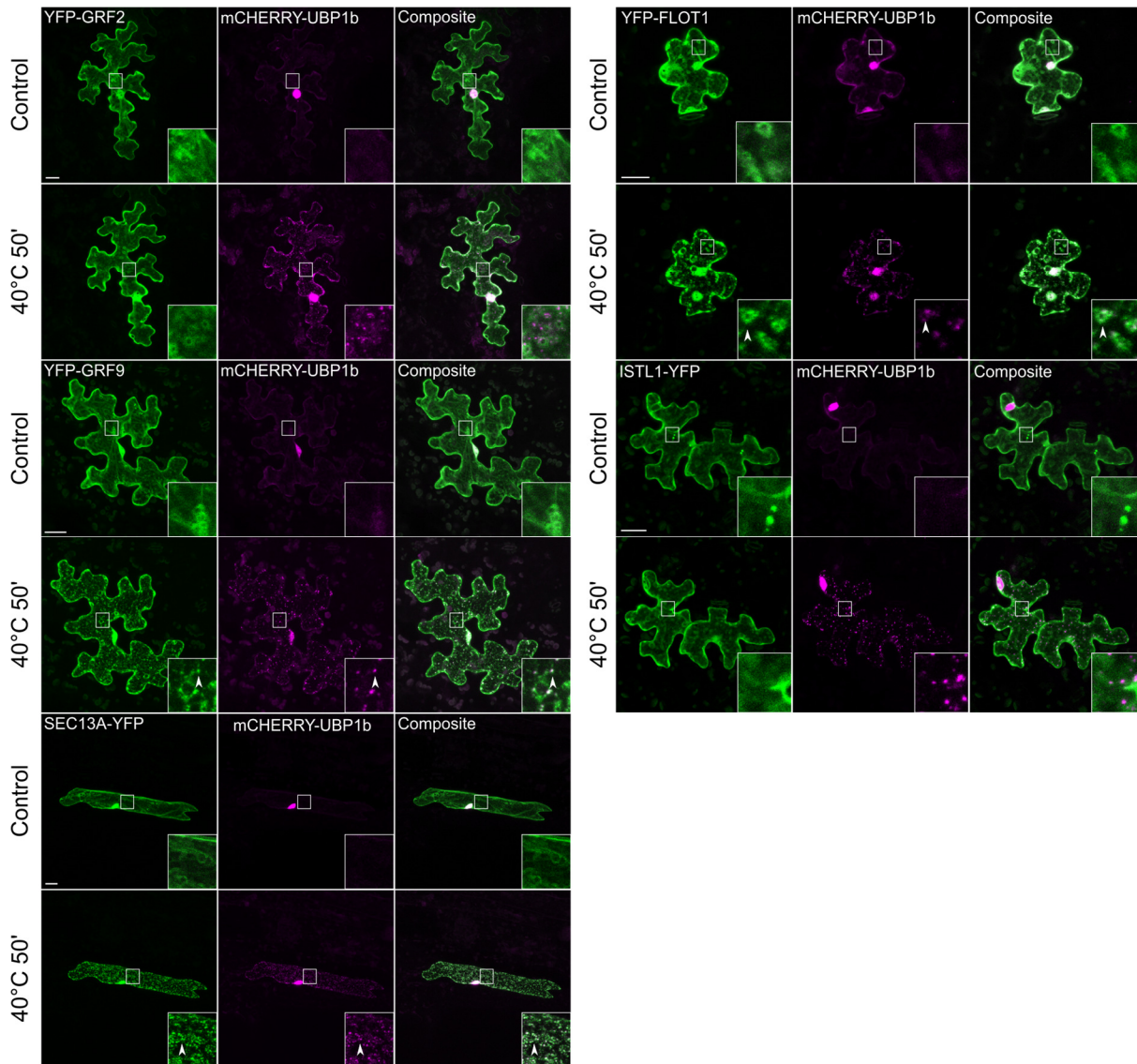


**Figure 3.22. Colocalization analysis of membrane trafficking candidates with mCHERRY-UBP1b.** Epidermal *A. thaliana* Col-0 cells were transiently double-transformed with a construct overexpressing an SKD1 interactome candidate in fusion with YFP and a construct overexpressing mCHERRY-UBP1b. The same cells were imaged by confocal microscopy with the same laser intensities before and after heat stress treatment at 40 °C for 50'. Depicted are representative maximum projections of stacks. Arrow heads indicate colocalizing structures. Bar = 20  $\mu$ m.

The expression of YFP-VPS18 in combination with mCHERRY-UBP1b was very weak and no imaging in a sufficient quality was possible. Therefore, the colocalization of VPS18 with other proteins was not continued in the context of this study.

The 14-3-3- proteins YFP-GRF2 and YFP-GRF9 were previously observed to localize in granules after heat stress, whereby GRF2 granule formation was weaker. In coexpression with mCHERRY-UBP1b, nearly no YFP-GRF2 granulation was observed while GRF9 colocalized with mCHERRY-UBP1b granules after heat stress treatment. SEC13A-YFP localized in heat-

triggered granules in single transformed cells as well as in coexpression with mCHERRY-UBP1b (mid vein cell). Furthermore, SEC13A-YFP and mCHERRY-UBP1b colocalized strongly.

The YFP-FLOT1 protein showed some aggregation after heat stress treatment and partial colocalization with mCHERRY-UBP1b granules. In contrast to that, ISTL1-YFP did not colocalize with mCHERRY-UBP1b.

As mentioned before, several candidates of the RNA metabolism category localized in cytosolic granules independent of treatment. This was also the case for the translation initiation factor eIF4B1-YFP in coexpression with mCHERRY-UBP1b (Figure 3.23). Interestingly, this coexpression caused mCHERRY-UBP1b to co-localize to eIF4B1-YFP granules in the absence of heat stress. After heat stress treatment, significantly more mCHERRY-UBP1b was present in cytosolic granules.

The two analyzed RNA helicases YFP-UAP56A and LOS4-YFP did not show a shift in localization upon heat stress treatment when coexpressed with mCHERRY-UBP1b. In contrast to that, CML10-YFP strongly colocalized with mCHERRY-UBP1b in granules after heat stress. Some CML10-YFP granules showed faint mCHERRY-UBP1b signal even in the absence of heat stress, indicating that CML10 has the capability to recruit mCHERRY-UBP1b to cytosolic granules in the absence of stress.

Similar to the two RNA-helicases, the deubiquitination protein UBP12-YFP and the putative RNA binding protein YFP-RRM did not change their localization when coexpressed with mCHERRY-UBP1b. The other analyzed RNA-binding protein, NTF2-YFP, was previously shown to localize in granules before heat treatment and in even stronger, more defined granules after heat treatment (Chapter 3.5.4 Figure 3.21). The same was observed in coexpression with mCHERRY-UBP1b. The effect of mCHERRY-UBP1b recruitment in granules in the absence of stress was even stronger for NTF2-YFP than for eIF4B1-YFP or CML10-YFP.

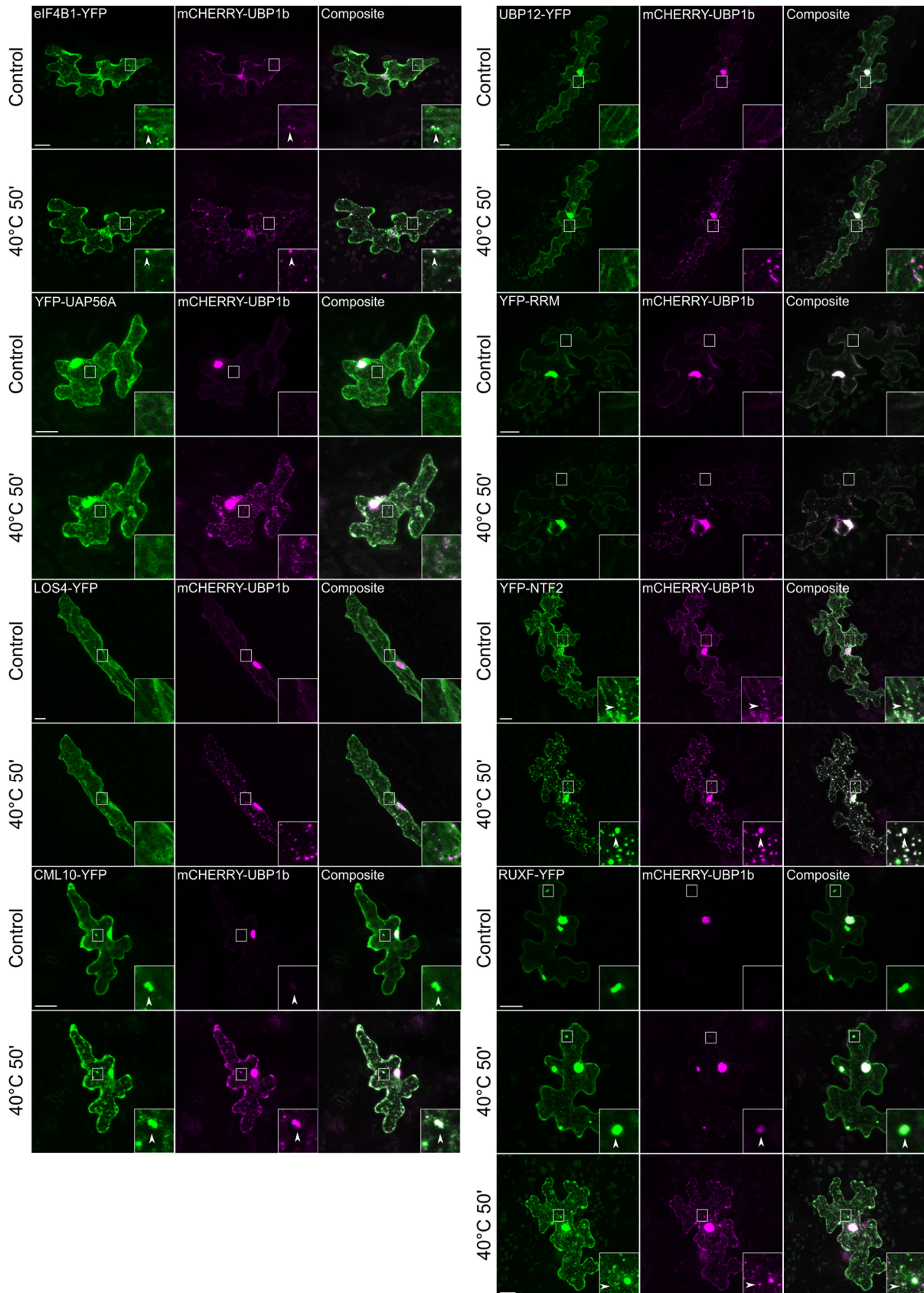


**Figure 3.23. Colocalization analysis of RNA metabolism candidates with mCHERRY-UBP1b.** Epidermal *A. thaliana* Col-0 cells were transiently double-transformed, treated and images as described in Figure legend Figure 3.22. An additional example of a heat treated cell is depicted for RUXF-YFP. Arrow heads indicate colocalizing structures. Bar = 20  $\mu$ m.

The RUXF-YFP protein localized either evenly distributed in the cytosol or in a few larger aggregates in the absence of stress. The same pattern of localization was observed when mCHERRY-UBP1b was coexpressed (Figure 3.23). Interestingly, cells which showed the aggregated state prior to heat treatment did not form a large amount of granules after heat stress. Further, this pre-induced aggregation changed the localization of mCHERRY-UBP1b so that it co-aggregated in these large structures instead of smaller cytosolic SGs. Not all cells showed this pattern and RUXF-YFP and mCHERRY-UBP1b also colocalized in normal-sized granules in some cells (second heat treated cell).

To summarize, the membrane trafficking candidates GRF2 and ISTL1 did not co-localize in granules with UB1b. SEC13A, GRF9 and, to a lesser extent, FLOT1 changed their localization upon heat stress treatment and colocalized with UB1b in granules. Only half of the RNA metabolism candidates colocalized with UB1b granules. However, when they did, the colocalization was strong and the granules were more distinct than for the membrane trafficking candidates. Furthermore, three of the four colocalizing proteins even induced UB1b aggregation in the absence of heat stress, which might point to an mRNP granule promoting activity of these components.

### **3.5.6 Colocalization analysis of interactome candidates with SKD1**

A prerequisite for protein interaction is spatial proximity. All of the analyzed components (with the exception of PIP1-1) showed at least a partial cytosolic localization, similar to SKD1. This part of the study aimed to answer the question whether the membrane trafficking and RNA metabolism candidates of the interactome also localize to heat-induced SKD1 granules. For that, similar to the colocalization study with UB1b, double-transformations of epidermal leaf cells with interactome candidates and SKD1-mCHERRY were performed. Treatment and imaging was done as described before and representative cells are shown in Figure 3.24 and Figure 3.25. Similar to VPS18, no good fluorescent signals of UB12-YFP and YFP-RRM were detected in coexpression with SKD1 and they were therefore not included in the colocalization analysis.

As in the previous localization studies, YFP-GRF2 did not change its localization upon heat treatment drastically and did not colocalize with heat-induced SKD1-mCHERRY granules. The other 14-3-3 protein, YFP-GRF9, colocalized with SKD1-mCHERRY granules and the same was true for the putative adaptor complex component SEC13A-YFP.

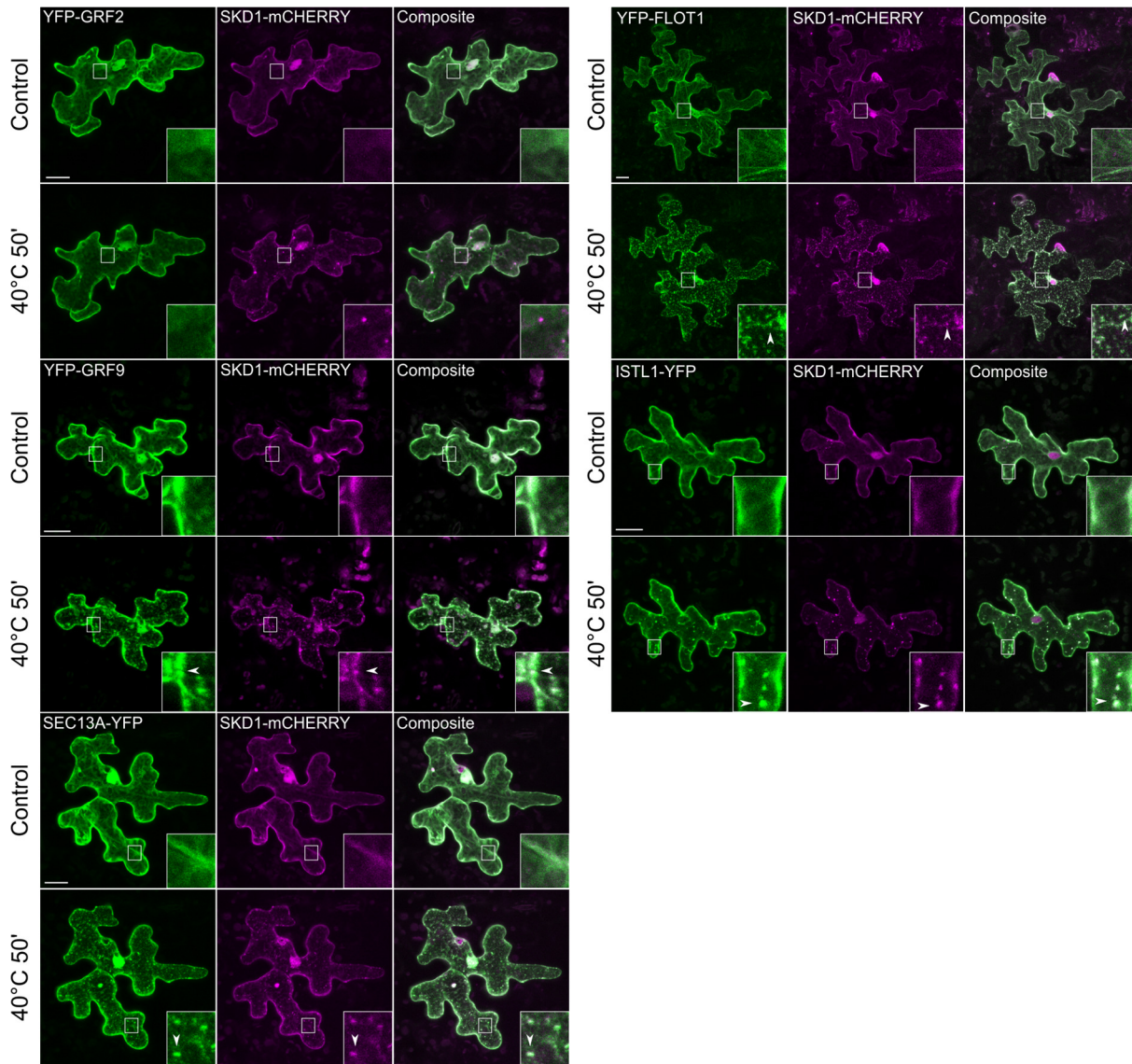


**Figure 3.24. Colocalization analysis of membrane trafficking candidates with SKD1-mCHERRY.** Epidermal *A. thaliana* Col-0 cells were transiently double-transformed with an SKD1 interactome candidate in fusion with YFP and SKD1-mCHERRY. The same cells were imaged by confocal microscopy with the same laser intensities before and after heat stress treatment (40°C 50'). Depicted are representative maximum projections of stacks. Arrow heads indicate colocalizing structures. Bar = 20  $\mu$ m.

The YFP-FLOT1 protein, which showed only weak granule formation when expressed alone or with UBP1b, showed stronger aggregation when coexpressed with SKD1-mCHERRY after heat stress treatment.

A surprising observation was made for the ISTL1-YFP localization in coexpression with SKD1-mCHERRY. Though ISTL1-YFP showed no strong granule formation when expressed alone and did not co-localize with UBP1b granules, it localized to SKD1-mCHERRY granules after heat stress.

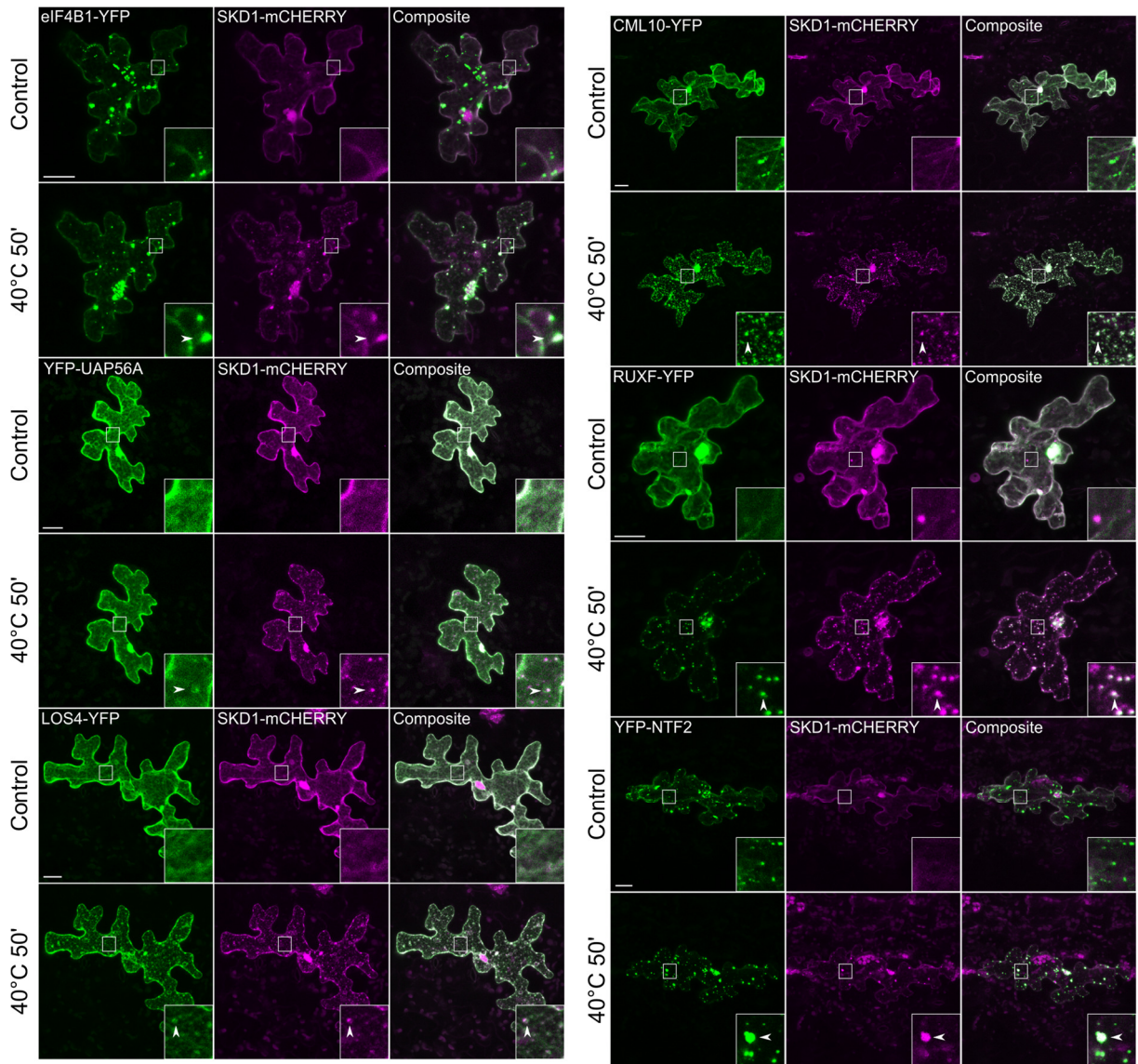


**Figure 3.25. Colocalization analysis of RNA metabolism candidates with SKD1-mCHERRY.** Epidermal *A. thaliana* Col-0 cells were transiently double-transformed as described in Figure legend Figure 3.24. Arrow heads indicate colocalizing structures. Bar = 20  $\mu$ m.

The coexpression of SKD1-mCHERRY did not change the localization of eIF4B1-YFP and vice versa (Figure 3.25). While eIF4B-YFP was able to recruit UBP1b into the cytosol and into granules, this was not the case for SKD1-mCHERRY. The two proteins colocalized only after heat stress treatment in granules.

An interesting observation was made for the two analyzed RNA-helicases YFP-UAP56A and LOS4-YFP. Both proteins did not undergo a heat-dependent shift in localization when expressed alone or together with UBP1b. However, in coexpression with SKD1-mCHERRY, both proteins showed some weak granulation and weakly colocalized with SKD1-mCHERRY labeled granules (Figure 3.25).

CML10-YFP localized in dots before and after heat stress whereby SKD1-mCHERRY only associated with those granules after heat stress treatment. RUXF-YFP showed once more a cytosolic localization. Heat stress induced granule formation and SKD1-mCHERRY colocalization.

YFP-NTF2 showed the same localization as before and was visible in very distinct granules, independent of the treatment. SKD1-mCHERRY only colocalized with NTF2-YFP granules after heat stress.

These results show that several of interactome candidates colocalized with SKD1 in heat-induced structures, which most likely represent mRNP granules. In contrast to the colocalization with UBP1b, the coexpression of eIF4B1, CML10 or NTF2 did not recruit SKD1 to granules in the absence of stress.

In addition to the heat-dependent subcellular localization of the interactome candidates in respect SKD1, it was of interest to see whether they are involved in ESCRT-dependent trafficking and localize to MVBs. To investigate that, leaf epidermal cells were co-transformed with the dominant-negative SKD1-AQ protein. As explained in Chapter 3.4.2, this ATPase-defective version of SKD1 inhibits the recycling of ESCRT components from endosomal membranes, thereby blocking MVB biogenesis and ESCRT-dependent trafficking. This block causes ESCRTIII components and interacting proteins to remain at MVBs. An enrichment of interactome candidate signal at SKD1-AQ-labeled structures (in the absence of stress) could indicate a function or general association at MVBs in an ESCRT-dependent manner.

As shown in Appendix, Figure A.4 and Figure A.5, only two candidate proteins colocalized with SKD1-AQ-labeled structures. One of them was ISTL1, which is not surprising since this protein is a well established ESCRTIII associated component (Azmi et al., 2008; Nickerson et al., 2010; Buono et al., 2016). The other candidate, which was found at SKD1-AQ-induced class E compartments, was RUXF. This is not easily explained since RUXF functions as a splicing factor.

### **3.5.7 Validation of candidate interactions with SKD1 by Y2H and LUMIER assays**

An important step to identify true interactions within a list of interactome candidates is the confirmation of protein interactions by additional methods. Therefore, a Y2H was performed. The selected membrane trafficking and RNA metabolism candidates were cloned in vectors allowing the N-terminal fusion of the GAL4-AD and were cotransformed with SKD1 in fusion with the GAL4-BD in yeast cells. As positive controls, the interactions of SKD1 with LIP5,

VPS32.1, VPS32.2, VPS60.1, and VPS60.2 were included in the analysis. As negative control, SKD1 in fusion with the GAL-BD was cotransformed with GFP in fusion with GAL4-AD. In total, nine biological replicates were evaluated for each combination and most of them were analyzed in three individual assays (see Appendix, Table 2.1).

Colony growth on the interaction medium was evaluated after nine to eleven days. For all combinations (including positive controls) colony growth was rather weak and nearly no combinations showed any growth on interaction medium which contained 5 mM 3-AT. Therefore, the combinations were evaluated on the plates without 3-AT. This was possible since the negative control of SKD1 showed no auto-activation in the absence of 3-AT.

From all positive controls, LIP5 showed the weakest colony growth (two out of nine replicates) and this number was used as a cut-off to determine positive growth. The membrane trafficking candidates VPS18, PIP1-1, SEC13A, FLOT1, and ISTL1 showed colony growth above the cut-off. From the RNA metabolism candidates, CML10 and UBP12 showed significant colony growth.

Nearly half of the candidate proteins showed interaction with SKD1 in the Y2H experiment. In order to further validate the interactions, a second protein interaction assay was performed. Similar to Y2H assays, the LUMIER assay is a high-throughput quantitative method for protein interaction determination (Barrios-Rodiles et al., 2005). In principle, the LUMIER assay is a pulldown-based method, in which human *HEK293TN* cells are double transfected with a construct expressing a ProtA tagged bait protein (pTREX-ProtA) and a prey protein fused to *Renilla reniformis* luciferase (pcDNA3-Renilla, see Chapter 2.7.2). As a negative control, SKD1 fused to ProtA and unfused luciferase were co-transfected. LIP5, VPS32.1, and VPS60.1 were used as positive controls for SKD1 interaction. All combinations were tested in at least two separate experiments and with at least two technical pulldown replicates (Appendix, Table A.12).

Two proteins were considered to interact, if a measured Relative Luminescence Intensity (RLI) was 1.5 times higher than the background (SKD1-ProtA with Renilla-w/o). Surprisingly, this was only the case for three interactome candidates (GRF2: 2.81, LOS4: 1.93, UBP12: 3.44) and for none of the positive controls.

The LUMIER assay was repeated in two initial experiments in which either fusions were switched (SKD1-Renilla, candidates fused to Prot-A) or cells were single transformed and cell lysates were mixed before immunoprecipitation. However, no interactions were identified by

these approaches (data not shown). To exclude a systemic problem, a protein interaction, which is well characterized in LUMIER assays, was included in one of the performed assays: TRANSPARENT TESTA GLABRA 1 (TTG1) and GLABRA3 (GL3), B. Zhang, unpublished). This combination yielded in a RLI 26.14-fold higher than the background, thus excluding a systemic error.

Another possible explanation for overall low or no SKD1 interactions might be that *A. thaliana* SKD1 is not well expressed or degraded in *HEK293TN* cells. Further, since SKD1 is known to associate with membranes, it is possible that the majority of protein is lost during cell debris removal. To answer this, cells were transformed with a construct expressing SKD1 in N-terminal fusion with YFP (pTREX-YFP) and cell lysates were prepared following the LUMIER protocol. The pellet, which was obtained during cell debris removal by centrifugation, was dissolved in the same volume as the supernatant. Lysate and pellet samples were prepared for SDS-PAGE and the YFP-SKD1 protein was detected via immunoblotting (see Appendix, Figure A.6). No strong degradation bands were detected, however, a large portion of SKD1 protein seemed to be lost in the pellet of the lysed cells. This result might explain the overall weak detected interactions of SKD1. This is even more likely in the case of the used positive control since they are known to interact with SKD1 primarily at membranes. Thus, the LUMIER method is not optimal for evaluating interactions of ESCRT components.

To the end of this study, the FLIM-FRET (Fluorescence Lifetime Imaging-Fluorescence Resonance Energy Transfer) method was started to be established for the SKD1 interaction analysis. This method allows the *in-vivo* analysis of protein interactions in *A. thaliana* and circumvents lysis steps in which proteins could be lost. Further, it allows the distinction between structures in which two proteins interact. Therefore, this method will provide a valuable tool for the future characterization of SKD1 interactions.

Altogether, several interactions for the interactome candidates with SKD1 were confirmed with at least one method. These results are summarized in Table 3.9 together with the localization results of Chapter 3.5.4-3.5.6.

**Table 3.9. Summary of localizations and interactions of the SKD1 interactome candidates.** n.d. = not determined. Symbols in brackets indicate weak granule formation, ++ indicates recruitment of UBP1b in granules without stress. Green and red backgrounds indicate positive or negative granule formation/colocalization/protein interaction, respectively.

Membrane trafficking						
Protein	in granules before heat	in granules after heat	in granules with UBP1b	in granules with SKD1	at class E compartments	Interaction in Y2H/LUMIER
VPS18	-	(+)	n.d.	n.d.	n.d.	+/-
GRF2	-	(+)	-	-	-	-/+
GRF9	-	+	+	+	-	-/-
PIP1-1	ER	ER	n.d.	n.d.	n.d.	+/-
SEC13A	-	+	+	+	-	+/-
FLOT1	-	(+)	(+)	+	-	+/-
ISTL1	(+)	(+)	-	+	+	+/-
RNA metabolism						
Protein	in granules before heat	in granules after heat	in granules with UBP1b	in granules with SKD1	at class E compartments	Interaction in Y2H/LUMIER
eIF4B1	+	+	++	+	-	-/-
UAP56A	-	-	-	(+)	-	-/-
LOS4	-	-	-	(+)	-	-/+
CML10	+	+	++	+	-	+/-
UBP12	-	-	-	n.d.	-	+/+
RUXF	(+)	+	+	+	+	-/-
RRM	(+)	(+)	-	n.d.	-	-/-
NTF2	+	+	++	+	-	-/-

Nearly all of the tested membrane trafficking candidates interacted with SKD1 in one of the two assays. Also, nearly all showed some degree of granule formation, in particular when coexpressed with SKD1. This might indicate that the membrane trafficking candidates associate only weakly with mRNP granules and need additional factors for colocalization. Same might be true for the RNA helicases UAP56A and LOS4, which only showed mild granule formation in coexpression with SKD1.

For the RNA metabolism candidates, only three were confirmed to interact with SKD1. This could be explained by only weak interactions with SKD1 or interactions which depend on specific plant co-factors. The future analysis of interactions with FLIM-FRET might answer this question. Independent of their associations with SKD1, several putative mRNP granules components were identified in this study. The translation initiation factor eIF4B1, the calcium-

sensor CML10 and the RNA-binding protein NTF2 form strong granules and are able to recruit the SG component UBP1b into granules in the absence of stress. Their further characterization in the context of mRNP granule formation might give new insight in this process in *A. thaliana*.

### **3.6 Impact of heat stress on PIN2 protein trafficking**

This study showed so far that the ESCRTIII associated protein SKD1 localizes to mRNPs granules after heat stress. A similar shift in localization was observed for the two ESCRTIII associated proteins VPS46.1 and VPS46.2, but not for the other analyzed ESCRTIII components. The ISTL1 protein did colocalize in strong granules after heat stress, but only in coexpression with SKD1. Furthermore, SKD1 co-precipitates with several proteins which function in RNA metabolism and some of these proteins have been shown to localize to mRNP granules. Altogether, these observations consolidate the hypothesis that SKD1 changes its localization from the cytosol and MVBs to mRNP granules after heat stress.

The removal of SKD1 from the cytosol might temporarily block the MVB pathway, which might be favourable for cells during acute heat stress. A similar mechanism was described for the TORC1 kinase in yeast and mammals after heat stress (Takahara and Maeda, 2012; Thedieck et al., 2013; Wippich et al., 2013). Active TORC1 promotes protein synthesis and cell growth while blocking catabolic processes such as autophagy. Upon nutrient starvation or stress, TORC1 is recruited from the vacuolar membrane (where it is active) into stress granules and thereby rendered inactive. This provides an extremely fast and reversible mechanism to switch the metabolic status of cells in stress situations.

So far, only one study has been published which analyzed ESCRT proteins in the context of heat stress in *A. thaliana* (Wang *et al.* 2015). This study showed that *lip5* mutants are susceptible to heat stress, accumulate more ubiquitinated proteins and that the LIP5 protein associates stronger with endosomal membranes during heat stress (Wang *et al.*, 2015). However, the transport of ESCRT cargo to the vacuole during or shortly after heat stress was not analyzed.

In a first attempt to explore, if heat-induced SKD1 removal from the cytosol to mRNP granules correlates with blocked MVB trafficking, the localization of the ESCRTIII cargo PIN2 was studied (Spitzer *et al.*, 2009). This auxin efflux carrier localizes to the PM in *A. thaliana* epidermal root cells, whereby it is enriched at the apical site. Under normal conditions, PIN2 undergoes constant endocytic cycling from the plasma membrane to endosomes and is finally internalized into MVBs for vacuolar degradation. The transition of PIN2 protein from recycling

endosomes to MVBs is dependent on BFA-sensitive ARF-GEFs and treatment with BFA causes PIN2 proteins to accumulate in so-called BFA-induced compartments (Geldner et al., 2001; Kleine-Vehn et al., 2008). If heat treatment causes an inhibition of MVB trafficking, an accumulation of PIN2 proteins in structures reminiscent of BFA-induced compartments should be visible.

To monitor PIN2 trafficking under normal conditions and after heat stress treatment, a stable rescue line which expressed the PIN2-GFP under its own promoter was used (*ProPIN2::PIN2-GFP*, Abas et al., 2006). As a reference for blocked PIN2-GFP trafficking, some seedlings were treated with 50  $\mu$ M BFA for 90' (Kleine-Vehn et al., 2008, Chapter 2.4.7). The roots of the seedling were imaged directly after treatment and representative pictures are shown in Figure 3.26.

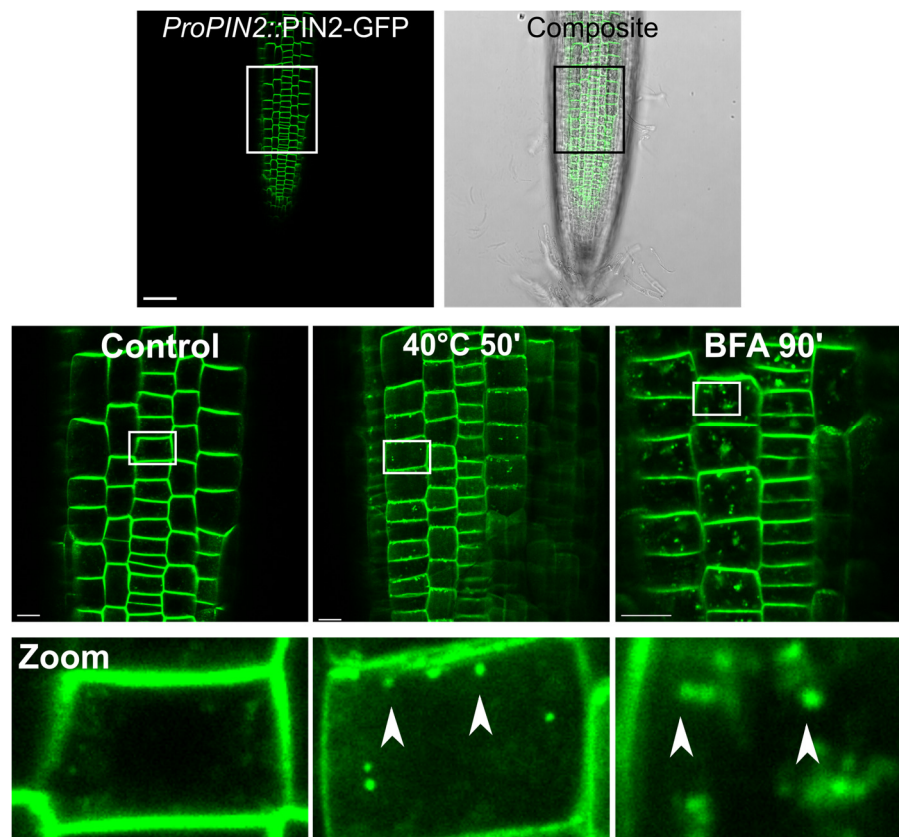


**Figure 3.26. Subcellular localization of PIN2-GFP after heat stress or BFA treatment.** *ProPIN2::PIN2-GFP* (*eir1-1*) seedlings were grown vertically on  $\frac{1}{2}$  MS for 5-7 d. Before imaging, the seedlings were transferred to tubes containing liquid  $\frac{1}{2}$  MS medium and were kept either at room temperature or were subjected to heat treatment (40°C 50'). For BFA treatment, the chemical was added to the medium to a final concentration of 50  $\mu$ M. Epidermal cells of the root transition zones (demonstrated in upper row) were imaged by confocal microscopy immediately after treatment. Representative pictures of single planes are given. Arrow head indicate PIN2-GFP aggregates. Bar = 50  $\mu$ m (upper row) or 10  $\mu$ m.

The localization of PIN2-GFP was studied in epidermal cells of the root transition zone (Verbelen et al., 2006). The approximate area is indicated in Figure 3.26 in the upper row. The PIN2-GFP protein exhibited the expected plasma membrane localization with a noticeable enrichment at apical cell boundaries. The application of heat treatment effected the localization of PIN2-GFP in the majority of roots: PIN2-GFP-labeled structures were now visible in the cytosol of epidermal root cells. After heat treatment, 10-times more PIN2-GFP-labeled structures were visible than in control roots (heat: 108 aggregates in 348 cells, control: 9 aggregates in 379 cells, Appendix, Table A.13). In comparison with the BFA samples, fewer cytosolic structures were visible in the heat-treated roots and the majority was smaller than BFA-induced compartments. Nonetheless, this phenotype was reminiscent of at least partially blocked PIN2 trafficking.

To further access the nature of the heat-induced PIN2-GFP structures, roots were stained with FM4-64 in addition to heat or BFA treatment in an initial experiment. Representative pictures of the staining results are given in Figure 3.27

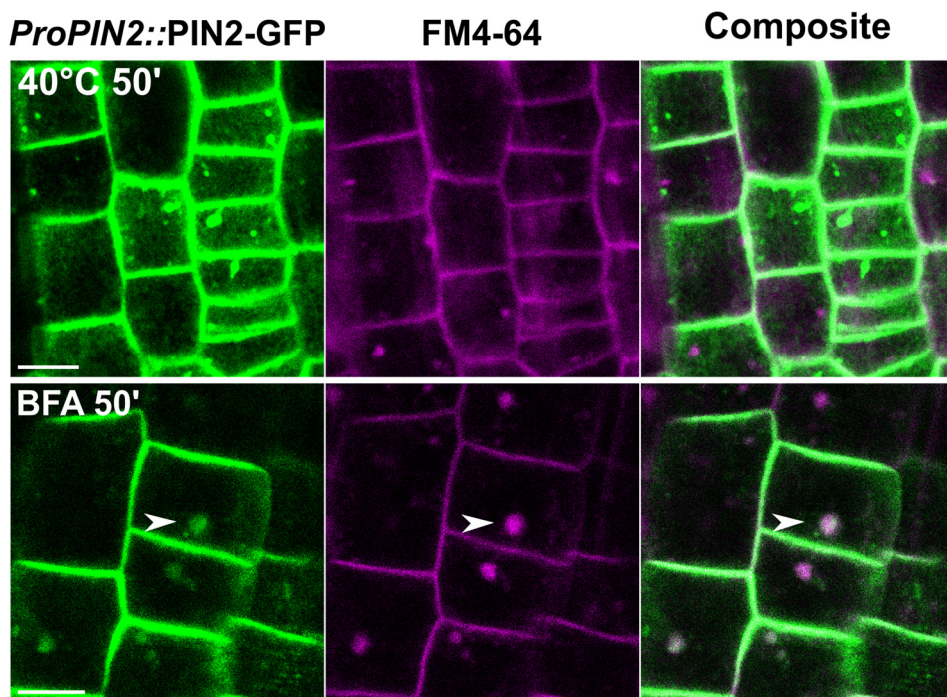


**Figure 3.27. FM4-64 staining of heat or BFA treated *ProPIN2::PIN2-GFP* roots.** Seedlings were grown and prepared for treatment as described in Figure legend Figure 3.26. Before(10')heat treatment, the FM4-64 dye was added to the medium (final concentration: 50  $\mu$ M, total staining time: 60'). BFA treatment and FM4-64 staining were done simultaneously, whereby the incubation time with the drug and dye was reduced to 50'. Imaging was done as described before. Arrow heads indicated colocalizing structures. Bar = 7.5  $\mu$ m.

The BFA-induced compartments showed an enrichment of FM4-64 staining. However, the heat-induced PIN2-GFP structures were not stained by the dye (five roots analyzed each). One explanation might be that heat treatment influences FM4-64 internalization differently than BFA treatment does. Indeed, it was previously shown that heat stress delays FM4-64 staining of late endosomal structures and the vacuolar membrane while it promotes accumulation in early endosomes in yeast (Meaden et al., 1999). Furthermore, a study in tobacco cell culture showed that BFA-treatment stimulates initial dye uptake by two-fold (Emans et al., 2002). Therefore, an adjustment of the staining time of the heat stressed roots might be necessary to see FM4-64 labeling of PIN2-GFP structures. In addition, the *ProPIN2::PIN2-GFP* line was crossed to the stable *35S::mCHERRY-ARA7* line. To the end of this study, seeds of the F1 generation were collected and a future colocalization analysis will show, if the heat-induced PIN2 structures co-localize with the MVB marker ARA7.

## 4 Discussion

As sessile organisms, plants have to quickly adapt to the onset of unfavorable conditions such as infection, salinity, drought, or significant temperature changes. The ongoing global climate change is predicted to significantly affect agricultural production by increasing regional weather extremes. This has been exemplified by the observation that the 2003 heat and drought wave in Europe caused a 30% decrease of crop production (Ciais et al., 2005). Thus, understanding abiotic stress responses is discussed to be one of the most important plant research fields (Hirayama and Shinozaki, 2010).

Although physiological outputs may vary, core processes of cellular heat stress responses are conserved among eukaryotes (Richter et al., 2010). In general, the onset of elevated temperatures triggers the global adjustment of gene transcription and translation. This is partially achieved by the enhanced transcription of aggregation protective proteins, such as chaperones and HSPs, by the transcription factor HSF1 (HEAT SHOCK FACTOR 1, Vihervaara and Sistonen, 2014). In addition to that, the pool of preexisting mRNAs is modulated by selective degradation in the cytosol or in P-bodies, and by the sequestration of transcripts in SGs (Anderson and Kedersha, 2008). Acute heat stress also affects membrane integrity and permeability. In addition, intracellular trafficking of proteins and membranes is affected, which has been linked to the impaired reorganization of the cytoskeleton (Richter et al., 2010).

Recent studies showed that the *A. thaliana* SPI protein regulates membrane remodeling in the process of MVB formation together with the ESCRTIII associated protein LIP5 (Steffens et al., 2017). Furthermore, it positively regulates P-bodies during salt stress and thereby modulates salt responsive transcript levels (Steffens et al., 2015). An initial Y2H experiment pointed to a potential interaction between ESCRTIII core and associated proteins and mRNP granule components. Therefore, this study investigated the connection between *A. thaliana* ESCRTIII proteins, in particular SKD1, and mRNP granules to find a potential crosslink between membrane trafficking processes and posttranscriptional regulation in the context of heat stress.

#### **4.1 SKD1 associates with mRNP granules after heat stress independent of endosomes**

This study extensively analyzed the subcellular localization of ESCRTIII core and associated proteins before and after heat treatment by confocal microscopy. The main focus was the essential ESCRTIII associated protein SKD1, since this AAA-ATPase executes the only energy consuming and rate-limiting step in MVB biogenesis (Haas et al., 2007; Shahriari et al., 2010). The importance of SKD1 for this process is demonstrated by the fact that the loss of SKD1 is lethal for *A. thaliana* (M. Jakoby, personal communication). Because SKD1 functions at MVBs, a dot-like subcellular localization would be expected in confocal studies. However, no association with MVBs under control conditions was visible (Chapter 3.2). This is in accordance with previously published localization studies and reflects the transient nature of the membrane association of ESCRTIII proteins (Shahriari et al., 2010). For example, membrane fractionation experiments showed that over 90% of the yeast SKD1 homolog is detected in the cytosol. A significant amount of SKD1 can only be detected in the membrane pellet after artificially enhancing membrane association, for example by mutating upstream ESCRTIII proteins (Babst et al., 1998; Babst et al., 2002b).

A similar approach was used to demonstrate, that the here used versions of SKD1 were still able to bind to MVBs. SKD1 was coexpressed with a C-terminally modified version of the ESCRTIII core protein VPS32.1 (Appendix, Figure A.3). C-terminal modifications of VPS32 proteins diminish the autoinhibitory effect of the C-terminal hairpin structure, thus leading to an increased association with endosomal membranes (Howard et al., 2001; Zamborlini et al., 2006; Hanson et al., 2008). Coexpression of VPS32.1-mCHERRY caused SKD1 to colocalize with it in large aggregated structures that represented class E compartments (enlarged MVBs).

The localization of SKD1 changed upon heat stress and granular structures became visible (Chapter 3.2). This was not caused by the fluorescent tag since free YFP did not form granules after heat stress (Appendix, Figure A.1). The shift in localization was independent of expression strength, transformation method, analyzed tissue and fusion orientation of the tag. Since SKD1 is known to function at MVBs, one would expect that this localization represents an enhanced association with membranes. However, heat-induced SKD1 granules were neither marked by FM4-64 staining nor shared a significant overlap with the two late endosomal markers ARA7 or RHA1 (Chapter 3.2 and Chapter 3.3.3). Instead, SKD1 granules significantly overlap with SG granules (UBP1b, RBP47b, and PAB2) and, to a lesser extent, P-bodies (DCP1, DCP5 and eIF(iso)4E, Chapter 3.3.3). The reciprocal test, if ARA7 or RHA1 co-localize with PAB2 or

DCP5 after heat treatment, showed no considerable degree of co-localization (Figure 3.11). This demonstrates that the association of SKD1 with mRNP granules is independent of endosomal structures. Further evidence for this observation might be given by mRNP granule purification and subsequent detection of SKD1, or by treatment with cyclohexamide, a translational inhibitor that reduces P-body and SG numbers (Xu et al., 2006; Weber et al., 2008; Jain et al., 2016).

P-bodies and SGs are both classes of mRNP granules. They are similar in size, share an overlap in proteins, and are often in proximity to each other (Buchan et al., 2008; Protter and Parker, 2016). These circumstances make it difficult to distinguish them in colocalization studies. One clear difference is that P-bodies are microscopically visible and mediate mRNA decay in the absence of stress (Stoecklin and Kedersha, 2013). SKD1 localized to granules only after heat stress, which suggests an association with SGs and no general function in P-bodies or mRNA decay. So far, there is no information about the presence of transcripts in SKD1 granules and their adenylation state (deadenylated: P-bodies, adenylated: SGs). Thus, no definite classification can be made and SKD1 is here described to associate with mRNP granules in general.

An interesting result of this study was that the ATPase-defective SKD1 version SKD1-AQ still localizes to mRNP granules (Chapter 3.4.4, Figure 3.16). This provides evidence that ATP binding and ATP hydrolysis are not essential for granule association. Instead, they might be mediated by other factors, such as interactions with granule recruiting factors or modifications such as phosphorylation. The quantification of the SKD1-AQ overlap with UBP1b showed a high, but significantly reduced overlap compared to wild type SKD1 (Figure 3.17). Large SKD1-AQ labeled structures, which represent class E compartments, were less often in colocalization with UBP1b than the heat-induced, small SKD1-AQ granules. This indicates that only the free cytosolic pool of SKD1-AQ is recruited to mRNP granules, while the membrane-associated pool remains at MVBs.

A key to understand the biological function of SKD1 recruitment to mRNP granules may lie in the identification of components or domains that regulate its relocalization. A possible recruiting factor is the SPI protein, which has been shown to directly interact with SKD1 and P-body components (Steffens et al., 2015 and 2017). SPI is discussed to contribute to P-body formation as a scaffolding component, thus increasing the interconnection of proteins. However, preliminary results of transient cellular localization studies showed that SKD1 is still present in granules after heat stress in epidermal leaf cells of *spi* mutants (data not shown). If

SPI is a stress-specific scaffolding factor (only during salt stress) or SKD1 depends on other factors or modifications, remains to be elucidated. First localization studies using SKD1 protein fragments suggest that the relevant domain for SKD1 recruitment lies in the highly structured ATPase domain and not in the MIT domain or the flexible linker region (data not shown). Further testing might confirm this observation and provide a starting point to search for relevant modifications or interaction sites.

## **4.2 Some ESCRTIII associated, but no core proteins localize to mRNP granules**

After the extensive analysis of the heat-dependent association of SKD1 with mRNP granules, it was questionable, whether other ESCRTIII proteins show a similar localization. Previous research showed that IDRs within protein sequences are a driving force in the formation of mRNP granules, such as for human TIA1 (Gilks et al., 2004). Furthermore, IDRs are overrepresented in proteins that form mRNP granules (Protter and Parker, 2016). This was confirmed for 12 *A.thaliana* mRNP granule components in this study using online prediction tools (Chapter 3.4.1, Table 3.5). While approximately 30% of the *A. thaliana* proteome are considered highly disordered (over 50% of aa in IDRs), over 90% of mRNP granule proteins fulfilled this criterion in this study (loop category, Pietrosemoli et al., 2013).

The same prediction tools were used to test, if the ESCRTIII core and associated proteins are highly disordered. From the analyzed subset, four of the ESCRTIII associated (SKD1, LIP5, VPS601, and VPS60.2) and none of the ESCRTIII core components were predicted to be highly disordered. Thus, a localization shift after heat stress was anticipated for LIP5 and VPS60.2. VPS60.2 showed some granules after heat stress, but did not colocalize to UBP1b (Chapter 3.4.4, Figure 3.16). LIP5 did not change its cytosolic localization after heat treatment. Instead, the less disordered VPS46.1 and VPS46.2 showed granulation and heat-induced colocalization with UBP1b. These results indicate that the IDR content of ESCRTIII proteins can only give a hint towards mRNP granule association but is not a good predictor on its own. This assumption is strengthened by the observation that a flexible linker in SKD1, which is highly disordered, is not essential for mRNP granule association (preliminary data, not shown).

The observed localization of LIP5 after heat stress was particularly surprising for two reasons. One was the fact that a heat-induced increase in LIP5 dots has been described previously (Wang et al., 2015). The authors showed that the formation of LIP5 dots correlated to an increase in ARA6-labeled structures (MVB marker) and a higher percentage of LIP5 protein in membrane fractions. Therefore, heat treatment enhanced the association of LIP5 with MVB membranes.

Their study used elevated temperatures (45°C) and longer incubation times (4 h). Thus, a change in LIP5 localization might only be visible at later time points. The other reason, why a heat-induced separation of SKD1 and LIP5 is surprising, is the fact that they form a tightly connected barrel structure, which is needed for full activity (see Chapter 1.3 Figure 1.3, Scott et al., 2005b; Azmi et al., 2006; Haas et al., 2007; Shahriari et al., 2010). LIP5 is not essential for SKD1 function, but becomes crucial for plant survival after prolonged stress (Wang et al., 2014 and 2015). The results of this study point to a separation of LIP5 and SKD1 during stress. This discrepancy is not easily resolved, but might be explained by different stages of stress responses. This study focused on early effects of heat stress on protein localization. It might be that an early separation of LIP5 and SKD1 downregulates MVB biogenesis while it is later on reactivated. However, this assumption is highly speculative and needs further confirmation by, for example, studying the number and morphology of MVBs at different timepoints after heat stress by electron microscopy.

VPS46.1 and VPS46.2 colocalized in mRNP granules, while LIP5 and VPS60.2 did not (Chapter 3.4.4, Figure 3.16). Thus, the ESCRTIII associated proteins are diverse in their response to heat stress and not all of them are simply sequestered in mRNP granules. Although they all stimulate SKD1 activity, they are not all synergistic in function. For example, yeast Ist1 forms a subcomplex with Did2 (VPS46) while Vta1 (LIP5) is synergistic to Vps60 (Rue et al., 2008). Therefore, the differential localization of ESCRTIII associated proteins might represent different modes of SKD1 activity regulation.

The ESCRTIII core proteins VPS32.1 and VPS24.1 did not colocalize to mRNP granules after heat stress (Chapter 3.4.4, Figure 3.16). This might be explained by their stronger association to membranes (e.g. filament formation, direct interaction with myristoylated VPS20, Babst et al., 2002b; Bowers et al., 2004; Lin et al., 2005). Interestingly, VPS24.1 was in distinct dots after heat stress, but they did not overlap with UBP1b. An explanation for this might be an enhanced association of VPS24.1 with membranes after heat stress, as it was observed for LIP5 by Wang and colleagues (Wang et al., 2015). It is known that the loss of SKD1 function or the coexpression of a dominant-negative version enhances membrane association of upstream ESCRT components (Babst et al., 2002b; Cai et al., 2014). Therefore, one could speculate that the heat-triggered reduction of cytosolic SKD1 inhibits the removal of ESCRTIII core components from MVBs. This would also fit to the observed weak formation of VPS60.2 dots after heat stress (Chapter 3.4.2, Figure 3.14). However, since VPS24 functions downstream of VPS32 in the process of MVB formation, a similar effect would be expected for VPS32 (Babst

et al., 2002b; Teis et al., 2008). Therefore, future experiments should clarify the identity of the heat-induced VPS24.1 and VPS60.2 structures.

In addition to the subcellular localization study, a systematic Y2H assay was carried out to identify interactions between ESCRTIII core and associated proteins with mRNP granule components (Chapter 3.1). Previous studies pointed to a broad interaction between ESCRT components and P-body proteins (Table 3.1). The results of this study did not confirm the previous results but found some other interactions, especially for LIP5 (Table 3.2). In the context of the subcellular colocalization study, this was not expected since LIP5 did not associate with mRNP granules. As the interaction assay was performed in yeast and not in plants, and in the absence of stress, a definite statement about specific protein interactions cannot be made. The results can rather be considered as a hint towards protein interactions between members of the two pathways. However, this demonstrates that additional methods, such as FLIM-FRET, are necessary to define direct interactions and that several approaches are needed to get a comprehensive idea about the connection of ESCRT and mRNP granule proteins.

### **4.3 Membrane trafficking and new mRNP granule proteins are in the SKD1 interactome**

The identification of the heat-dependent interactome of SKD1 was another approach to further investigate the localization shift of SKD1. To this end, proteins were extracted from leaves of stable lines and subjected to immunoprecipitation, followed by LC-MS/MS analysis (Chapter 3.5). By filtering, a total of 192 potential SKD1 interactors were identified, whereby 15 of them were control-specific and 18 specific for the heat treated samples. There were no treatment-specific significant differences in relative protein abundance between the shared interactors. This could be explained by the transient nature of protein-protein interactions within mRNP granules (Jain et al., 2016). The here used protocol was a first approach to identify new SKD1 interactors and although no striking heat-specific differences were observed, several new putative interactors were described. As a next step, formaldehyde fixation prior to cell lysis might be used to highlight treatment-specific differences in interactor abundances.

From the interactome candidates, 46 proteins were annotated to be or to function in mitochondria or chloroplasts (Figure 3.19). This number of organelle proteins is not unusual for the used material and extraction protocol (leaf material, no centrifugation to remove organelles, S. Müller, Proteomics Core Facility Cologne, personal communication). Without the organelle proteins, 146 candidates remained. This is somewhat higher but comparable to

similar interactome studies of *A. thaliana* VPS2.2 and CML38 (89 proteins: Ibl et al., 2012; 106 proteins: Lokdarshi et al., 2016). The majority of candidates was annotated to be involved in diverse metabolic or biosynthetic processes (termed “others”). Future studies might reveal crosslinks between candidates of this list and SKD1 function, yet their analysis was beyond the scope of this study.

19 candidates with protein folding activity were identified in the interactome, the majority of them being HSPs and TCP-1 chaperones (Appendix, Table A.10). All of the seven identified TCP-1 proteins were also identified in the interactomes of the *A. thaliana* SG protein RBP45b and CML38 (Lokdarshi et al., 2016; Muthuramalingam et al., 2017). TCP-1 proteins, also known as CCT complex proteins, form cytosolic ring complexes and assist in the protein folding of a variety of cytosolic proteins (Leitner et al., 2012). They have been identified in purified yeast SGs and were shown to negatively regulate SG formation in mutant studies (Jain et al., 2016). The presence of several TCP-1 proteins in the SKD1, RBP45b, and CML38 interactome might hint towards a similar role of this class of chaperones in plant mRNP granules. Therefore, their role in mRNP granule formation is worth testing in the future.

The SKD1 interactome also contained 17 proteins which participate in RNA-related processes such as splicing, transport, topology, or translation. Some of them contained known RNA-binding domains or are known to localize in mRNP granules (Appendix, Table A.10). VCS, a large scaffolding protein and core component of P-bodies, was also among the potential interactors, further confirming the microscopically visible association of SKD1 with mRNP granules. From the 17 RNA-associated proteins, eight were further characterized. Interestingly, three of the eight tested proteins already formed distinct granules, which also recruited UBP1b, in the absence of stress (Figure 3.23, eIF4B1, CML10, NTF2). The overexpression of mRNP granule components, such as mammalian TIA1, G3BP, or yeast Pab1, can induce granule formation in the absence of stress and can induce the association of other components (Stoeckling et al., 2004; Kedersha et al., 2005; Takahara and Maeda, 2012). Thus, the recruiting effect of eIF4B1, CML10, and NTF2 overexpression onto UBP1b might indicate a function in granule induction. Their overexpression did not recruit SKD1 in the absence of stress and only additional heat treatment induced colocalization (Figure 3.25). Thus, it might be that stress directly triggers modifications of SKD1 (e.g. phosphorylation), which are essential for the localization shift, and that the presence of mRNP granules alone is not sufficient for recruitment.

Some of the other analyzed RNA metabolism proteins showed little or no granule formation after heat treatment (UBP12, UAP56A, RRM, and LOS4, Figure 3.21). It might be that these tested candidates do not associate with mRNP granules. Another explanation might be that the fluorescent tag interferes with their localization. Interestingly, the coexpression of SKD1 seemed to increase the granulation of UAP56A and LOS4 slightly, although the majority of protein signal remained cytosolic (Figure 3.24). This effect was not observed by coexpression with UBP1b, making it unlikely that the increased protein load caused their granulation (Figure 3.22). Thus, SKD1 itself might influence the localization of interacting components to mRNP granules after stress.

Since SKD1 regulates MVB biogenesis, one focus was what other membrane trafficking proteins are present in the interactome and a total of 23 proteins have been identified (e.g. putative coat proteins, tethering complex proteins, cargo transport proteins, Appendix, Table A.10). Two ESCRTIII associated proteins, ISTL1 and VPS46.2, were identified, which increases the confidence in the identified interactors. Interestingly, VPS46.2 was present in all heat treated samples, but only in one of the control replicates (Appendix, Table A.10). This could be interpreted as an increased interaction of SKD1 with VPS46.2 after heat treatment, which in turn correlates with the observed shift in localization of SKD1 and VPS46.2.

An interesting group of membrane trafficking candidates are the HOPS/CORVET complex proteins. This conserved tethering complex functionally connects Rab GTPases with SNAREs (Soluble NSF Attachment protein REceptor) and is of high importance for MVB to vacuole (CORVET) and homotypic vacuole to vacuole (HOPS) fusions (Vukašinović and Žárský, 2016; Takemoto et al., 2018). They share a common set of four core proteins consisting of VPS11, VPS18, VCL1/VPS16, and VPS33. From those, VCL1/VPS16 and VPS18 were identified in the SKD1 interactome. Furthermore, the HOPS specific VPS41 protein was identified. HOPS/CORVET complexes are essential for the regulation of endosomal maturation and have been speculated to directly interact with other endosomal maturation machineries such as the ESCRT machinery (Solinger and Spang, 2013). Evidence for a direct interaction is still missing in the literature, but an antagonistic function of HOPS and ESCRT has been described in yeast (Bugnicourt et al., 2004). The identification of several HOPS/CORVET proteins in the SKD1 interactome provides first evidence that a functional link with the ESCRT machinery might be based on direct protein interactions. Since the cloning of VPS41 and VCL1/VPS16 was not successful in this study, only the interaction of VPS18 with SKD1 was confirmed by Y2H (Table 3.9). Further analysis of SKD1 interaction with HOPS/CORVET proteins might confirm

the results of this study and provide insights on how this interaction influences maturation and fusion of MVBs.

The subcellular localization of seven membrane trafficking candidates was analyzed in the context of heat-induced mRNP granules. With the exception of ISTL1, none of the membrane trafficking proteins colocalized to Class E compartments (SKD1-AQ coexpression, Appendix, Figure A.4 and Figure A.5). Since the inhibition of SKD1 function causes an accumulation of ESCRT trafficking proteins at MVBs, this indicates that their function lies not in ESCRT-trafficking. Surprisingly, the small mRNP RUXF colocalized with SKD1-AQ aggregates. However, since RUXF formed aggregates on its own in some cells, the observed co-localization might be an artifact.

Six of the analyzed membrane trafficking proteins showed some degree granulation after heat treatment (Figure 3.20). The granules were not as distinct as for the RNA metabolism candidates. Only the putative coat protein SEC13A and the 14-3-3 protein GRF9 showed a stronger granulation and colocalization with UBP1b (Figure 3.22). It remains to be determined, if this weak granule formation of some of the membrane trafficking proteins is also visible when the proteins are not overexpressed, as it was shown for SKD1 (Figure 3.1). In this case, the here obtained results might indicate that components from several membrane trafficking routes are sequestered in mRNP granules in response to heat stress.

Apart from the subcellular localization study, the identified interactome candidates were subjected to Y2H and LUMIER assays to confirm their interaction with SKD1 (Chapter 3.5.7). The interaction of six out of seven membrane trafficking candidates with SKD1 was confirmed. From the RNA metabolism candidates, only two out of the eight tested combinations were positive. This difference might be explained by weak interactions of SKD1 with other mRNP granules proteins. Also, the tests were not made in plants and in the absence of stress. The LUMIER assay was not optimal to test interactions with *A. thaliana* SKD1 since the majority of protein got lost in the process of sample preparation, presumably due to enhanced membrane association (Appendix, Figure A.6). Additional modifications of the assay would be needed to use it for SKD1 interaction confirmation. However, since the use of heterologous assays always bares the risk to fail to confirm species-specific interactions, the use of another *in-vivo* method, such as FLIM-FRET, is more promising.

#### **4.4 What is the functional relevance of SKD1 relocalization under heat stress?**

At the end of this study the following question remains: What is the function of SKD1 association with mRNP granules during heat stress? Although some approaches were made to address this aspect, no definite answer can be given. The following paragraphs will point out working hypotheses, which are being followed up in further studies.

One possibility is an active and direct function of SKD1 in mRNP granule formation or stability. An argument for this hypothesis is the function of the direct SKD1 interactor SPI in P-bodies (Steffens et al., 2015). SPI has no known enzymatic function but contains several protein-protein interaction domains (e.g. five WD40 repeats). Therefore, it was speculated that SPI functions as a scaffolding factor in P-bodies. SKD1 is no scaffolding factor and has a highly structured AAA-ATPase cassette with enzymatic activity (Haas et al., 2007; Shahriari et al., 2010). Therefore, an enzymatic function of SKD1 in mRNP granules would be expected. A direct function of AAA-ATPases in SGs has been described in yeast (Jain et al., 2016). The study demonstrated that cellular availability of ATP is essential for granule formation and also largely influences their movement, fusion and exchange of protein content after formation. In this context, proteins of the AAA-ATPase complexes MCM (MINI-CHROMOSOME MAINTENANCE) and Rvb have been shown to inhibit SG disassembly by removing disassembly factors of remodeling SG content to facilitate the association of additional SG components. MCM and Rvb are DNA/RNA helicases that are known to modulate nucleic acid-protein complexes. SKD1 is well established in its function to disassemble large proteins complexes. Therefore, a remodeling function in mRNP granules is imaginable. The observation that SKD1 coexpression can enhance granule association for some putative mRNP granule components might point in that direction (UAP56A and LOS4, Figure 3.25). The colocalization studies using the ATPase-defective version SKD1-AQ did not indicate an inhibitory effect on mRNP granule formation (Figure 3.17). However, this study did not evaluate the dynamics of mRNP granule formation or disassembly. In epidermal leaf cells of stable lines, PAB2-labeled granules appear after 10 min of heat stress and are completely dissolved after 4 h (H. Bhasin, personal communication). The comparative analysis of granule numbers within this time frame in PAB2 and the SKD1-overexpressing PAB2 line might provide evidence for a direct involvement of SKD1 in granule dynamics.

Independent of a direct function at mRNP granules, one consequence of the recruitment of SKD1 to mRNP granules might be a temporary inhibition of ESCRT-dependent trafficking to

the vacuole. VPS24.1 and, to a lesser extent, VPS60.2 can be seen in dots after heat stress, which do not colocalize with mRNP granule marker (Figure 3.16). This supports the hypothesis as the loss of SKD1 activity at MVBs causes an enhanced association of ESCRT proteins with membranes (Babst et al., 2002).

To test this potential inhibition, an experiment was performed in which the heat-dependent localization of the transmembrane protein PIN2 was tested (Chapter 3.6). PIN2 is a well established marker for ESCRT-trafficking and its accumulation in cytosolic structures is an indicator for defects in vacuolar trafficking (Geldner et al., 2001; Spitzer et al, 2009). Epidermal cells of heat treated roots contained 10-times more PIN2-labeled cytosolic structures than untreated cells (Figure 3.26). A first attempt to demonstrate that these structures are membranous by FM4-64 staining failed (Figure 3.27). Therefore, the positioning of the heat-induced PIN2 structures within the endomembrane system still needs to be done. Colocalization studies with different endosomal markers might clarify at which step PIN2 trafficking might be inhibited by heat.

The analysis of PIN2 localization provided first evidence that heat might block vacuolar trafficking. Therefore, the additional analysis of ESCRT-dependent cargo trafficking to the vacuole, such as for the vacuolar enzymes CPY or AALP, would be interesting (Rojo et al., 2003; Shahriari et al., 2010). The future study of heat-dependent MVB morphology and number by electron microscopy is crucial to strengthen the hypothesis of a heat-induced block of ESCRT trafficking. However, these kind of studies could only demonstrate a correlation of SKD1 recruitment to mRNP granules and a blockage of MVB trafficking. The investigation of a causative link is much more complicated. A classical approach would be the complementation with an SKD1 version that does not relocate to mRNP granules during heat stress. Preliminary results of the interactome candidate study indicated that membrane trafficking proteins of other transport processes associate with mRNP granules after heat stress. Therefore, blocked MVB trafficking during heat might not only depend on SKD1 recruitment. An approach, which could provide a first functional link between general recruitment of membrane trafficking proteins to mRNP granules and the block of cellular transport processes, might be the combinatorial treatment of cells with heat and cyclohexamide to prevent granule formation.

Acute, sublethal heat stress affects nearly every cellular process. Membrane trafficking has been described to be mainly affected by changes in membrane fluidity and permeability. Furthermore, the reorganization or the loss of cytoskeletal organization impairs proper membrane trafficking, which finally leads to aberrant organelle structures, e.g. fragmentation

of the Golgi or ER and a reduced number of lysosomes (Welch and Suhan, 1985; Richter et al., 2010). Heat stress also triggers the association of HSP70 with membranes, which stimulates the endocytosis of PM receptors. This has been discussed to modulate cellular homeostasis during heat stress in mammalian cells (Vega et al., 2010). Heat stress can also cause the misfolding of transmembrane proteins, which in turn triggers their degradation. This is thought to be mediated by the ESCRT machinery, since yeast and plant ESCRT mutants have been shown to be heat stress sensitive (Jarolim et al., 2013; Wang et al., 2015). Thus, one would expect an increase in vacuolar trafficking via MVBs during heat stress, which is contradictory to the hypothesis of a temporal ESCRT trafficking block.

Interestingly, it seems that different steps of trafficking are differently regulated by heat stress. Previous studies in yeast showed that heat treatment delays FM4-64 staining of late endosomal structures and of the vacuolar membrane, indicating a specific inhibition of late trafficking events (Meaden et al., 1999). A similar observation was made in a study investigating the function of the Huntington's disease protein HUNTINGTIN during heat stress (Nath et al., 2015). The authors showed that heat stress induces the rapid association of HUNTINGTIN with EEs, which causes the arrest of EE to LE and EE to RE maturation. This effect was quicker than other canonical heat stress responses, such as mRNP granule formation or the induction of the unfolded protein response. This block is speculated to save energy for the later heat stress responses.

But how are cell surface receptors then degraded during heat stress when endosomal maturation or MVB trafficking is inhibited? Two studies from 2017 showed that an ESCRT-independent degradation pathway for PM receptors and channels is activated in yeast during cellular stress such as heat stress or general TOR signaling (McNally et al., 2017; McNally and Brett, 2017). This pathway relies on the homotypic fusion of lysosomes, whereby the cargo is enriched in the lysosomal membrane at the vertex of the fusing lysosomes, making the step of membrane invagination dispensable and thus the process potentially more energy-efficient. The authors of the study speculated that this mechanism of ESCRT-independent protein degradation might be present in other eukaryotes since the underlying machinery is conserved. Future studies will show, if a similar, energy-saving mechanism is active in *A. thaliana* during heat stress and if this process coincides or even depends on SKD1 recruitment to mRNP granules.

## 5 Appendix

**Table A.1. List of specific plasmids used or generated in this study.** The plasmids contained the CDS of the listed genes either with a stop codon (+) or a glycine (-) for C-terminal fusion. For some genes, CDS with and without stop codon were available.

Gene name	ATG	Vectors	Reference/Origin
<b>LIP5 (+/-)</b>	AT4G26750	pDONR201	Shahriari et al., 2010
		pAS	Shahriari et al., 2010
		pACT	Shahriari et al., 2010
		pEXSG-YFP	Steffens et al., 2017
		pAUBERGINE	A. Steffens
		pcDNA3	This study (LR)
<b>SKD1 (+/-)</b>	AT2G27600	pDONR201	Shahriari et al., 2010
		pAS	Shahriari et al., 2010
		pACT	Shahriari et al., 2010
		pEXSG-YFP (SKD1 promoter fragment)	M. Jakoby
		pEXSG-YFP	A. Steffens
		pAUBERGINE	A. Steffens
		pTREX	This study (LR)
		pTREX-YFP	This study (LR)
<b>SKD1-AQ (+)</b>	AT2G27600	pENSG-YFP	Shahriari et al., 2010
		pAMARENA-UBQ10	A. Steffens
<b>VPS46.1 (+)</b>	AT1G17730	pDONR201	Shahriari et al., 2010
		pAS	Shahriari et al., 2010
		pAMARENA	A. Steffens
<b>VPS46.2 (+)</b>	AT1G73030	pDONR201	Shahriari et al., 2010
		pAS	Shahriari et al., 2010
		pENSG-YFP	A. Steffens
<b>VPS60.1 (+)</b>	AT3G10640	pDONR201	M. Jakoby
		pAS	M. Jakoby
		pACT	M. Jakoby
		pcDNA3	This study (LR)
<b>VPS60.2 (+/-)</b>	AT5G04850	pDONR201	M. Jakoby
		pAS	M. Jakoby
		pACT	M. Jakoby
		pEXSG-YFP	M. Jakoby
<b>VPS20.1 (+)</b>	AT5G63880	pAS	Shahriari et al., 2010
		pACT	Shahriari et al., 2010
<b>VPS24.1 (+/-)</b>	AT5G22950	pAS	Shahriari et al., 2011
		pEXSG-YFP	A. Steffens
<b>VPS32.1 (+/-)</b>	AT2G19830	pDONR201	Shahriari et al., 2010
		pAS	Shahriari et al., 2010
		pACT	Shahriari et al., 2010
		pENSG-YFP	A. Steffens
		pAMARENA	A. Steffens
		pAUBERGINE	A. Steffens
		pcDNA3	This study (LR)

<b>Gene name</b>	<b>ATG</b>	<b>Vectors</b>	<b>Reference/Origin</b>
<b>VPS32.2 (+)</b>	AT4G29160	pAS	Shahriari et al., 2011
		pACT	Shahriari et al., 2011
<b>DCP1 (+/-)</b>	AT1G08370	pACT	Steffens et al., 2015
		pEXSG-CFP	Steffens et al., 2015
<b>DCP2 (+)</b>	AT5G13570	pACT	Steffens et al., 2015
<b>DCP5 (+/-)</b>	AT1G26110	pAS	Steffens et al., 2015
		pACT	A. Steffens
		pEXSG-YFP	A. Steffens
<b>VCS (+)</b>	AT3G13300	pACT	Steffens et al., 2015
<b>eIF4E1(+)</b>	AT4G18040	pACT	A. Steffens
<b>XRN4(+)</b>	AT1G54490	pACT	A. Steffens
<b>UBP1b (+)</b>	AT1G17370	pDONR201	Bhasin and Hülkamp, 2017
		pACT	This study (LR)
		pENSG-YFP	Bhasin and Hülkamp, 2017
		pAMARENA	H. Bhasin
<b>PAB2(+)</b>	AT4G34110	pDONR201	Bhasin and Hülkamp, 2017
		pACT	This study (LR)
		pAMARENA	Bhasin and Hülkamp, 2017
<b>RBP47b(+)</b>	AT3G19130	pDONR201	Bhasin and Hülkamp, 2017
		pACT	This study (LR)
		pAMARENA	H. Bhasin
<b>RBP45b(+)</b>	AT1G11650	pDONR201	Bhasin and Hülkamp, 2017
		pACT	This study (LR)
<b>GRP7(+)</b>	AT2G21660	pDONR201	Bhasin and Hülkamp, 2017
		pACT	This study (LR)
<b>GRP2(+)</b>	AT4G13850	pDONR201	Bhasin and Hülkamp, 2017
		pACT	This study (LR)
<b>eIF(iso)4E(+)</b>	AT5G3562	pENSG-YFP	H. Bhasin
<b>VPS18 (+)</b>	AT1G12470	pDONR201	This study (BP)
		pACT	This study (LR)
		pENSG-YFP	This study (LR)
		pcDNA3	This study (LR)
<b>GRF2 (+/-)</b>	AT1G78300	pDONR207	This study (BP)
		pACT	This study (LR)
		pENSG-YFP	This study (LR)
		pcDNA3	This study (LR)
<b>GRF9 (+/-)</b>	AT2G42590	pDONR201	This study (BP)
		pACT	This study (LR)
		pENSG-YFP	This study (LR)
		pcDNA3	This study (LR)
<b>PIP1-1 (+/-)</b>	AT3G61430	pDONR207	This study (BP)
		pACT	This study (LR)
		pENSG-YFP	This study (LR)
		pEXSG-YFP	This study (LR)
		pcDNA	This study (LR)
<b>SEC13A (+/-)</b>	AT3G01340	pDONR201	This study (BP)
		pACT	This study (LR)
		pEXSG-YFP	This study (LR)
		pcDNA3	This study (LR)
<b>FLOT1 (+/-)</b>	AT5G25250	pDONR201	This study (BP)
		pACT	This study (LR)

Gene name	ATG	Vectors	Reference/Origin
		pENSG-YFP	This study (LR)
		pcDNA3	This study (LR)
<b>ISTL1 (+/-)</b>	AT1G34220	pDONR201	This study (BP)
		pACT	This study (LR)
		pEXSG-YFP	This study (LR)
		pcDNA3	This study (LR)
<b>eIF4B1 (+/-)</b>	AT3G26400	pDONR201	This study (BP)
		pACT	This study (LR)
		pEXSG-YFP	This study (LR)
		pcDNA3	This study (LR)
<b>UAP56A (+/-)</b>	AT5G11170	pDONR207	This study (BP)
		pACT	This study (LR)
		pENSG-YFP	This study (LR)
		pcDNA3	This study (LR)
<b>LOS4 (-)</b>	AT3G53110	pDONR201	This study (BP)
		pACT	This study (LR)
		pEXSG-YFP	This study (LR)
		pcDNA3	This study (LR)
<b>CML10 (+/-)</b>	AT2G41090	pDONR201	This study (BP)
		pACT	This study (LR)
		pEXSG-YFP	This study (LR)
		pcDNA3	This study (LR)
<b>UBP12 (-)</b>	AT5G06600	pDONR201	This study (BP)
		pACT	This study (LR)
		pEXSG-YFP	This study (LR)
		pcDNA3	This study (LR)
<b>RUXF (+/-)</b>	AT4G30220	pDONR201	This study (BP)
		pACT	This study (LR)
		pEXSG-YFP	This study (LR)
		pcDNA3	This study (LR)
<b>RRM (+)</b>	AT3G23900	pDONR201	This study (BP)
		pACT	This study (LR)
		pENSG-YFP	This study (LR)
		pcDNA3	This study (LR)
<b>NTF2 (+/-)</b>	AT5G60980	pDONR207	This study (BP)
		pACT	This study (LR)
		pENSG-YFP	This study (LR)
		pcDNA3	This study (LR)
<b>GFP</b>	-	pACT	A. Steffens
<b>w/o</b>	-	pcDNA	This study (LR with pENTRA)
<b>TTG1</b>	AT5G24520	pTREX	B. Zhang
<b>GL3</b>	AT5G41315	pcDNA	B. Zhang

**Table A.2. Y2H of ESCRTIII core and associated proteins with mRNP granule proteins.** Raw data of Table 3.2. Constructs expressing ESCRTIII core and associated proteins in fusion with GAL4-BD and an mRNP granule protein in fusion with the GAL4-AD were cotransformed in yeast. Colonies were transferred to plates selecting for successful double transformation (SD-LW) as a control and onto plates with the interaction medium (SD-LWH, 0 mM, 5 mM, 15 mM, 30 mM). Colony growth was evaluated after 7-9 days on SD-LWH plates with different concentrations of 3-AT. Colony growth on the day of analysis is indicated with an X, no growth is indicated by a 0. All combinations were tested with at least two technical replicates and in two repetitions. A tested combination was considered positive, if half of the transferred colonies grew on a 3-AT concentration which was higher than for the corresponding negative control (GFP-AD). Pictures of the evaluated plates are documented in the laboratory journal number IV, pages 143-144, H. Wolff, AG Hülkamp, University of Cologne.

	pAS	pACT	L W	0 mM	5 mM	15 mM	30 mM	LW	0 mM	5 mM	15 mM	30 mM						
	pAS	pACT	Set 1 day 7					Repeat Set 1 day 7										
1	LIP5	DCP1	x	x	x	x	0	0	x	x	x	x	x	x	0	0	0	0
2	SKD1	DCP1	x	x	0	x	0	x	0	x	0	x	x	0	0	0	0	0
3	VPS46.1	DCP1	x	x	0	x	0	x	0	x	0	0	x	x	0	0	0	0
4	VPS46.2	DCP1	x	x	0	0	0	0	0	0	0	0	x	x	0	x	0	0
5	VPS60.1	DCP1	x	x	x	x	x	x	x	x	x	0	x	x	x	x	x	x
6	LIP5	DCP2	x	x	x	x	0	0	0	0	0	0	x	x	x	0	0	0
7	SKD1	DCP2	x	x	0	0	0	0	0	0	0	0	x	x	0	0	0	0
8	VPS46.1	DCP2	x	x	0	0	0	0	0	0	0	0	x	x	0	0	0	0
9	VPS46.2	DCP2	x	x	0	0	0	0	0	0	0	0	x	x	0	0	0	0
10	VPS60.1	DCP2	x	x	x	x	x	x	x	x	0	0	x	x	x	x	x	0
11	LIP5	DCP5	x	x	x	x	x	0	0	0	0	0	x	x	x	x	x	0
12	SKD1	DCP5	x	x	0	x	0	x	0	0	0	0	x	x	0	0	0	0
13	VPS46.1	DCP5	x	x	0	0	0	0	0	0	0	0	x	x	0	0	0	0
14	VPS46.2	DCP5	x	x	0	0	0	0	0	0	0	0	x	x	0	0	0	0
15	VPS60.1	DCP5	x	x	x	x	x	x	x	x	x	0	x	x	x	x	x	0
16	LIP5	VCS	x	x	x	x	0	x	0	0	0	0	x	x	x	x	0	0
17	SKD1	VCS	x	x	0	0	0	0	0	0	0	0	x	x	0	0	0	0
18	VPS46.1	VCS	x	x	0	0	0	0	0	0	0	0	x	x	0	0	0	0
19	VPS46.2	VCS	x	x	0	0	0	0	0	0	0	0	x	x	0	x	0	0
20	VPS60.1	VCS	x	x	x	x	x	x	x	x	x	x	x	x	x	x	x	x
21	LIP5	XRN4	x	x	x	x	0	0	0	0	0	0	x	x	x	x	0	0
22	SKD1	XRN4	x	x	0	0	0	0	0	0	0	0	x	x	x	0	0	0
23	VPS46.1	XRN4	x	x	0	0	0	0	0	0	0	0	x	x	0	0	0	0
24	VPS46.2	XRN4	x	x	0	0	0	0	0	0	0	0	x	x	0	x	0	0
25	VPS60.1	XRN4	x	x	x	x	x	x	x	x	x	0	x	x	x	x	x	0
26	LIP5	GRP2	x	x	x	x	0	0	0	0	0	0	x	x	x	x	0	0
27	SKD1	GRP2	x	x	x	0	0	0	0	0	0	0	x	x	0	0	0	0
28	VPS46.1	GRP2	x	x	0	0	0	0	0	0	0	0	x	x	0	0	0	0
29	VPS46.2	GRP2	x	x	0	0	0	0	0	0	0	0	x	x	0	0	0	0
30	VPS60.1	GRP2	x	x	x	x	x	x	x	x	0	0	x	x	x	x	x	x
31	LIP5	UBP1b	x	x	x	x	0	0	0	0	0	0	x	x	x	x	x	0
32	SKD1	UBP1b	0	0	0	x	0	0	0	0	0	0	0	0	0	0	0	0
33	VPS46.1	UBP1b	x	x	0	0	0	x	0	0	0	0	x	x	0	0	0	0
34	VPS46.2	UBP1b	x	x	0	0	0	0	0	0	0	0	x	x	x	0	0	0
35	VPS60.1	UBP1b	x	x	x	x	x	x	x	x	x	x	x	x	x	x	x	x
36	LIP5	GFP	x	x	x	0	0	0	0	0	0	0	x	x	x	0	0	0
37	SKD1	GFP	x	x	0	0	0	0	0	0	0	0	x	x	0	0	0	0
38	VPS46.1	GFP	x	x	0	0	0	0	0	0	0	0	x	x	0	0	0	0
39	VPS46.2	GFP	x	x	0	0	0	0	0	0	0	0	x	x	0	0	0	0
40	VPS60.1	GFP	x	x	x	x	x	x	x	0	0	0	x	x	x	x	x	0

Appendix

	pAS	pACT	L W	0 mM	5 mM	15 mM	30 mM	LW	0 mM	5 mM	15 mM	30 mM										
41	DCP2	DCP1	x	x	0	x	0	x	0	x	0	x	x	x	x	0	x	0	x	0	0	0
42	DCP5	DCP2	x	x	x	x	x	x	0	x	0	0	x	x	x	x	x	0	0	0	0	0
43	DCP2	DCP5	x	x	0	0	0	0	0	0	0	0	x	x	0	0	0	0	0	0	0	0
44	DCP2	VCS	x	x	x	x	x	x	x	x	x	x	x	x	0	0	0	0	0	0	0	0
45	DCP2	XRN4	x	x	0	0	0	0	0	0	0	0	x	x	0	0	0	0	0	0	0	0
46	UBP1b	GRP2	x	x	0	0	0	0	0	0	0	0	x	x	0	0	0	0	0	0	0	0
47	UBP1b	UBP1b	x	x	0	0	0	0	0	0	0	x	x	0	0	0	0	0	0	0	0	0
48	LIP5	SKD1	x	x	x	x	x	x	0	0	0	0	x	x	x	x	x	x	0	0	0	0
Set 2 day 7								Repeat Set 2 day 9														
	pAS	pACT	L W	0 mM	5 mM	15 mM	30 mM	LW	0 mM	5 mM	15 mM	30 mM										
1	LIP5	PABP2	x	x	x	x	x	x	0	0	0	0	x	x	x	x	x	x	0	0	0	0
2	SKD1	PABP2	x	x	0	0	0	0	0	0	0	0	x	x	0	0	0	0	0	0	0	0
3	VPS46.1	PABP2	x	x	0	0	0	0	0	0	0	0	x	x	x	x	0	0	0	0	0	0
4	VPS46.2	PABP2	x	x	x	0	0	0	0	0	0	0	x	x	x	x	0	0	0	0	0	0
5	VPS60.1	PABP2	x	x	x	x	x	x	x	x	x	x	x	x	x	x	x	x	x	x	x	x
6	VPS60.2	PABP2	x	x	x	x	x	x	x	x	x	x	x	x	x	x	x	x	x	x	x	x
7	LIP5	RBP47 b	x	x	x	x	x	x	0	0	0	0	x	x	x	x	x	x	0	0	0	0
8	SKD1	RBP47 b	x	x	0	0	0	0	0	0	0	0	x	x	0	0	0	0	0	0	0	0
9	VPS46.1	RBP47 b	x	x	0	0	0	0	0	0	0	0	x	x	0	0	0	0	0	0	0	0
10	VPS46.2	RBP47 b	x	x	0	0	0	0	0	0	0	0	x	x	x	x	0	0	0	0	0	0
11	VPS60.1	RBP47 b	x	x	x	x	x	x	x	x	x	x	x	x	x	x	x	x	x	x	x	x
12	VPS60.2	RBP47 b	x	x	x	x	x	x	x	0	0	0	x	x	x	x	x	x	x	x	x	x
13	LIP5	RBP45 b	x	x	x	x	x	x	0	0	0	0	x	x	x	x	x	x	0	0	0	0
14	SKD1	RBP45 b	x	x	0	0	0	0	0	0	0	0	x	x	0	0	0	0	0	0	0	0
15	VPS46.1	RBP45 b	x	x	0	0	0	0	0	0	0	0	x	x	x	x	0	0	0	0	0	0
16	VPS46.2	RBP45 b	x	x	x	x	0	0	0	0	0	0	x	x	x	x	0	0	0	0	0	0
17	VPS60.1	RBP45 b	x	x	x	x	x	x	x	x	x	x	x	x	x	x	x	x	x	x	x	x
18	VPS60.2	RBP45 b	x	x	x	x	x	x	x	x	x	x	x	x	x	x	x	x	x	x	x	x
19	LIP5	GFP	x	x	x	x	0	0	0	0	0	0	x	x	x	x	x	x	0	0	0	0
20	SKD1	GFP	x	x	0	0	0	0	0	0	0	0	x	x	x	x	0	0	0	0	0	0
21	VPS46.1	GFP	x	x	0	0	0	0	0	0	0	0	x	x	x	x	0	0	0	0	0	0
22	VPS46.2	GFP	x	x	0	0	0	0	0	0	0	0	x	x	x	x	0	0	0	0	0	0
23	VPS60.1	GFP	x	x	x	x	x	x	x	x	x	x	x	x	x	x	x	x	x	x	x	x
24	VPS60.2	GFP	x	x	x	x	x	x	x	x	x	x	x	x	x	x	x	x	x	x	x	x
25	PABP2	GFP	0	0	0	0	0	0	0	0	0	0	x	x	x	x	0	0	0	0	0	0
26	RBP45b	GFP	0	0	0	0	0	0	0	0	0	0	x	x	x	x	0	0	0	0	0	0
27	RBP47b	GFP	0	0	0	0	0	0	0	0	0	0	x	x	x	x	0	0	0	0	0	0
28	DCP5	GFP	x	x	x	x	x	x	0	0	0	0	x	x	x	x	x	x	x	x	0	0
29	DCP2	GFP	x	x	0	0	0	0	0	0	0	0	x	x	x	x	0	0	0	0	0	0
30	UBP1b	GFP	x	x	0	0	0	0	0	0	0	0	x	x	0	0	0	0	0	0	0	0
31	LIP5	SKD1	0	0	0	0	0	0	0	0	0	0	x	x	x	x	x	x	x	0	0	0
32	PABP2	PABP2	0	0	0	0	0	0	0	0	0	0	x	x	x	x	0	0	0	0	0	0
33	RBP45b	RBP47 b	0	0	0	0	0	0	0	0	0	0	x	x	x	x	0	0	0	0	0	0
34	RBP47b	RBP45 b	0	0	0	0	0	0	0	0	0	0	x	x	x	x	0	0	0	0	0	0
35	DCP5	DCP1	x	x	x	x	x	x	0	x	x	x	x	x	x	x	x	x	x	x	x	0
36	DCP5	DCP2	x	x	x	x	x	x	0	x	0	0	x	x	x	x	x	x	x	x	0	0

Appendix

	pAS	pACT	L W	0 mM	5 mM	15 mM	30 mM	LW	0 mM	5 mM	15 mM	30 mM										
37	DCP2	DCP5	x	x	0	0	0	0	0	0	0	0	x	x	x	x	0	0	0	0	0	0
38	DCP5	VCS	x	x	x	x	x	x	0	0	x	0	x	x	x	x	x	x	x	x	x	x
39	DCP5	XRN4	x	x	x	x	x	x	0	0	0	0	x	x	x	x	x	x	x	x	x	0
40	UBP1b	GRP2	x	x	0	0	0	0	0	0	0	0	x	x	x	x	0	0	0	0	0	0
41	UBP1b	UBP1b	x	x	0	0	0	0	0	0	0	0	x	x	x	x	0	0	0	0	0	0
42	VPS60.2	DCP1	x	x	x	x	x	x	x	x	x	x	x	x	x	x	x	x	x	x	x	x
43	VPS60.2	DCP2	x	x	x	x	x	x	x	0	x	0	x	x	x	x	x	x	x	x	x	x
44	VPS60.2	DCP5	x	x	x	x	x	x	x	x	0	0	x	x	x	x	x	x	x	x	x	x
45	VPS60.2	VCS	x	x	x	x	x	x	x	x	x	x	x	x	x	x	x	x	x	x	x	x
46	VPS60.2	XRN4	x	x	x	x	x	x	x	x	x	0	x	x	x	x	x	x	x	x	x	x
47	VPS60.2	GRP2	x	x	x	x	x	x	x	x	0	0	x	x	x	x	x	x	x	x	x	x
48	VPS60.2	UBP1b	x	x	x	x	x	x	x	x	x	x	x	x	x	x	x	x	x	x	x	x
Set4 day 8													Repeat Set4 day 7									
	pAS	pACT	L W	0 mM	5 mM	15 mM	30 mM	LW	0 mM	5 mM	15 mM	30 mM										
1	LIP5	PABP2	x	x	x	x	x	x	0	0	0	0	x	x	x	x	x	0	0	0	0	0
2	SKD1	PABP2	x	x	0	0	0	0	0	0	0	0	x	x	x	0	0	0	0	0	0	0
3	VPS46.1	PABP2	x	x	x	0	0	0	0	0	0	0	x	x	0	0	0	0	0	0	0	0
4	VPS46.2	PABP2	x	x	x	x	0	0	0	0	0	0	x	x	0	0	0	0	0	0	0	0
5	VPS60.1	PABP2	x	x	x	x	x	x	x	x	x	x	x	x	x	x	x	x	x	x	x	x
6	VPS60.2	PABP2	x	x	x	x	x	x	x	x	x	x	x	x	x	x	x	x	x	x	x	x
7	LIP5	RBP47 b	x	x	x	x	x	0	0	0	0	0	x	x	x	x	0	0	0	0	0	0
8	SKD1	RBP47 b	x	x	0	0	0	0	0	0	0	0	x	x	0	0	0	0	0	0	0	0
9	VPS46.1	RBP47 b	x	x	0	0	0	0	0	0	0	0	x	x	x	0	x	0	x	0	0	0
10	VPS46.2	RBP47 b	x	x	0	0	0	0	0	0	0	0	x	x	0	0	0	0	0	0	0	0
11	VPS60.1	RBP47 b	x	x	x	x	x	x	x	x	x	x	x	x	x	x	x	x	x	x	x	x
12	VPS60.2	RBP47 b	x	x	x	x	x	x	x	x	x	x	x	x	x	x	x	x	x	x	x	x
13	LIP5	RBP45 b	x	x	x	x	x	x	0	0	0	0	x	x	x	x	x	x	0	0	0	0
14	SKD1	RBP45 b	0	0	0	0	0	0	0	0	0	0	x	x	0	0	0	0	0	0	0	0
15	VPS46.1	RBP45 b	x	x	x	0	0	0	0	0	0	0	x	x	0	0	0	0	0	0	0	0
16	VPS46.2	RBP45 b	x	x	x	x	0	0	0	0	0	0	x	x	x	0	0	0	0	0	0	0
17	VPS60.1	RBP45 b	x	x	x	x	x	x	x	x	x	x	x	x	x	x	x	x	x	x	x	x
18	VPS60.2	RBP45 b	x	x	x	x	x	x	x	x	x	x	x	x	x	x	x	x	x	x	x	x
19	LIP5	GFP	x	x	x	x	x	0	0	0	0	0	x	x	0	0	0	0	0	0	0	0
20	SKD1	GFP	x	x	0	0	0	0	0	0	0	0	x	x	0	0	0	0	0	0	0	0
21	VPS46.1	GFP	x	x	0	0	0	0	0	0	0	0	x	x	0	0	0	0	0	0	0	0
22	VPS46.2	GFP	x	x	0	0	0	0	0	0	0	0	x	x	0	0	0	0	0	0	0	0
23	VPS60.1	GFP	x	x	x	x	x	x	x	x	x	x	x	x	x	x	x	x	x	x	x	0
24	VPS60.2	GFP	x	x	x	x	x	x	x	x	x	0	x	x	x	x	x	x	x	x	x	0
25	PABP2	GFP	x	x	0	0	0	0	0	0	0	0	x	x	0	0	0	0	0	0	0	0
26	RBP45b	GFP	x	x	x	0	0	0	0	0	0	0	x	x	x	x	0	0	0	0	0	0
27	RBP47b	GFP	x	x	0	0	0	0	0	0	0	0	x	x	x	0	0	0	0	0	0	0
28	DCP5	GFP	x	x	x	x	x	x	x	x	0	0	x	x	x	x	x	x	0	0	0	0
29	DCP2	GFP	x	x	x	x	x	x	x	x	x	x	x	x	x	x	x	x	x	x	x	0
30	UBP1b	GFP	x	x	0	0	0	0	0	0	0	0	x	x	x	0	0	0	0	0	0	0
31	LIP5	SKD1	x	x	x	x	x	x	x	0	0	0	x	x	x	x	x	0	0	0	0	0
32	PABP2	PABP2	x	x	0	0	0	0	0	0	0	0	x	x	x	0	0	0	0	0	0	0

	pAS	pACT	L W	0 mM	5 mM	15 mM	30 mM	LW	0 mM	5 mM	15 mM	30 mM										
33	RBP45b	RBP47 b	x	x	x	x	0	0	0	0	0	0	x	x	x	x	0	0	0	0		
34	RBP47b	RBP45 b	x	x	x	x	0	0	0	0	0	0	x	x	x	x	0	0	0	0		
35	DCP5	DCP1	x	x	x	x	x	x	x	x	x	0	x	x	x	x	x	x	0	0		
36	DCP5	DCP2	x	x	x	x	x	0	x	0	0	0	x	x	x	x	x	0	0	0		
37	DCP2	DCP5	x	x	0	0	0	0	0	0	0	0	x	x	0	0	0	0	0	0		
38	DCP5	VCS	x	x	x	x	x	x	x	x	x	0	x	x	x	x	x	x	0	0	0	
39	DCP5	XRN4	x	x	x	x	x	x	x	x	0	0	x	x	x	x	0	0	0	0		
40	UBP1b	GRP2	x	x	0	0	0	0	0	0	0	0	x	x	0	0	0	0	0	0		
41	UBP1b	UBP1b	x	x	0	0	0	0	0	0	0	0	x	x	0	0	0	0	0	0		
42	VPS60.2	DCP1	x	x	x	x	x	x	x	x	x	x	x	x	x	x	x	x	x	x		
43	VPS60.2	DCP2	x	x	x	x	x	x	x	x	0	0	x	x	x	x	x	x	x	0		
44	VPS60.2	DCP5	x	x	x	x	x	x	0	x	0	0	x	x	x	x	x	x	0	0		
45	VPS60.2	VCS	x	x	x	x	x	x	x	x	x	x	x	x	x	x	x	x	x	x		
46	VPS60.2	XRN4	x	x	x	x	x	x	x	x	0	0	x	x	x	x	x	x	x	x		
47	VPS60.2	GRP2	x	x	x	x	x	x	x	x	0	0	x	x	x	x	x	x	x	0		
48	VPS60.2	UBP1b	x	x	x	x	x	x	x	x	x	x	x	x	x	x	x	x	x	x		
			SET5 day 7					SET5 repeat day 9														
	pAS	pACT	L W	0 mM	5 mM	15 mM	30 mM	LW	0 mM	5 mM	15 mM	30 mM										
1	LIP5	eIF4E1	x	x	x	x	x	0	0	0	0	0	x	x	x	x	0	0	0	0		
2	SKD1	eIF4E1	x	x	0	0	0	0	0	0	0	0	x	x	x	0	x	0	0	0		
3	VPS46.1	eIF4E1	x	x	0	0	0	0	0	0	0	0	x	x	0	0	0	0	0	0		
4	VPS46.2	eIF4E1	x	x	x	0	x	0	0	0	0	0	x	x	x	0	0	0	0	0		
5	VPS60.1	eIF4E1	x	x	x	x	x	x	x	0	0	0	x	x	x	x	x	x	x	x		
6	VPS60.2	eIF4E1	x	x	x	x	x	x	x	0	0	0	x	x	x	x	x	x	x	x		
7	LIP5	GRP7	x	x	x	x	x	0	0	0	0	0	x	x	x	x	x	x	0	0		
8	SKD1	GRP7	x	x	0	0	0	0	0	0	0	0	x	x	x	0	0	0	0	0		
9	VPS46.1	GRP7	x	x	0	0	0	0	0	0	0	0	x	x	0	0	0	0	0	0		
10	VPS46.2	GRP7	x	x	0	0	0	0	0	0	0	0	x	x	x	0	0	0	0	0		
11	VPS60.1	GRP7	x	x	x	x	x	x	x	0	0	0	x	x	x	x	x	x	x	x		
12	VPS60.2	GRP7	x	x	x	x	x	x	x	0	0	0	x	x	x	x	x	x	x	x		
13	LIP5	GFP	x	x	x	x	0	0	0	0	0	0	x	x	x	0	0	0	0	0		
14	SKD1	GFP	x	x	0	0	0	0	0	0	0	0	x	x	0	0	0	0	0	0		
15	VPS46.1	GFP	x	x	0	0	0	0	0	0	0	0	x	x	x	0	0	0	0	0		
16	VPS46.2	GFP	x	x	0	0	0	0	0	0	0	0	x	x	x	0	0	0	0	0		
17	VPS60.1	GFP	x	x	x	x	x	x	x	0	0	0	x	x	x	0	x	x	x	x		
18	VPS60.2	GFP	x	x	x	x	x	x	x	0	0	0	x	x	x	x	x	x	x	x		
19	VPS20.1	eIF4E1	x	x	0	0	0	0	0	0	0	0	x	x	0	0	0	0	0	0		
20	VPS24.1	eIF4E1	x	x	0	0	0	0	0	0	0	0	x	x	0	0	0	0	0	0		
21	VPS22	eIF4E1	x	x	0	0	0	0	0	0	0	0	x	x	0	0	0	0	0	0		
22	VPS32.1	eIF4E1	x	x	x	x	0	0	0	0	0	0	x	x	x	x	0	0	0	0		
23	VPS32.2	eIF4E1	x	x	x	x	0	0	0	0	0	0	x	x	x	x	0	0	0	0		
24	VPS2.1	eIF4E1	x	x	0	0	0	0	0	0	0	0	x	x	0	0	0	0	0	0		
25	VPS2.2	eIF4E1	x	x	0	0	0	0	0	0	0	0	x	x	x	0	0	0	0	0		
26	VPS2.3	eIF4E1	x	x	x	x	0	0	0	0	0	0	x	x	x	x	0	0	0	0		
27	VPS20.1	GRP7	x	x	0	0	0	0	0	0	0	0	x	x	0	0	0	0	0	0		
28	VPS24.1	GRP7	x	x	0	0	0	0	0	0	0	0	x	x	0	0	0	0	0	0		
29	VPS22	GRP7	x	x	0	0	0	0	0	0	0	0	x	x	0	0	0	0	0	0		
30	VPS32.1	GRP7	x	x	x	x	0	0	0	0	0	0	x	x	x	x	0	0	0	0		
31	VPS32.2	GRP7	x	x	x	x	0	0	0	0	0	0	x	x	x	x	0	0	0	0		
32	VPS2.1	GRP7	x	x	0	0	0	0	0	0	0	0	x	x	0	0	0	0	0	0		
33	VPS2.2	GRP7	x	x	0	0	0	0	0	0	0	0	x	x	0	0	0	0	0	0		
34	VPS2.3	GRP7	x	x	x	x	0	0	0	0	0	0	x	x	x	x	0	0	0	0		
35	VPS20.1	GFP	x	x	0	0	0	0	0	0	0	0	x	x	0	0	0	0	0	0		
36	VPS24.1	GFP	x	x	0	0	0	0	0	0	0	0	x	x	0	0	0	0	0	0		
37	VPS22	GFP	x	x	0	0	0	0	0	0	0	0	x	x	0	0	0	0	0	0		

	pAS	pACT	L	0	5	15	30	LW	0	5	15	30										
			W	mM	mM	mM	mM		mM	mM	mM	mM										
38	VPS32.1	GFP	x	x	x	x	0	0	0	0	0	0	x	x	x	x	0	0	0	0	0	0
39	VPS32.2	GFP	x	x	x	x	0	0	0	0	0	0	x	x	x	x	0	0	0	0	0	0
40	VPS2.1	GFP	x	x	0	0	0	0	0	0	0	0	x	x	0	0	0	0	0	0	0	0
41	VPS2.2	GFP	x	x	0	0	0	0	0	0	0	0	x	x	0	0	0	0	0	0	0	0
42	VPS2.3	GFP	x	x	x	x	0	0	0	0	0	0	x	x	x	0	0	0	0	0	0	0
43	UBP1b	GFP	x	x	0	0	0	0	0	0	0	0	x	x	0	0	0	0	0	0	0	0
44	GRP2	GFP	x	x	0	0	0	0	0	0	0	0	x	x	0	0	0	0	0	0	0	0
45	UBP1b	eIF4E1	x	x	0	0	0	0	0	0	0	0	x	x	0	0	0	0	0	0	0	0
46	GRP2	GRP7	x	x	0	0	0	0	0	0	0	0	x	x	0	0	0	0	0	0	0	0
47	LIP5	SKD1	x	x	x	x	0	0	0	0	0	0	x	x	x	x	x	0	x	0	0	0
48	VPS32.1	SKD1	x	x	0	0	0	0	0	0	0	0	x	x	x	x	0	0	0	0	0	0

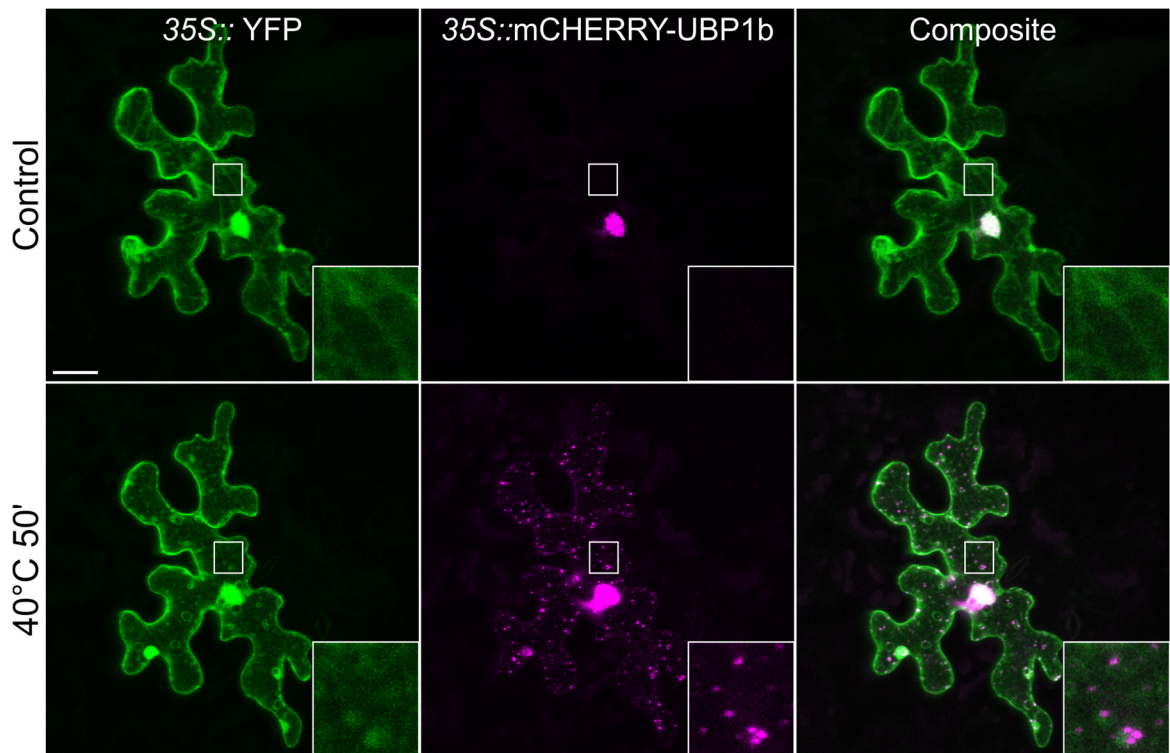


**Figure A.1. Subcellular localization of free YFP and mCHERRY-UBP1b before and after heat.** Epidermal cells of *A. thaliana* Col-0 rosette leaves were transiently transformed by particle bombardment with a construct overexpressing free YFP and mCHERRY-UBP1b. The same cells were imaged by confocal microscopy with the same laser intensities before and after heat treatment at 40°C for 50'. Depicted are representative maximum projections of stacks. Bar = 20  $\mu$ m.

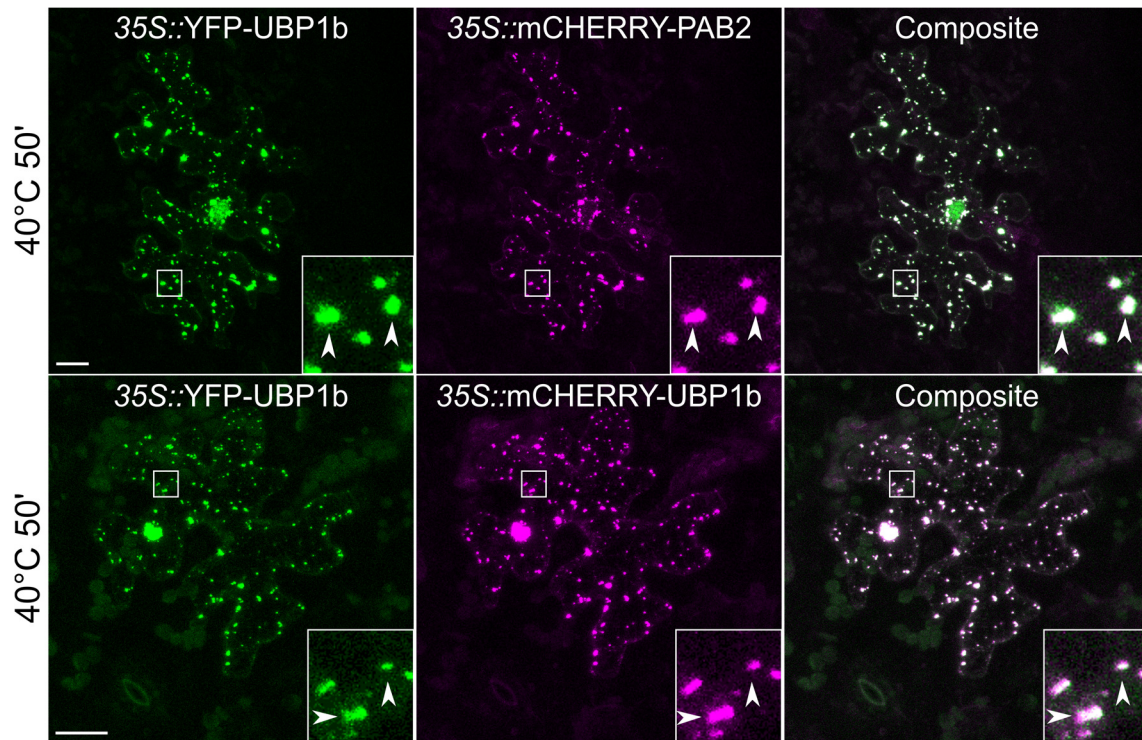


**Figure A.2. Representative pictures of the positive controls for the colocalization quantification.** Epidermal cells of *A. thaliana* Col-0 rosette leaves were transiently transformed by particle bombardment with a construct overexpressing YFP-UBP1b and mCHERRY-PAB2 or mCHERRY-UBP1b. The cells were imaged by confocal microscopy after heat treatment at 40°C for 50'. Depicted are representative maximum projections of stacks. Arrow heads indicate colocalizing structures. Bar =20  $\mu$ m.

**Table A.3. PCCs of transiently double transformed epidermal leaf cells.** Epidermal leaf cells of Col-0 plants were transiently double transformed for colocalization quantification. All used constructs overexpressed the respective protein under the control of the *35S CaMV* promoter. The transformed cells were subjected to heat stress treatment at 40°C for 50' and maximum projections of stacks were generated (confocal microscopy). For each combination, ten cells were imaged and three ROIs were analyzed for fluorescent signal overlap using the PCC (ImageJ, JACoP). Raw data from Figure 3.7.

<b>UBP1b UBP1b</b>	<b>UBP1b PAB2</b>	<b>UBP1b SKD1-</b>	<b>RBP47b SKD1</b>	<b>PAB2 SKD1</b>	<b>eIF(iso)4E SKD1</b>	<b>DCP1 SKD1</b>	<b>DCP5 SKD1</b>	<b>UBP1b UBP1b tilt</b>
0.776	0.565	0.789	0.771	0.428	0.654	0.614	0.609	-0.032
0.783	0.578	0.749	0.703	0.637	0.55	0.706	0.578	0.187
0.706	0.653	0.747	0.696	0.636	0.555	0.83	0.346	-0.015
0.538	0.717	0.751	0.752	0.508	0.516	0.575	0.416	0.101
0.564	0.76	0.72	0.789	0.432	0.586	0.522	0.617	0
0.551	0.79	0.816	0.826	0.474	0.502	0.452	0.411	0.148
0.727	0.681	0.717	0.582	0.357	0.499	0.567	0.401	0.015
0.861	0.723	0.702	0.565	0.484	0.527	0.597	0.333	0.019
0.684	0.67	0.813	0.481	0.431	0.409	0.395	0.487	-0.032
0.857	0.63	0.744	0.616	0.502	0.63	0.27	0.399	0.154
0.834	0.542	0.753	0.62	0.614	0.436	0.42	0.144	0.023
0.856	0.553	0.823	0.581	0.619	0.404	0.314	0.269	-0.087
0.633	0.692	0.638	0.449	0.589	0.388	0.526	0.597	-0.061
0.853	0.717	0.617	0.636	0.584	0.43	0.457	0.481	-0.136
0.764	0.721	0.623	0.546	0.647	0.495	0.414	0.508	-0.016
0.686	0.743	0.737	0.685	0.65	0.577	0.482	0.618	0.006
0.61	0.786	0.679	0.689	0.599	0.496	0.516	0.432	-0.016
0.837	0.743	0.773	0.58	0.718	0.552	0.399	0.584	0.103
0.78	0.563	0.694	0.34	0.583	0.682	0.443	0.51	-0.026
0.8	0.502	0.611	0.614	0.581	0.771	0.536	0.646	0.069
0.81	0.556	0.705	0.515	0.53	0.74	0.252	0.38	-0.087
0.719	0.754	0.741	0.809	0.598	0.65	0.476	0.346	0.153
0.763	0.864	0.87	0.781	0.614	0.575	0.607	0.721	0.043
0.832	0.84	0.676	0.628	0.598	0.692	0.421	0.337	0.032
0.83	0.81	0.828	0.645	0.476	0.646	0.678	0.445	0.046
0.806	0.84	0.59	0.665	0.578	0.571	0.421	0.661	0.147
0.735	0.811	0.623	0.679	0.535	0.551	0.579	0.366	-0.004
0.754	0.814	0.806	0.645	0.488	0.425	0.317	0.377	-0.009
0.823	0.845	0.799	0.626	0.603	0.384	0.422	0.362	0.008
0.85	0.876	0.854	0.738	0.424	0.443	0.718	0.55	-0.094

**Table A.4. Statistical analysis of colocalization between transient double transformations.** All datasets were normally distributed with the exception of UB1b/UB1b (Shapiro-Wilk-test). Normally distributed datasets were evaluated for significant colocalization differences using the Welch's two sample t-test. For comparisons with the UB1b/UB1b dataset, the Wilcoxon-Mann-Whitney-test was used.

	UB1b UB1b	UB1 b PAB2	UB1 b SKD1	RBP47b SKD1	PAB2 SKD 1	eFiso4E SKD1	DCP1 SKD1	DCP5 SKD1	UB1b UB1b tilt
UB1b UB1b		0.1296	0.158	0.000158 4	1.557 e-08	2.952e-08	9.247e- 09	1.41e-09	3.014e-11
UB1b PAB2	0.1296		0.379	0.01708	4.363 e-08	1.296e-07	9.362e-0 9	1.371e-1 0	2.2e-16
UB1b SKD1	0.158	0.379		0.000496 8	4.599 e-10	1.608e-10	1.05e-10	1.05e-10	2.2e-16
RBP47b SKD1	0.000158 4	0.0170 8	0.0004 968		0.000 7267	0.000936 8	3.114e-0 5	6.266e-0 7	2.2e-16
PAB2 SKD1	1.557e-08	4.363e- 08	4.599e- 12	0.000726 7		0.8085	0.07488	0.004401	2.2e-16
eFiso4E SKD1	2.952e-08	1.296e- 07	1.608e- 10	0.000936 8	0.808 5		0.1386	0.01245	2.2e-16
DCP1 SKD1	9.247e-09	9.362e- 09	1.05e-1 0	3.114e-05	0.074 88	0.1386		0.3419	2.2e-16
DCP5 SKD1	1.41e-09	1.371e- 10	1.05e-1 0	6.266e-07	0.004 401	0.0124	0.3419		2.2e-16
UB1b UB1b tilt	3.014e-11	2.2e-16	2.2e-16	2.2e-16	2.2e-1 6	2.2e-16	2.2e-16	2.2e-16	

**Table A.5. PCCs of stable lines.** Epidermal leaf cells of crossed stable marker lines were imaged by confocal microscopy for colocalization quantification. The following lines were used: *35S::YFP-RHA1x35S::PAB2-mRFP*, *35S::DCP5-mTQx35S::mCHERRY-ARA7*, and *35S::DCP5-mTQx35S::PAB2-mRFP*. Leaves were subjected to heat stress treatment at 40°C for 50' and maximum projections of stacks were generated. Raw data from Figure 3.11.

SKD1-GFP x PABP2- mRFP	DCP5-mTQ x PABP2- mRFP	YFP-RHA1 x PABP2- mRFP	SKD1-GFP x mCHERRY- ARA7	DCP5-mTQ x mCHERRY- ARA7	SKD1-GFP x PABP2-mRFP tilt
0.536	0.546	0.222	0.271	0.199	0.014
0.534	0.409	0.292	0.194	0.115	0.035
0.646	0.428	0.138	0.159	0.227	0.14
0.596	0.401	0.299	0.171	0.186	0.172
0.435	0.463	0.321	0.256	0.121	0.023
0.544	0.408	0.323	0.296	0.128	-0.136
0.403	0.389	0.208	0.276	0.121	0.045
0.545	0.446	0.376	0.416	0.174	0.092
0.601	0.535	0.341	0.328	0.212	-0.085
0.423	0.351	0.35	0.297	0.068	0.064
0.368	0.371	0.495	0.266	0.138	0.008
0.389	0.385	0.271	0.23	0.088	-0.018
0.5	0.463	0.15	0.192	0.189	-0.13
0.568	0.429	0.313	0.269	0.19	0.052
0.425	0.448	0.228	0.313	0.213	0.068
0.415	0.34	0.222	0.338	0.057	-0.063
0.267	0.47	0.368	0.267	0.199	0.033
0.548	0.43	0.383	0.282	0.072	0.206
0.578	0.358	0.454	0.243	0.204	-0.014
0.657	0.374	0.471	0.404	0.102	0.059
0.679	0.36	0.252	0.247	0.168	0.082
0.392	0.435	0.39	0.314	0.201	-0.031
0.464	0.434	0.373	0.266	0.122	-0.043
0.591	0.435	0.371	0.138	0.149	0.183
0.459	0.382	0.134	0.384	0.161	-0.017
0.413	0.485	0.32	0.423	0.22	-0.025
0.44	0.496	0.394	0.354	0.246	0.007
0.53	0.416	0.234	0.258	0.094	0.194
0.406	0.479	0.234	0.274	0.104	0.07
0.417	0.393	0.318	0.24	0.35	-0.002

**Table A.6. Statistical analysis of colocalization between the stable lines.** All datasets were normally distributed (Shapiro-Wilk-test). Significant colocalization differences were tested by the Welch's two sample t-test.

	<b>SKD1x PAB2</b>	<b>DCP5x PAB2</b>	<b>RHA1x PAB2</b>	<b>SKD1x ARA7</b>	<b>DCP5x ARA7</b>	<b>SKD1x PAB2 tilt</b>
<b>SKD1xPAB2</b>		0.001975	5.879e-10	3.666e-13	2.2e-16	2.2e-16
<b>DCP5xPAB2</b>	0.001975		3.084e-07	2.489e-12	2.2e-16	2.2e-16
<b>RHA1xPAB2</b>	5.879e-10	3.084e-07		0.179	3.174e-09	2.2e-16
<b>SKD1xARA7</b>	3.666e-13	2.489e-12	0.179		8.039e-09	2.2e-16
<b>DCP5xARA7</b>	2.2e-16	2.2e-16	3.174e-09	8.039e-09		3.136e-08
<b>SKD1/PAB2 tilt</b>	2.2e-16	2.2e-16	2.2e-16	2.2e-16	2.2e-16	

**Table A.7. Predicted IDR content within *A. thaliana* ESCRTIII core, ESCRTIII associated, P-body, and SG proteins.** *A. thaliana* ESCRTIII core and associated, P-body and SG proteins were analyzed by DisEMBL and GlobPlot for their IDR content (Linding et al., 2003; Linding, 2003). The specific identifiers, protein lengths and amino acid (aa) stretches, which were predicted to be disorders, are indicated. Long IDRs (30 or more residues) are depicted in bold and italic. Percentages of IDRs are given in respect to the total length of the analyzed proteins. The total number of aa in IDRs or long IDRs are shown in brackets.

			DisEMBL		GlobPlot	
		AGI	aa	loops	H-loops	disordered region
ESCRTIII core	VPS20.1	AT5G 63880	243	1-12, <b><i>186-243</i></b>	1-16, 63-75, <b><i>201-243</i></b>	209-219
	VPS24.1	AT5G 22950	229	1-16, 151-160, 190-200	1-19, 33-43, 51-62, 67-77, 177-200	<i>none</i> <i>none</i>
	VPS32.1	AT2G 19830	194	98-105, 125-137, <b><i>151-180</i></b>	11-39, 94-105	161-173
	VPS32.2	AT4G 29160	219	1-11, 116-123, 145-154, 173-200	1-17, <b><i>36-70</i></b> , 113-123,	178-197
	VPS2.1	AT2G 06530	225	1-11, 149-160, 178-194, 201-213	1-17, 31-42, 50-59, 80-87, 202-214	2-6, 206-213
	VPS2.2	AT5G 44560	243	1-15, 76-85, 95-102, 149-157, <b><i>173-207</i></b>	<b><i>1-39</i></b> , 48-56, 74-86, 93-102, <b><i>175-211</i></b>	195-201
	VPS2.3	AT1G 03950	210	1-12, 147-159, 175-200	<b><i>1-39</i></b> , 48-58, 176-200	1-10, 180-195
ESCRTIII associated	LIP5	AT4G 26750	421	20-27, 38-51, 65-80, 91-106, 119-131, <b><i>147-376</i></b> , 411-421	41-52, 146-162, 167-177, 408-421	1-6, 70-76, 123-127, <b><i>148-374</i></b> , 412-419
	SKD1	AT2G 27600	435	17-29, <b><i>74-113</i></b> , 121-135, <b><i>148-179</i></b> , 222-229, 234-248, 261-268, 291-301, <b><i>311-379</i></b> , 389-400	<b><i>73-113</i></b> , 240-250, 391-400	<b><i>74-112</i></b> , 168-178, 237-244, 313-323, 328-336, 362-379, 431-435
	VPS46.1	AT1G 17730	203	136-152, 164-187	<b><i>13-53</i></b> , 173-191	141-149, 168-178
	VPS46.2	AT1G 73030	203	139-152, 164-188	<b><i>1-53</i></b> , 173-191	142-149, 168-178
	VPS60.1	AT3G 10640	235	1-22, 49-58, 75-89, 149-163, <b><i>174-235</i></b>	<b><i>1-35</i></b> , 46-61, 220-235	9-23, 151-162, <b><i>178-217</i></b> , 228-235
	VPS60.2	AT5G 04850	272	1-21, 47-57, 75-89, 149-169, 188-197, <b><i>210-272</i></b>	<b><i>1-33</i></b> , 40-60	5-22, 153-164, <b><i>216-257</i></b> , 265-272
P-body	DCP1	AT1G 08370	367	1-17, 64-73, 92-105, <b><i>139-185</i></b> , <b><i>191-300</i></b>	1-16, 64-82, 139-165, 287-300	<b><i>164-262</i></b> , <b><i>266-334</i></b>
	DCP2	AT5G 13570	386	1-23, 31-40, 58-72, 83-91, 99-114, 127-147, 203-214, 224-241, 259-275, <b><i>282-370</i></b>	1-19, 34-41, 99-106, 127-144, 174-181, 203-212, 263-273, <b><i>283-338</i></b> , 343-355	6-19, 131-142, 264-270, 285-293, 353-366
	DCP5	AT1G 26110	611	1-15, 24-31, <b><i>38-72</i></b> , <b><i>80-392</i></b> , <b><i>399-611</i></b>	1-16, 38-47, 55-70, 319-331, <b><i>400-445</i></b> , <b><i>487-571</i></b> , 594-611	3-13, 54-69, <b><i>89-264</i></b> , <b><i>271-305</i></b> , <b><i>320-369</i></b> , 374-387, <b><i>412-453</i></b> , 482-500, 517-532, <b><i>553-611</i></b>
	VCS	AT3G 13300	1344	<b><i>1-107</i></b> , <b><i>115-202</i></b> , 214-221, 268-279, 290-306, <b><i>317-364</i></b> , <b><i>384-427</i></b> , <b><i>437-467</i></b> , 499-509, 520-535, 553-573, <b><i>580-786</i></b> , 797-819, <b><i>827-896</i></b> , 905-917, 945-954, <b><i>1179-1212</i></b> , 1248-1260, 1293-1303, 1318-1326	1-14, 141-153, 269-280, 325-343, 405-417, 582-599, 706-731, 747-757, <b><i>763-818</i></b> , 860-870, 875-894, 945-955, 966-975, 1046-1059, 1228-1237	<b><i>2-64</i></b> , <b><i>82-112</i></b> , 117-127, 139-156, 397-409, 501-507, 523-532, 557-567, 583-602, 626-653, 659-667, 684-695, 721-742, 775-781, 802-810, <b><i>838-873</i></b> , 882-896, 1180-1193

			DisEMBL		GlobPlot	
	AGI	aa	loops	H-loops	disordered region	
	<b>eIF4E1</b>	<b>AT4G18040</b>	235	<i>1-92, 103-150, 228-235</i>	1-26, 218-226	4-8, 22-26, 35-61, 130-143, 227-233
	<b>XRN4</b>	<b>AT1G54490</b>	947	<i>11-75, 104-113, 153-166, 196-207, 217-231, 256-298, 312-324, 338-351, 371-378, 413-462, 485-580, 612-623, 631-655, 660-749, 763-847, 855-877, 888-927, 937-947</i>	<i>8-43, 104-117, 132-140, 393-444, 450-465, 719-739, 821-831, 934-947</i>	<i>22-51, 59-74, 158-163, 200-204, 219-229, 271-288, 422-439, 523-537, 543-555, 638-656, 667-676, 695-704, 719-728, 767-845, 858-872, 888-923, 939-945</i>
SG	<b>UBP1b</b>	<b>AT1G17370</b>	419	<i>22-60, 68-103, 113-151, 160-190, 211-230, 238-258, 265-275, 319-360, 374-389, 394-408</i>	217-232, 238-257	30-54, 219-227, 240-254, <b>326-358</b> , 377-384, 401-405
	<b>PAB2</b>	<b>AT4G34110</b>	629	<i>1-51, 73-87, 98-148, 157-169, 188-213, 223-239, 247-264, 275-296, 315-333, 338-369, 407-538, 545-553</i>	1-19, 75-89, <b>200-232</b> , 274-300, 311-322, 340-360, 406-422, 615-629	7-33, 116-121, 160-164, 250-259, 345-362, <b>417-497</b> , 513-538, 624-629
	<b>RBP47b</b>	<b>AT3G19130</b>	435	<i>1-30, 62-109, 120-135, 145-153, 169-256, 264-290, 300-365, 388-435</i>	1-19, 172-180, <b>220-257, 375-405</b>	2-29, 69-79, 171-182, 202-208, 239-249, 299-324, <b>390-435</b>
	<b>GRP7</b>	<b>AT2G21660</b>	176	<i>32-57, 68-176</i>	30-58, 69-78, 85-98, 157-176	<i>69-75, 83-174</i>
	<b>RBP45b</b>	<b>AT1G11650</b>	405	<i>1-59, 97-106, 123-158, 176-185, 193-205, 216-275, 287-304, 326-405</i>	144-153, <b>175-226</b> , 231-242, 248-259, 389-405	4-24, 29-54, 125-132, 144-155, 220-239, 248-266, <b>326-395</b>
	<b>GRP2</b>	<b>AT4G13850</b>	158	<i>1-33, 40-49, 68-88</i>	10-20, 71-87, 92-100	4-8, 12-24, 42-47, 76-82, <b>105-156</b>

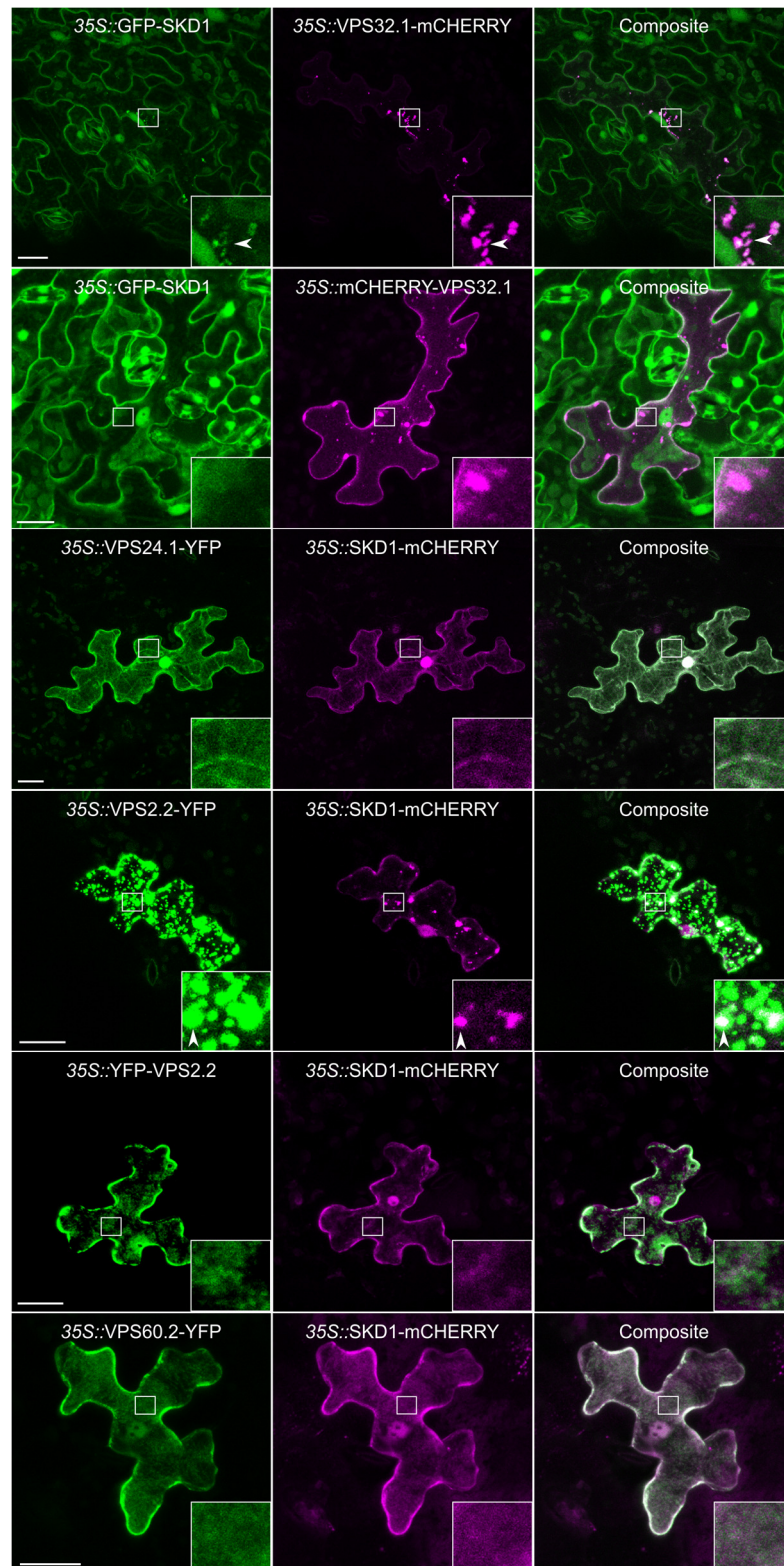


**Figure A.3. Colocalization of ESCRTIII core and associated proteins with SKD1.** Epidermal leaf cells were transiently transformed. For colocalization analysis of VPS32.1 with SKD1, epidermal leaf cells of the stable *35S::GFP-SKD1* line were transformed either with a construct overexpressing VPS32.1-mCHERRY or mCHERRY-VPS32.1 (row 1-2). For the colocalization of VPS24.1-YFP (row3), VPS2.2-YFP and YFP-VPS2.2 (row 4-5), and VPS60.2-YFP (row6), Col-0 cells were transiently double transformed with the respective ESCRTIII protein and SKD1-mCHERRY. The cells were imaged by confocal microscopy and representative maximum projections of stacks are depicted. Arrow heads indicate colocalization with SKD1. Bar = 20  $\mu$ m.

## Appendix

**Table A.8. PCCs of ESCRTIII core or associated proteins and UBP1b.** Epidermal leaf cells of Col-0 plants were transiently double transformed. In addition to the indicated ESCRTIII proteins, the cells were transformed with UBP1b in N-terminal fusion with the opposing fluorescent proteins (YFP or mCHERRY). For each combination, ten cells were imaged after heat stress and three ROIs were analyzed for fluorescent signal overlap using the PCC (ImageJ, JACoP). Raw data from Figure 3.17.

VPS24.1	VPS32.1	VPS2.2 YFP	YFP VPS2.2	VPS46.1	VPS46.2	VPS60.2	LIP5	SKD1-AQ
0.279	0.181	0.417	0.41	0.345	0.215	0.3	0.344	0.41
0.254	0.268	0.342	0.086	0.251	0.315	0.277	0.386	0.763
0.358	0.367	0.438	0.316	0.335	0.338	0.102	0.581	0.626
0.126	0.178	0.562	0.492	0.608	0.473	0.341	0.115	0.424
0.185	0.143	0.645	0.416	0.688	0.373	0.32	0.156	0.443
0.157	0.24	0.424	0.48	0.582	0.453	0.295	0.265	0.476
0.299	0.181	0.311	0.395	0.536	0.534	0.289	0.272	0.643
0.139	0.38	0.324	0.393	0.672	0.453	0.297	0.221	0.652
0.243	0.388	0.181	0.109	0.348	0.46	0.162	0.303	0.604
0.226	0.309	0.271	0.324	0.363	0.601	0.159	0.311	0.651
0.207	0.188	0.266	0.261	0.356	0.591	0.384	0.375	0.643
0.384	0.243	0.398	0.17	0.385	0.622	0.216	0.393	0.569
0.272	0.267	0.252	0.38	0.241	0.421	0.157	0.341	0.69
0.15	0.287	0.136	0.362	0.535	0.323	0.144	0.296	0.749
0.385	0.259	0.24	0.337	0.36	0.312	0.233	0.197	0.765
0.152	0.428	0.253	0.358	0.453	0.647	0.411	0.396	0.676
0.175	0.27	0.17	0.362	0.475	0.62	0.375	0.375	0.632
0.3	0.259	0.275	0.265	0.475	0.65	0.413	0.397	0.602
0.184	0.19	0.299	0.422	0.485	0.36	0.131	0.197	0.456
0.201	0.132	0.225	0.42	0.453	0.385	0.495	0.195	0.297
0.169	0.221	0.296	0.438	0.376	0.327	0.149	0.4	0.385
0.159	0.248	0.296	0.327	0.255	0.427	0.029	0.376	0.527
0.22	0.385	0.44	0.44	0.129	0.407	0.115	0.364	0.499
0.112	0.38	0.534	0.291	0.171	0.39	0.222	0.246	0.545
0.334	0.205	0.195	0.271	0.419	0.799	0.279	0.33	0.633
0.23	0.17	0.187	0.309	0.339	0.829	0.185	0.224	0.585
0.309	0.325	0.107	0.162	0.289	0.815	0.402	0.234	0.513
0.161	0.273	0.441	0.357	0.497	0.434	0.311	0.231	0.548
0.21	0.275	0.488	0.511	0.486	0.458	0.461	0.27	0.642
0.211	0.247	0.495	0.212	0.072	0.468	0.379	0.446	0.708

**Table A.9. Statistical analysis of colocalization of ESCRTIII core and associated proteins with UBP1b.** All datasets were normally distributed with the exception of VPS46.2 (Shapiro-Wilk-test). Normally distributed datasets were evaluated for significant colocalization differences using the Welch's two sample t-test. For comparisons with the VPS46.2 dataset, the Wilcoxon-Mann-Whitney-test was used. The obtained PCCs were compared to the values of the SKD1-mCHERRY/YFP-UBP1b overlap and the negative control YFP-UBP1b/mCHERRY-UBP1b tilt (Chapter 3.3.2).

	VPS 32.1	VPS 24.1	VPS 2.2 YFP	YFP VPS 2.2	VPS 46.1	VPS 46.2	VPS 60.2	LIP5	SKD1 AQ	SKD1	UBP1b UBP1b tilt
VPS 32.1		0.0738 4	0.0221	0.0043 17	6.22e-05	2.285e-08	0.851 8	0.056 48	2.2e-16	2.2e-16	2.2e-16
VPS 24.1	0.0738 4		0.0006 055	3.492e-05	1.147e-06	1.12e-09	0.112 9	0.000 7392	2.2e-16	2.2e-16	2.772e-14
VPS 2.2-YFP	0.0221	0.0006 055		0.8595	0.0646 6	0.0002 603	0.060 51	0.465 8	2.83e-10	2.2e-16	2.236e-14
YFP-VPS2.2	0.0043 17	3.492e-05	0.8595		0.0648 5	0.0003 664	0.023 32	0.300 2	1.74e-11	2.2e-16	2.2e-16
VPS 46.1	6.22e-05	1.147e-06	0.0646 6	0.0648 5		0.1188	0.000 3763	0.007 257	3.279e-06	1.147e-06	7.804e-16
VPS 46.2	2.285e-08	1.12e-09	0.0002 603	0.0003 664	0.1188		6.524e-07	5.853e-06	0.005 443	1.66e-07	3.012e-11
VPS 60.2	0.8518	0.1129	0.0605 1	0.0233 2	0.0003 763	6.524e-07		0.158 6	1.256e-14	2.2e-16	8.734e-13
LIP5	0.0564 8	0.0007 392	0.4658	0.3002	0.0072 57	5.853e-06	0.158 6		1.365e-13	2.2e-16	2.2e-16
SKD1 AQ	2.2e-16	2.2e-16	2.83e-10	1.74e-11	3.279e-06	0.0054 43	1.256e-14	1.365e-13		1.889e-07	2.2e-16
SKD1	2.2e-16	2.2e-16	2.2e-16	2.2e-16	1.147e-06	1.66e-07	2.2e-16	2.2e-16	1.889e-07		2.2e-16
UBP1b UBP1b tilt	2.2e-16	2.772e-14	2.236e-14	2.2e-16	7.804e-16	3.012e-11	8.734e-13	2.2e-16	2.2e-16	2.2e-16	

**Table A.10. List of filtered SKD1 interactome candidates.** List of proteins, which were identified by LC-MS/MS analysis in at least three replicates of one condition of the *35S::GFP-SKD1* samples and not present in any of the *35S::YFP* samples. Names, UniProt Protein IDs and ATG gene identifier are given. The columns SKD1 control and SKD1 heat indicate the number of replicates in which the respective protein was identified (0- 3). Annotations and short descriptions are based on TAIR annotations and available literature. Proteins were grouped based on functional classification. Gray = mitochondria and chloroplast, orange = membrane trafficking, pink = protein processing, lilac = RNA metabolism, green = protein folding, no color = others. The column “in other interactome” indicates, if an identified SKD1 interactor was found in an *A. thaliana* interactome of the SG proteins CML38 (Lokdarshi et al., 2016), RBP45b (Muthuramalingam et al., 2017) or VPS2.2 (Ibl et al., 2012).

Protein names/Gene names	Protein IDs	ATG	SKD1 control	SKD1 heat	Annotations and descriptions	In other interactome
<b>SKD1 shared interactors</b>						
	F4HY33	AT1G21630	3	2	calcium-binding EF hand family protein	
Formate dehydrogenase, mitochondrial, FDH1	Q9S7E4	AT5G14780	3	2	NAD-dependent formate dehydrogenase	
ADP-ribosylation factor 2-A	Q9M1P5	AT3G62290	3	2	ARF GTPase family, vesicle coating/ uncoting function	
26S proteasome non-ATPase regulatory subunit 14 homolog	Q9LT08	AT5G23540	3	2	26S proteasome regulatory subunit, putative	CML38
Puromycin-sensitive aminopeptidase	F4I3R4	AT1G63770	3	2	peptidase M1 family protein, proteolysis	
	F4HNU6	AT1G06900	3	2	metalloendopeptidase, cytosol	
VPS18 homolog	F4IDS7	AT1G12470	3	2	Vps18, CORVET/HOPS complex, endosome to vacuole fusion	
NADP-dependent glyceraldehyde-3-phosphate dehydrogenase, ALDH11A3	F4INS6	AT2G24270	3	2	oxidation-reduction processes	
Small nuclear ribonucleoprotein F, RUXF	F4JPK5	AT4G30220	3	2	mRNA splicing	
Proteasome subunit beta type, PBA1	F4JRY2	AT4G31300	3	2	plant caspase-3-like enzyme, ER-stress, apoptosis	
DEAD-box ATP-dependent RNA helicase 56, UAP56A	F4JWF3	AT5G11170	3	2	RNA helicase, interact with mRNA export factors	CML38
nuclear transport factor 2 (NTF2) family protein	F4K1Y4	AT5G60980	3	2	(RRM)-containing protein, nucleocytoplasmic transport	RBP45b, VPS2.2
Serine hydroxymethyltransferase 4, SHM4	O23254	AT4G13930	3	2	L-serine metabolic process	CML38
Superoxide dismutase [Cu-Zn] 2, chloroplastic, CSD2	O78310	AT2G28190	3	2	zinc superoxide dismutase, chloroplast	
Reticulon-like protein B5, RTNLB5	O82352	AT2G46170	3	2	ER-Golgi trafficking, vesicle formation and membrane morphogenesis	
glutamate-tRNA ligase, putative	O82462	AT5G26710	3	2	glutamyl-tRNA aminoacylation	
T-complex protein 1 subunit alpha, ATTCP-1	P28769	AT3G20050	3	2	TCP-1 chaperonine	CML38
Calnexin homolog 1, CNX1	P29402	AT5G61790	3	2	protein folding, calcium ion binding	
3-oxoacyl-[acyl-carrier-protein] reductase, chloroplastic	P33207	AT1G24360	3	2	fatty acid biosynthetic process, oxidation-reduction process	

Appendix

Protein names/Gene names	Protein IDs	ATG	SKD1 control	SKD1 heat	Annotations and descriptions	In other interactome
Glucose-1-phosphate adenylyltransferase small subunit, chloroplastic, APS1	P55228	AT5G48300	3	2	glycogen biosynthetic process	
Vacuolar protein sorting-associated protein 41 homolog, VPS41	P93043	AT1G08190	3	2	Vps41,HOPS complex, endosome to vacuole fusion	
14-3-3-like protein GF14 omega, GRF2	Q01525	AT1G78300	3	2	post golgi protein trafficking, PIN polarity establishment	
Probable glycerol-3-phosphate acyltransferase 8,GPAT8	Q5XF03	AT4G00400	3	2	CDP-diacylglycerol biosynthetic process	
COP9 signalosome complex subunit 5b, CSN5B	Q8LAZ7	AT1G22920	3	2	COP9 signalosome,regulation of photomorphogenesis, cell cycle	
Rhodanese-like/PpiC domain-containing protein 12	Q93W10	AT5G19370	3	2	cytokinin response	
ABC transporter G family member 22, ABCG22	Q93YS4	AT5G06530	3	2	water transport	
Tetratricopeptide repeat (TPR)-like superfamily protein	Q93ZI7	AT5G35430	3	2		
DEAD-box ATP-dependent RNA helicase 2, eIF4AIII	Q94A52	AT3G19760	3	2	RNA helicase,	
ATP-dependent Clp protease proteolytic subunit 4, chloroplastic, CLPP4	Q94B60	AT5G45390	3	2	caseinolytic protease, chloroplast	
ZKT	Q94BS2	AT1G55480	3	2	binding / protein binding	
Copper transport protein, ATX1	Q94BT9	AT1G66240	3	2	copper chaperone, metal ion homeostasis	
Pentatricopeptide repeat-containing protein , mitochondrial	Q9C977	AT1G80270	3	2	mitochondrial RNA editing	
importin beta-2, putative	Q9FJD4	AT5G53480	3	2	protein import to nucleus	
CBS domain-containing protein CBSCBSPB1	Q9FMV3	AT5G63490	3	2	integral membrane component	
WEB family protein, chloroplastic	Q9LFE4	AT5G16730	3	2	microtubule-associated	
BAK1-ASSOCIATING RECEPTOR-LIKE KINASE 1, BARK1	Q9LK43	AT3G23750	3	2	protein kinase family protein, cell surface receptor	
Peroxiredoxin-2F, mitochondrial, PRXIIIF	Q9M7T0	AT3G06050	3	2	cell redox homeostasis	
Fructose-1,6-bisphosphatase, cytosolic	Q9MA79	AT1G43670	3	2	carbon metabolism	
Delta-aminolevulinic acid dehydratase 1, chloroplastic, HEMB1	Q9SFH9	AT1G69740	3	2	chlorophyll biosynthesis.	
26S proteasome non-ATPase regulatory subunit 8 homolog A, RPN12A	Q9SGW3	AT1G64520	3	2	ubiquitin mediated 26 proteasome degradation,	
SOUL heme-binding family protein	Q9SHG8	AT1G17100	3	2	antioxidant pathway	
TPX2	Q9SJ62	AT2G35880	3	2		
CRS2-associated factor 1, chloroplastic, CAF1	Q9SL79	AT2G20020	3	2	RNA binding, mRNA processing in chloroplast	
SEC13A homolog	Q9SR11	AT3G01340	3	2	COPII vesicle budding, protein transport	
ISTL1	Q9XIC8	AT1G34220	3	2	Regulator of SKD1 activity, ESCRTIII associated	
	Q8VYF2	AT4G15790	2	3		

Appendix

Protein names/Gene names	Protein IDs	ATG	SKD1 control	SKD1 heat	Annotations and descriptions	In other interactome
Phospholipase A I	F4HX14	AT1G61850	2	3	non-specific lipase	
Protochlorophyllide reductase C, chloroplastic, POR C	F4I2F8	AT1G03630	2	3	chlorophyll biosynthetic processes	
Alanine--tRNA ligase, ALATS	F4I4Z2	AT1G50200	2	3	alanyl-tRNA aminoacylation	CML38
	F4IDE8	AT1G72640	2	3		
alpha/beta-Hydrolases superfamily protein	F4J447	AT3G23600	2	3	hydrolase activity	
E3 ubiquitin-protein ligase, KEG	F4K3Z6	AT5G13530	2	3	RING E3 ligase, promotes ubiquitin dependent 26S proteasome pathway.	
26S proteasome non-ATPase regulatory subunit 12 homolog A, EMB2107	F4KFD7	AT5G09900	2	3	proteasome complex regulation	
2,3-bisphosphoglycerate-independent phosphoglycerate mutase 1, PGM1	O04499	AT1G09780	2	3	glucose catabolic process	
Glycine--tRNA ligase 1, mitochondrial, GLYRS-1	O23627	AT1G29880	2	3	glycine-tRNA ligase	
Metacaspase-4, AMC4	O64517	AT1G79340	2	3	stress-induced programmed cell death (PCD), metacaspase	
Aspartate aminotransferase, mitochondrial, ASP1	P46643	AT2G30970	2	3	biosynthetic process, mitochondrion	
Aldehyde dehydrogenase family 2 member C4, ALDH2C4	Q56YU0	AT3G24503	2	3	oxidation-reduction process	
serine/threonine protein phosphatase 2A regulatory subunit B gamma, BGAMMA	Q8VZQ4	AT5G28900	2	3	Calcium-binding EF-hand family protein	
Pyruvate dehydrogenase E1 component subunit alpha-2, mitochondrial, IAR4	Q8H1Y0	AT1G24180	2	3	acetyl-CoA biosynthetic process	
COP9 signalosome complex subunit 4, CSN4	Q8L5U0	AT5G42970	2	3	COP9 signalosome complex	
S-formylglutathione hydrolase, SFGH	Q8LAS8	AT2G41530	2	3	formaldehyde catabolic process	
Probable clathrin assembly protein	Q8S9J8	AT4G32285	2	3	adaptor protein , membrane trafficking	
Beta carbonic anhydrase 4, BCA4	Q94CE4	AT1G70410	2	3	regulation of stomatal movement	
Ferritin/ribonucleotide reductase-like family protein	Q94JV2	AT3G27050	2	3		
Nucleosome assembly protein 1, NAP1	Q94K07	AT5G56950	2	3	nucleosome assembly	
Peroxisome biogenesis protein 5, PEX5	Q9FMA3	AT5G56290	2	3	peroxisomal protein translocation	
RAN GTPase-activating protein 1, RANGAP1	Q9LE82	AT3G63130	2	3	RAN GTPase activator, involved in nuclear import	
Alpha-glucan phosphorylase 1, PHS1	Q9LIB2	AT3G29320	2	3	starch metabolism, plastidic	
Developmentally-regulated G-protein 1,	Q9LQK0	AT1G17470	2	3	SMALL GTPase, associates with Heat Shock proteins and ribosomes	
Obg-like ATPase 1, ENGD-1	Q9SA73	AT1G30580	2	3	GTP binding, negativ regulator of salt stress response	
photosystem II 5 kD protein	Q9SYE2	AT1G51400	2	3	photosynthesis	
Outer envelope pore protein 16-1, chloroplastic, OEP161	Q9ZV24	AT2G28900	2	3	protein transmembrane transporter, import into chloroplast stroma	

Appendix

Protein names/Gene names	Protein IDs	ATG	SKD1 control	SKD1 heat	Annotations and descriptions	In other interactome
Glyoxylate/succinic semialdehyde reductase 1	Q9LSV0	AT3G25530	3	3	phosphogluconate dehydrogenase	
Probable UTP--glucose-1-phosphate uridylyltransferase 2	Q9M9P3	AT3G03250	3	3	UDP-glucose pyrophosphorylase	
haloacid dehalogenase-like hydrolase family protein, chloroplastic	Q8VZ10	AT1G56500	3	3	thylakoid membrane protein	
DNAJ heat shock protein, putative	Q0WN54	AT1G80030	3	3	Molecular chaperone Hsp40/DnaJ family protein	
DnaJ protein ERDJ2B	F4JIN3	AT4G21180	3	3	DNAJ heat shock N-terminal domain-containing protein, protein folding	
disease resistance protein (TIR-NBS class), putative, RLM3	Q9FT77	AT4G16990	3	3		
Organellar oligopeptidase A, chloroplastic/mitochondrial, OOP	Q94AM1	AT5G65620	3	3	metalloprotease	
DNA damage-binding protein 1a, DDB1A	Q9M0V3	AT4G05420	3	3	DNA damage repair	
Heat shock 70 kDa protein 14, HSP70-14	Q9S7C0	AT1G79930	3	3	protein folding/chaperone	
	F4HZS8	AT1G22060	3	3		
S-adenosyl-L-methionine-dependent methyltransferases superfamily protein	Q9ZVU4	AT1G55450	3	3		
myosin-related, SYP41 interactor, TNO1	F4I9A1	AT1G24460	3	3	putative tethering factor, interacts with SYP41, vacuolar trafficking/HOPS	
threonyl-tRNA synthetase, mitochondrion and chloroplast, EMB2761	F4IFC5	AT2G04842	3	3		
14-3-3-like protein GF14 mu, GRF9	F4IP53	AT2G42590	3	3	PIN polarity establishment	
Chaperonin CPN60-like 1, mitochondrial, HSP60-2	F4IVR2	AT2G33210	3	3		
Phosphoinositide phospholipase C, PLC2	F4IX90	AT3G08510	3	3	phospholipase C, ER stress response	
Magnesium-protoporphyrin IX monomethyl ester cyclase, chloroplastic, CRD1	F4J0U9	AT3G56940	3	3		
Clustered mitochondria protein homolog	F4J5S0	AT3G52140	3	3	tetratricopeptide repeat (TPR)-containing protein,	
Ubiquitin carboxyl-terminal hydrolase, UBP12	F4K3X1	AT5G06600	3	3	deubiquitination, involved in JA signaling and circadian clock regulation	
pleckstrin homology (PH) domain-containing protein	F4JNE4	AT4G17140	3	3		
Myosin-6, MYA2	F4K7C5	AT5G43900	3	3		
1-deoxy-D-xylulose 5-phosphate reductoisomerase, chloroplastic, DXR	F4K7T6	AT5G62790	3	3	isopentenyl diphosphate biosynthetic process	
TRANSDUCIN/WD40-2 PROTEIN, TWD40-2	F4KIH8	AT5G24710	3	3		
T-complex protein 1 subunit epsilon	O04450	AT1G24510	3	3	TCP-1 chaperonine	RBP45b
Biotin carboxylase, chloroplastic, CAC2	O04983	AT5G35360	3	3	fatty acid biosynthetic process	CML38
NADPH-dependent thioredoxin reductase 3, NTRC	O22229	AT2G41680	3	3	cell redox homeostasis, chloroplast	

Appendix

Protein names/Gene names	Protein IDs	ATG	SKD1 control	SKD1 heat	Annotations and descriptions	In other interactome
Zinc-metallopeptidase, peroxisomal, PXM16	O22941	AT2G41790	3	3	peptidase M16 family protein	
Calmodulin-binding transcription activator 5, CMTA5	O23463	AT4G16150	3	3	Calcium transcription activator	
KINESIN LIGHT CHAIN-RELATED 1, KLCR1,	O81629	AT4G10840	3	3	microtubule, calcium sensing	
Phosphomethylpyrimidine synthase, chloroplastic, THIC	O82392	AT2G29630	3	3	thiamine biosynthesis	
Phosphoglycolate phosphatase 1B, chloroplastic, PGLP1B	P0DKC4	AT5G36790	3	3	Haloacid dehalogenase-like hydrolase (HAD) superfamily protein	
Chaperone protein dnaJ 2, ATJ2	P42825	AT5G22060	3	3	chaperone, protein folding, response to heat	
26S proteasome non-ATPase regulatory subunit 4 homolog, RPN10	P55034	AT4G38630	3	3	proteasome subunit, autophagy	
60S ribosomal protein L10a-3, RPL10AC	P59231	AT5G22440	3	3	60S ribosomal protein L10A	
Aquaporin PIP1-1	P61837	AT3G61430	3	3	transmembrane water transport at PM, transport ESCRT-dependent	
Thylakoid lumenal 19 kDa protein, chloroplastic	P82658	AT3G63540	3	3	calcium-ion binding, thylakoid	
ATP synthase protein MI25, AtMg00640	Q04613	ATMG00640	3	3	mitochondrial ATP synthase	
Aquaporin PIP1-3	Q08733	AT1G01620	3	3	transmembrane water transport at PM	
Serine/threonine-protein phosphatase regulatory subunit A alpha isoform, RCN1	Q38845	AT1G25490	3	3	role in PIN polarity by regulation vesicle trafficking of PIN	
Myosin-5, XI-1	Q39160	AT1G17580	3	3	motor protein	
Cell division protein FtsZ homolog 1, chloroplastic, FTSZ1	Q42545	AT5G55280	3	3	cell cycle, chloroplast fission	
Phosphoenolpyruvate carboxylase 2, PPC2	Q5GM68	AT2G42600	3	3	carbon fixation	RBP45b
dihydrolipoamide S-acetyltransferase, putative, mitochondrial	Q5M729	AT1G54220	3	3	pyruvate dehydrogenase	
Fe-S cluster assembly factor HCF101, chloroplastic, HCF101	Q6STH5	AT3G24430	3	3	chloroplast scaffold protein	
Aldehyde dehydrogenase family 3 member F1, ALDH3F1	Q70E96	AT4G36250	3	3	aldehyde metabolic processes	
T-complex protein 1 subunit gamma	Q84WV1	AT5G26360	3	3	TCP-1 chaperonin	CML38
Monothiol glutaredoxin-S16, chloroplastic, GRXS16	Q8H7F6	AT2G38270	3	3	calcium transporter chloroplast	
sodium/calcium exchanger family protein	Q8L636	AT1G53210	3	3	Calcium homeostasis	
TCP-1/cpn60 chaperonin family protein	Q9M888	AT3G02530	3	3	TCP-1 chaperonin	CML38, RBP45b
Thioredoxin-like 2-2, chloroplastic	Q8LCT3	AT4G29670	3	3	cell redox homeostasis	
	Q8VZ74	AT5G66470	3	3		
elongation factor P (EF-P) family protein, chloroplast,	Q8VZW6	AT3G08740	3	3	elongation factor chloroplast	
MA3 domain-containing protein	Q8W4Q4	AT4G24800	3	3	MA3 domain-containing protein	

Appendix

Protein names/Gene names	Protein IDs	ATG	SKD1 control	SKD1 heat	Annotations and descriptions	In other interactome
V-type proton ATPase subunit a3, VHA-a3	Q8W4S4	AT4G39080	3	3	vacuolar proton transport	
Protein VACUOLELESS1, VCL1	Q93VQ0	AT2G38020	3	3	CORVET/HOPS complex, late endosome to tonoplast transport/fusion	
GDP-mannose 3,5-epimerase	Q93VR3	AT5G28840	3	3	L-ascorbic acid biosynthetic process	
Coatomer subunit delta	Q93Y22	AT5G05010	3	3	protein transport, COPI vesicles	
DEAD-box ATP-dependent RNA helicase 38, LOS4	Q93ZG7	AT3G53110	3	3	DEAD-box RNA Helicase, nuclear envelope and cytosol,mRNA export from nucleus	
Chaperonin CPN60-like 2, mitochondrial, HSP60-3A	Q93ZM7	AT3G13860	3	3	chaperonin, putative	
Phosphomethylethanolamine N-methyltransferase, NMT2	Q944H0	AT1G48600	3	3	phosphatidylcholine biosynthetic process	CML38
Multicopper oxidase LPR2	Q949X9	AT1G71040	3	3	copper ion binding	
TCP-1 chaperonine, putative	Q94K05	AT3G03960	3	3	TCP-1 chaperonine	RBP45b
30S ribosomal protein, putative	Q94K97	AT5G24490	3	3		
Plasma membrane-associated cation-binding protein 1,PCAP1	Q96262	AT4G20260	3	3	plasmamebrane associated, binds calmodulin	
Mitochondrial dicarboxylate/tricarboxylate transporter DTC	Q9C5M0	AT5G19760	3	3	mitochondrial carrier protein	
myosin heavy chain-related	Q9C7V7	AT1G64330	3	3		
DNA helicase, putative	Q9FJW0	AT5G67630	3	3	transcription	
TIM-barrel signal transduction protein, chloroplast	Q9FJZ7	AT5G66420	3	3		
Magnesium-chelatase subunit ChlH, chloroplastic, GUN5	Q9FNB0	AT5G13630	3	3	magnesium chelatase, plastid-to-nucleus signal transduction.	
Translation factor GUF1 homolog, chloroplastic	Q9FNM5	AT5G08650	3	3	translation elongation	
6-phosphogluconate dehydrogenase, decarboxylating 3	Q9FWA3	AT3G02360	3	3	peroxisomal dehydrogenase	CML38
Chaperonin 60 subunit beta 2, chloroplastic, CPN60B2	Q9LJE4	AT3G13470	3	3	chaperonin, putative	
V-type proton ATPase subunit d1, VHA-d1	Q9LJI5	AT3G28710	3	3	ATPase, V0/A0 complex, subunit C/D	
26S proteasome non-ATPase regulatory subunit 3 homolog A, RPN3A	Q9LNU4	AT1G20200	3	3	26S proteasom component	
Enhancer of mRNA-decapping protein 4, VCS	Q9LTT8	AT3G13300	3	3	P-body, decapping	CML38, RBP45b
T-complex protein 1 subunit delta	Q9LV21	AT3G18190	3	3	TCP-1 chaperonine	CML38, RBP45b
26S protease regulatory subunit S10B homolog B, RPT4B	Q9MAK9	AT1G45000	3	3	26S proteasom component	
6-phosphofructo-2-kinase/fructose-2,6-bisphosphatase, FKFBP	Q9MB58	AT1G07110	3	3	photosynthetic carbon metabolism	
Serine/threonine-protein kinase STN7, chloroplastic, STN7	Q9S713	AT1G68830	3	3	kinase/ protein kinase	
Inosine-5-monophosphate dehydrogenase 2	Q9SA34	AT1G16350	3	3	aldolase TIM barrel protein	CML38

Protein names/Gene names	Protein IDs	ATG	SKD1 control	SKD1 heat	Annotations and descriptions	In other interactome
Alpha-glucan water dikinase 1, chloroplastic, SEX1	Q9SAC6	AT1G10760	3	3	starch metabolism/degradation	
AP-4 complex subunit mu, AP4M	Q9SB50	AT4G24550	3	3	clathrin adaptor complex, vacuolar sorting of storage proteins	
Methylenetetrahydrofolate reductase 1, MTHFR1	Q9SE60	AT3G59970	3	3	methionine biosynthetic process	
TCP-1/cpn60 chaperonin family protein	Q9SF16	AT3G11830	3	3	TCP-1 chaperonine	CML38
DEK domain-containing chromatin associated protein	Q9SMM8	AT3G48710	3	3	GTP binding / RNA binding	
Elongation factor Tu, mitochondrial, TUFA	Q9ZT91	AT4G02930	3	3		CML38
<b>SKD1 control interactors</b>						
Protein names/Gene names	Protein IDs	ATG	SKD1 control	SKD1 heat	Annotations and descriptions	In other interactome
Spactacin carboxy terminus protein	F4JW21	AT4G39420	3	0	spatacsin carboxy-terminus protein	
Kinesin-like protein KCA2	Q9FKP4	AT5G65460	3	0	motorprotein	
eukaryotic translation initiation factor 4B1, EIF4B1	Q9LIN5	AT3G26400	3	0	translation initiation	
transcription elongation factor protein (computational), mRNA binding	F4J0L7	AT3G50370	3	1		
semialdehyde dehydrogenase family protein	Q8VYI4	AT1G14810	3	1	lysine and threonine/methionine biosynthesis	
Phosphatidylinositol 4-kinase alpha 1, PI4KA1	Q9SXA1	AT1G49340	3	1	phosphatidylinositol phosphorylation	
Phosphoglycerate kinase	F4I3L1	AT1G56190	3	1	glycolytic process	
Eukaryotic translation initiation factor 3 subunit M	F4J2B4	AT3G02200	3	1	proteasome family protein	
DNAJ heat shock N-terminal domain-containing protein	F4J6A8	AT3G11450	3	1	putative Hsp40	
V-type proton ATPase subunit B2	F4JTQ0	AT4G38510	3	1	vacuolar transporter	
NAD(P)H-quinone oxidoreductase subunit M, chloroplastic, ndhM	Q2V2S7	AT4G37925	3	1	NADH dehydrogenase complex (plastoquinone) assembly	
AP-2 complex subunit alpha-2, ALPHAC-AD	Q8LPK4	AT5G22780	3	1	adaptor protein complex, endocytosis, vesicle transport	
S-adenosyl-L-methionine-dependent tRNA 4-demethylwyosine synthase	Q8RXN5	AT1G75200	3	1	tRNA processing, mitochondrion	
LINC3 (LITTLE NUCLEI3)	Q9CA42	AT1G68790	3	1	nuclear lamina regulation	
Bidirectional sugar transporter SWEET11	Q9SMM5	AT3G48740	3	1	sugar transport at pm and tonoplast	
<b>SKD1 heat interactors</b>						
Protein names/Gene names	Protein IDs	ATG	SKD1 control	SKD1 heat	Annotations and descriptions	In other interactome
RNA recognition motif (RRM)-containing protein	F4J5A9	AT3G23900	0	3	RNA binding	
Myosin-14, XI-H	F4JM19	AT4G28710	0	3	motor protein,	
17.6 kDa class II heat shock protein, HSP17.6	P29830	AT5G12020	0	3	chaperone	

Protein names/Gene names	Protein IDs	ATG	SKD1 control	SKD1 heat	Annotations and descriptions	In other interactome
Calmodulin-like protein 10, CML10	P30187	AT2G41090	0	3	calmodulin-like calcium-binding protein	
23.6 kDa heat shock protein, mitochondrial, HSP23.6	Q96331	AT4G25200	0	3	chaperone	
15.7 kDa heat shock protein, peroxisomal, HSP15.7	Q9FHQ3	AT5G37670	0	3	HSP20-like chaperones superfamily protein, response to heat stress	
17.8 kDa class I heat shock protein, HSP17.8	Q9LNW0	AT1G07400	0	3	HSP20-like chaperones superfamily protein, response to heat stress	
UDP-glycosyltransferase 85A2, UGT85A2	F411C6	AT1G22360	1	3	metabolic processes	
leucine-rich repeat protein kinase, putative	F41B63	AT1G51805	1	3	kinase activity	
Jacalin-related lectin 34, JAL34	O04310	AT3G16460	1	3		
SAP domain-containing protein	O65655	AT4G39680	1	3	DNA binding	
Peptidyl-prolyl cis-trans isomerase CYP18-4	Q42406	AT4G34870	1	3	cyclophilins, including roles as chaperones	
Flotillin-like protein 1, FLOT1	Q501E6	AT5G25250	1	3	hypoxia response, membrane invagination, endocytosis	
Phosphoethanolamine N-methyltransferase 3, NMT3	Q9C6B9	AT1G73600	1	3	phosphatidylcholine biosynthetic process	
Proline-rich receptor-like protein kinase PERK15,	Q9C821	AT1G52290	1	3	protein kinase family protein, eIF2 $\alpha$ phosphorylation	
phosphatidylinositol 3-kinase complex, chloroplast	Q9LPK9	AT1G21500	1	3		
fructose-bisphosphate aldolase, putative	Q9SJQ9	AT2G36460	1	3	gluconeogenesis	
VPS46.2	Q9SSM4	AT1G73030	1	3	Regulator of SKD1 activity, ESCRTIII associated component	VPS2.2

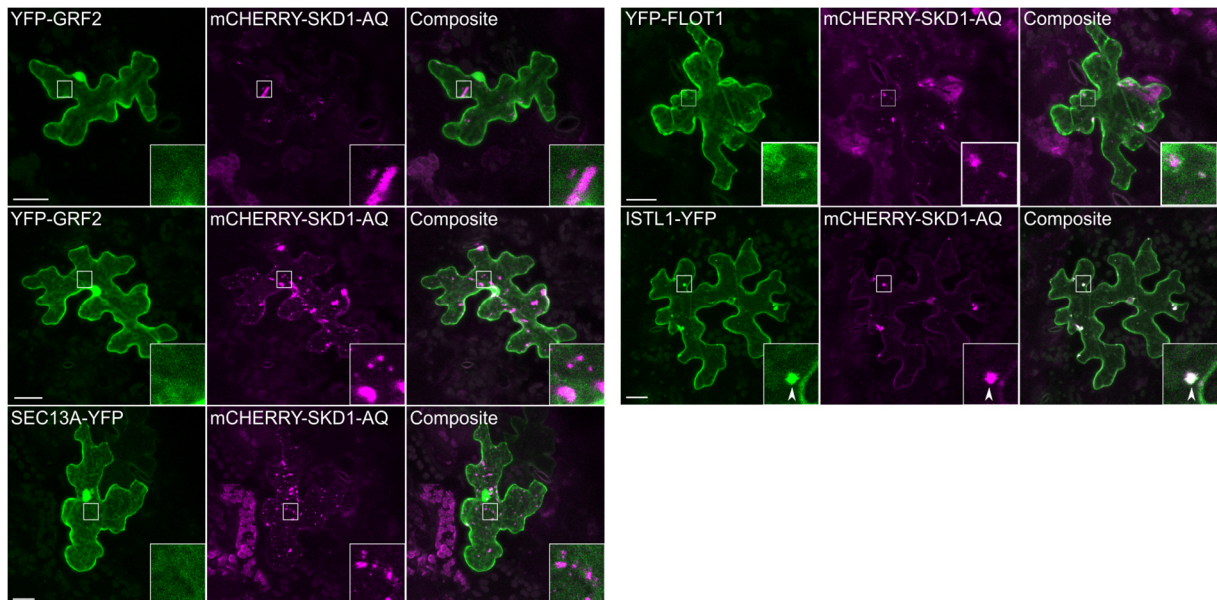


**Figure A.4. Colocalization of membrane trafficking candidates with mCHERRY-SKD1-AQ.** Epidermal *A. thaliana* Col-0 cells were transiently transformed with a construct overexpressing an SKD1 interactome candidate in fusion with YFP and a construct overexpressing (*UBQ10* promoter) mCHERRY-SKD1-AQ. Cells were imaged by confocal microscopy and representative maximum projections of stacks are depicted. Arrow heads indicate colocalizing structures. Bar = 20  $\mu$ m.

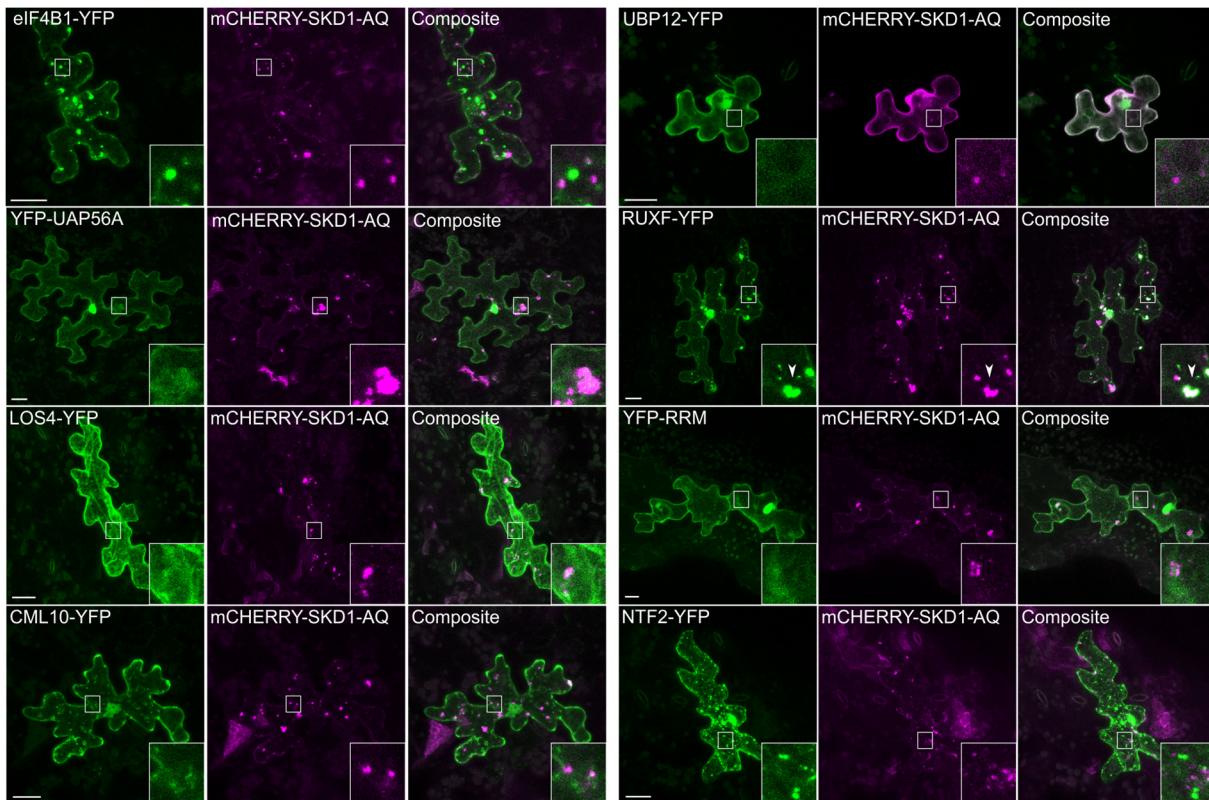


**Figure A.5. Colocalization of RNA metabolism candidates with mCHERRY-SKD1-AQ.** Epidermal *A. thaliana* Col-0 cells were transiently double-transformed and imaged as described in Figure legend Figure A.4. Arrow heads indicate co-localizing structures. Bar = 20  $\mu$ m.

**Table A.11. Results of SKD1 interactome Y2H assays.** Constructs expressing SKD1 in fusion with GAL4-BD and an interactome candidate in fusion with the GAL4-AD were transformed in yeast. Colonies were transferred to plates selecting for successful double transformation (SD-LW) as a control and onto plates with the interaction medium (SD-LWH). Colony growth was evaluated after 9-11 days on SD-LWH plates without 3-AT since no auto-activation was detected for the negative control (SKD1 *versus* GFP). X indicates colony growth. The majority of combinations was tested in three replicates (xxx) over three sets. VPS18, UBP12 and RRM were tested in two sets with three and six biological replicates. SEC13A and eIF4B1 were tested in one set with nine biological replicates. The lowest number of colony growth among the positive controls was observed for LIP5 (2). All combinations, which showed the same or higher number of growth on the interaction medium, were considered positive (gray background). Pictures of the evaluated plates are documented in the laboratory journal number IV, pages 103-104, 117, and 122, H. Wolff, AG Hülkamp, University of Cologne.

GAL4-BD	GAL4-AD	SET 1 day 10		SET 2 day 9		SET 3 day 11		total	
		SD-LW	SD-LWH 0mM	SD-LW	SD-LWH 0mM	SD-LW	SD-LWH 0mM	SD-LW	SD-LWH 0mM
SKD1	LIP5	xxx	x	xxx	0	xxx	x	9	2
SKD1	VPS32.1	xxx	xx	xxx	0	xxx	x	9	3
SKD1	VPS32.2	xxx	xxx	xxx	xxx	xxx	xxx	9	9
SKD1	VPS60.1	xxx	xx	xxx	xxx	xxx	xx	9	7
SKD1	VPS60.2	xxx	x	xxx	xx	xxx	xxx	9	8
SKD1	GFP	xxx	0	xxx	0	xxx	0	9	0
SKD1	VPS18	n.d.	n.d.	xxx	x	xxxxxxx	xxx	9	4
SKD1	GRF2	xxx	0	xxx	0	xxx	x	9	1
SKD1	GRF9	xxx	0	xxx	0	xxx	0	9	0
SKD1	PIP1-1	xxx	xx	xxx	x	xxx	xxx	9	6
SKD1	SEC13A	n.d.	n.d.	n.d.	n.d.	xxxxxxx xxx	xx	9	2
SKD1	FLOT1	xxx	x	xxx	0	xxx	xxx	9	4
SKD1	ISTL1	xxx	xx	xxx	xxx	xxx	xx	9	7
SKD1	eIF4B1	n.d.	n.d.	n.d.	n.d.	xxxxxxx xxx	0	9	0
SKD1	UAP56A	xxx	0	xxx	x	xxx	0	9	1
SKD1	LOS4	xxx	0	xxx	0	xxx	0	9	0
SKD1	CML10	xxx	xx	xxx	0	xxx	0	9	2
SKD1	UBP12	n.d.	n.d.	xxx	x	xxxxxxx	xxx	9	4
SKD1	RUXF	xxx	0	xxx	0	xxx	0	9	0
SKD1	RRM	n.d.	n.d.	xxx	0	xxxxxxx	x	9	1
SKD1	NTF2	xxx	0	xxx	0	xxx	0	9	0

**Table A.12. Results of SKD1 interactome LUMIER assay.** Constructs expressing SKD1 in fusion with ProtA (pTREX) and an interactome candidate in fusion with the Renilla luciferase (pcDNA3) were transfected in HEK293TN cells. After 48 h, total proteins were extracted from the cells and the Relative Luminescence Intensity (RLI) was measured (Input). Afterwards, cell lysates were incubated with  $\alpha$ -ProtA magnetic beads, washed and pulldown RLI was measured. All combinations were tested in at least two sets with at least two technical pulldown replicates. As a negative control, cells were co-transfected with SKD1-ProtA and unfused Renilla luciferase. As positive controls, SKD1-ProtA was co-transfected with VPS32.1, VPS60.1, and LIP5 in fusion with Renilla. Further, the combination TTG1-ProtA with GL3-Renilla was included in one set to exclude systemic problems. A combination was considered to interact if the measured RLI was 1.5 times higher than the background (marked by gray background).

		Relative Luminescence Intensity [RLI]											
		SET1			SET2			SET3					
ProtA	Renilla	Input	Pulldown			Input	Pulldown		Input	Pulldown		total	
pTREX	pcDNA3	1:10 diluted	rep1	rep2	rep3	1:10 diluted	rep1	rep2	1:10 diluted	rep1	rep2	Mean RLI	fold background
SKD1	VPS32.1	1330	241	242	240	1135	235	232	n.d.	n.d.	n.d.	238	0,98
SKD1	VPS60.1	3504	260	265	261	1397	233	233	n.d.	n.d.	n.d.	250	1,03
SKD1	LIP5	1585	244	244	243	1417	237	239	n.d.	n.d.	n.d.	241	1,00
SKD1	wo	2422	238	239	237	3489	230	231	4724	264	258	242	1,00
SKD1	VPS18	497	242	245	250	674	238	240	n.d.	n.d.	n.d.	243	1,00
<b>SKD1</b>	<b>GRF2</b>	<b>41878</b>	<b>547</b>	<b>618</b>	<b>624</b>	<b>n.d.</b>	<b>n.d.</b>	<b>n.d.</b>	<b>62279</b>	<b>801</b>	<b>822</b>	<b>682</b>	<b>2,81</b>
SKD1	GRF9	827	243	239	n.d.	1006	230	230	n.d.	n.d.	n.d.	236	0,97
SKD1	PIP1-1	3286	264	267	269	2911	230	239	n.d.	n.d.	n.d.	254	1,05
SKD1	SEC13A	725	250	247	250	1137	236	237	n.d.	n.d.	n.d.	244	1,01
SKD1	FLOT1	2272	289	292	274	1513	236	235	n.d.	n.d.	n.d.	265	1,09
SKD1	ISTL1	864	241	239	245	1268	235	235	n.d.	n.d.	n.d.	239	0,99
SKD1	eF4B1	514	235	235	242	1100	230	231	n.d.	n.d.	n.d.	235	0,97
SKD1	UAP56A	16979	243	247	261	34213	244	242	n.d.	n.d.	n.d.	247	1,02
<b>SKD1</b>	<b>LOS4</b>	<b>3186</b>	<b>428</b>	<b>420</b>	<b>442</b>	<b>7311</b>	<b>395</b>	<b>399</b>	<b>13943</b>	<b>559</b>	<b>634</b>	<b>468</b>	<b>1,93</b>
SKD1	CML10	1354	239	238	237	3194	235	237	n.d.	n.d.	n.d.	198	0,82
<b>SKD1</b>	<b>UBP12</b>	<b>3222</b>	<b>535</b>	<b>585</b>	<b>587</b>	<b>937</b>	<b>1126</b>	<b>1206</b>	<b>6678</b>	<b>932</b>	<b>868</b>	<b>834</b>	<b>3,44</b>
SKD1	RUXF	1011	277	283	273	2297	306	319	n.d.	n.d.	n.d.	292	1,20
SKD1	RRM	520	240	236	236	519	255	232	n.d.	n.d.	n.d.	240	0,99
SKD1	NTF2	3335	245	242	243	2833	233	234	n.d.	n.d.	n.d.	239	0,99
<b>TTG1</b>	<b>GL3</b>	<b>n.d.</b>	<b>n.d.</b>	<b>n.d.</b>	<b>n.d.</b>	<b>2205</b>	<b>6463</b>	<b>6209</b>	<b>n.d.</b>	<b>n.d.</b>	<b>n.d.</b>	<b>6336</b>	<b>26,14</b>

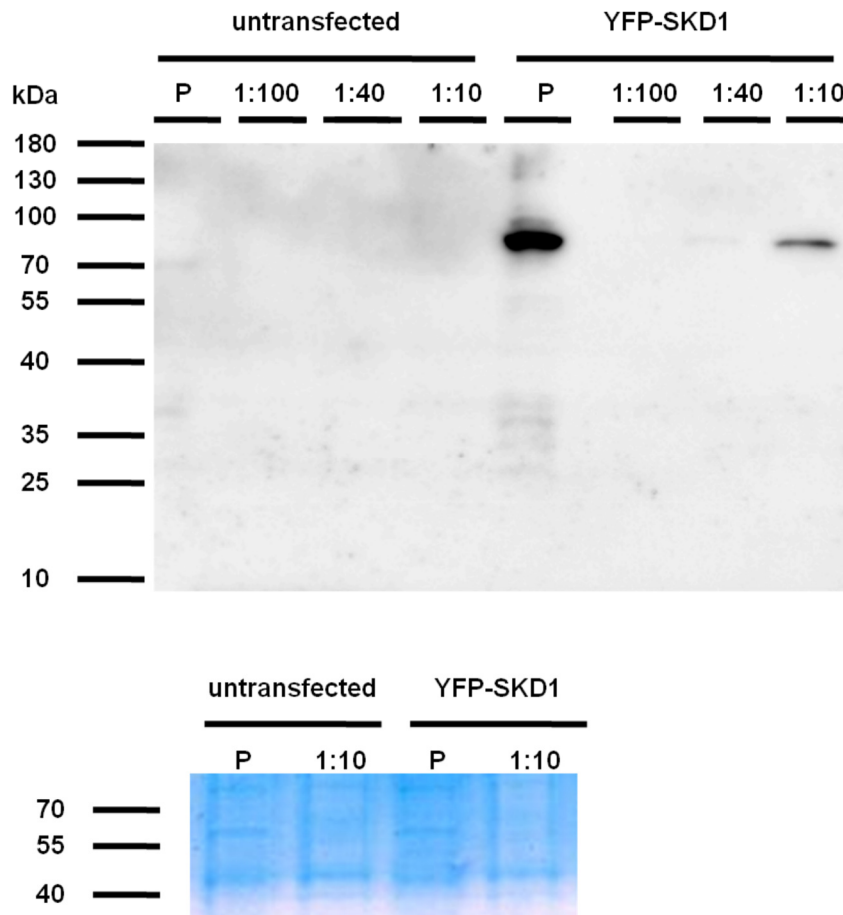


**Figure A.6. Test of SKD1 expression and purification from HEK293TN cells by SDS-PAGE and immunoblotting.** Human HEK293TN cells were transfected with a construct expressing YFP-SKD1 (pTREX-YFP-SKD1). After 48 h, transfected and untransfected cells (as a control) were lysed and cell debris were removed by centrifugation (15000 *g* for 15'). The generated pellets (P) were dissolved in the same volumes as the supernatants and prepared for SDS-PAGE followed either by immunoblotting ( $\alpha$ -GFP 1:2000, exposure time = 100'') or Coomassie staining. For blotting, supernatants were used in 1:10 to 1:100 dilutions and equal protein amounts were applied for SDS-PAGEs (1:10 dilution 15  $\mu$ l, P 2  $\mu$ l, approximately same protein amount in Coomassie staining). YFP-SKD1 is expected to migrate at approximately 77 kDa.

**Table A.13. Quantification of PIN2-GFP aggregates.** *ProPIN2::PIN2-GFP* seedlings were grown vertically on ½ MS plates for 5 d. The seedlings were transferred to ½ MS liquid and either kept at RT or subjected to heat treatment (40°C 50'). For each condition, seven roots were analyzed for the presence of PIN2-GFP aggregates in the cytosol. For that, single plane pictures of the transition zone of each root were taken by confocal microscopy. All cells for which the cell boundaries were clearly visible were counted and the number of aggregates was determined.

No treatment			40°C 50'		
Root No.	PIN2-GFP aggregates	Cells	Root No.	PIN2-GFP aggregates	Cells
1	0	62	1	17	53
2	2	77	2	37	50
3	3	57	3	9	64
4	0	54	4	18	48
5	3	41	5	12	45
6	0	39	6	7	32
7	1	49	7	8	51
MEAN	1.29	54.1	MEAN	15.43	49
STDEV	1.38	13	STDEV	10.44	9.6
SUM	9	379	SUM	108	343

## 6 References

- Abas, L., Benjamins, R., Malenica, N., Paciorek, T., Wiśniewska, J., Moulinier–Anzola, J.C., Sieberer, T., Friml, J., and Luschnig, C. (2006). Intracellular trafficking and proteolysis of the Arabidopsis auxin-efflux facilitator PIN2 are involved in root gravitropism. *Nat. Cell Biol.* 8, 249–256.
- Aizer, A., Kalo, A., Kafri, P., Shraga, A., Ben-Yishay, R., Jacob, A., Kinor, N., and Shav-Tal, Y. (2014). Quantifying mRNA targeting to P-bodies in living human cells reveals their dual role in mRNA decay and storage. *J. Cell Sci.* 127, 4443–4456.
- Alonso Y Adell, M., and Teis, D. (2011). Assembly and disassembly of the ESCRT-III membrane scission complex. *FEBS Lett.* 585, 3191–3196.
- Altschul, S.F., Madden, T.L., Schäffer, A.A., Zhang, J., Zhang, Z., Miller, W., and Lipman, D.J. (1997). Gapped BLAST and PSI-BLAST: a new generation of protein database search programs. *Nucleic Acids Res.* 25, 3389–3402.
- Amerik, A.Y., Nowak, J., Swaminathan, S., and Hochstrasser, M. (2000). The Doa4 deubiquitinating enzyme is functionally linked to the vacuolar protein-sorting and endocytic pathways. *Mol. Biol. Cell* 11, 3365–3380.
- Anderson, P., and Kedersha, N. (2008). Stress granules: the Tao of RNA triage. *Trends Biochem. Sci.* 33, 141–150.
- Azmi, I., Davies, B., Dimaano, C., Payne, J., Eckert, D., Babst, M., and Katzmann, D.J. (2006). Recycling of ESCRTs by the AAA-ATPase Vps4 is regulated by a conserved VSL region in Vta1. *J. Cell Biol.* 172, 705–717.
- Azmi, I.F., Davies, B.A., Xiao, J., Babst, M., Xu, Z., and Katzmann, D.J. (2008). ESCRT-III Family Members Stimulate Vps4 ATPase Activity Directly or via Vta1. *Dev. Cell* 14, 50–61.
- Babst, M., Wendland, B., Estepa, E.J., and Emr, S.D. (1998). The Vps4p AAA ATPase regulates membrane association of a Vps protein complex required for normal endosome function. *EMBO J.* 17, 2982–2993.
- Babst, M., Katzmann, D.J., Snyder, W.B., Wendland, B., and Emr, S.D. (2002a). Endosome-associated complex, ESCRT-II, recruits transport machinery for protein sorting at the multivesicular body. *Dev. Cell* 3, 283–289.
- Babst, M., Katzmann, D.J., Estepa-Sabal, E.J., Meerloo, T., and Emr, S.D. (2002b). Escrt-III: an endosome-associated heterooligomeric protein complex required for mvb sorting. *Dev. Cell* 3, 271–282.
- Bache, K.G., Brech, A., Mehlum, A., and Stenmark, H. (2003). Hrs regulates multivesicular body formation via ESCRT recruitment to endosomes. *J. Cell Biol.* 162, 435–442.
- Bajorek, M., Schubert, H.L., McCullough, J., Langelier, C., Eckert, D.M., Stubblefield, W.-M.B., Uter, N.T., Myszka, D.G., Hill, C.P., and Sundquist, W.I. (2009). Structural basis for ESCRT-III protein autoinhibition. *Nat. Struct. Mol. Biol.* 16, 754–762.
- Barrios-Rodiles, M., Brown, K.R., Ozdamar, B., Bose, R., Liu, Z., Donovan, R.S., Shinjo, F., Liu, Y., Dembowy, J., Taylor, I.W., et al. (2005). High-Throughput Mapping of a Dynamic Signaling Network in Mammalian Cells. *Science* 307, 1621.
- Basbous-Serhal, I., Pateyron, S., Cochet, F., Leymarie, J., and Bailly, C. (2017). 5' to 3' mRNA Decay Contributes to the Regulation of Arabidopsis Seed Germination by Dormancy. *Plant Physiol.* 173, 1709–1723.
- Beelman, C.A., Stevens, A., Caponigro, G., LaGrandeur, T.E., Hatfield, L., Fortner, D.M., and Parker, R. (1996). An essential component of the decapping enzyme required for normal rates of mRNA turnover. *Nature* 382, 642–646.

## References

---

- Bertani, G. (1951). Studies on lysogenesis. I. The mode of phage liberation by lysogenic *Escherichia coli*. *J. Bacteriol.* 62, 293–300.
- Bhasin, H., and Hülskamp, M. (2017). ANGUSTIFOLIA, a Plant Homolog of CtBP/BARS Localizes to Stress Granules and Regulates Their Formation. *Front. Plant Sci.* 8.
- Bhattacharyya, S.N., Habermacher, R., Martine, U., Closs, E.I., and Filipowicz, W. (2006). Relief of microRNA-Mediated Translational Repression in Human Cells Subjected to Stress. *Cell* 125, 1111–1124.
- Bi, X., Ren, J., and Goss, D.J. (2000). Wheat germ translation initiation factor eIF4B affects eIF4A and eIFiso4F helicase activity by increasing the ATP binding affinity of eIF4A. *Biochemistry (Mosc.)* 39, 5758–5765.
- Bilodeau, P.S., Urbanowski, J.L., Winistorfer, S.C., and Piper, R.C. (2002). The Vps27p–Hse1p complex binds ubiquitin and mediates endosomal protein sorting. *Nat. Cell Biol.*
- Bilodeau, P.S., Winistorfer, S.C., Kearney, W.R., Robertson, A.D., and Piper, R.C. (2003). Vps27-Hse1 and ESCRT-I complexes cooperate to increase efficiency of sorting ubiquitinated proteins at the endosome. *J. Cell Biol.* 163, 237–243.
- Blanc, C., Charette, S.J., Mattei, S., Aubry, L., Smith, E.W., Cosson, P., and Letourneur, F. (2009). Dictyostelium Tom1 Participates to an Ancestral ESCRT-0 Complex. *Traffic* 10, 161–171.
- Bolte, S., Talbot, C., Boutte, Y., Catrice, O., Read, N.D., and Satiat-Jeunemaitre, B. (2004). FM-dyes as experimental probes for dissecting vesicle trafficking in living plant cells. *J. Microsc.* 214, 159–173.
- Bonnerot, C., Boeck, R., and Lapeyre, B. (2000). The two proteins Pat1p (Mrt1p) and Spb8p interact in vivo, are required for mRNA decay, and are functionally linked to Pab1p. *Mol. Cell. Biol.* 20, 5939–5946.
- Boursiac, Y., Chen, S., Luu, D.-T., Sorieul, M., van den Dries, N., and Maurel, C. (2005). Early effects of salinity on water transport in *Arabidopsis* roots. Molecular and cellular features of aquaporin expression. *Plant Physiol.* 139, 790–805.
- Bouveret, E., Rigaut, G., Shevchenko, A., Wilm, M., and Séraphin, B. (2000). A Sm-like protein complex that participates in mRNA degradation. *EMBO J.* 19, 1661–1671.
- Bowers, K., Lottridge, J., Helliwell, S.B., Goldthwaite, L.M., Luzio, J.P., and Stevens, T.H. (2004). Protein-Protein Interactions of ESCRT Complexes in the Yeast *Saccharomyces cerevisiae*: Protein-Protein Interactions of ESCRT Complexes. *Traffic* 5, 194–210.
- Bregues, M., Teixeira, D., and Parker, R. (2005). Movement of eukaryotic mRNAs between polysomes and cytoplasmic processing bodies. *Science* 310, 486–489.
- Buchan, J.R., and Parker, R. (2009). Eukaryotic Stress Granules: The Ins and Outs of Translation. *Mol. Cell* 36, 932–941.
- Buchan, J.R., Muhrad, D., and Parker, R. (2008). P bodies promote stress granule assembly in *Saccharomyces cerevisiae*. *J. Cell Biol.* 183, 441–455.
- Buchan, J.R., Kolaitis, R.-M., Taylor, J.P., and Parker, R. (2013). Eukaryotic stress granules are cleared by granulophagy and Cdc48/VCP function. *Cell* 153, 1461–1474.
- Buchkovich, N.J., Henne, W.M., Tang, S., and Emr, S.D. (2013). Essential N-Terminal Insertion Motif Anchors the ESCRT-III Filament during MVB Vesicle Formation. *Dev. Cell* 27, 201–214.
- Bugnicourt, A., Froissard, M., Sereti, K., Ulrich, H.D., Haguenaer-Tsapis, R., and Galan, J.-M. (2004). Antagonistic roles of ESCRT and Vps class C/HOPS complexes in the recycling of yeast membrane proteins. *Mol. Biol. Cell* 15, 4203–4214.

## References

---

- Buono, R.A., Paez-Valencia, J., Miller, N.D., Goodman, K., Spitzer, C., Spalding, E.P., and Otegui, M.S. (2016). Role of SKD1 Regulators LIP5 and IST1-LIKE1 in Endosomal Sorting and Plant Development. *Plant Physiol.* 171, 251–264.
- Cai, Y., Zhuang, X., Gao, C., Wang, X., and Jiang, L. (2014). The Arabidopsis Endosomal Sorting Complex Required for Transport III Regulates Internal Vesicle Formation of the Prevacuolar Compartment and Is Required for Plant Development. *Plant Physiol.* 165, 1328.
- Chantarachot, T., and Bailey-Serres, J. (2018). Polysomes, Stress Granules, and Processing Bodies: A Dynamic Triumvirate Controlling Cytoplasmic mRNA Fate and Function. *Plant Physiol.* 176, 254–269.
- Chen, J., Chiang, Y.-C., and Denis, C.L. (2002). CCR4, a 3'-5' poly(A) RNA and ssDNA exonuclease, is the catalytic component of the cytoplasmic deadenylase. *EMBO J.* 21, 1414–1426.
- Chen, R., Hilson, P., Sedbrook, J., Rosen, E., Caspar, T., and Masson, P.H. (1998). The arabidopsis thaliana AGRVITROPIC 1 gene encodes a component of the polar-auxin-transport efflux carrier. *Proc. Natl. Acad. Sci. U. S. A.* 95, 15112–15117.
- Cho, K.-M., Nguyen, H.T.K., Kim, S.Y., Shin, J.S., Cho, D.H., Hong, S.B., Shin, J.S., and Ok, S.H. (2016). CML10, a variant of calmodulin, modulates ascorbic acid synthesis. *New Phytol.* 209, 664–678.
- Chung, K.P., Zeng, Y., and Jiang, L. (2016). COPII Paralogs in Plants: Functional Redundancy or Diversity? *Trends Plant Sci.* 21, 758–769.
- Ciais, P., Reichstein, M., Viovy, N., Granier, A., Ogée, J., Allard, V., Aubinet, M., Buchmann, N., Bernhofer, C., Carrara, A., et al. (2005). Europe-wide reduction in primary productivity caused by the heat and drought in 2003. *Nature* 437, 529–533.
- Colanzi, A., Grimaldi, G., Catara, G., Valente, C., Cericola, C., Liberali, P., Ronci, M., Lalioti, V.S., Bruno, A., Beccari, A.R., et al. (2013). Molecular mechanism and functional role of brefeldin A-mediated ADP-ribosylation of CtBP1/BARS. *Proc. Natl. Acad. Sci. U. S. A.* 110, 9794–9799.
- Conibear, E., and Stevens, T.H. (1998). Multiple sorting pathways between the late Golgi and the vacuole in yeast. *Biochim. Biophys. Acta* 1404, 211–230.
- Contento, A.L., and Bassham, D.C. (2012). Structure and function of endosomes in plant cells. *J. Cell Sci.* 125, 3511–3518.
- Cougot, N., Babajko, S., and Séraphin, B. (2004). Cytoplasmic foci are sites of mRNA decay in human cells. *J. Cell Biol.* 165, 31–40.
- Cui, X., Lu, F., Li, Y., Xue, Y., Kang, Y., Zhang, S., Qiu, Q., Cui, X., Zheng, S., Liu, B., et al. (2013). Ubiquitin-Specific Proteases UBP12 and UBP13 Act in Circadian Clock and Photoperiodic Flowering Regulation in Arabidopsis. *PLANT Physiol.* 162, 897–906.
- Cullinane, A.R., Schäffer, A.A., and Huizing, M. (2013). The BEACH Is Hot: A LYST of Emerging Roles for BEACH-Domain Containing Proteins in Human Disease: BEACH-Domain Containing Proteins in Human Disease. *Traffic* 14, 749–766.
- Decker, C.J., Teixeira, D., and Parker, R. (2007). Edc3p and a glutamine/asparagine-rich domain of Lsm4p function in processing body assembly in *Saccharomyces cerevisiae*. *J. Cell Biol.* 179, 437–449.
- Dhonukshe, P., Aniento, F., Hwang, I., Robinson, D.G., Mravec, J., Stierhof, Y.-D., and Friml, J. (2007). Clathrin-Mediated Constitutive Endocytosis of PIN Auxin Efflux Carriers in Arabidopsis. *Curr. Biol.* 17, 520–527.
- Dimaano, C., Jones, C.B., Hanono, A., Curtiss, M., and Babst, M. (2008). Ist1 regulates Vps4 localization and assembly. *Mol. Biol. Cell* 19, 465–474.

## References

---

- Dunckley, T., and Parker, R. (1999). The DCP2 protein is required for mRNA decapping in *Saccharomyces cerevisiae* and contains a functional MutT motif. *EMBO J.* 18, 5411–5422.
- Dunckley, T., Tucker, M., and Parker, R. (2001). Two related proteins, Edc1p and Edc2p, stimulate mRNA decapping in *Saccharomyces cerevisiae*. *Genetics* 157, 27–37.
- Dunker, A.K., Brown, C.J., Lawson, J.D., Iakoucheva, L.M., and Obradović, Z. (2002). Intrinsic Disorder and Protein Function. *Biochemistry (Mosc.)* 41, 6573–6582.
- Dunn, K.W., Kamocka, M.M., and McDonald, J.H. (2011). A practical guide to evaluating colocalization in biological microscopy. *Am. J. Physiol.-Cell Physiol.* 300, C723–C742.
- Efeyan, A., Zoncu, R., and Sabatini, D.M. (2012). Amino acids and mTORC1: from lysosomes to disease. *Trends Mol. Med.* 18, 524–533.
- Emans, N. (2002). Uptake of a Fluorescent Marker in Plant Cells Is Sensitive to Brefeldin A and Wortmannin. *PLANT CELL ONLINE* 14, 71–86.
- Fenger-Grøn, M., Fillman, C., Norrild, B., and Lykke-Andersen, J. (2005). Multiple Processing Body Factors and the ARE Binding Protein TTP Activate mRNA Decapping. *Mol. Cell* 20, 905–915.
- Ferraiuolo, M.A., Basak, S., Dostie, J., Murray, E.L., Schoenberg, D.R., and Sonenberg, N. (2005). A role for the eIF4E-binding protein 4E-T in P-body formation and mRNA decay. *J. Cell Biol.* 170, 913–924.
- Fields, S., and Song, O. (1989). A novel genetic system to detect protein-protein interactions. *Nature* 340, 245–246.
- Finken-Eigen, M., Röhricht, R.A., and Köhrer, K. (1997). The VPS4 gene is involved in protein transport out of a yeast pre-vacuolar endosome-like compartment. *Curr. Genet.* 31, 469–480.
- Fujita, H. (2003). A dominant negative form of the AAA ATPase SKD1/VPS4 impairs membrane trafficking out of endosomal/lysosomal compartments: class E vps phenotype in mammalian cells. *J. Cell Sci.* 116, 401–414.
- Gallie, D.R. (2014). The role of the poly(A) binding protein in the assembly of the Cap-binding complex during translation initiation in plants. *Translation* 2, e959378.
- Gälweiler, L., Guan, C., Müller, A., Wisman, E., Mendgen, K., Yephremov, A., and Palme, K. (1998). Regulation of polar auxin transport by AtPIN1 in *Arabidopsis* vascular tissue. *Science* 282, 2226–2230.
- Gao, C., Luo, M., Zhao, Q., Yang, R., Cui, Y., Zeng, Y., Xia, J., and Jiang, L. (2014). A Unique Plant ESCRT Component, FREE1, Regulates Multivesicular Body Protein Sorting and Plant Growth. *Curr. Biol.* 24, 2556–2563.
- Gao, C., Zhuang, X., Shen, J., and Jiang, L. (2017). Plant ESCRT Complexes: Moving Beyond Endosomal Sorting. *Trends Plant Sci.* 22, 986–998.
- Garrus, J.E., Von Schwedler, U.K., Pornillos, O.W., Morham, S.G., Zavitz, K.H., Wang, H.E., Wettstein, D.A., Stray, K.M., Côté, M., and Rich, R.L. (2001). Tsg101 and the vacuolar protein sorting pathway are essential for HIV-1 budding. *Cell* 107, 55–65.
- Geldner, N., Friml, J., Stierhof, Y.D., Jürgens, G., and Palme, K. (2001). Auxin transport inhibitors block PIN1 cycling and vesicle trafficking. *Nature* 413, 425–428.
- Geldner, N., Dénervaud-Tendon, V., Hyman, D.L., Mayer, U., Stierhof, Y.-D., and Chory, J. (2009). Rapid, combinatorial analysis of membrane compartments in intact plants with a multicolor marker set. *Plant J.* 59, 169–178.

## References

---

- Gietz, R.D., Schiestl, R.H., Willems, A.R., and Woods, R.A. (1995). Studies on the transformation of intact yeast cells by the LiAc/SS-DNA/PEG procedure. *Yeast* Chichester Engl. 11, 355–360.
- Gilks, N., Kedersha, N., Ayodele, M., Shen, L., Stoecklin, G., Dember, L.M., and Anderson, P. (2004). Stress granule assembly is mediated by prion-like aggregation of TIA-1. *Mol. Biol. Cell* 15, 5383–5398.
- Gill, D.J., Teo, H., Sun, J., Perisic, O., Veprintsev, D.B., Emr, S.D., and Williams, R.L. (2007). Structural insight into the ESCRT-I/-II link and its role in MVB trafficking. *EMBO J.* 26, 600–612.
- Gong, Z. (2005). A DEAD Box RNA Helicase Is Essential for mRNA Export and Important for Development and Stress Responses in Arabidopsis. *PLANT CELL ONLINE* 17, 256–267.
- Gong, Z., Lee, H., Xiong, L., Jagendorf, A., Stevenson, B., and Zhu, J.-K. (2002). RNA helicase-like protein as an early regulator of transcription factors for plant chilling and freezing tolerance. *Proc. Natl. Acad. Sci. U. S. A.* 99, 11507–11512.
- Gorvel, J.-P., Chavier, P., Zerial, M., and Gruenberg, J. (1991). rab5 controls early endosome fusion in vitro. *Cell* 64, 915–925.
- Grunewald, W., and Friml, J. (2010). The march of the PINs: developmental plasticity by dynamic polar targeting in plant cells. *EMBO J.* 29, 2700–2714.
- Haas, T.J., Sliwinski, M.K., Martinez, D.E., Preuss, M., Ebine, K., Ueda, T., Nielsen, E., Odorizzi, G., and Otegui, M.S. (2007). The Arabidopsis AAA ATPase SKD1 Is Involved in Multivesicular Endosome Function and Interacts with Its Positive Regulator LYST-INTERACTING PROTEIN5. *PLANT CELL ONLINE* 19, 1295–1312.
- Hanahan, D. (1983). Studies on transformation of *Escherichia coli* with plasmids. *J. Mol. Biol.* 166, 557–580.
- Hanson, P.I., Roth, R., Lin, Y., and Heuser, J.E. (2008). Plasma membrane deformation by circular arrays of ESCRT-III protein filaments. *J. Cell Biol.* 180, 389–402.
- Hartmann, C., Chami, M., Zachariae, U., de Groot, B.L., Engel, A., and Grütter, M.G. (2008). Vacuolar Protein Sorting: Two Different Functional States of the AAA-ATPase Vps4p. *J. Mol. Biol.* 377, 352–363.
- Hatfield, L., Beelman, C.A., Stevens, A., and Parker, R. (1996). Mutations in trans-acting factors affecting mRNA decapping in *Saccharomyces cerevisiae*. *Mol. Cell. Biol.* 16, 5830–5838.
- Henne, W.M., Buchkovich, N.J., Zhao, Y., and Emr, S.D. (2012). The Endosomal Sorting Complex ESCRT-II Mediates the Assembly and Architecture of ESCRT-III Helices. *Cell* 151, 356–371.
- Hirayama, T., and Shinozaki, K. (2010). Research on plant abiotic stress responses in the post-genome era: past, present and future. *Plant J.* 61, 1041–1052.
- Hooper, C.M., Castleden, I.R., Tanz, S.K., Aryamanesh, N., and Millar, A.H. (2017). SUBA4: the interactive data analysis centre for Arabidopsis subcellular protein locations. *Nucleic Acids Res.* 45, D1064–D1074.
- Howard, T.L., Stauffer, D.R., Degnin, C.R., and Hollenberg, S.M. (2001). CHMP1 functions as a member of a newly defined family of vesicle trafficking proteins. *J. Cell Sci.* 114, 2395–2404.
- Huotari, J., and Helenius, A. (2011). Endosome maturation: Endosome maturation. *EMBO J.* 30, 3481–3500.
- Hurley, J.H., and Hanson, P.I. (2010). Membrane budding and scission by the ESCRT machinery: it's all in the neck. *Nat. Rev. Mol. Cell Biol.* 11, 556–566.
- Iakoucheva, L.M., Brown, C.J., Lawson, J.D., Obradović, Z., and Dunker, A.K. (2002). Intrinsic Disorder in Cell-signaling and Cancer-associated Proteins. *J. Mol. Biol.* 323, 573–584.

## References

---

- Ibl, V., Csaszar, E., Schlager, N., Neubert, S., Spitzer, C., and Hauser, M.-T. (2012). Interactome of the Plant-specific ESCRT-III Component AtVPS2.2 in *Arabidopsis thaliana*. *J. Proteome Res.* 11, 397–411.
- Jaag, H.M., and Nagy, P.D. (2009). Silencing of *Nicotiana benthamiana* Xrn4p exoribonuclease promotes tombusvirus RNA accumulation and recombination. *Virology* 386, 344–352.
- Jain, S., Wheeler, J.R., Walters, R.W., Agrawal, A., Barsic, A., and Parker, R. (2016). ATPase-Modulated Stress Granules Contain a Diverse Proteome and Substructure. *Cell* 164, 487–498.
- James, P., Halladay, J., and Craig, E.A. (1996). Genomic libraries and a host strain designed for highly efficient two-hybrid selection in yeast. *Genetics* 144, 1425–1436.
- Jarolim, S., Ayer, A., Pillay, B., Gee, A.C., Phrakaysone, A., Perrone, G.G., Breitenbach, M., and Dawes, I.W. (2013). *Saccharomyces cerevisiae* Genes Involved in Survival of Heat Shock. *G3 GenesGenomesGenetics* 3, 2321–2333.
- Jeong, J.S., Jung, C., Seo, J.S., Kim, J.-K., and Chua, N.-H. (2017). The Deubiquitinating Enzymes UBP12 and UBP13 Positively Regulate MYC2 Levels in Jasmonate Responses. *Plant Cell* tpc.00216.2017.
- Kabsch, W., and Sander, C. (1983). Dictionary of protein secondary structure: pattern recognition of hydrogen-bonded and geometrical features. *Biopolymers* 22, 2577–2637.
- Kammel, C., Thomaier, M., Sørensen, B.B., Schubert, T., Längst, G., Grasser, M., and Grasser, K.D. (2013). *Arabidopsis* DEAD-Box RNA Helicase UAP56 Interacts with Both RNA and DNA as well as with mRNA Export Factors. *PLoS ONE* 8, e60644.
- Kamura, T., Burian, D., Khalili, H., Schmidt, S.L., Sato, S., Liu, W.-J., Conrad, M.N., Conaway, R.C., Conaway, J.W., and Shilatifard, A. (2001). Cloning and Characterization of ELL-associated Proteins EAP45 and EAP20: A ROLE FOR YEAST EAP-LIKE PROTEINS IN REGULATION OF GENE EXPRESSION BY GLUCOSE. *J. Biol. Chem.* 276, 16528–16533.
- Kanno, T., Lin, W.-D., Fu, J.L., Matzke, A.J.M., and Matzke, M. (2017). A genetic screen implicates a CWC16/Yju2/CCDC130 protein and SMU1 in alternative splicing in *Arabidopsis thaliana*. *RNA N. Y. N* 23, 1068–1079.
- Kastenmayer, J.P., and Green, P.J. (2000). Novel features of the XRN-family in *Arabidopsis*: evidence that AtXRN4, one of several orthologs of nuclear Xrn2p/Rat1p, functions in the cytoplasm. *Proc. Natl. Acad. Sci. U. S. A.* 97, 13985–13990.
- Kato, M., Han, T.W., Xie, S., Shi, K., Du, X., Wu, L.C., Mirzaei, H., Goldsmith, E.J., Longgood, J., Pei, J., et al. (2012). Cell-free Formation of RNA Granules: Low Complexity Sequence Domains Form Dynamic Fibers within Hydrogels. *Cell* 149, 753–767.
- Katsiarimpa, A., Anzenberger, F., Schlager, N., Neubert, S., Hauser, M.-T., Schwechheimer, C., and Isono, E. (2011). The *Arabidopsis* Deubiquitinating Enzyme AMSH3 Interacts with ESCRT-III Subunits and Regulates Their Localization. *Plant Cell* 23, 3026–3040.
- Katsiarimpa, A., Kalinowska, K., Anzenberger, F., Weis, C., Ostertag, M., Tsutsumi, C., Schwechheimer, C., Brunner, F., Huckelhoven, R., and Isono, E. (2013). The Deubiquitinating Enzyme AMSH1 and the ESCRT-III Subunit VPS2.1 Are Required for Autophagic Degradation in *Arabidopsis*. *Plant Cell* 25, 2236–2252.
- Katzmann, D.J., Babst, M., and Emr, S.D. (2001). Ubiquitin-dependent sorting into the multivesicular body pathway requires the function of a conserved endosomal protein sorting complex, ESCRT-I. *Cell* 106, 145–155.
- Katzmann, D.J., Stefan, C.J., Babst, M., and Emr, S.D. (2003). Vps27 recruits ESCRT machinery to endosomes during MVB sorting. *J. Cell Biol.* 162, 413–423.

## References

---

- Kedersha, N., Stoecklin, G., Ayodele, M., Yacono, P., Lykke-Andersen, J., Fritzler, M.J., Scheuner, D., Kaufman, R.J., Golan, D.E., and Anderson, P. (2005). Stress granules and processing bodies are dynamically linked sites of mRNP remodeling. *J. Cell Biol.* 169, 871–884.
- Kedersha, N., Ivanov, P., and Anderson, P. (2013). Stress granules and cell signaling: more than just a passing phase? *Trends Biochem. Sci.* 38, 494–506.
- Kedersha, N.L., Gupta, M., Li, W., Miller, I., and Anderson, P. (1999). RNA-binding proteins TIA-1 and TIAR link the phosphorylation of eIF-2 alpha to the assembly of mammalian stress granules. *J. Cell Biol.* 147, 1431–1442.
- Keicher, J., Jaspert, N., Weckermann, K., Möller, C., Throm, C., Kintzi, A., and Oecking, C. (2017). Arabidopsis 14-3-3 epsilon members contribute to polarity of PIN auxin carrier and auxin transport-related development. *ELife* 6.
- Kleine-Vehn, J., Dhonukshe, P., Swarup, R., Bennett, M., and Friml, J. (2006). Subcellular Trafficking of the Arabidopsis Auxin Influx Carrier AUX1 Uses a Novel Pathway Distinct from PIN1. *PLANT CELL ONLINE* 18, 3171–3181.
- Kleine-Vehn, J., Leitner, J., Zwiewka, M., Sauer, M., Abas, L., Luschnig, C., and Friml, J. (2008). Differential degradation of PIN2 auxin efflux carrier by retromer-dependent vacuolar targeting. *Proc. Natl. Acad. Sci.* 105, 17812–17817.
- Kolb, C., Nagel, M.-K., Kalinowska, K., Hagmann, J., Ichikawa, M., Anzenberger, F., Alkofer, A., Sato, M.H., Braun, P., and Isono, E. (2015). FYVE1 Is Essential for Vacuole Biogenesis and Intracellular Trafficking in Arabidopsis. *Plant Physiol.* 167, 1361–1373.
- Korbei, B., Moulinier-Anzola, J., De-Araujo, L., Lucyshyn, D., Retzer, K., Khan, M.A., and Luschnig, C. (2013). Arabidopsis TOL Proteins Act as Gatekeepers for Vacuolar Sorting of PIN2 Plasma Membrane Protein. *Curr. Biol.* 23, 2500–2505.
- Kostelansky, M.S., Schluter, C., Tam, Y.Y.C., Lee, S., Ghirlando, R., Beach, B., Conibear, E., and Hurley, J.H. (2007). Molecular Architecture and Functional Model of the Complete Yeast ESCRT-I Heterotetramer. *Cell* 129, 485–498.
- Kranz, A., Kinner, A., and Kolling, R. (2001). A Family of Small Coiled-Coil-forming Proteins Functioning at the Late Endosome in Yeast. *Mol. Biol. Cell* 12, 711–723.
- Krapp, S., Greiner, E., Amin, B., Sonnewald, U., and Krenz, B. (2017). The stress granule component G3BP is a novel interaction partner for the nuclear shuttle proteins of the nanovirus pea necrotic yellow dwarf virus and geminivirus abutilon mosaic virus. *Virus Res.* 227, 6–14.
- Lambermon, M.H., Simpson, G.G., Wieczorek Kirk, D.A., Hemmings-Mieszczak, M., Klahre, U., and Filipowicz, W. (2000). UBP1, a novel hnRNP-like protein that functions at multiple steps of higher plant nuclear pre-mRNA maturation. *EMBO J.* 19, 1638–1649.
- Landsberg, M.J., Vajjhala, P.R., Rothnagel, R., Munn, A.L., and Hankamer, B. (2009). Three-Dimensional Structure of AAA ATPase Vps4: Advancing Structural Insights into the Mechanisms of Endosomal Sorting and Enveloped Virus Budding. *Structure* 17, 427–437.
- Lange, A., Castañeda, C., Hoeller, D., Lancelin, J.-M., Fushman, D., and Walker, O. (2012). Evidence for Cooperative and Domain-specific Binding of the Signal Transducing Adaptor Molecule 2 (STAM2) to Lys 63-linked Diubiquitin. *J. Biol. Chem.* 287, 18687–18699.
- Lee, M.H., and Hwang, I. (2014). Adaptor proteins in protein trafficking between endomembrane compartments in plants. *J. Plant Biol.* 57, 265–273.

## References

---

- Lee, G.-J., Sohn, E.J., Lee, M.H., and Hwang, I. (2004). The Arabidopsis rab5 homologs rha1 and ara7 localize to the prevacuolar compartment. *Plant Cell Physiol.* 45, 1211–1220.
- Leitner, A., Joachimiak, L.A., Bracher, A., Mönkemeyer, L., Walzthoeni, T., Chen, B., Pechmann, S., Holmes, S., Cong, Y., Ma, B., et al. (2012). The molecular architecture of the eukaryotic chaperonin TRiC/CCT. *Struct. England* 1993 20, 814–825.
- Leung, K.F., Dacks, J.B., and Field, M.C. (2008). Evolution of the Multivesicular Body ESCRT Machinery; Retention Across the Eukaryotic Lineage. *Traffic* 9, 1698–1716.
- Li, R., Liu, P., Wan, Y., Chen, T., Wang, Q., Mettbaach, U., Baluska, F., Samaj, J., Fang, X., Lucas, W.J., et al. (2012). A Membrane Microdomain-Associated Protein, Arabidopsis Flot1, Is Involved in a Clathrin-Independent Endocytic Pathway and Is Required for Seedling Development. *Plant Cell* 24, 2105–2122.
- Lin, Y., Kimpler, L.A., Naismith, T.V., Lauer, J.M., and Hanson, P.I. (2005). Interaction of the Mammalian Endosomal Sorting Complex Required for Transport (ESCRT) III Protein hSnf7-1 with Itself, Membranes, and the AAA + ATPase SKD1. *J. Biol. Chem.* 280, 12799–12809.
- Lin, Y., Protter, D.S.W., Rosen, M.K., and Parker, R. (2015). Formation and Maturation of Phase-Separated Liquid Droplets by RNA-Binding Proteins. *Mol. Cell* 60, 208–219.
- Linding, R. (2003). GlobPlot: exploring protein sequences for globularity and disorder. *Nucleic Acids Res.* 31, 3701–3708.
- Linding, R., Jensen, L.J., Diella, F., Bork, P., Gibson, T.J., and Russell, R.B. (2003). Protein Disorder Prediction. *Structure* 11, 1453–1459.
- Lokdarshi, A., Conner, W.C., McClintock, C., Li, T., and Roberts, D.M. (2016). Arabidopsis CML38, a Calcium Sensor That Localizes to Ribonucleoprotein Complexes under Hypoxia Stress. *Plant Physiol.* 170, 1046–1059.
- Lorković, Z.J., Wiczorek Kirk, D.A., Klahre, U., Hemmings-Mieszczak, M., and Filipowicz, W. (2000). RBP45 and RBP47, two oligouridylate-specific hnRNP-like proteins interacting with poly(A)+ RNA in nuclei of plant cells. *RNA N. Y. N* 6, 1610–1624.
- Lottridge, J.M., Flannery, A.R., Vincelli, J.L., and Stevens, T.H. (2006). Vta1p and Vps46p regulate the membrane association and ATPase activity of Vps4p at the yeast multivesicular body. *Proc. Natl. Acad. Sci. U. S. A.* 103, 6202–6207.
- Lu, Q., Hope, L.W., Brasch, M., Reinhard, C., and Cohen, S.N. (2003). TSG101 interaction with HRS mediates endosomal trafficking and receptor down-regulation. *Proc. Natl. Acad. Sci. U. S. A.* 100, 7626–7631.
- Luschnig, C., Gaxiola, R.A., Grisafi, P., and Fink, G.R. (1998). EIR1, a root-specific protein involved in auxin transport, is required for gravitropism in Arabidopsis thaliana. *Genes Dev.* 12, 2175–2187.
- Lykke-Andersen, J. (2002). Identification of a Human Decapping Complex Associated with hUpf Proteins in Nonsense-Mediated Decay. *Mol. Cell. Biol.* 22, 8114–8121.
- Mackintosh, C. (2004). Dynamic interactions between 14-3-3 proteins and phosphoproteins regulate diverse cellular processes. *Biochem. J.* 381, 329–342.
- Manders, E.M., Stap, J., Brakenhoff, G.J., Van Driel, R., and Aten, J.A. (1992). Dynamics of three-dimensional replication patterns during the S-phase, analysed by double labelling of DNA and confocal microscopy. *J. Cell Sci.* 103, 857–862.
- Martin-Serrano, J., Yarovoy, A., Perez-Caballero, D., Bieniasz, P.D., and Yarovoy, A. (2003). Divergent retroviral late-budding domains recruit vacuolar protein sorting factors by using alternative adaptor proteins. *Proc. Natl. Acad. Sci. U. S. A.* 100, 12414–12419.

## References

---

- Mateju, D., Franzmann, T.M., Patel, A., Kopach, A., Boczek, E.E., Maharana, S., Lee, H.O., Carra, S., Hyman, A.A., and Alberti, S. (2017). An aberrant phase transition of stress granules triggered by misfolded protein and prevented by chaperone function. *EMBO J.* 36, 1669–1687.
- Mayberry, L.K., Allen, M.L., Dennis, M.D., and Browning, K.S. (2009). Evidence for Variation in the Optimal Translation Initiation Complex: Plant eIF4B, eIF4F, and eIF(iso)4F Differentially Promote Translation of mRNAs. *PLANT Physiol.* 150, 1844–1854.
- Mazroui, R., Di Marco, S., Kaufman, R.J., and Gallouzi, I.-E. (2007). Inhibition of the ubiquitin-proteasome system induces stress granule formation. *Mol. Biol. Cell* 18, 2603–2618.
- McCue, A.D., Nuthikattu, S., Reeder, S.H., and Slotkin, R.K. (2012). Gene Expression and Stress Response Mediated by the Epigenetic Regulation of a Transposable Element Small RNA. *PLoS Genet.* 8, e1002474.
- McCullough, J., Clippinger, A.K., Talledge, N., Skowrya, M.L., Saunders, M.G., Naismith, T.V., Colf, L.A., Afonine, P., Arthur, C., and Sundquist, W.I. (2015). Structure and membrane remodeling activity of ESCRT-III helical polymers. *Science* 350, 1548–1551.
- McNally, E.K., and Brett, C. (2017). ESCRT-Independent Surface Receptor And Transporter Protein Degradation By The ILF Pathway. *BioRxiv* 167411.
- McNally, E.K., Karim, M.A., and Brett, C.L. (2017). Selective Lysosomal Transporter Degradation by Organelle Membrane Fusion. *Dev. Cell* 40, 151–167.
- Meaden, P.G., Arneborg, N., Guldeldt, L.U., Siegumfeldt, H., and Jakobsen, M. (1999). Endocytosis and vacuolar morphology in *Saccharomyces cerevisiae* are altered in response to ethanol stress or heat shock. *Yeast* 15, 1211–1222.
- Méresse, S., Gorvel, J.-P., and Chavrier, P. (1995). The rab7 GTPase resides on a vesicular compartment connected to lysosomes. *J. Cell Sci.* 108, 3349–3358.
- Merret, R., Descombin, J., Juan, Y., Favory, J.-J., Carpentier, M.-C., Chaparro, C., Charng, Y., Deragon, J.-M., and Bousquet-Antonelli, C. (2013). XRN4 and LARP1 Are Required for a Heat-Triggered mRNA Decay Pathway Involved in Plant Acclimation and Survival during Thermal Stress. *Cell Rep.* 5, 1279–1293.
- Mi, H., Dong, Q., Muruganujan, A., Gaudet, P., Lewis, S., and Thomas, P.D. (2010). PANTHER version 7: improved phylogenetic trees, orthologs and collaboration with the Gene Ontology Consortium. *Nucleic Acids Res.* 38, D204–D210.
- Miki, T., Park, J.A., Nagao, K., Murayama, N., and Horiuchi, T. (1992). Control of segregation of chromosomal DNA by sex factor F in *Escherichia coli*. Mutants of DNA gyrase subunit A suppress letD (ccdB) product growth inhibition. *J. Mol. Biol.* 225, 39–52.
- Minamisawa, N., Sato, M., Cho, K.-H., Ueno, H., Takechi, K., Kajikawa, M., Yamato, K.T., Ohyama, K., Toyooka, K., Kim, G.-T., et al. (2011). ANGUSTIFOLIA, a plant homolog of CtBP/BARS, functions outside the nucleus: ANGUSTIFOLIA on TGN. *Plant J.* 68, 788–799.
- Molliex, A., Temirov, J., Lee, J., Coughlin, M., Kanagaraj, A.P., Kim, H.J., Mittag, T., and Taylor, J.P. (2015). Phase Separation by Low Complexity Domains Promotes Stress Granule Assembly and Drives Pathological Fibrillization. *Cell* 163, 123–133.
- Motomura, K., Le, Q.T.N., Hamada, T., Kutsuna, N., Mano, S., Nishimura, M., and Watanabe, Y. (2015). Diffuse Decapping Enzyme DCP2 Accumulates in DCP1 Foci Under Heat Stress in *Arabidopsis thaliana*. *Plant Cell Physiol.* 56, 107–115.

## References

---

- Müller, A., Guan, C., Gälweiler, L., Tänzler, P., Huijser, P., Marchant, A., Parry, G., Bennett, M., Wisman, E., and Palme, K. (1998). AtPIN2 defines a locus of Arabidopsis for root gravitropism control. *EMBO J.* 17, 6903–6911.
- Murashige, T., and Skoog, F. (1962). A Revised Medium for Rapid Growth and Bio Assays with Tobacco Tissue Cultures. *Physiol. Plant.* 15, 473–497.
- Muthuramalingam, M., Wang, Y., Li, Y., and Mahalingam, R. (2017). Interacting protein partners of Arabidopsis RNA-binding protein AtRBP45b. *Plant Biol.* 19, 327–334.
- Muzioł, T., Pineda-Molina, E., Ravelli, R.B., Zamborlini, A., Usami, Y., Göttlinger, H., and Weissenhorn, W. (2006). Structural Basis for Budding by the ESCRT-III Factor CHMP3. *Dev. Cell* 10, 821–830.
- Nath, S., Munsie, L.N., and Truant, R. (2015). A huntingtin-mediated fast stress response halting endosomal trafficking is defective in Huntington's disease. *Hum. Mol. Genet.* 24, 450–462.
- Nguyen, A.H., Matsui, A., Tanaka, M., Mizunashi, K., Nakaminami, K., Hayashi, M., Iida, K., Toyoda, T., Nguyen, D.V., and Seki, M. (2015). Loss of Arabidopsis 5'–3' Exoribonuclease AtXRN4 Function Enhances Heat Stress Tolerance of Plants Subjected to Severe Heat Stress. *Plant Cell Physiol.* 56, 1762–1772.
- Nguyen, C.C., Nakaminami, K., Matsui, A., Kobayashi, S., Kurihara, Y., Toyooka, K., Tanaka, M., and Seki, M. (2016). Oligouridylylate Binding Protein 1b Plays an Integral Role in Plant Heat Stress Tolerance. *Front. Plant Sci.* 7, 853.
- Nguyen, C.C., Nakaminami, K., Matsui, A., Watanabe, S., Kanno, Y., Seo, M., and Seki, M. (2017). Overexpression of oligouridylylate binding protein 1b results in ABA hypersensitivity. *Plant Signal. Behav.* 12, e1282591.
- Nickerson, D.P., West, M., and Odorizzi, G. (2006). Did2 coordinates Vps4-mediated dissociation of ESCRT-III from endosomes. *J. Cell Biol.* 175, 715–720.
- Nickerson, D.P., Brett, C.L., and Merz, A.J. (2009). Vps-C complexes: gatekeepers of endolysosomal traffic. *Curr. Opin. Cell Biol.* 21, 543–551.
- Nishi, T., and Forgac, M. (2002). The vacuolar (H<sup>+</sup>)-ATPases — nature's most versatile proton pumps. *Nat. Rev. Mol. Cell Biol.* 3, 94–103.
- Obita, T., Saksena, S., Ghazi-Tabatabai, S., Gill, D.J., Perisic, O., Emr, S.D., and Williams, R.L. (2007). Structural basis for selective recognition of ESCRT-III by the AAA ATPase Vps4. *Nature* 449, 735–739.
- Olmos, Y., Hodgson, L., Mantell, J., Verkade, P., and Carlton, J.G. (2015). ESCRT-III controls nuclear envelope reformation. *Nature* 522, 236–239.
- Paciorek, T., Zažímalová, E., Ruthardt, N., Petrášek, J., Stierhof, Y.-D., Kleine-Vehn, J., Morris, D.A., Emans, N., Jürgens, G., Geldner, N., et al. (2005). Auxin inhibits endocytosis and promotes its own efflux from cells. *Nature* 435, 1251–1256.
- Parida, A.P., Sharma, A., and Sharma, A.K. (2017). AtMBD6, a methyl CpG binding domain protein, maintains gene silencing in Arabidopsis by interacting with RNA binding proteins. *J. Biosci.* 42, 57–68.
- Parker, R., and Song, H. (2004). The enzymes and control of eukaryotic mRNA turnover. *Nat. Struct. Mol. Biol.* 11, 121–127.
- Peng, J., Yang, J., Yan, F., Lu, Y., Jiang, S., Lin, L., Zheng, H., Chen, H., and Chen, J. (2011). Silencing of NbXrn4 facilitates the systemic infection of Tobacco mosaic virus in *Nicotiana benthamiana*. *Virus Res.* 158, 268–270.

- Pesch, M., Schultheiss, I., Digiuni, S., Uhrig, J.F., and Hülkamp, M. (2013). Mutual control of intracellular localisation of the patterning proteins AtMYC1, GL1 and TRY/CPC in Arabidopsis. *Development* 140, 3456–3467.
- Pfaff, C., Ehrnsberger, H.F., Flores-Tornero, M., Soerensen, B.B., Schubert, T., Längst, G., Griesenbeck, J., Sprunck, S., Grasser, M., and Grasser, K.D. (2018). ALY RNA-binding proteins are required for nucleocytoplasmic mRNA transport and modulate plant growth and development. *Plant Physiol.* pp.00173.2018.
- Pietrosemoli, N., García-Martín, J.A., Solano, R., and Pazos, F. (2013). Genome-Wide Analysis of Protein Disorder in Arabidopsis thaliana: Implications for Plant Environmental Adaptation. *PLoS ONE* 8, e55524.
- Pineda-Molina, E., Belrhali, H., Piefer, A.J., Akula, I., Bates, P., and Weissenhorn, W. (2006). The Crystal Structure of the C-Terminal Domain of Vps28 Reveals a Conserved Surface Required for Vps20 Recruitment: Crystal Structure of Vps28. *Traffic* 7, 1007–1016.
- Protter, D.S.W., and Parker, R. (2016). Principles and Properties of Stress Granules. *Trends Cell Biol.* 26, 668–679.
- Reijns, M.A.M., Alexander, R.D., Spiller, M.P., and Beggs, J.D. (2008). A role for Q/N-rich aggregation-prone regions in P-body localization. *J. Cell Sci.* 121, 2463–2472.
- Ren, X., and Hurley, J.H. (2010). VHS domains of ESCRT-0 cooperate in high-avidity binding to polyubiquitinated cargo. *EMBO J.* 29, 1045–1054.
- Reyes, F.C., Buono, R.A., Roschztardt, H., Di Rubbo, S., Yeun, L.H., Russinova, E., and Otegui, M.S. (2014). A Novel Endosomal Sorting Complex Required for Transport (ESCRT) Component in Arabidopsis thaliana Controls Cell Expansion and Development. *J. Biol. Chem.* 289, 4980–4988.
- Richardson, L.G.L., Howard, A.S.M., Khoo, N., Gidda, S.K., McCartney, A., Morphy, B.J., and Mullen, R.T. (2011). Protein-Protein Interaction Network and Subcellular Localization of the Arabidopsis Thaliana ESCRT Machinery. *Front. Plant Sci.* 2.
- Richter, K., Haslbeck, M., and Buchner, J. (2010). The Heat Shock Response: Life on the Verge of Death. *Mol. Cell* 40, 253–266.
- Rieder, S.E., Banta, L.M., Köhrer, K., McCaffery, J.M., and Emr, S.D. (1996). Multilamellar endosome-like compartment accumulates in the yeast vps28 vacuolar protein sorting mutant. *Mol. Biol. Cell* 7, 985–999.
- Rink, J., Ghigo, E., Kalaidzidis, Y., and Zerial, M. (2005). Rab Conversion as a Mechanism of Progression from Early to Late Endosomes. *Cell* 122, 735–749.
- Rogers, G.W., Richter, N.J., Lima, W.F., and Merrick, W.C. (2001). Modulation of the Helicase Activity of eIF4A by eIF4B, eIF4H, and eIF4F. *J. Biol. Chem.* 276, 30914–30922.
- Rojo, E., Gillmor, C.S., Kovaleva, V., Somerville, C.R., and Raikhel, N.V. (2001). VACUOLELESS1 is an essential gene required for vacuole formation and morphogenesis in Arabidopsis. *Dev. Cell* 1, 303–310.
- Rojo, E., Zouhar, J., Kovaleva, V., Hong, S., and Raikhel, N.V. (2003). The AtC-VPS Protein Complex Is Localized to the Tonoplast and the Prevacuolar Compartment in Arabidopsis. *Mol. Biol. Cell* 14, 361–369.
- Roy, R., and Bassham, D.C. (2017). TNO1, a TGN-localized SNARE-interacting protein, modulates root skewing in Arabidopsis thaliana. *BMC Plant Biol.* 17.
- Rue, S.M., Mattei, S., Saksena, S., and Emr, S.D. (2008). Novel Ist1-Did2 complex functions at a late step in multivesicular body sorting. *Mol. Biol. Cell* 19, 475–484.
- Saedler, R., Jakoby, M., Marin, B., Galiana-Jaime, E., and Hülkamp, M. (2009). The cell morphogenesis gene SPIRRIG in Arabidopsis encodes a WD/BEACH domain protein. *Plant J.* 59, 612–621.

## References

---

- Schmidt, O., and Teis, D. (2012). The ESCRT machinery. *Curr. Biol.* CB 22, R116-120.
- Schmidt, A.E., Miller, T., Schmidt, S.L., Shiekhattar, R., and Shilatifard, A. (1999). Cloning and characterization of the EAP30 subunit of the ELL complex that confers derepression of transcription by RNA polymerase II. *J. Biol. Chem.* 274, 21981–21985.
- Schneider, C.A., Rasband, W.S., and Eliceiri, K.W. (2012). NIH Image to ImageJ: 25 years of image analysis. *Nat. Methods* 9, 671–675.
- Schuh, A.L., Hanna, M., Quinney, K., Wang, L., Sarkeshik, A., Yates, J.R., and Audhya, A. (2015). The VPS-20 subunit of the endosomal sorting complex ESCRT-III exhibits an open conformation in the absence of upstream activation. *Biochem. J.* 466, 625–637.
- von Schwedler, U.K., Stuchell, M., Müller, B., Ward, D.M., Chung, H.-Y., Morita, E., Wang, H.E., Davis, T., He, G.-P., Cimbara, D.M., et al. (2003). The protein network of HIV budding. *Cell* 114, 701–713.
- Scott, A., Gaspar, J., Stuchell-Brereton, M.D., Alam, S.L., Skalicky, J.J., and Sundquist, W.I. (2005a). Structure and ESCRT-III protein interactions of the MIT domain of human VPS4A. *Proc. Natl. Acad. Sci.* 102, 13813–13818.
- Scott, A., Chung, H.-Y., Gonciarz-Swiatek, M., Hill, G.C., Whitby, F.G., Gaspar, J., Holton, J.M., Viswanathan, R., Ghaffarian, S., and Hill, C.P. (2005b). Structural and mechanistic studies of VPS4 proteins. *EMBO J.* 24, 3658–3669.
- Shahriari, M., Keshavaiah, C., Scheuring, D., Sabovljevic, A., Pimpl, P., Häusler, R.E., Hülskamp, M., and Schellmann, S. (2010a). The AAA-type ATPase AtSKD1 contributes to vacuolar maintenance of *Arabidopsis thaliana*: Vacuolar maintenance by AtSKD1. *Plant J.* no-no.
- Shahriari, M., Hülskamp, M., and Schellmann, S. (2010b). Seeds of *Arabidopsis* plants expressing dominant-negative AtSKD1 under control of the GL2 promoter show a transparent testa phenotype and a mucilage defect. *Plant Signal. Behav.* 5, 1308–1310.
- Shen, Q.-T., Schuh, A.L., Zheng, Y., Quinney, K., Wang, L., Hanna, M., Mitchell, J.C., Otegui, M.S., Ahlquist, P., Cui, Q., et al. (2014). Structural analysis and modeling reveals new mechanisms governing ESCRT-III spiral filament assembly. *J. Cell Biol.* 206, 763–777.
- Sheth, U., and Parker, R. (2003). Decapping and decay of messenger RNA occur in cytoplasmic processing bodies. *Science* 300, 805–808.
- Shim, S., Kimpler, L.A., and Hanson, P.I. (2007). Structure/Function Analysis of Four Core ESCRT-III Proteins Reveals Common Regulatory Role for Extreme C-Terminal Domain. *Traffic* 8, 1068–1079.
- Skalicky, J.J., Aarii, J., Wenzel, D.M., Stubblefield, W.-M.B., Katsuyama, A., Uter, N.T., Bajorek, M., Myszka, D.G., and Sundquist, W.I. (2012). Interactions of the Human LIP5 Regulatory Protein with Endosomal Sorting Complexes Required for Transport. *J. Biol. Chem.* 287, 43910–43926.
- Slagsvold, T., Aasland, R., Hirano, S., Bache, K.G., Raiborg, C., Trambaiolo, D., Wakatsuki, S., and Stenmark, H. (2005). Eap45 in Mammalian ESCRT-II Binds Ubiquitin via a Phosphoinositide-interacting GLUE Domain. *J. Biol. Chem.* 280, 19600–19606.
- Sohn, E.J. (2003). Rha1, an *Arabidopsis* Rab5 Homolog, Plays a Critical Role in the Vacuolar Trafficking of Soluble Cargo Proteins. *PLANT CELL ONLINE* 15, 1057–1070.
- Solinger, J.A., and Spang, A. (2013). Tethering complexes in the endocytic pathway: CORVET and HOPS. *FEBS J.* 280, 2743–2757.

## References

---

- Sorenson, R., and Bailey-Serres, J. (2014). Selective mRNA sequestration by OLIGOURIDYLATE-BINDING PROTEIN 1 contributes to translational control during hypoxia in Arabidopsis. *Proc. Natl. Acad. Sci.* 111, 2373–2378.
- Spallek, T., Beck, M., Ben Khaled, S., Salomon, S., Bourdais, G., Schellmann, S., and Robatzek, S. (2013). ESCRT-I Mediates FLS2 Endosomal Sorting and Plant Immunity. *PLoS Genet.* 9, e1004035.
- Spitzer, C., Schellmann, S., Sabovljevic, A., Shahriari, M., Keshavaiah, C., Bechtold, N., Herzog, M., Muller, S., Hanisch, F.-G., and Hülskamp, M. (2006). The Arabidopsis elch mutant reveals functions of an ESCRT component in cytokinesis. *Development* 133, 4679–4689.
- Spitzer, C., Reyes, F.C., Buono, R., Sliwinski, M.K., Haas, T.J., and Otegui, M.S. (2009). The ESCRT-Related CHMP1A and B Proteins Mediate Multivesicular Body Sorting of Auxin Carriers in Arabidopsis and Are Required for Plant Development. *PLANT CELL ONLINE* 21, 749–766.
- Steffens, A., Bräutigam, A., Jakoby, M., and Hülskamp, M. (2015). The BEACH Domain Protein SPIRRIG Is Essential for Arabidopsis Salt Stress Tolerance and Functions as a Regulator of Transcript Stabilization and Localization. *PLoS Biol.* 13.
- Steffens, A., Jakoby, M., and Hülskamp, M. (2017). Physical, Functional and Genetic Interactions between the BEACH Domain Protein SPIRRIG and LIP5 and SKD1 and Its Role in Endosomal Trafficking to the Vacuole in Arabidopsis. *Front. Plant Sci.* 8.
- Steiger, M., Carr-Schmid, A., Schwartz, D.C., Kiledjian, M., and Parker, R. (2003). Analysis of recombinant yeast decapping enzyme. *RNA N. Y. N* 9, 231–238.
- Stoecklin, G., and Kedersha, N. (2013). Relationship of GW/P-Bodies with Stress Granules. In *Ten Years of Progress in GW/P Body Research*, E.K.L. Chan, and M.J. Fritzler, eds. (New York, NY: Springer New York), pp. 197–211.
- Stoecklin, G., Stubbs, T., Kedersha, N., Wax, S., Rigby, W.F.C., Blackwell, T.K., and Anderson, P. (2004). MK2-induced tristetraprolin:14-3-3 complexes prevent stress granule association and ARE-mRNA decay. *EMBO J.* 23, 1313–1324.
- Strack, B., Calistri, A., Craig, S., Popova, E., and Göttlinger, H.G. (2003). AIP1/ALIX is a binding partner for HIV-1 p6 and EIAV p9 functioning in virus budding. *Cell* 114, 689–699.
- Stuchell-Brereton, M.D., Skalicky, J.J., Kieffer, C., Karren, M.A., Ghaffarian, S., and Sundquist, W.I. (2007). ESCRT-III recognition by VPS4 ATPases. *Nature* 449, 740–744.
- Suzuki, Y., Arae, T., Green, P.J., Yamaguchi, J., and Chiba, Y. (2015). AtCCR4a and AtCCR4b are Involved in Determining the Poly(A) Length of Granule-bound starch synthase 1 Transcript and Modulating Sucrose and Starch Metabolism in Arabidopsis thaliana. *Plant Cell Physiol.* 56, 863–874.
- Takahara, T., and Maeda, T. (2012). Transient Sequestration of TORC1 into Stress Granules during Heat Stress. *Mol. Cell* 47, 242–252.
- Takemoto, K., Ebine, K., Askani, J.C., Krüger, F., Gonzalez, Z.A., Ito, E., Goh, T., Schumacher, K., Nakano, A., and Ueda, T. (2018). Distinct sets of tethering complexes, SNARE complexes, and Rab GTPases mediate membrane fusion at the vacuole in Arabidopsis. *Proc. Natl. Acad. Sci.* 115, E2457–E2466.
- Teis, D., Saksena, S., and Emr, S.D. (2008). Ordered Assembly of the ESCRT-III Complex on Endosomes Is Required to Sequester Cargo during MVB Formation. *Dev. Cell* 15, 578–589.
- Teo, H., Perisic, O., González, B., and Williams, R.L. (2004). ESCRT-II, an endosome-associated complex required for protein sorting: crystal structure and interactions with ESCRT-III and membranes. *Dev. Cell* 7, 559–569.

## References

---

- Teo, H., Gill, D.J., Sun, J., Perisic, O., Veprintsev, D.B., Vallis, Y., Emr, S.D., and Williams, R.L. (2006). ESCRT-I Core and ESCRT-II GLUE Domain Structures Reveal Role for GLUE in Linking to ESCRT-I and Membranes. *Cell* 125, 99–111.
- Tharun, S., He, W., Mayes, A.E., Lennertz, P., Beggs, J.D., and Parker, R. (2000). Yeast Sm-like proteins function in mRNA decapping and decay. *Nature* 404, 515.
- Thedieck, K., Holzwarth, B., Prentzell, M.T., Boehlke, C., Kläsener, K., Ruf, S., Sonntag, A.G., Maerz, L., Grellscheid, S.-N., Kremmer, E., et al. (2013). Inhibition of mTORC1 by Astrin and Stress Granules Prevents Apoptosis in Cancer Cells. *Cell* 154, 859–874.
- Thomas, P.D., Campbell, M.J., Kejariwal, A., Mi, H., Karlak, B., Daverman, R., Diemer, K., Muruganujan, A., and Narechania, A. (2003). PANTHER: a library of protein families and subfamilies indexed by function. *Genome Res.* 13, 2129–2141.
- Tian, Q., Streuli, M., Saito, H., Schlossman, S.F., and Anderson, P. (1991). A polyadenylate binding protein localized to the granules of cytolytic lymphocytes induces DNA fragmentation in target cells. *Cell* 67, 629–639.
- Tompa, P., Dosztányi, Z., and Simon, I. (2006). Prevalent Structural Disorder in *E. coli* and *S. cerevisiae* Proteomes. *J. Proteome Res.* 5, 1996–2000.
- Tourrière, H., Chebli, K., Zekri, L., Courselaud, B., Blanchard, J.M., Bertrand, E., and Tazi, J. (2003). The RasGAP-associated endoribonuclease G3BP assembles stress granules. *J. Cell Biol.* 160, 823–831.
- Tucker, M., Valencia-Sanchez, M.A., Staples, R.R., Chen, J., Denis, C.L., and Parker, R. (2001). The transcription factor associated Ccr4 and Caf1 proteins are components of the major cytoplasmic mRNA deadenylase in *Saccharomyces cerevisiae*. *Cell* 104, 377–386.
- Ueda, T., Yamaguchi, M., Uchimiya, H., and Nakano, A. (2001). Ara6, a plant-unique novel type Rab GTPase, functions in the endocytic pathway of *Arabidopsis thaliana*. *EMBO J.* 20, 4730–4741.
- Vajjhala, P.R., Wong, J.S., To, H.-Y., and Munn, A.L. (2006). The  $\beta$  domain is required for Vps4p oligomerization into a functionally active ATPase. *FEBS J.* 273, 2357–2373.
- Vega, V.L., Charles, W., and De Maio, A. (2010). A new feature of the stress response: increase in endocytosis mediated by Hsp70. *Cell Stress Chaperones* 15, 517–527.
- Verbelen, J.-P., Cnodder, T.D., Le, J., Vissenberg, K., and Baluška, F. (2006). The root apex of *Arabidopsis thaliana* consists of four distinct zones of growth activities: meristematic zone, transition zone, fast elongation zone and growth terminating zone. *Plant Signal. Behav.* 1, 296–304.
- Vietri, M., Schink, K.O., Campsteijn, C., Wegner, C.S., Schultz, S.W., Christ, L., Thoresen, S.B., Brech, A., Raiborg, C., and Stenmark, H. (2015). Spastin and ESCRT-III coordinate mitotic spindle disassembly and nuclear envelope sealing. *Nature* 522, 231–235.
- Vihervaara, A., and Sistonen, L. (2014). HSF1 at a glance. *J. Cell Sci.* 127, 261–266.
- Viotti, C., Bubeck, J., Stierhof, Y.-D., Krebs, M., Langhans, M., van den Berg, W., van Dongen, W., Richter, S., Geldner, N., Takano, J., et al. (2010). Endocytic and Secretory Traffic in *Arabidopsis* Merge in the Trans-Golgi Network/Early Endosome, an Independent and Highly Dynamic Organelle. *Plant Cell* 22, 1344–1357.
- Vukašinović, N., and Žárský, V. (2016). Tethering Complexes in the *Arabidopsis* Endomembrane System. *Front. Cell Dev. Biol.* 4.
- Wang, F., Shang, Y., Fan, B., Yu, J.-Q., and Chen, Z. (2014). *Arabidopsis* LIP5, a Positive Regulator of Multivesicular Body Biogenesis, Is a Critical Target of Pathogen-Responsive MAPK Cascade in Plant Basal Defense. *PLoS Pathog.* 10, e1004243.

## References

---

- Wang, F., Yang, Y., Wang, Z., Zhou, J., Fan, B., and Chen, Z. (2015). A Critical Role of Lyst-Interacting Protein5, a Positive Regulator of Multivesicular Body Biogenesis, in Plant Responses to Heat and Salt Stresses. *Plant Physiol.* 169, 497–511.
- Wang, H.-J., Hsu, Y.-W., Guo, C.-L., Jane, W.-N., Wang, H., Jiang, L., and Jauh, G.-Y. (2017). VPS36-Dependent Multivesicular Bodies Are Critical for Plasmamembrane Protein Turnover and Vacuolar Biogenesis. *Plant Physiol.* 173, 566–581.
- Ward, J.J., Sodhi, J.S., McGuffin, L.J., Buxton, B.F., and Jones, D.T. (2004). Prediction and Functional Analysis of Native Disorder in Proteins from the Three Kingdoms of Life. *J. Mol. Biol.* 337, 635–645.
- Weber, C., Nover, L., and Fauth, M. (2008). Plant stress granules and mRNA processing bodies are distinct from heat stress granules. *Plant J.* 56, 517–530.
- Welch, W.J., and Suhan, J.P. (1985). Morphological study of the mammalian stress response: characterization of changes in cytoplasmic organelles, cytoskeleton, and nucleoli, and appearance of intranuclear actin filaments in rat fibroblasts after heat-shock treatment. *J. Cell Biol.* 101, 1198–1211.
- Wernimont, A.K., and Weissenhorn, W. (2004). Crystal structure of subunit VPS25 of the endosomal trafficking complex ESCRT-II. *BMC Struct. Biol.* 4, 10.
- Winter, V., and Hauser, M.-T. (2006). Exploring the ESCRTing machinery in eukaryotes. *Trends Plant Sci.* 11, 115–123.
- Wippich, F., Bodenmiller, B., Trajkovska, M.G., Wanka, S., Aebersold, R., and Pelkmans, L. (2013). Dual Specificity Kinase DYRK3 Couples Stress Granule Condensation/Dissolution to mTORC1 Signaling. *Cell* 152, 791–805.
- Wolff, H. (2016). The unifying power of stress: Bringing together mRNAs and proteins. CEPLAS Planter's Punch. <https://www.ceplas.eu/en/discover/planters-punch/2016/the-unifying-power-of-stress-bringing-together-mrnas-and-proteins/>
- Xiang, L., Etxeberria, E., and Van den Ende, W. (2013). Vacuolar protein sorting mechanisms in plants. *FEBS J.* 280, 979–993.
- Xiao, J., Xia, H., Yoshino-Koh, K., Zhou, J., and Xu, Z. (2007). Structural Characterization of the ATPase Reaction Cycle of Endosomal AAA Protein Vps4. *J. Mol. Biol.* 374, 655–670.
- Xiao, J., Xia, H., Zhou, J., Azmi, I.F., Davies, B.A., Katzmann, D.J., and Xu, Z. (2008). Structural Basis of Vta1 Function in the Multivesicular Body Sorting Pathway. *Dev. Cell* 14, 37–49.
- Xie, H., Vucetic, S., Iakoucheva, L.M., Oldfield, C.J., Dunker, A.K., Uversky, V.N., and Obradovic, Z. (2007). Functional Anthology of Intrinsic Disorder. 1. Biological Processes and Functions of Proteins with Long Disordered Regions. *J. Proteome Res.* 6, 1882–1898.
- Xu, J., and Chua, N.-H. (2009). Arabidopsis Decapping 5 Is Required for mRNA Decapping, P-Body Formation, and Translational Repression during Postembryonic Development. *Plant Cell* 21, 3270–3279.
- Xu, J., Yang, J.-Y., Niu, Q.-W., and Chua, N.-H. (2006). Arabidopsis DCP2, DCP1, and VARICOSE Form a Decapping Complex Required for Postembryonic Development. *PLANT CELL ONLINE* 18, 3386–3398.
- Yu, M., Liu, H., Dong, Z., Xiao, J., Su, B., Fan, L., Komis, G., Šamaj, J., Lin, J., and Li, R. (2017). The dynamics and endocytosis of Flot1 protein in response to flg22 in Arabidopsis. *J. Plant Physiol.* 215, 73–84.
- Zamborlini, A., Usami, Y., Radoshitzky, S.R., Popova, E., Palu, G., and Göttlinger, H. (2006). Release of autoinhibition converts ESCRT-III components into potent inhibitors of HIV-1 budding. *Proc. Natl. Acad. Sci.* 103, 19140–19145.

## 7 Danksagung

An dieser Stelle möchte ich mich bei Prof. Dr. Martin Hülkamp für die jahrelange Unterstützung bedanken, ohne die diese Dissertation nicht möglich gewesen wäre. Zudem bedanke ich mich für die vielen Diskussionen und Ideen, die mich sehr motiviert haben. Bei Prof. Dr. Jane Parker und Prof. Dr. Niels Gehring bedanke ich mich für die Hilfe bei der Gestaltung dieses Projektes und den vielen Anregungen.

Mein ganz besonderer Dank gilt Dr. Marc Jakoby, der zu jeder Zeit bereit war in diesem Projekt mitzudenken und Hilfestellung zu leisten. Sowohl seine wissenschaftliche Betreuung als auch die vielen nichtwissenschaftlichen Gespräche haben mich geprägt und zum Nachdenken angeregt.

Ich bedanke mich bei Dr. Stefan Müller und bei der Proteomic Facility Cologne für die Hilfe bei der Umsetzung und Auswertung des SKD1 Proteoms. Des Weiteren möchte ich mich bei dem Exzellenzcluster CEPLAS für die Finanzierung dieser Doktorarbeit bedanken. Der CEPLAS Graduiertenschule danke ich für die Einblicke in die verschiedensten Bereiche der Pflanzenwissenschaften und für die Gelegenheit eine Vielzahl talentierter junger Wissenschaftler kennen gelernt zu haben.

Für die ausgezeichnete Hilfe bei Klonierungsarbeiten, Transformationen und Hefeexperimenten bedanke ich mich bei Birgit Kernebeck und Hanna Bechtel.

Meinen lieben Mitdotorandinnen Eva Koebke, Jessica Pietsch und Lisa Stephan danke ich für den unerschütterlichen Zusammenhalt. Außerdem bedanke ich mich für die Hilfe bei Experimenten und der Korrektur dieser Arbeit. Die vielen lustigen Stunden im Büro und im Labor, aber vor allem die an der frischen Luft, haben mir viel Kraft gegeben.

Ich bedanke mich bei jedem Mitglied der AGHülkamp für die gegenseitige Unterstützung. Der vortreffliche Teamgeist war stets aufmunternd und motivierend.

Meinen Jägersfreunden Olga Bondarenko, Rafael Campos-Martin, Arijit Das und Henrik Failmezger danke ich für unvergessliche Zeit und den großen Spaß, den ich dank ihnen während dieser Arbeit hatte.

Mein größter Dank gilt meiner Familie: Meinen Eltern Gisela und Ernst Wolff, meiner Schwester Selma Wolff, meinen Großeltern Sieglinde und Ludwig Wolff. Jeder von ihnen hat mich auf diesem Weg solange er konnte begleitet und stets an mich geglaubt.

## **8 Erklärung zur Dissertation**

Ich versichere, dass ich die von mir vorgelegte Dissertation selbständig angefertigt, die benutzten Quellen und Hilfsmittel vollständig angegeben und die Stellen der Arbeit –einschließlich Tabellen, Karten und Abbildungen –, die anderen Werken im Wortlaut oder dem Sinn nach entnommen sind, in jedem Einzelfall als Entlehnung kenntlich gemacht habe; dass diese Dissertation noch keiner anderen Fakultät oder Universität zur Prüfung vorgelegen hat; dass sie –abgesehen von unten angegebenen Teilpublikationen –noch nicht veröffentlicht worden ist, sowie, dass ich eine solche Veröffentlichung vor Abschluss des Promotionsverfahrens nicht vornehmen werde. Die Bestimmungen der Promotionsordnung sind mir bekannt. Die von mir vorgelegte Dissertation ist von Prof. Dr. Martin Hülskamp betreut worden.

Heike Wolff

Köln, den